PRESSURE FLUCTUATIONS IN THE PLUNGE POOL OF AN IMPINGING JET SPILLWAY

(VOLUME I OF II – MAIN TEXT)

A THESIS ON PLUNGE POOL ENERGY DISSIPATORS FOR THE DEGREE OF DOCTOR OF PHILOSOPHY

BY: WILLIAM JAMES WITHERS
DEPARTMENT OF CIVIL ENGINEERING
UNIVERSITY OF GLASGOW
FEBRUARY 1991

To Mother, Father and R.F.C.

ACKNOWLEDGEMENTS

I am most grateful to my mother, father and girlfriend, Gloria, for their patience, kindness and support during the course of my studies. This is especially true for the hectic last few months.

Special thanks and appreciation to my supervisor, Dr. D.A. Ervine, for his excellent teaching, encouragement and advice. His knowledge of hydraulics, particularly in the field of hydraulic structures, was basic to the completion of this dissertation. Without Dr. Ervine's input during the numerous readings of the various versions of this thesis, the standard would be nowhere near that which has been attained.

I would also like to express my gratitude to Mr. A. Gray, hydraulics technician, for his assistance in the design of the experimental apparatus. Mr Gray also fabricated the rig single–handedly and contributed substantially with the experimental programme.

I would also like to thank Mr. A. Burnett, superintendent, for the procurement of materials and express my gratitude to the remainder of the Glasgow University technical staff.

Of the faculty staff, Mr Hewitt (Statistics), Mr Watson (Instrument design) and Dr. Williams (Dynamics) were of assistance in the cited areas, and I am most grateful.

Many thanks also to Dr. D. Green for allowing the use of the Glasgow University facilities.

Concerning my fellow research students, I appreciate the assistance of Mr. A. Khan during turbulence testing and Mr J. Wark and Dr. Y.R. Fares for helpful discussions which can be attributed to the solution of many problems in this research. Thanks also to Dr. H. K. Jasem for his assistance in the preparation of this thesis.

Financial contributions:
I would like to thank the Science and Engineering Research Council for providing

financial assistance during the course of this research.

The administrators of the Wylie/Dunlop Bequest are also thanked for providing funds to purchase elements of the experimental apparatus, instrumentation and the computer system.

Last, but not least, I would like to thank W. A. Fairhurst and Partners for funding the production costs of this thesis. Their contribution is greatly appreciated.

ABSTRACT

The primary purpose of this dissertation is to define the range of pressure fluctuations produced at a plunge pool floor due to spillway jet impingement.

At high head dams the spillway flow sometimes takes the form of free–falling jets. Energy dissipation of the spillway flow is achieved by dispersion of the free–falling jets in the atmosphere, diffusion of the impinging flow in a water cushion at the dam base and impact of the remaining flow with the plunge pool floor.

The plunge pool may be formed naturally through scouring of the bedrock by the spillway flow or may consist of a man–made stilling basin. Whichever method is adopted, impingement of the spillway jets with the plunge pool tailwater promotes a large degree of air entrainment while mixing of the pool fluid with the incoming flow generates a large amount of turbulence. Associated with the turbulence are large pressure fluctuations which act on the sides and floor of the stilling basin. In the case of lined pools, the fluctuations can cause uplift and removal of the concrete base slabs from the stilling basin. Damage of this form may become severe and, if left unchecked, produce subsequent failure of the dam. Vibration of the dam due to coincidence of the structures natural frequency with that of the applied loading is also a threat. In natural plunge pools, excessive scour can be produced, possibly undermining the dam foundations.

In general, lack of information has meant that current stilling basin design procedures usually fail to include these pressure fluctuations in the structural design of the plunge pool. The objective of this research is to establish information describing pressure fluctuations for design use and prevent these forms of operational problems.

The highly complex flow situation was simulated by construction of an experimental rig at the University of Glasgow. Design of the apparatus was such that the main parameters affecting the flow could be altered to cover a wide range of scenarios. As well as measurement of instantaneous pressures on the plunge pool floor, turbulence readings within the plunging jet were taken as the behaviour of the free–falling flow has a profound effect on the subsequent plunge pool diffusion.

The current state of technology allowed data acquisition and control by means of a micro–computer. By development of analytical procedures and specialised routines from commercial software, the computer was used to facilitate measurement of pressure fluctuations at selected locations on the plunge pool floor and velocity fluctuations within the plunging jet. The raw data was then statistically analysed with the primary interest being the magnitude, frequency and extent of pressure fluctuations at the pool base and the turbulence development within the plunging jet. From the jet turbulence results, methods were produced to determine the jet condition at impact with the pool surface for comparison with measured values.

The statistical pressure head results were compared with other available research and parameters were introduced to take account of the effects of plunging jet behaviour in the atmosphere on the subsequent plunge pool diffusion process. Through analysis, explanation of the values of mean pressure head and the level of fluctuations generated at the pool floor was provided. Application of the results to plunge pool design was also included.

PRESSURE FLUCTUATIONS IN THE PLUNGE POOL OF AN IMPINGING JET SPILLWAY (VOLUME I OF II – MAIN TEXT)

GENERAL CONTENTS

CONTENTS OF EACH CHAPTER. Page

NOTATION

Symbol	Meaning
A_1	area of total head tube
A_2	area of shock chamber
B_1, B_2	plan dimensions of pool
b	value of radius at which U=Um/2 (length scale)
b	slot thickness
bp	value of radius at which P=Pm/2 (length scale)
C	air concentration
Cc	centre line air concentration
Cp'	R.M.S. pressure coefficient
Cp^+	maximum pressure coefficient
Cp^-	minimum pressure coefficient
d,D	diameter and gate opening
Dp	depth of penetration of air bubbles
E	Young's modulus and kinetic energy
F	force on bubble
F(f)	frequency response
f	frequency
fc	Nyquist frequency
fd	natural frequency of transducer
fo	natural frequency of instrument
f(p)	probability
G(f)	power spectral density function
g	gravitational acceleration
H	total available head
$\bar{H}m$	total mean pressure head
$(\bar{H}m-Y)$	dynamic mean pressure head
Hmax	instantaneous total peak head
Hmin	instantaneous total minimum head
h	pressure head
hs	mean pressure head above hydrostatic at stagnation point
Δh	pressure head deviation from mean

	and head difference at manometer
Kd	spring constant
L	jet fall height
L_B	jet break-up length
Lo	length of upstream nozzle
L_1	total length of total head tube
L_2	length of shock chamber
ℓ	eddy length and distance from outlet
M	momentum flux
N	total number of time intervals
P_1, P_2	probability of encountering water
P	pressure
Pm	dynamic mean pressure at jet centre line
Ps	stagnation pressure
Q	flow rate
q	unit discharge
R	radius of curvature of jet surface undulations
Rj	radius of jet
Rp	distance from jet centre line on pool floor
Rp*	radial extent of deflection region
r,Φ,z	cylindrical coordinates
r	radial distance from jet centre line
rj	distance from jet centre line to turbulence probe
T	time period
Tu	turbulence intensity
t	time
u,v,w	velocity components in x,y,z direction
U	jet velocity in longitudinal direction
Ubr	bubble rise velocity
Ue	minimum entrainment velocity
Um	maximum jet velocity (centre line) - velocity scale
U*	shear velocity
V	velocity in radial direction
Ve	entrainment velocity
W	jet velocity and slot width
X,Y,Z	cartesian coordinates
X	longitudinal distance from outlet

y, Y	plunge pool depth
Yc	length of submerged core
Ys	limiting depth for central pressure
Y*	longitudinal extent of deflection region
Z	diaphragm deflection

Dimensionless numbers

Fr	Froude number	$[U/\sqrt{(gD)}]$
Re	Reynolds number	$[UD/\nu]$
We	Weber number	$[U/\sqrt{(\sigma/\rho D)}]$
Oh	Ohnesorge number	$[W_e/R_e]$

Greek symbol

α	jet convergence angle
α_e	entrainment coefficient
β	air/water ratio
β_D	damping factor
δ_1, δ_2	inner and outer jet spread angle in atmosphere
δ_0	amplitude of initial surface disturbance
δ	boundary layer extent (and denotes partial differentiation)
∇	vector operator
ϵ	dynamic eddy viscosity and magnitude of surface disturbances
η	Poisson's ratio
θ	similarity variable and angle to horizontal
μ	dynamic viscosity
ν	kinematic viscosity
ρ	density
ρd	density of diaphragm
σ	standard deviation and surface tension
τ	shear stress
Φ	angle of nozzle convergence
ω	vorticity

Subscript

a	pertaining to air
i	denotes pool impact and submerged outlet conditions
o	denotes outlet section
r	restricted jet conditions
u	unrestricted jet conditions
w	pertaining to water

Superscript

–	mean component of quantity
~	denotes proportionality and fluctuating components
'	R.M.S. of fluctuating component

CHAPTER 1

INTRODUCTION TO IMPINGING JET SPILLWAYS

CONTENTS

CHAPTER 1

1.1 GENERAL INTRODUCTION.

Impact of a plunging liquid jet with a liquid surface has numerous applications including, use as an energy dissipator, enhanced mixing in some gas–liquid reactors and assistance in fermentation, waste treatment and purification processes by promoting oxygenation. This dissertation will address the plunging jet system as a form of energy dissipator.

During the last twenty to thirty years an increasing number of high head dams have been constructed around the world. The spillways for such dams have had to carry higher velocities, because of higher heads, and have also been subjected to higher specific discharge rates for economic reasons. Correspondingly, stilling basins have been designed to dissipate much larger magnitudes of incoming energy. Typical examples of the use of impinging jets to enhance energy dissipation and promote air entrainment at high head dams, are shown in Figs. 1.1 and 1.2 (Vol.II) for Morrow Point Dam and Crystal Dam respectively. Both dams are in Colorado, U.S.A., and come under the control of the United States Bureau of Reclamation. In the case of Morrow Point Dam, spillway jets pass under sluice gates high up in the dam structure and plunge through the atmosphere, with almost vertical entry into the plunge pool. The jet droplength is of the order of 110m. The jets diffuse in the concrete–lined plunge pool, producing a great deal of turbulence from the incoming kinetic energy, and fully dissipates the remaining flow through impact with the pool base. Pressure fluctuations occur on the pool base and require to be investigated in case of potential vibration damage. In model tests, mean impact pressures of roughly one–third of the overall head of 110m were measured. Flow in the stilling basin returns to the river course over the plunge pool end weir. It can be seen from Fig. 1.1 that the entire process is accompanied by a great deal of spray and aeration.

At Crystal Dam, Fig. 1.2, on the other hand, the spillway flow is in the form of a free–falling rectangular nappe, produced at the overflow crest, which plunges into a pre–excavated pool. Another alternative is to allow the spillway

jets to erode the bed rock in the jet impact zone and hence form a natural scour hole. An example of this type of dissipator is shown in Fig. 1.3 for Kariba Dam (Africa).

1.2 DEFINITION OF PROBLEMS RELATING TO PLUNGING JET ENERGY DISSIPATORS.

Whichever solution is adopted, the free-falling impinging jet spillway and plunge pool has the advantage over more conventional spillway designs and energy dissipators for high head dam structures, in that a much simpler and more economic method is provided. Simple in the sense that basically a man-made waterfall is produced and economic in that it will dispense with a flow transport structure from dam crest to stilling basin. However, with dispersion, and occasionally interaction of the spillway jets in space, plunge pool air entrainment and further diffusion in the plunge pool, a highly complex flow phenomona is apparent which is not yet amenable to a purely theoretical analysis. Furthermore, and more importantly, difficulties have arisen during operation of this form of dissipator.

Associated with the vast amounts of turbulence generated within the plunge pool during spillway jet impingement are large pressure fluctuations which act on the floor and walls of the stilling basin. In some instances this can produce vibration of the structure, often due to coincidence of the plunge pool natural structural frequency with that of the applied loading. Of more concern, in terms of damage, is penetration of the peak fluctuating pressures to the underside of the pool base slabs, through cracks or joints, or into fissures in the bed rock. Large differential upward forces can then be applied which are significantly greater than the downward force from the weight of rock or concrete and the hydrostatic pressure from the water in the plunge pool. The result is that plunge pool base slabs may be uplifted in a lined pool or severe erosion can occur relatively quickly in a natural scour hole due to this rapidly fluctuating upward force.

This action is evidenced in the damage sustained by some prototype structures. At Granget Dam (U.S.A.), for example, blocks of concrete and debris weighing more than 10 tons was moved out of the lined basin. The scouring

potential of rock from plunging jets can be equally spectacular. At Kariba Dam (Fig. 1.3) the bed rock downstream from the dam has eroded to a depth over two– thirds the height of the dam despite the cushioning effect of 20m of water over the impact zone. The scour depth has not yet reached equilibrium and has proved extremely unpredictable. Obviously the integrity of the dam foundations have been called into question due to this excessive scour. Damage caused by fluctuating pressures and forces has also been sustained by some hydraulic jump stilling basins. Turbulence in the stilling basin at Malpaso Dam in Mexico, for example, resulted in displacement and transport of floor slabs. Remedial work consisted of replacing almost 50% of the basin floor.

These problems have occured as current spillway and stilling basin design procedures often fail to include pressure fluctuations in the structural design, due in part to the lack of information concerning the pressure fluctuations, and also to lack of an accepted design procedure. For lined pools in particular, the design engineer is faced with the problem of determining the depth of the plunge pool that should be supplied for a particular spillway configuration to avoid generation of excessively large pressures and, once selected, to ascertain what actual pressures will be generated when the plunge pool of a certain depth is provided.

1.3 PROGRAMME OF RESEARCH.

Following a visit by Dr. Ervine to the United States Bureau of Reclamation (Denver) in 1985, the impetus was gained to tackle some of the problems inherent in the operation of this particular form of energy dissipator. The questions that had so far been unanswered regarding impinging jet spillways, centred on the jet behaviour in the atmosphere, the jet behaviour in the plunge pool, as well as the effect of plunge pool depth, entrained air and turbulence on the pressure fluctuation level. In particular the following were the main points of interest :

(i) Can the prototype situation be simulated in a model study ?

(ii) What factors affect the jet spread as it plunges through the atmosphere ?

(iii) What happens to the inner core of the jet during the plunge through the atmosphere ?

(iv) How would maximum dispersion of the spillway jets be achieved during the plunge ?

(v) What is the effect of air entrainment on plunge pool pressures ?

(vi) How does the impinging jet spread in the plunge pool ?

(vii) What is the effect of plunge pool geometry both in terms of depth and plan area ?

(viii) What is the magnitude of mean and fluctuating pressures on the pool floor for various plunge pool depths ?

(ix) How do pressures in the plunge pool in the model relate to those in the prototype ?

It was decided to undertake, first, an extensive literature search to determine how much research had already been done on this subject, and how far each of the topics above had been covered. Although several practical studies had been conducted on certain aspects of the behaviour of the plunging jet dissipator, it was found that there were various areas in which further work was necessary. The literature review in Chapter 2 clearly demonstrates a lack of information on a vital area of interest : the magnitude, frequency and distribution of turbulence induced pressure fluctuations at the plunge pool floor.

Subsequently, an experimental programme was devised at the University of Glasgow to gain further information on plunging jet spillways, plunge pool stilling basins and, in particular, the pressure fluctuations generated on a solid surface beneath free–falling jets.

To establish this information it was decided to take measurements of mean and fluctuating pressures on the solid floor of a model stilling basin for various impinging jet flow conditions. Measurements were also taken within the plunging jet to determine the jet condition in the atmosphere. This was facilitated by

use of a microcomputer linked to pressure transducers located on the floor of the test plunge pool as well as a turbulence probe situated within the free–falling jet. The computer was used to sample pressure fluctuations and instantaneous jet velocities, to analyse the signal statistically, to define the magnitude, frequency spectra, and distribution of the data time–history, to store the information on disc and output the results to a printer. An additional feature of this study is the software that was utilised to accomplish the above tasks. This is one of the first studies of this kind to use the microcomputer in data acquisition, control and analysis.

While the acquired data is of immediate interest in the design of plunge pools for large dams, the overall research can be considered as a fundamental study of an important flow phenomena; the plunging jet energy dissipator.

CHAPTER 2

LITERATURE REVIEW AND INTRODUCTION TO FLOW PHENOMENA

CONTENTS

2.7 PRESSURE FLUCTUATIONS AT HYDRAULIC STRUCTURES.

2.7.1 Introduction

2.7.2 Turbulence - pressure fluctuation relationships

2.8 MODELLING IMPINGING JET SPILLWAYS.

2.9 MODELLING SCOUR IN NATURAL PLUNGE POOLS.

2.10 SUMMARY.

CHAPTER 2

2.1 INTRODUCTION.

An attempt has been made in this chapter to draw together the various strands of research connected with jet behaviour, both in the atmosphere and submerged pool conditions. It is evident from Chapter 1 that the physical processes involved are complex or even chaotic. Thus a breadth of knowledge is required to promote understanding of the phenomenon, including a knowledge of turbulence, aeration, stability, pressure fluctuations and the behaviour of jet flows in general. This chapter will attempt, therefore, to act like a literature survey / review but will also attempt to introduce the reader to each of the flow phenomena mentioned.

Despite the importance of defining impact pressures on the rigid base of plunge pools below free–falling spillway jets, research into this topic has been sparse. Previous studies have tended to concentrate on the scouring capacity of impinging spillway jets on erodible material, which does have some relevance to the above situation but tends to concentrate more on rock and soil behaviour. Work has also been carried out on jet behaviour in the atmosphere, whilst separate studies have been undertaken into submerged jet discharge into fluid below the water surface. Both of these areas give indications of the physical processes occuring at free overfall spillway dams, but they cannot be treated separately from each other in this case, as the atmospheric jet has a great influence on the dissipation of energy within the plunge pool.

Various studies have considered the unsteady dynamic forces due to turbulence induced pressure fluctuations produced at energy dissipators. This work is of great interest and will be reviewed in detail as it gives an indication of the magnitudes of pressure fluctuations which may be encountered, and allows empirical relations between the turbulent flow field which generates the pressure fluctuations and the fluctuations themselves.

The purpose of this chapter, therefore, is to begin with the fundamentals, to introduce the reader to basic concepts of turbulence and jet behaviour, and as

the chapter proceeds to introduce more and more of how the fundamentals might be applied to real situations involving impinging jet spillways and scour in plunge pools.

In a general sense the chapter moves from the basics to the applications, from idealised situations to real situations, from theory to empiricism, hopefully building up in complexity to give some insights into the physical behaviour involved.

2.2 A BRIEF NOTE ON TURBULENCE.

2.2.1 Basic background

At the most basic level, the physical behaviour of a jet plunging through the atmosphere, diffusing in the plunge pool, generating coherent and random turbulent structures and producing pressure fluctuations on the plunge pool floor is largely governed by fluid turbulence.

Turbulence is classified by the random chaotic motion of fluid particles which exists when disturbances in the flow are not completely damped by viscosity. Turbulence is characterised by large fluctuations in velocity, large variation in eddy length and being random in direction. Turbulence can also be characterised to some extent by the Reynolds Number (Re) of the flow. This is a measure of the ratio of disturbing forces in the flow to viscous damping. At low Reynolds Number, disturbances in general cannot extract enough energy from the flow to maintain themselves and the flow is said to be laminar. When laminar flow exists in a system the fluid flows in smooth layers called laminae. Any disturbances which appear are damped out by viscosity. The change from laminar to turbulent flow is at Re = 2000. Turbulent flow, on the other hand, usually exists at a Reynolds Number greater than 2000. In this case eddies and vortices mix the fluid by moving particles tortuously about the system.

A feature of well–developed turbulence is the hierarchy of scales, known as eddy length scales, with a transfer of kinetic energy from the largest to the smallest. The scale of the largest eddy motion may occupy the full depth of an

open channel flow or half the diameter of a pipe flow. The scale of the smallest eddy motions, known as the Kolmogoroff micro scale, may involve tiny distances a fraction of a millimetre in diameter. At this end of the eddy length scale spectrum, turbulent energy is transferred to heat. An example of the variation of turbulent energy in each length scale is shown in Fig. 2.1(a) with energy transferred down the length scales, dissipation by viscosity and finally transfer into heat. The large variation in turbulent eddy lengths prompted Prandtl [1] to devise a characteristic eddy length ℓ, which is akin to the mean free distance travelled by a lump of fluid before being embedded in an adjacent lump of fluid. In engineering type flows, the eddy length is considered to vary in size linearly from a solid boundary, Fig. 2.1(b), although this is not physically the case.

The source of the energy varies from flow to flow. In the case of jet flow it is the initial kinetic energy of the fluid. Whatever the source, the energy extraction can be ascribed to an interaction between the mean flow and large, fairly well-ordered elements of the turbulence. The smallest motions of the turbulence, with the largest shearing stresses, are responsible for the dissipation of turbulence energy and energy transfers within the turbulent flow are conceived to be a cascade of energy from the largest, energy-extracting scales of motion to the smallest, dissipating scales.

Another feature of turbulent flow is velocity fluctuations. The passage of successive turbulent eddies past a point in the flow will produce velocity fluctuations, in a given direction, as sketched in Fig. 2.2(a). The velocity at a given point will vary randomly with time. Reynolds [2] in 1894 inaugurated a statistical approach to analyse the random nature of the turbulent motions. This assumes that the flow can be divided into temporal mean and turbulent parts, thus the velocity component in the mean flow or x direction is written :

$$U = \overline{U} + \underset{\sim}{U} \qquad (2.1)$$

where $\underset{\sim}{U}$ = turbulent velocity fluctuation part.

The distribution of velocity fluctuation magnitudes has been found experimentally to follow the Gaussian or normal error curve closely. This is shown in Fig. 2.2(b). Since the standard deviation of such a distribution

represents a suitable statistical measure, it is sometimes used in the definition of turbulence intensity. The root–mean–square (RMS) value of the turbulent velocity fluctuations (U') is given by :

$$U' = \sqrt{(\overline{\underset{\sim}{U}}^2)} \qquad (2.2)$$

The ratio of this value to the mean flow velocity (i.e. the relative intensity), is termed the intensity (Tu) :

$$Tu = U'/\overline{U} \qquad (2.3)$$

The fluctuating components are considered to vary differently in all three orthogonal directions as shown in Fig. 2.2(c). The RMS value is U' in the (x) direction, V' in the lateral (y) direction and W' in the vertical (z) direction.

When the turbulence is not isotropic, the mean value of all three components may be used, if they have been measured, as more appropriate to define the turbulence intensity.

Thus the three dimensional relative turbulence intensity becomes,

$$Tu = 1/\overline{U}\ \sqrt{[(U'^2 + V'^2 + W'^2)/3]} \qquad (2.4)$$

Turbulence in a fluid might be described by the concept of shear stress, which is the interchange of molecules and the associated transfer of momentum between two adjacent layers. In turbulent flow, there is continuous interchange of not only the molecules over small distances but particles over large distances. These particles carry momentum from one layer of flow to the other. Therefore, as a result, the interchange action of molecules can be described as a shear stress rather in the same manner as the viscous shear is related to the velocity gradient, $\tau = \mu du/dy$. Boussinesq [3] described the turbulent shear stress in the same way $\tau = \epsilon du/dy$, where ϵ is a kind of viscosity for particle exchange and transfer. The total internal shear stress (τ) could consequently be defined as :

$$\tau = (\mu + \epsilon)\ \partial\overline{U}/\partial y \qquad (2.5)$$

where μ = molecular viscosity

ϵ = dynamic eddy viscosity. = $\rho \nu_t$

$\overline{U}$ = average velocity in longitudinal (x) direction

The eddy viscosity is almost independent of fluid properties but depends on the degree of turbulence and location of the point considered. Equation (2.5) was suggested by Boussinesq [3] as early as 1877. In fully turbulent conditions, $\epsilon/\mu >> 1$ normally, and thus the direct contribution of molecular viscosity is negligible. The introduction of eddy viscosity or turbulent viscosity provides a possible way toward a turbulence model but it does not itself constitute a model for there remains the task of expressing the turbulent viscosity in terms of known or calculable quantities.

2.2.2 Simple turbulence models

The most fundamental expression of the conservation of momentum in fluid flow is given by the Navier–Stokes equations. Derivation of these equations is given in many standard fluid mechanics texts. Reynolds modified the Navier–Stokes equations by substituting a mean $\overline{U}$ and RMS fluctuating velocity U', in place of the instantaneous velocity, as already described in Equations (2.1) and (2.2).

The result is given below for the three–dimensional coordinate system. In the x–direction we obtain,

$$\frac{\partial \bar{u}}{\partial t} + \overline{U}\frac{\partial \bar{u}}{\partial x} + \overline{V}\frac{\partial \bar{u}}{\partial y} + \overline{W}\frac{\partial \bar{u}}{\partial z} = -\frac{1}{\rho}\frac{\partial}{\partial x}(\overline{P} + \gamma h)$$

$$+ \frac{\mu}{\rho}\nabla^2 u - \left[\frac{\partial u'^2}{\partial x} + \frac{\partial u'v'}{\partial y} + \frac{\partial u'w'}{\partial z}\right] \qquad (2.6)$$

The main interest in Equation (2.6) is the final term in brackets representing the turbulent shear stress. This latter term appears as an additional stress set and is termed the Reynolds stresses. The Reynolds stresses, for the simplified two dimensional case, can be written in tensor form, thus :

$$\tau_{ij} = - \begin{bmatrix} \rho u'^2 & \rho u'v' \\ \rho u'v' & \rho v'^2 \end{bmatrix} \qquad (2.7)$$

The cross product term $-\rho u'v'$ is recognised as the turbulent shear stress, or merely the shear stress since, except in localised regions, the laminar–viscous shear stress in turbulent flows is negligible.

It can be noted that whilst in viscous–laminar motions, it is most difficult to find solution for the Navier–Stokes equations, the additional terms introduced in the Reynolds equations mean that they are quite intractible. Statistical theory of turbulence, although yielding insight into the nature of turbulent motion, is unable to give even mean flow solutions. The solution has therefore been to resort entirely to empiricism or develop some simple or workable model of turbulence which does allow mean–flow solutions. Several models have been introduced such as Boussinesq's eddy viscosity concept, $\tau = \epsilon\ \partial u/\partial y$, Prandtl's [1] mixing length model and momentum transfer, Taylor's [4] vorticity transfer, and Von Karman's [5] similarity hypothesis. One feature of the simplified turbulence model approach is that, at best, only the form of the mean–flow solution is obtained and one or more coefficients always remain unknown, to be obtained empirically via comparison with experimental results.

Mixing length models

Perhaps the most usable phenomenological model for turbulence is the momentum–transfer, mixing–length model of L. Prandtl. Here it is assumed that eddies move about in a fluid in the same way that molecules move around in a gas. Consider a flow in the x–direction with a lateral or vertical velocity gradient $\bar{U}$ = function (y), as sketched in Fig. 2.3. A fluid element or lump (considered for the moment to retain its entity without diffusing) has a mean velocity $\bar{U}_1$ at point 1. At some instant a lateral turbulence fluctuation $\underset{\sim}{v}$ appears to transport this lump laterally some distance ℓ (the mixing length) before it loses its identity and acquires that of the fluid at point 2. Considering the new point, where the lump is to stop and mingle with the ambient fluid, the mean velocity there is $\bar{U}_2 = \bar{U}_1 + \ell\,\partial\bar{u}/\partial y$. The lump, however, arrives at point 2 with the instantaneous x–component velocity that it started with, i.e. $\bar{U}_1$. The velocity difference between the two points is then considered proportional to the

longitudinal turbulence fluctuation given by,

$$\underset{\sim}{U} = -\ell \, \partial\bar{U}/\partial y \qquad (2.8)$$

Although the real fluctuation process is continuous, this model is still usable. It leads to an understanding of the process by which turbulence in a mean velocity gradient flow produces shear stresses, via lateral momentum transfer.

The Reynolds stress indicates the relation between shear stress and the turbulence fluctuations :

$$\tau yx = -\rho \, u'v' \qquad (2.9a)$$

Assuming $\underset{\sim}{V}$ to be proportional to $\underset{\sim}{U}$ and absorbing the proportionality factor into ℓ, the shear stress may be written :

$$\tau yx = \rho\ell^2 \, (\partial\bar{u}/\partial y)^2 = \rho l^2 \, |\partial\bar{u}/\partial y| \, (\partial\bar{u}/\partial y) \qquad (2.9b)$$

All that is now required to obtain the mean-velocity solution $\bar{U}$ = function (y) is the variation in shear stress and mixing length.

T. Von Karman in 1930 introduced his so-called "Similarity" hypothesis as :

$$\ell = K \, [\, (\partial\bar{u}/\partial y) \, / \, (\partial^2\bar{u}/\partial y^2) \,] \qquad (2.10)$$

The analysis implied that ℓ was the ratio of the first to the second spatial derivatives of mean velocity, where K was thought to be a universal constant of 0.40. The ingenuity of the proposal was the removal of the need to prescribe the mixing length profile.

However, later experimental results show variations of K, as already shown in Fig. 2.1(b). The reason that this formula is not in agreement with measurements, except in the vicinity of a wall, may presumably be explained by the fact that the length scale is not determined solely by local properties of the mean flow, but is influenced by the properties at other locations in the vicinity. The shortcomings of the Von Karman formula become apparent when a turbulent

jet and its mixing layer is considered. Jet velocity profiles have inflection points, where $\partial^2\bar{u}/\partial y^2 = 0$, at the position of maximum shear stress. Von Karman's relationship suggests an infinite mixing length at that point, and therefore cannot be used to compute a finite shear stress.

One of the main defects of the mixing length hypothesis itself lies in its simplicity. The mixing length, which can now be computed directly from measured quantities, is found to be a complicated function of the coordinates, thus, the principal advantage of the mixing length theories, namely the introduction of a "simple" length, is not correct. It has also been found that the main results of these theories can be obtained by dimensional reasoning, without the introduction of a hypothesis on the mechanism of turbulence.

Other eddy viscosity models

In some respects the mixing length model described above is a sub-branch of eddy viscosity models, which in general assume an analogy between molecular motion and turbulent motion. The Boussinesq concept relates the turbulent shear to the eddy viscosity in the form :

$$\tau = \rho \nu t \partial u/\partial y \qquad (2.11)$$

where eddy viscosity has units m^2/s and hence can be considered to be composed of a length scale times a turbulent velocity scale

$$\nu t \alpha\ U' \ell' \qquad (2.12)$$

For open channel flow, for instance, where the velocity U' scales on the shear velocity $U_* = \sqrt{(\tau_0/\rho)}$ and eddy length scales on the depth of flow, then, when bed friction is dominant,

$$\nu t = kU_* h \qquad (2.13)$$

where $k = 0.16$ for river flows.

For shear layers the velocity scale may be chosen as Umax − Umin over a shear layer cross section and ℓ' may scale on the shear layer width δ, then a

model may be used in the form

$$\upsilon t = k\ \delta\ |Umax - Umin| \qquad (2.14)$$

where $k \simeq 0.01$ for a plane shear layer.

Another approach consists of a more complex model where the eddy viscosity is related to the kinetic turbulent energy (k) of the flow in the form :

$$\upsilon_t \propto \ell' \sqrt{(k)} \qquad (2.15)$$

This requires an additional transport equation for υ_t (derived from the Navier–Stokes equations), involving higher order covariances and requiring more empirical coefficients.

Both kinetic energy and shear stress models require a substantial computational effort with large modern computers. Individual models have usually been verified with a limited type of experiment only (mostly boundary layer types). There is no model for which failure cannot be shown under certain circumstances, as discussed for the turbulent jet previously. Thus, the models fall considerably short of a complete description of turbulent phenomena.

Some features of fully turbulent motion are slightly more helpful when it comes to analysis. Flows where the mean motion and larger scales of turbulence are independent of viscosity are termed self–preserving. Viscosity has a passive function, as in turbulent dissipation ; it is dominant in the smallest scales, but plays no direct part in specifying the overall pattern and activity. Self–preservation implies that a length and velocity scale of the mean motion can be used to reduce velocity profiles to a common form. In effect, the characteristics of the mean flow pattern should be dynamically similar under all conditions. Such a situation is the starting point for dimensional analysis and allied similarity techniques, and these methods reveal some simple features of self–similar flow.

Another important simplifying feature of many turbulent (and laminar) flows is the thinness of the highly sheared region. For moderate and larger Reynolds Numbers, the angle of jet spread is small due to the relative slowness of lateral

diffusion in comparison with the basic convection of the mean flow. Many features of thin flows can be described with sufficient accuracy using simplified equations of motion, the simplification achieved by neglecting terms that are relatively small by virtue of the nearly parallel mean flow. When the flow is both thin and self–similar, the process of predicting its main features is much simpler. Work on defining the mean jet flow characteristics, through theory and experiments, will now be covered.

2.3 SUBMERGED JET BEHAVIOUR IN AN INFINITE MEDIUM.

2.3.1 Introduction

The behaviour of submerged jets in a stagnant environment has been investigated thoroughly both in a theoretical and experimental manner. Most of the work has considered jet diffusion into an infinite medium with similar properties, although many experiments have also been carried out to determine the effects of a solid boundary on the process. As the jets of interest in this thesis initially plunge through a gaseous atmosphere, additional factors such as air entrainment and bubble transport in the pool along with non–uniform impact conditions will be considered in later sections, to see how this alters the classical diffusion pattern.

The following section will consider mainly submerged diffusion of a circular jet, as the expressions developed are slightly simpler than the corresponding plane jet formulations and also as a circular jet was used in this work. A schematic representation of the jet diffusion pattern is shown in Fig. 2.4 as proposed by Albertson et al. [6]. As the jet, with uniform velocity profile, is discharged into the initially quiescent fluid there will be a pronounced discontinuity between inflow and the ambient surroundings. A shear layer is set–up and becomes turbulent very close to the outlet, with the kinetic energy of the incoming flow being steadily converted into kinetic energy of turbulence. Lateral mixing between the jet and surroundings will occur into both the uniform velocity jet and the ambient fluid. This lateral mixing process causes retardation of the jet while, in a balanced manner, fluid from the surrounding region will be gradually accelerated or entrained into the diffusing jet. Continuity and turbulent shear

considerations dictate the expansion rate of the jet causing the increase in flow rate and velocity reduction. When the mixing regions have penetrated to the jet centre line (Fig. 2.4) the flow may be considered to be fully established. At this point the constant velocity or potential core has completely diminished. From this point onwards the entire central portion of the jet has become turbulent and the diffusion process continues without essential change in character. Further entrainment of the surrounding fluid by the expanding shear layer is balanced by reduction in velocity of the entire central region. Albertson [6] reported that this velocity will eventually read a negligible magnitude, but not until a very great distance from the efflux section.

The diffusion pattern in an infinite medium therefore will consist of two distinct regions. Region 1 is a zone of flow establishment which extends from the nozzle exit to the apex of the potential core. The so–called potential core is the central portion of the flow in which the velocity remains constant and equal to the velocity at the nozzle exit. Region 2 is a zone of established flow which is beyond the apex of the potential core in the jet flow direction. It is characterised by a dissipation of the centre line velocity and by spreading of the jet in the transverse direction. The situation is simplified by considering the boundary between the zone of establishment and established flow to be sharply defined (indicated by the vertical broken line in Fig. 2.4), if the zone of transition which necessarily exists between two distinct flow regions is neglected.

Because of the statistical nature of the mixing process it is virtually impossible to locate precisely the point at which the eddies from opposite side of the jet meet in the inner core region. So the boundary of the diffusion region, like the border between the two zones, must be accepted as a convenient nominal designation. The nominal limits of the diffusion region are therefore also shown as broken lines.

Other authors have slightly different views on the classical diffusion pattern described above. Shih I Pai [7] states that laminar flow and turbulent flow exist in tandem. In general, in the initial part of the diffusing jet the flow is laminar, followed by a transition region, and finally the flow becomes turbulent. Pai pointed out that the flow in the transition region is still not well understood but consists essentially of laminar flow with instabilities which may either be damped out or grow in magnitude as turbulence.

Davies [8] suggests that in the submerged jet, the flow is laminar only near the exit of the nozzle. Davies argued that a free submerged jet is usually considered to have four flow regions :

(1) A region of flow establishment. Flow in this region has a core velocity about the same as the discharge velocity at the exit and the length of this region is about 6.4 D, where D is the nozzle diameter.
(2) A transition region between 6.4 D to 8 D.
(3) A region of established flow, extending out to about 100 D.
(4) A region where the centre line velocity decreases steeply to zero (terminal region). These regions are sketched in Fig. 2.5 with shear layer boundaries represented as straight lines.

Davies also pointed out that the jet spread angle is best defined as a half–angle of the cone formed by the locus of the points where the velocity is half that of the jet centre line, as sketched in Fig. 2.5.

A.J. Reynolds [9] explanation of the jet flow pattern consisted of two stages in the turbulent development. In the first stage, the cylindrical shear layer between jet and ambient fluid becomes unstable. The initial well–organised vortices disintegrate into turbulence which spreads both inwards and outwards, and finally absorbs completely the laminar (or potential) core of the jet.

In the second stage of development, the turbulence can spread only at the outer shear layer boundary, and the jet adopts a pattern of growth consistent with the unchanging interaction between the internal turbulence and the quiescent outer fluid. Reynolds [9] also noted that the point of transition moves closer to the efflux section (nozzle exit) as the jet Reynolds Number increases indicating more rapid breakdown of ordered vortices and more rapid turbulent diffusion. Apart from these small differences in interpretation, the general aspects of the jet diffusion pattern are well understood.

2.3.2 Theoretical treatment of an axisymmetric jet diffusing in an infinite medium

Experimentation on submerged jet diffusion has usually concentrated on the properties of air efflux into a stagnant environment. However, results produced by Forstall and Gaylord [10] have shown that the turbulent diffusion of velocity and material in an axially symmetric water jet is like that of an air jet of constant density, and hence constants obtained by others for experiments in air can be applied to water.

The earliest experimental results on circular jets appear to be those of Trupel [11]. The mean velocity distributions at various cross-sections in the region of established flow are reproduced in Fig. 2.6 and a definition sketch of the circular turbulent jet is given in Fig. 2.7. The coordinate system for the later theoretical treatment and the velocity and length scale is given in this figure.

It can be found that the velocity distribution at different sections fall on one common curve, if the ordinates are made dimensionless by division with the appropriate velocity and length scales. At each section, if the velocity is divided by Um at that section and the radial distance is converted to a dimensionless form by division with b, where b is the value of r at U = Um/2, then the velocity profiles can be shown to be similar, Fig. 2.8. This observation has been confirmed by the experiments of Corrsin [12], Hinze and Zijnen [13], Albertson [6] and others. In order to use these similarity profiles for predicting the mean velocity field in any particular problem, prediction must be made of the manner in which the velocity (Um) and length (b) scale vary. This can be carried out by consideration of the fundamental equations of motion.

It is appropriate at this stage to investigate the theoretical formulation of an axisymmetric submerged jet entering a large volume of fluid.

Applying boundary-layer approximations to the Reynolds equations in the cylindrical co-ordinate system (r,Φ,z), the following is appropriate for circular jets without swirl, $V\Phi = 0$ and all terms containing $V\Phi$ and its derivatives disappear. Furthermore, axial velocities Vz are considered much greater than radial velocities, $Vz >> Vr$, whilst gradients in the radial direction are much larger

than those in the axial direction. Viscous stresses are assumed to be much smaller than the corresponding turbulent shear stresses, provided the nozzle Reynolds Number is sufficiently high. Also, turbulent normal stresses are approximately equal in the radial and peripheral directions (Wygnanski and Fiedler [14]).

With these simplifications, the equations of motion in the radial and axial directions for steady axisymmetric and incompressible flow become :

$$1/\rho \; \partial\bar{P}/\partial r = - \partial/\partial r \; Vr'^2 \tag{2.16}$$

$$\bar{V}r.\partial\bar{V}z/\partial r + \bar{V}z \; \partial\bar{V}z/\partial z = - 1/\rho.\partial\bar{P}/\partial z - (\partial/\partial r.Vr'Vz' + (Vr'Vz')/r + \partial/\partial z.Vz'^2) \tag{2.17}$$

The continuity equation is written as :

$$\partial/\partial r.r \; \bar{V}r + \partial/\partial z.r\bar{V}z = 0 \tag{2.18}$$

where $\bar{V}r,\bar{V}z$ = time mean velocities in radial and axial direction.

Vr',Vz' = fluctuating velocities in radial and axial direction.

Integrating (2.16), substituting in (2.17) and simplifying; Equation (2.17) becomes:

$$\bar{V}r.\partial\bar{V}z/\partial r + \bar{V}z.\partial\bar{V}z/\partial z = -1/\rho.\partial\bar{P}/\partial z - 1/r.\partial/\partial r \; (rVr'Vz') \tag{2.19}$$

Where $\bar{P}$ now is the mean pressure outside the jet. For convenience, and to proceed with the formulation in a similar form to Equation (2.6) stated previously, the axial direction will be called X and the velocity components in the axial and radial directions will be $\bar{U}$ and $\bar{V}$ respectively. Letting $-\rho Vr'Vz' = \tau$, the remaining equations become :

$$\bar{U}.\partial\bar{U}/\partial x + \bar{V}.\partial\bar{U}/\partial r = - 1/\rho.\partial\bar{P}/\partial x + 1/\rho r.\partial r\tau/\partial r \tag{2.20}$$

$$\partial/\partial x.r\bar{u} + \partial/\partial r. \; r\bar{v} = 0 \tag{2.21}$$

For a more complete derivation of these equations see Schlichting [15].

According to Forthmann [16] the pressure in a horizontal diffusing jet is

invariable and equal to that of the ambient surroundings. Therefore, the pressure gradient in the axial direction is approximately zero. As a result Equation (2.20) further simplifies to :

$$\bar{U}.\partial\bar{U}/\partial x + \bar{V}.\partial\bar{U}/\partial r = 1/\rho.1/r.\partial r\ \tau/\partial r \qquad (2.22)$$

Multiplying Equation (2.22) by ρr and integrating with respect to r from r = 0 to r = ∞, the equation takes the form :

$$\int_0^\infty \rho\ \bar{U}r\ \partial\bar{U}/\partial x.dr + \int_0^\infty \rho\ \bar{V}r\ \partial\bar{U}/\partial r.dr = \int_0^\infty \partial r\tau/\partial r.dr \qquad (2.23)$$

Considering each of the different terms in the above equation:

$$\int_0^\infty \rho.\bar{U}r.\partial\bar{U}/\partial x.dr = 1/4\pi.d/dx.\ \int_0^\infty 2\pi.r.\partial r.\rho.\bar{U}^2 \qquad (2.24)$$

(by Liebnitz rule)

$$\int_0^\infty \rho\ \bar{V}r\ \partial\bar{U}/\partial r.dr = \Big|\ \rho\bar{U}\bar{V}r\ \Big|_0^\infty - \int_0^\infty \rho.\bar{U}.\partial r\bar{V}/\partial r.dr =$$

$$\int_0^\infty \rho\bar{U}\ \partial r\bar{U}/\partial r.dr = 1/4\pi\ d/dx \int_0^\infty 2\pi r.dr.\rho.\bar{U}^2 \qquad (2.25)$$

$$\int_0^\infty \partial r\tau/\partial r.dr = \Big|\ r\tau\ \Big|_0^\infty = r\tau(\infty) - r\tau(0) = 0 \qquad (2.26)$$

In Equation (2.26), $r\tau(0) = 0$ from considerations of symmetry and it is reasonable to assume $r\tau(\infty)$ is zero. Hence Equation (2.23) becomes :

$$d/dx \int_0^\infty 2\pi r\ dr\ \rho\ \bar{U}^2 = 0 \qquad (2.27)$$

Equation (2.27) states that the rate of change of the axial momentum flux in the axial direction is zero or that the momentum flux in the axial direction is conserved.

Without resort to this elegant solution, it can be seen, for jet diffusion into a stagnant environment of the same fluid where the pressure distribution is hydrostatic, that the sole force producing the deceleration of the jet and the acceleration of the surrounding fluid is the tangential shear within the mixing shear layer region. As this is a wholly internal process, no external force exists and therefore the momentum flux must be a constant for all normal sections of a given flow pattern. Using Equation (2.27), a relationship can be developed for the jet diffusion velocity and length scales as follows. Let :

$$\bar{U}/Um = f\ (r/b) = f\ (\eta) \tag{2.28}$$

$$Um \propto X^{P} \tag{2.29}$$

$$\text{and } b \propto X^{q} \tag{2.30}$$

With these substitutions, (2.27) becomes :

$$d/dx\ \rho Um^2 b^2 \int_0^{\infty} 2\pi\eta\ f^2 d\eta = 0 \tag{2.31}$$

Since the value of the definite integral in (2.31) is a constant :

$$Um^2\ b^2 \propto X^0 \tag{2.32}$$

$$\text{or :} \quad 2p + 2q = 0 \tag{2.33}$$

$$\text{or :} \quad p + q = 0 \tag{2.34}$$

To evaluate these exponents one further equation is required and this can be developed in a number of ways. These methods consist of either a similarity analysis of the equations of motion, the integral energy equation or thirdly using the entrainment hypothesis proposed by Morton et al. [17]. The simplest of the methods, in terms of mathematics, will be detailed below, namely the entrainment hypothesis.

If Qi is the flow rate from the nozzle and Q is the flow rate in the jet at any cross–section, it is known that the ratio Q/Qi is greater than unity and

increases with X. This means that the jet entrains the surrounding fluid. The following could then be written.

$$Q = \int_0^\infty 2\pi r dru \tag{2.35}$$

$$dQ/dx = d/dx \int_0^\infty 2\pi r dru = 2\pi \bar{b} Ve \tag{2.36}$$

where $\bar{b}$ is the nominal outer boundary of the jet where U is very small (i.e. close to zero) and Ve is the entrainment velocity. From dimensional considerations the following could be stated :

$$Ve \propto Um \quad or \quad Ve = \alpha_e Um \tag{2.37}$$

where α_e is the entrainment coefficient. Since $\bar{b}$ is another length scale, it could by assumed :

$$\bar{b} \propto x^q \tag{2.38}$$

Hence, (2.36) becomes :

$$d/dx \ (Um\ b^2 \int_0^\infty 2\pi\eta f d\eta) = 2\pi \bar{b} Ve \tag{2.39}$$

$$or : \quad d/dx \ (Um\ b^2) \ / \ \bar{b} V_e \propto X^0 \tag{2.40}$$

$$i.e. \quad p + 2q - 1 - q - p = 0 \tag{2.41}$$

Therefore, $q = 1$ and from (2.34) $p = -1$. It can then be shown that the centre line jet velocity Um and the shear layer width b will vary as follows :

$$Um \propto 1/x \quad and \quad b \propto x \tag{2.42}$$

Useful expressions for the velocity and length scales can be obtained using the principles of dimensional analysis. As the momentum flux at the submerged nozzle (Mi) is an important parameter of the jet, it can be written for the established flow region:

$$Um = f(Mi, \rho, x) \qquad (2.43)$$

Molecular viscosity is neglected as the Reynolds Number is assumed to be large. Using the Buckingham π— theorem, the following expression for the velocity scale can be obtained for a circular jet;

$$Um/Ui = 1/2C_1 . Di/x \qquad (2.44)$$

where Di = Initial jet diameter at inflow, Ui is the mean initial velocity and x the axial direction. Similarly for the length scale :

$$b/x = C_2 \qquad (2.45)$$

In other words, the angle of jet diffusion in the zone of established flow is a constant. Furthermore, the increase in flow rate due to radial entrainment can be shown as :

$$Q/Qi = C_3 \, x/Di \qquad (2.46)$$

where Qi is the flow rate from the submerged nozzle and the constants C_1, C_2 and C_3 are determined from experimental measurements.

A similar process was carried out by Albertson [6]. In this case, however, a velocity distribution to characterise every section in the diffusion region was actually selected to fit experimental data. The experimental results were found to follow the general trend of the Gaussian normal probability function, which was defined by the centre line velocity (Um) and the standard or root— mean deviation (σ), shown in Fig. 2.9. The analysis differed slightly from the dimensional considerations mentioned above, as the length scale was taken as the standard deviation of the velocity distribution rather than the previously defined length scale (b). Under the condition of dynamic similarity, the relationship for the variation of σ with X was given by :

$$\sigma/X = C_4 \qquad (2.47)$$

Considering the constancy of momentum, an expression for the velocity scale was determined in a form similar to Equation (2.44) as follows :

$$Um/Ui = 1/2C_4 . Di/X \qquad (2.48)$$

At the end of the potential core Um = Ui, therefore, the distance from the nozzle to the apex of the potential core (Xc) could be expressed as :

$$Xc/Di = 1/2C_4 = K_1 \qquad (2.49)$$

Having explored the Reynolds equations for two-dimensional axisymmetric jet flow and the resultant simplifications, as well as investigating suitable velocity and length scales for diffusing jets, we are now in a position to review the main early theoretical investigations. These investigations were aimed primarily at estimating the mean axial velocity distribution U(r,x) by considering the 2-D equation typified by

$$\bar{u}\, \partial\bar{u}/\partial x + \bar{v}\, \partial\bar{u}/\partial r = 1/\rho r . \partial r . \tau/\partial r \qquad \text{(Equa. 2.22)}$$

With only two equations of motion and three unknowns ($\bar{u}$,$\bar{v}$, and τ), one more equation must be produced for solution. It is therefore necessary, in obtaining the velocity distribution, to express the turbulent shear stress (τ) in terms of parameters of the main flow. The first theoretical investigation of this nature was carried out by Tollmien [18] in 1926. The turbulent shear stress was related to the mixing length by use of the Prandtl mixing length formula already discussed in Section 2.2. The mixing length itself was related to the flow by assuming its magnitude was proportional to the distance from the efflux section,

$$\ell = CX \qquad (2.50)$$

and therefore, the mixing length was assumed constant at each cross-section of the jet. Tollmien's estimate of the turbulent shear stress was therefore based on the general turbulence equation :

$$\tau = \rho\, \ell^2\, (\partial u/\partial r)^2 \qquad (2.51)$$

$$= \rho\, C^2X^2\, (\partial u/\partial r)^2 \qquad (2.52)$$

By solving the resulting equations numerically, Tollmien produced a solution which closely approximated observations of the mean flow pattern as shown in Fig.2.10.

Later studies by Goertler [19] introduced the concept of constant eddy viscosity across any section of the diffusion zone. As already discussed, the turbulent eddy viscosity scales on a product of velocity and the length scale which Goertler assumed as Um (centre line velocity) multiplied by the half shear layer width (b). The relationship between eddy viscosity and the flow parameters was given as

$$\epsilon = KUmb \tag{2.53}$$

where K is a constant. Using the earlier results for Um and b (i.e. $b = C_2X$ and letting $n = UiDi/2C_1$, then $Um = n/x$), Equation (2.53) becomes :

$$\epsilon = KnC_2 \tag{2.54}$$

As mentioned, for a circular turbulent jet with this stress model, the eddy viscosity ϵ ($= \rho\upsilon t$) is a constant. Hence the turbulent shear stress is given as :

$$\tau = \epsilon(\partial u/\partial r) = KnC_2(\partial u/\partial r) \tag{2.55}$$

The solution produced by Goertler is slightly simpler and is shown in Fig. 2.11 along with Tollmien's curve and experimental results from Reichardt [20]. It is found that near the axis of the jet, the Goertler–type curve is slightly superior to the Tollmien curve whereas, in the outer regions, the Tollmien curve agrees with the experimental observations much better than the Goertler–type curve. Clearly the assumptions of constant mixing length and constant eddy viscosity over a cross–section produce reasonable agreement with experiment, but are obviously crude assumptions.

2.3.3 Experimental observations

The following section will summarise the experimental results obtained by various researchers investigating submerged circular jet diffusion. The results were used to determine the velocity, jet width and flow variations with distance from the nozzle outlet that have been described in the previous section ; Equations (2.44–2.48).

During the solution of the mean velocity profile, Tollmien [18] had introduced a similarity variable as :

$$\theta = r/ax \tag{2.56}$$

When the ratio U/Um = 0.5 (i.e. where r = b), it was found that $\theta = 1.23$. The expression above could then be written as :

$$b = 1.23ax \tag{2.57}$$

By obtaining the coefficient a experimentally, the equation for the length scale (b) could be evaluated. The constant, a, also came into the relation for the velocity scale, derived from Tollmien's solution, as ;

$$Um/U_i = 0.48\ Di/ax \tag{2.58}$$

Similarly an expression for the velocity scale from Goertler's solution [19] including an unknown constant δ was as follows :

$$Um/Ui = \delta/3.22.(Di/X) \tag{2.59}$$

From the experiments of Trupel [11], in which the velocity distribution at the submerged nozzle was almost uniform, gave a = 0.066. Abramovich [21] found that a increases linearly with the ratio of the average to the maximum velocity at the nozzle. Further, the value of a appears to increase with the turbulence level of the jet. For a nozzle, with uniform velocity distribution and taking a = 0.066, the relation for the velocity scale from Equation (2.58) becomes :

$$Um/Ui = 7.3(X/Di)^{-1} \tag{2.60}$$

From the Goertler–type solution, taking $\delta = 18.5$, as was determined using the experimental observations of Reichardt [20], the equation for the velocity scale from Equaton (2.59) becomes ;

$$Um/Ui = 5.75(X/Di)^{-1} \tag{2.61}$$

Hinze and Zijnen [13] from their experimental observations suggested :

$$Um/Ui = 6.39/(X/Di + 0.6) \qquad (2.62)$$

The value of X is the longitudinal distance from the nozzle. The origin of the spreading jet, termed the virtual origin, is found from their work to be located 0.6 Di behind the nozzle, hence the 0.6 term in Equation (2.62). Abramovich [21], on the other hand, obtained a value of 2.2 Di for this distance. Because of the uncertainty involved in predicting the distance of the virtual origin from the nozzle, it is suggested that the virtual origin be located at the nozzle itself.

Using a = 0.066 and Equation (2.57), Tollmien's solution gives C_2 (=1.23a) in Equation (2.45) as 0.082. Abramovich suggested a value of C_2 = 0.097 to be more appropriate. Using this value and working back to the value of a = 0.079, the equation for velocity scale from Equation (2.58) then becomes :

$$Um/Ui = 6.1(X/Di)^{-1} \qquad (2.63)$$

The variation of core length with Reynolds Number was investigated by Hrycak et al. [22]. It was found that for Reynolds number > 10000, the experimental core length varied between 6.0 to about 6.7 jet diameters. Albertson [6] determined the position of the apex of the potential core by considering the centre line velocity decay in the established flow region, Fig. 2.12. The value of the constant C_4 in Equations (2.47) and (2.48) was found to be 0.081. Thus equation (2.48) takes the form :

$$Um/Ui = 6.2(X/Di)^{-1} \qquad (2.64)$$

In the flow establishment region Albertson described the velocity profile by two symmetrical halves of the selected probability curve connected with a straight line through the constant velocity core, Fig. 2.13. Comparison of the non–linear portion of Albertson's velocity profile in this region with experimental values resulted in disagreement, Fig. 2.14. This is because one and the same experimental constant had been used to cover both flow regions, which is incorrect

From Albertson's data a value of 0.0965 was found for C_4 in Equation (2.45), which is in good agreement with the data of Hinze and Zijnen

($C_2 = 0.094$) and the suggestion from Abramovich noted above. For practical purposes the relation could be given as :

$$b = 0.10\ x \tag{2.65}$$

This is exactly the same as that for a plane jet.

Regarding flow entrainment by the jet, the following result has been obtained:

$$Q/Q_i = 0.32\ X/D_i \tag{2.66}$$

If E is the kinetic energy of the jet at any section and Ei is the kinetic energy at the nozzle, the reduction in energy can be calculated from Albertson's expression:

$$E/E_i = 4.1(X/D_i)^{-1} \tag{2.67}$$

Measurements of the turbulence characteristics of the free circular jet have been made by Corrsin [12] and [23], Liepmann and Laufer [24] and more recently by Wygnanski and Fiedler [25]. The observations show that the constancy of mixing length and eddy viscosity appears to be in error. In fact, the sensitivity of the mean velocity distribution function to the type of turbulence structure is not good enough and detailed measurements of the turbulence show considerable discrepancy between assumption and fact. Details of the turbulence measurements will be given in a later section.

2.4 SUBMERGED JET BEHAVIOUR IN A CONFINED SPACE.

The discussion so far has centred on jet behaviour in a very large body of receiving fluid, which is not exactly comparable to jets impinging in plunge pools downstream of dams. In terms of space confinement on the diffusing plunge pool jet, the main confinement is in the axial direction as sketched in Fig. 2.15. The dimensions of the impinging jet are usually small compared to the plan area of the pool which means that side wall confinement is not significant.

However, the depth of the pool is often relatively shallow, for economic reasons, which implies that the recognised stages in flow development outlined in Section 2.3.1 are going to be interrupted and significantly altered as the diffusing jet suddenly impinges on the solid plunge pool base producing a transfer from velocity to pressure and the possibility of large recirculation eddies, as sketched in Fig. 2.15.

If the development of the spreading jet shear layer is impeded by a solid boundary as sketched in Fig. 2.15 then, as the flow approaches the stagnation point, the jet axial velocity decreases rapidly and the pressure increases above the ambient. At the stagnation point, the velocity is zero and the pressure is a maximum. In comparison with free jet development, the energy is not only dissipated by turbulent shear action with the surrounding fluid but also by shear at the solid boundary of the basin. For impinging jets, two stages of energy dissipation can be distinguished depending on the depth of tailwater and jet impact conditions. At shallow to moderate tailwater depths (relative to the jet impact diameter) energy transformation occurs in the form of a hydraulic jump, as sketched in Fig. 2.16. At moderate to substantial depths, energy is dissipated through turbulent mixing before impingement, analogous to a vertical drowned hydraulic jump.

In terms of design, the magnitude and distribution of the dynamic pressure developed at the solid boundary due to jet impingement is of paramount importance. Experiments have consequently been carried out to determine the mean pressures generated. At large pool depths, four distinct flow regions have been characterised and are shown in Fig. 2.17. The regions are as follows,

(i) Region 1 is the region of flow establishment
(ii) Region 2 is the region of established flow

] free jet regions

(iii) Region 3 is that region in which the jet is deflected from the axial direction, termed the deflection region. In this zone the most severe hydrodynamic actions of the flow are located.

(iv) Region 4 is known as the wall jet region, where the directed flow increases in thickness as the boundary layer builds up along the solid surface.

The disturbance created by a solid boundary on an impinging jet is

propogated upstream at a rate dependent on the sonic and fluid velocity. With increase in fluid velocity the disturbance created by the solid boundary would be less able to propogate upstream. In a theoretical study reported by Levey [26] the effect of the impingement surface was not felt by the jet as close as only 1 slot width away from the surface. An experimental study reported by Tani and Komatsu [27] confirms the theoretical result ; no surface effect on the jet was observed beyond about 2 jet diameters from the solid boundary. Consequently, a deflected jet can be considered to behave like a free jet except in the immediate vicinity of the solid boundary of deflection. For submerged jet deflection, Fig. 2.18 shows the centre line velocity decay for various values of the distance between the outlet nozzle and deflection surface. Close examination of this figure verifies the fact that the jet behaves like a free jet except within a few nozzle diameters of the impingement surface.

Mean pressures at the deflection point have been determined using the free jet principles by evaluating the arrival velocity. The arrival velocity is that velocity which would exist in the jet at the same distance from the nozzle as the stagnation point if no impingement surface were present. An alternative method has been to equate the reaction of the floor to the impinging jet momentum. Hausler [28] has used both of these methods to calculate the mean pressure distribution at the pool floor for comparison with mean pressure measurements. The mean pressure results had been obtained in an earlier study by Hausler [29] for a free–falling jet which impinged vertically into the tailwater. Fig. 2.19 shows the comparison of the measured mean pressure at the pool floor with the theoretical profiles. In the figure, the pool depths tested were greater than the potential core length and the pressure values were made dimensionless by division with the corresponding central pressure at the same depth in the pool. It can be seen from the figure that the results are in general above the pressure profile calculated on the basis of an arrival velocity (velocity–head profile) and below the profile developed from considering the reaction of the pool floor to the impinging jet momemtum (pressure profile for jet deflection).

For submerged circular jet diffusion, more precise formulations of wall pressure have been obtained based on dimensional considerations and experimentation. In the neighbourhood of the stagnation point, Poreh and Cermak [30], testing a vertical water jet, developed expressions based on irrotational flow considerations. For a jet impinging at the solid boundary when

the flow was fully established, the mean pressure head above the hydrostatic at the stagnation point (hs) was found to be, in dimensionless form :

$$hs/\ Ui^2/2g = 60.5(Di/Y)^2 \qquad (2.68)$$

where Ui and Di are the velocity and jet diameter at the pool surface and Y is the plunge pool depth.

An expression for the mean dynamic pressure head distribution, termed the additional pressure head at the boundary, for the stagnation zone in the radial direction was also determined by Poreh and Cermak [30]. The simplified expression is given as :

$$\bar{h}/hs = 1 - 124.7\ (Rp/Y)^2 \qquad (2.69)$$

where Rp is the radial distance from the jet axis on the boundary and $\bar{h}$ is the mean pressure head above the hydrostatic at Rp.

Fig. 2.20 shows Equation (2.69) for the mean dynamic pressure distribution on the boundary and the experimental values obtained by Poreh and Cermak. From the plot of the pressure distribution (Fig. 2.20) and velocity measurements it was concluded that the limit of applicability of Equation (2.69) could be defined as the interior of a hemisphere with centre at the stagnation point and with a radius of 0.05Y. The effect of diffusion is important beyond these limits. On the boundary of this hemisphere, the pressure intensity deviates from the parabolic shape resulting from Equation (2.69) and approaches the ambient static pressure with increasing radius (Rp/Y), see Fig. 2.20.

The radial extent of the deflection region (Region 3 defined previously) from the stagnation point was found by determining where the pressure gradient was approximately zero, shown in Fig. 2.20. The longitudinal magnitude of this region, on the other hand, was taken to be where no effect on the axial velocity by the boundary was apparent. A definition sketch of the deflection region and the zone of the stagnation point is given in Fig. 2.21. In this figure the longitudinal extent of the deflection region from the solid boundary is termed Y* and the radial extent of this region from the stagnation point is termed as Rp*. From experimentation, the limits of the deflection region were found by Poreh

and Cermak [30] to be $Y^* = 0.2Y$ and $Rp^* = 0.3Y$.

From their experiments on high velocity submerged air jets, Beltaos and Rajaratnam [31] found slightly different values for the longitudinal and radial extent of the deflection (or impingement) region. In this case Y^* was found to equal 0.14Y and, from boundary pressure considerations, Rp^* was found to be equal to 0.22Y. It was also found by Beltaos and Rajaratnam [31] that, for a fully established jet (Y/Di= 21.2– 65.7), the dimensionless mean pressure profiles in the radial direction for the deflection region and at the solid boundary are similar and can be described by :

$$\bar{P}/P_m = \exp.[-0.693\ (Rp/bp)^2] \qquad (2.70)$$

where Pm = Dynamic mean pressure at jet centre line.
bp = Value of radius at which $P = 1/2\ P_m$ (Length scale).
$\bar{P}$ = Mean dynamic pressure value at any radius.

Fig. 2.22 shows the experimental values determined by Beltaos and Rajaratnam [31] for the dimensionless pressure profiles near to and at the solid boundary along with the fitted similarily expression, Equation (2.70).

At the solid boundary, the mean dynamic pressure at the jet centre line will equal the stagnation value (Ps). It was also found that the length scale at the boundary was :

$$bp = 0.078Y \qquad (2.71)$$

where bp is again the radial distance to the point where the pressure is half that of the centre line pressure and Y is the plunge pool depth.

Therefore, an expression for the dimensionless boundary pressure profile throughout the radial extent of the deflection region was determined by Beltaos and Rajaratnam [31] as :

$$\bar{P}/Ps = \exp.[-114\ (Rp/Y)^2] \qquad (2.72)$$

Fig. 2.23 shows the experimental results of this study along with those of Poreh

and Cermak [30], mentioned previously, and the fitted expression, Equation (2.72). An equation for the variation of the stagnation pressure (Ps) with pool depth relative to pool inlet conditions (Ui and Di) was also developed by Beltaos and Rajaratnam [31]. In a comparable form to Equation (2.68), the expression was as follows :

$$Ps / \rho Ui^2/2 = 50 (Di/Y)^2 \qquad (2.73)$$

Similar tests were carried out to determine the mean pressure distribution at the solid floor beneath a submerged impinging jet by Hrycak et al. [22], but with lower values of submergence ratio than had previously been considered (i.e. Y/Di = 4–20). The dimensionless mean pressure values were plotted against the ratio of radial distance over jet diameter at the submerged nozzle (R_p/Di), Fig. 2.24. From the figure it can be seen that at a (Y/Di) value of 4, the fitted curve showed a maximum pressure level at the stagnation point (Rp/Di = 0) and a rapid decrease followed by an asymptotic approach to zero ; at a distance of Rp/Di = 3, the curve was near to the horizontal axis, and the pressure was about equal to the ambient pressure. As the value of Y/Di increases, both the slope of the pressure distribution and the maximum mean value decrease.

For the case of short jet impingement (i.e. with the stagnation point located within the potential core – Y/Di $<$4), Davanipour and Sami [32] found that the pressure profiles could again be shown to be similar. With potential core deflection, the value of stagnation pressure itself was found, as expected, to be equal to the total dynamic pressure at the submerged nozzle ($\rho Ui^2/2$). At these short deflection depths, the presence of strong adverse pressure gradients caused the flow to experience the effects of the stagnation zone almost immediately and the characteristics of the flow were clearly dependent upon the pool depth, Y. Secondary effects produced by the surface may be characterised by lateral oscillation of the complete jet flow or by changes in core length and jet spreading rate.

Work in this general field has also been carried out for rectangular jet deflection. The diffusion pattern of a submerged plane jet and the pressures generated at the boundary below the jet were recorded by Cola [33]. The measured mean pressure head above the hydrostatic at the boundary was found to be slightly higher than that calculated purely from free jet velocity decay, Fig.

2.25. For a submergence of 44.3 slot widths, the calculated centre line arrival velocity, based on Albertson's [6] relation, would be 0.344 Ui which corresponds to a kinetic energy head of 0.118 $Ui^2/2g$. As can be seen from the figure, at the stagnation point the mean pressure head above the hydrostatic was found to be 0.145 $Ui^2/2g$. The results were limited, however, as only one submergence ratio was considered. Later work by Kamoi and Tanaka [34] considered rectangular jet diffusion at various angles of jet impingement and for various pool depths. The boundary pressure profiles were again shown to be similar. Of more interest, however, are the measurements of boundary pressure fluctuations. It was found by Kamoi and Tanaka [34] that the position of the maximum pressure fluctuations on the boundary was located outwith the stagnation point when testing at low submergence ratios. As the pool depth was increased, the location of the maximum fluctuations was found to move towards the stagnation point. For a constant outlet size it was also found that as the turbulence level was increased, this transition occured at lower pool depths. This observation may be attributed to the development of the pool turbulence, see Fig. 2.26. In the potential core region, the maximum level of longitudinal turbulence is located in the mixing layer rather than at the jet axis while, in the region of established flow, the maximum turbulence level is at the jet centre line.

As the expressions and observations noted in this section relate to submerged jet diffusion in a confined space, the influence of entrained air is not considered. Therefore, the following section will discuss the effect of pool air entrainment on the diffusion process to properly understand the action of a spillway jet which impinges on a plunge pool surface.

2.5 INFLUENCE OF ENTRAINED AIR ON THE JET DIFFUSION PROCESS.

It will be appreciated that spillway jets impinging on a plunge pool surface will entrain large quantities of air which are likely to have a significant effect on the subsequent jet diffusion process, the pressures generated at the plunge pool floor as well as the degree of scour produced in a natural plunge pool. Air bubble diffusion in plunge pools has been investigated by Ciborowski and Bin[35], Kumagai and Imai [36], Smigelschi and Suciu [37], van de Sande [38] and McKeogh [39] to name but a few. The effect of entrained air on pressures

generated in plunge pools has been investigated by Johnson[40], Tabushi [41] and Ervine and Falvey [42] while the influence of air bubbles on scour reduction has been investigated by Mason [43].

The mechanisms and quantities of air entrained at a jet plunge point will be discussed in Section 2.6, whereas in this section the discussion will centre on the bubble diffusion process.

The most fundamental study of this nature has been carried out by Auton, Sene, Hunt and Thomas [44] for the case of bubble diffusion in a plane shear layer. This is illustrated in Fig. 2.27 showing the four forces acting on a single bubble. Considering buoyancy, inertial components, vorticity and drag, ignoring the density of air ($\rho a << \rho w$) and applying the force– momentum equation to an air bubble an expression can be produced for the resultant force on a bubble as follows :

$$F = \underbrace{-\rho w \bar{V} g}_{1} + \underbrace{\rho w \bar{V} \, dU/dt}_{2} - \underbrace{\rho w \bar{V} Cvm \, (\partial Ub/\partial t - dU/dt)}_{3}$$

$$\underbrace{-\rho w \bar{V} CL \, (Ub - U) \wedge \omega}_{4} - \underbrace{\rho w \bar{V} g \, \frac{Ub-U}{Ubr} \left| \frac{Ub-U}{Ubr} \right|}_{5} \qquad (2.74)$$

where 1 = buoyancy
2 = particle acceleration
3 = virtual mass force
4 = lift force due to vorticity
5 = drag force on bubble

F = resultant force on the bubble
$\bar{V}$ = bubble volume
U = local water velocity vector
Ub = bubble velocity vector
Ubr = bubble rise velocity in fluid at rest
$d/dt = \partial/\partial t + U.\nabla$
Cvm = virtual mass coefficient (=0.5)
CL = lift coefficient (=0.53)
ω = vorticity vector ($\nabla \wedge U$)

Equation (2.74) has been written in terms of the acceleration (total derivative) of the bubble for the simplified case of $\partial Ub/\partial t = 0$ in the virtual mass force as follows :

$$\frac{dUb}{dt} = -g + \frac{dU}{dt} + Cvm\left(\frac{dU}{dt} - \frac{dUb}{dt}\right) - CL\,(Ub-U) \wedge \omega - g\,\frac{(Ub-U)}{Ubr}\left|\frac{Ub-U}{Ubr}\right|$$

which becomes : ---------- (2.75)

$$\underset{\text{(inertia)}}{\frac{dUb}{dt}} = \underset{\text{(buoyancy)}}{\frac{3.dU}{dt}} - \underset{\text{lift(vorticity)}}{2g - 2CL\,(Ub-U) \wedge \omega} - \underset{\text{(drag)}}{2g\,\frac{(Ub-U)}{Ubr}\left|\frac{Ub-U}{Ubr}\right|} \qquad (2.76)$$

Auton, Sene, Hunt and Thomas [44] used a form of Equation (2.76) above to investigate the behaviour of bubbles rising under buoyancy from a point below a vortex core. Ultimately this type of analysis by Auton et al. [44] will lead to more accurate predictions of bubble behaviour which can be used to compute a bubble path in a shear layer including detrainment and bubble transport. The analysis, however, requires extensive computer modelling and is not yet at a stage of development to become common place in the Civil Engineering context.

A more simplified and empirical approach was adopted by McKeogh [39] in his study of air bubble diffusion in plunge pools. McKeogh considered that entrained air bubbles were transported in vortices in the shear layer down into the plunge pool. Beyond a certain depth in the pool, buoyancy forces counteract the downward motion and the bubbles escape and rise to the free surface. To determine the effect of air presence on the plunge pool base pressure, the composition of the two-phase shear layer region must be investigated. The factors which contributed to the rate of air entrainment will consequently effect the air distribution in the pool. The most critical parameter influencing the shape and composition of the aerated region is the condition of the impinging jet.

McKeogh [39] commenced his experimental studies using very low turbulence impinging jets. Jets with low turbulence intensity at impact produce an entrainment pattern which can be described as a cone shaped core of descending bubbles surrounded by a cylindrical volume of ascending bubbles. The depth of

penetration (Dp) of the bubbles will be very large, provided no boundary impedes the jet development, whereas the overall air concentration (C) within the diffusion zone is low (C $\leq$ 2%). C is defined as :

$$C\ \% = \frac{Q_{AIR}}{Q_{AIR} + Q_{WATER}} \times 100 \quad \text{(with U air = U water)} \tag{2.77}$$

The air bubbles were considered to rise to the free surface when the downward water velocity equals 0.26 m/s, see Fig. 2.28. This is the velocity at which a 2mm diameter bubble will rise within a column of water, Haberman and Morton [45].

McKeogh found that the presence of air bubbles in the pool excites the turbulence level in the shear layer and hence the dissipation process is affected in terms of the jet spreading angle and inner core decay. With the low concentrations of entrained air, typical values of spreading angle were found by McKeogh to be between 10–11° in the zone of flow establishment and around 14° in the established flow zone. The inner core was also found to decay at an angle between 7–8°. Fig. 2.29 shows a comparison of these values with Albertson's [6] results for free jet diffusion. For the submerged jet the spreading angle is 6° in the zone of establishment and 11° in the established flow zone while the inner core decays at an angle of 4.5°. It is interesting to note an almost 50% increase in the angle of inner core decay and outer jet spread in the zone of flow establishment when only a low concentration of air is entrained.

For very low intensity turbulent impinging jets, the following expression was derived for the jet centre line velocity decay by McKeogh and Ervine [46]:

$$Um/Ui = 3.3(Di/Y)^{1.1} \tag{2.78}$$

where Ui and Di are the velocity and diameter at the impact point and Y is the vertical distance into the pool from the free surface. Comparison of the above expression with that found for a free submerged jet by Albertson shows a large increase in velocity decay even for such small air concentrations. This is shown clearly in Fig. 2.30.

McKeogh then commenced tests using high turbulence intensity impinging jets. As the turbulence level of the impacting jet increases it was found that the entrainment pattern changes dramatically. The penetration depth of the bubbles is substantially reduced, the average air concentration within the diffusion zone is greatly increased and the outer spread angle of the two–phase shear layer is also increased. Overall the pattern produced is much more random in nature. Each of these points will be considered in turn.

As the spreading jet will penetrate to smaller depths, greater energy loss efficiency will be obtained. For rough turbulent impinging jets, which are far more common in Civil Engineering structures, the maximum depth of penetration of air bubbles was related to the momentum of the issuing jet. It should be noted at this juncture, however, that the maximum bubble penetration depth (Dp) is not strictly defined, since the lower limit of the bubble swarm fluctuates continuously, but a time average value can be estimated. A general expression for the penetration depth was given as

$$Dp = K\ Uo^m\ Do^n \qquad (2.79)$$

where Do = diameter of nozzle situated at distance L above plunge pool surface (m)

Uo = jet velocity at nozzle (m/s).

Considering experimental data from Bin [47], Bonsignore et al. [48], McKeogh and Ervine [46], van de Donk [49] and van de Sande and Smith [50] for $UoDo < 0.1\ m^2/s$ then $m = n = 0.66$ and $K = 2.4$. A separate correlation by Vigander [51] gave :

$$Dp/Do \simeq 1.5\ Uo/Ubr \qquad (2.80)$$

Assuming Ubr (bubble rise velocity) approximately equal to 0.26 m/s the expression could be written as :

$$Dp \simeq 6\ Uo\ Do \qquad (2.81)$$

The expressions for penetration depth showed good agreement over the range of velocity and diameter tested in defining Equation (2.79), see Fig. 2.31.

A typical set of air concentration profiles is shown in Fig. 2.32, from the work of McKeogh and Ervine [46]. The example is for a rough (5%) turbulent jet where the fall height through the atmosphere (L) was set equal to the jet disintegration length to achieve maximum aeration (this point will be discussed in Section 2.6.3). The graphs show that the maximum value of air concentration (C) occurs at the centre line of the jet. There is a decrease in the axial value of C and a broadening of the profiles as the distance from the point of jet impact increases. Unfortunately velocity profiles for this condition could not be obtained due to the presence of large amounts of air. Considering the maximum possible air concentration in the pool, it was found that Cmax on the jet centre line was around 38%. This is in good agreement with the work of Brauer [52] who stated that a maximum transport capacity must exist in air–water flows and hence a maximum possible air concentration. Tests yielded a maximum possible air concentration of approximately 40% .

An expression for the centre line air concentration (Cc) was given by McKeogh and Ervine [46] as :

$$Cc/Cmax = 1/\ [1+3\ (Y/Dp)]^3 \qquad (2.82)$$

However, it should be noted that when the depth into the plunge pool (Y) equals the depth of penetration (Dp) then the ratio of centre line to maximum air concentration equals 0.25 from Equation (2.82), while by definition this value should be approaching zero.

Considering the increase in outer jet spread angle, a value of 13–14° was obtained from experiments which agreed well with the work of Sene [53]. Sene shows that, for turbulent jets, the outer spread of the bi–phasic zone is of the order of 14° when moderate to large quantities of air are entrained. The angle of inner core decay has not been measured successfully but is estimated to be around 8°. Hence the value of the depth of inner core decay (Yc) would be conservatively around 4 Di.

The influence of air bubbles on the resulting pressures in a plunge pool, and in fact, at hydraulic structures in general, has not been widely investigated. A study by Frizell [54] on pressures in a tunnel spillway after air injection revealed a reduction in mean dynamic pressures due to air presence but an increase in

pressure fluctuation magnitude. A specific study of the influence of air bubbles on plunge pool pressures was undertaken by Johnson [40]. The result of this experimental study revealed that mean dynamic pressures at the plunge pool floor could be reduced by up to 40% .

The influence of air on the boundary pressures can be estimated approximately by determining the air concentration variation with plunge pool depth. This can be done using empirical expressions or assuming a linear reduction in $\bar{C}$ with depth having estimated the initial air concentration, the bubble penetration depth and considering flow entrainment into the spreading jet. This process was carried out by Ervine and Falvey [42]. The reduction in mean pressure due to the presence of air bubbles is achieved by approximating the bi-phasic shear layer with a pseudo-fluid whose density is $(1 - \bar{C})\rho w$. This will result in the following expressions for mean dynamic pressure derived below:-

The mean dynamic pressure at any point on the plunge pool is given by :

$$\bar{P} = (1 - \bar{C})1/2\rho w\ U^2 \qquad (2.83)$$

where $\bar{C}$ is the mean air concentration and U the vertical velocity component at that point. For plunge pool depth (Y) shallower than Yc, the value of U should be taken as the impact velocity Ui, and $\bar{C}$ may be taken as zero, because an unaerated solid core may exist. Therefore :

$$\bar{P} = 1/2\rho w\ Ui^2 \qquad (2.84)$$

that is, the mean dynamic pressure may be as high as the reservoir head.

For $Y > Yc$, judicious assesment of suitable values of $\bar{C}$ and U is required. $\bar{C}$ may be assessed by the method mentioned above. Assuming a linear velocity decay and taking $Yc = 4\ Di$, established previously, an expression for the centre line velocity at depth Y ($> Yc$) related to the impact velocity could be written, similar to Albertson [6] as :

$$U \propto 4\ Ui.Di/Y \qquad (2.85)$$

hence the centre line mean dynamic pressure ($Y > Yc$) would be given by :

$$\bar{P} \simeq (1-\bar{C})\ 1/2\rho w\ Ui^2\ [\ 16(Di/Y)^2\ ] \qquad (2.86)$$

Using the largest centre line air concentration of 40% would thus produce a pseudo–density of 60% of water and hence maximum reduction of mean dynamic pressure of the order of 40%.

The designation of the diameter at impact remains a problem in the above expression and this will be discussed in Section 2.8. Further problems exist in this form of analysis, which is based on modifications to free (unconfined) jet principles. Firstly, as mentioned, the velocity decay in such highly aerated flow has not been determined. Secondly, it has been found that with increasing air concentration ($C > 2\%$) the velocity profiles are no longer universal, McKeogh [39], and simplifications subsequently introduced (Section 2.3.2) are no longer valid. Considering the air quantities in the pool, the boundary influence will alter the diffusion and air concentration pattern to some degree, as also noted by McKeogh, see Fig. 2.33. Therefore, values for free jet spreading will not give precise results for air concentration and arrival velocity at the floor of the basin. However, although not precisely quantified, it is apparent from this section that entrainment of large amounts of air has a profound effect on the plunge pool diffusion process.

In the realm of bubble diffusion, scale effects in terms of geometric similarity (ratio of bubble size to boundary scale) and dynamic similarity (ratio of bubble rising velocity to water velocity) are evident. For Froude models the scale effects are two fold.

(i) Surface tension effects mean that the physical size of the air bubble (which is about the same size in model as in prototype) is relatively too large in the model giving relatively too large rise velocities compared to the downward drag (jet) velocity acting on the bubble.

(ii) The other scale effect lies in the fact that the Reynolds Number is not modelled correctly, and hence neither is the turbulence characteristics (turbulence intensity, turbulent energy spectrum) of the flow. To overcome these effects the model Reynolds Number must be sufficiently high or models of various sizes must be tested to determine the influence of non–simulated parameters.

For scour at natural plunge pools, the influence of entrained air on the depth of scour hole has been investigated by Mason [43]. This work, amongst others on scour, will be detailed in a separate section of this chapter (Section 2.9).

2.6 BEHAVIOUR OF TURBULENT JETS IN THE ATMOSPHERE.

2.6.1 Introduction

Turbulent water jets plunging through the atmosphere have received little attention as a research topic. The physical mechanisms are complex, and also crucial to our understanding of the jet conditions as it impacts with the plunge pool free water surface. In Sections 2.6.2 and 2.6.3, the author will review two of the most important aspects affecting pressures in the plunge pool, namely, jet stability (or how the jet disintegrates during the plunge) and secondly, plunge point air entrainment (or how much air is entrained into the plunge pool).

In this introduction, however, it is important to introduce the reader to some general characteristics of jet behaviour in the atmosphere. Consider first the idealised case of a circular jet issuing from a vertical circular nozzle as shown in Fig. 2.34.

If the nozzle is short, the boundary layer at the edge of the jet will be thin. For very long nozzles the boundary layer may be fully developed. At the point of entry into the atmosphere the jet will contain some turbulence which will be more pronounced at the edges compared with the centre. Relative turbulences for short or long nozzles are sketched in Fig. 2.35. Turbulence in the jet will immediately act on the surface tension "skin" of the jet to cause surface disturbances which grow in size in the axial direction. This is analogous to the submerged jet behaviour where the eddy length is considered to grow linearly in the axial direction $\ell = cx$ as explained in Equation (2.50).

As well as causing surface disturbances, the internal fluid turbulence also spreads rapidly inward towards the jet centre line. This is an exact parallel with the zone of flow establishment in a submerged jet (Section 2.3.1), only in the case of an atmospheric jet, the ambient fluid has a density which is only 1/800

of the jet density.

An important aspect of atmospheric jet behaviour is that the equal pressure around the jet periphery will produce a zero pressure gradient across the jet width and hence ultimately a zero velocity gradient (ignoring air resistance) across the jet width. This is shown in Fig. 2.36. A zero velocity gradient will in turn mean that no new turbulence is generated as per the relation, $\tau = \rho \ell^2 (\partial u/\partial r)^2$. If there is no turbulence generated along the jet length then existing turbulence after redistribution (advection) will be dissipated in the usual way of energy transfer down the eddy length scales. Davies [8] also postulates that turbulence is dissipated by the impact of turbulent eddies with the free surface causing bulges or disturbances. A graph showing the growth of surface disturbances in the axial direction is shown from Davies [8] in Fig. 2.37. Davies [8] showed that disturbances ϵ vary with x, the distance from the nozzle. It was found that $\epsilon \propto (\sqrt{x})$ and similarly with the internal jet turbulent velocity, $U' \propto (\sqrt{(1/x)})$.

The influence of air resistance at higher velocities magnifies the growth of jet surface disturbances. This is also true for the total trajectory length of the jet, as shown in Fig. 2.38 from Novak [55], indicating the physical reduction in jet trajectory due to air resistance. In the figure, considering flow leaving a flip bucket, it can be seen that the effect of air resistance is small whenever the exit velocity (Uo) is less than about 20 m/s, but as the velocity increases to 40 m/s the throw distance could be reduced by as much as 30% from the value given by projectile theory.

Ervine and Falvey [42] have produced a simple model for the ability of the jet to spread laterally and to cause free surface aeration. For a jet issuing horizontally from a straight pipe at velocities into the prototype range, measurements were taken by Ervine and Falvey [42] to determine the influence of turbulence on the flow behaviour in the atmosphere. To investigate the effect of turbulence on the spread, distortion and break–up of free jets, the axial turbulence intensity at jet exit was related to the half angle of jet spread taken from high speed photographs. Fig. 2.39(a) shows the relation between the jet spread and the jet axial turbulence intensity at the orifice outlet and Fig.2.39(b) shows the simplified condition of the spreading turbulent jet. With limited data, the rate of jet spread was found to be :

$$\delta_2/x = 0.38\ U'/Uo \qquad (2.87)$$

where δ_2 is the lateral spread of the jet; x is the distance from the orifice; and Uo is the average velocity at the plane of the orifice. Further, it was argued that the outer spread angle was equal to the lateral component of turbulence (v'/Uo). Hence

$$\delta_2/x = v'/Uo \qquad (2.88)$$

Extension of the jet spread model to the estimation of the jet disintegration length will be discussed in Section 2.6.2.

Since, according to Equation (2.88), the jet spreads laterally at a rate proportional to the turbulence intensity, the jet particles moving perpendicular to the flow must have adequate kinetic energy to overcome the restraining surface tension. Representing the lateral turbulent kinetic energy as $1/2\ \rho v'^2$ and the restraining surface tension pressure as $2\sigma/R$, see Fig. 2.40, the criterion for jet spreading is :

$$1/2\rho v'^2 \geq 2\ \sigma/R \qquad (2.89)$$

or from equation (2.87) :

$$1/2\rho u'^2 \geq 13.8\ \sigma/R \qquad (2.90)$$

where R is the radius of curvature of the jet surface undulation and σ is the surface tension parameter.

Equation (2.89) is stipulated as a criterion for the onset of free surface aeration, as air bubbles will not be entrained across the free surface until there is sufficient turbulent energy relative to the surface tension forces. A further criterion for the onset of aeration concerns the value of R, the radius of curvature of surface undulations. An estimate of the value of R can be obtained making the following assumptions :

(a) At the onset of aeration, the radius of the eddies in the jet have the same order of magnitude as the surface disturbance amplitude (Fig. 2.40).

(b) The magnitude of the surface disturbances are proportional to the kinetic

energy of the turbulent fluctuations $u'^2/2g$, as advocated by Sene [53]. Thus, from Equation (2.89), assuming isotropic turbulence meantime ($U' = V'$),

$$R \geq 4\ \sigma/\rho u'^2 \sim \epsilon \sim u'^2/2g \tag{2.91}$$

giving :

$$u'^4 \sim 8\ \sigma g/\rho \tag{2.92}$$

or

$$u' \sim 0.275 \text{ m/s at } 10^\circ \text{ C}$$

as the criterion for the entrainment of bubbles at a free surface. In an equal and opposite action, this should also be the criterion for the creation of drops of water or spray at the air–water interface. Equation (2.92) may also be expressed in the form of jet velocity :

$$U = \frac{0.275}{u'/u} = \frac{0.275}{Tu} \tag{2.93}$$

where u is the jet velocity at the onset of aeration.

With reference to the Morrow Point Dam spillway, Fig. 2.41, it can be seen that although the lateral spreading of the plunging jet is approximately the same in both the model and the prototype, there is a major difference in the free surface aeration and spray at the plunge point between the model and the prototype. In addition, the prototype exhibits free surface aeration around the entire jet periphery. The problem is that some important processes in free jets are dependent on Weber and Reynolds Numbers and cannot be easily simulated in Froude models. Considering the relations, derived by Ervine and Falvey [42], that have been outlined above, the reasons for the problems associated with modelling turbulent jet behaviour become apparent. For example, with a relative turbulence intensity of approximately 4–5% in both the Morrow Point model and prototype, a jet velocity of 5.5–7 m/s would be required for aeration, from Equation (2.93). The model jet exists at velocities much less than 5 m/s, whereas the prototype has an exit velocity around 10 m/s.

Hoyt and Taylor [56] also used a sophisticated photographic technique to

determine the turbulence structure in a water jet discharging in air. However, the process of free surface aeration is attributed by Hoyt and Taylor [56] to the falling droplet hypothesis rather than the mechanism postulated by Ervine and Falvey [42]. According to the falling droplet hypothesis of aeration, as the initial jet surface disturbances are amplified, sufficient turbulent energy close to the free surface overcomes surface tension and propels a droplet of water radially into the atmosphere. The returning end of the spray filament then acts as a re-entrant jet, carrying with it an air bubble. These air bubbles persist in the jet surface until the jet breaks up. However, this mechanism is clearly not possible on the under-side of a jet as a water droplet propelled out of the flow is unable to return to the flow, and yet a similar order of magnitude of air entrainment has been noted to occur at both the upper and lower sides of the jet.

At the final stage of air entrainment, as the jet moves through the air, viscous forces and large scale instabilities cause the jet to break-up, according to Hoyt and Taylor [56]. In addition to the air bubbles riding in the jet surface, air is physically entrained and carried along as the jet breaks up. Fig.2.42 (a-d) shows the nature of the horizontal water jet at various distances from the nozzle outlet. Before the jet breaks up into droplets it can be seen from the figure that these large scale motions appear to be helical-type instabilities, as contrasted to the axisymmetric instabilities seen near the nozzle exit. No guidance is given by Hoyt and Taylor [56] on the cause of this jet motion, but the jet axial swirl may be due to the Coriolis component, see Fig. 2.43. This point will be returned to in Section 2.6.2.

Finally, it can be noted that the most recent research on chaos and non-linear dynamics has suggested that jets issuing from an orifice can be chaotic. According to Mullin [57] this may be true of laminar jets or jets of intermittent low turbulence issuing into an ambient fluid. The path taken by the jet may vary randomly, be unpredictable and therefore not amenable to conventional analysis. The following section will deal with the methods that have been employed to determine the jet stability in the atmosphere.

2.6.2 Jet stability in the atmosphere

The stability of a jet refers to the behaviour of the coherent portion of the jet, and how the jet breaks–up or disintegrates during a plunge through the atmosphere. The significance of this topic is that if the jet plunge length is sufficient to allow break–up into discrete elements, then the mean pressures on the plunge pool floor will be greatly reduced, and air entrainment into the pool will be by a droplet mechanism. A sketch of jet break–up is shown in Fig.2.44.

Due to the complex interaction of hydrodynamic and aerodynamic forces on the plunging jet, a theoretical treatment has only been possible for the simplest cases. Experimentation and observation have been utilised to determine empirical formulations (from dimensional relationships) to allow estimation of break–up lengths for jets other than the ideal. The jet break–up length LB is hence defined as the jet length from nozzle exit to the point where is jet first becomes totally discontinuous (see Fig. 2.44).

Early work by Rayleigh [58] on the stability of low velocity laminar jets, due to the growth of axisymmetric disturbances, resulted in equations for the break–up length dependent only on surface tension and inertial forces. Further analysis was carried out by Weber [59], who also took account of the effect of viscosity on the jet break–up characteristics. The dimensionless break–up length was given by :

$$L_B/D = \ln (r/\delta_0) \left[(We) + 3(We^2/Re) \right] \qquad (2.94)$$

where D = diameter of outlet
r = jet radius
δ_0 = amplitude of initial surface disturbance.
We = Weber Number $[\rho U^2 D/\sigma)]$
Re = Reynolds Number (UD/υ)

The value of $\ln (r/\delta_0)$ had to be found experimentally. Weber reported a value of 12, based on data by Haenlein [60], whereas Smith and Moss [61] found a value of 13 to be more appropriate. For glycerol/water solutions, Grant and Middleman [62] reported an average value of 13.4 for $\ln (r/\delta_0)$, in good agreement with earlier work.

As a convenient means of representing experimental jet stability data, stability curves are commonly constructed. A schematic example is shown in Fig. 2.45, which applies to a particular liquid and outlet configuration. The linear portion of the stability curve (AB) is well defined by the previously outlined equations. Grant and Middleman proposed a similar expression for the linear break– up region as follows:

$$L_B/D = 19.5\ (We + 3\ We^2/Re)^{0.85} \qquad (2.95)$$

They also proposed that the initial disturbance ln (r/δ_0) is a variable and is more appropriately represented by the correlation:

$$\ln (r/\delta_0) = -2.66\ \ln (Oh) + 7.68 \qquad (2.96)$$

where Oh (Ohnesorge or stability number) = We/Re

This is an important number in jet stability analysis as it represents the ratio of restraining to disturbing forces.

This relationship was used, along with a correlation for the maximum point in the linear break– up region, to modify Weber's expression so that the calculated values of the critical point (B) in Fig. 2.45 agreed with their experimental data. Subsequent testing of the modified theory at ambient pressures other than atmosphere however proved unsuccessful. Another point to note is that the experiments to measure break– up length, by photographs or observation, were generally for small scale, horizontal jets issuing from long pipes, acting as the nozzle outlet. Peculiarities arose during experimental work when outlets other than long pipes were used. This point will be discussed later.

Beyond the initial linear portion of the stability curve (Fig. 2.45), break– up lengths reduce with velocity, reportedly attributable to the onset of turbulence [61] or in other instances the increased influence of aerodynamic forces [62].

In the turbulent jet region (CD in Figure 2.45), which is more applicable to this research field, break– up lengths begin to increase with velocity once more. This seems to imply that turbulence will stabilize the jet. However, as can be seen from the slope of the stability graph in this region (Fig. 2.45), the time to

break– up decreases with increasing velocity. This corresponds to an increase in the rate of growth of a disturbance and hence the jet becomes less stable as velocity is increased.

The mechanism of break– up for low velocity turbulent jets plunging through the atmosphere has been proposed by Ervine [63]. On exit from the outlet constraint, lateral turbulence will induce surface disturbances against restraining surface tension. An air boundary layer set up by the plunging jet generates shear stresses which can further disrupt the jet surface undulations. Further acceleration of the jet will amplify the jet surface undulations until they can no longer be sustained. The jet will break– up into discrete droplets if the fall height is sufficient. Just before break– up, according to Ervine [63], the jet surface will display a sinuous nature, Fig. 2.46. The main parameters defining the break– up process are the development of the boundary layer in the nozzle / outlet and the level of turbulence in the boundary layer itself, refer to previous figure (2.34).

Various empirical correlations for the break– up of small scale turbulent jets have been put forward. For instance, Grant and Middleman [62] developed a relation for jets issuing horizontally from long smooth nozzles as follows :

$$L_B/D = 8.51\ (We)^{0.64} \qquad (2.97)$$

Chen and Davis [64] produced a further correlation for this region. For fully developed turbulent flow issuing from horizontal pipes, the following relationship was given :

$$L_B/D = 1.15\ We + 30 \qquad (2.98)$$

Using the dimensional analysis approach, Baron [65] also provided a relationship, this time including surface tension and viscosity, as follows :

$$L_B/D = 537\ We/(Re)^{5/8} \qquad (2.99)$$

Horeni [66] investigated the break– up of a free rectangular jet of water in air. From experimental results the break– up length was found to be a function of the Reynolds Number :

$$LB = 7.8\ Re^{0.319} \qquad (2.100)$$

Van de Sande and Smith [67] developed a relationship for free vertical jets from circular outlets where turbulence was fully developed :

$$LB = 320\ Uj\ D^{1.5} \qquad (2.101)$$

where Uj = jet velocity at break–up point.

McCarthy and Molloy [68] pointed out in a review of jet stability that the lack of consistency in the various correlations, some of which have been listed, may be due to ommision of the effect of the initial velocity profile on jet stability. Velocity profile relaxation produces radial velocity components which lead to disintegration of the jet. To standardise the velocity profile at jet formation, many workers used long nozzles so that the jet would be fully developed and hence this effect would be reduced.

Ervine, McKeogh and Elsawy [69] argued that the turbulence level of the issuing jet was the main parameter causing perturbations on the jet surface and jet disintegration. As various turbulence levels can be attained at constant Reynolds Number, due to nozzle geometry, then relationships without this parameter would not be representative. By careful alteration of flow conditions in the header tank, the above authors managed to determine break–up lengths of low velocity, circular jets at various turbulence levels. The jets plunged near vertically into a receiving pool below. As expected, when the turbulence level was increased, holding other parameters constant, the break–up length was substantially reduced. The break–up length was related to outflow in a general form as follows :

$$LB = C\ Q^{X} \qquad (2.102)$$

The constant (C) and exponent (x) were determined by the relative turbulence intensity of the issuing jet. Typical values of C and x for low to high turbulence are given in Table (2.1) (Vol.II). As the turbulence intensity was increased it was also found that the minimum entrainment velocity reduced. That is, the minimum velocity to entrain air into the plunge pool is also a function of the relative turbulence of the jet at the end of the nozzle.

When the jet velocity and scale increases, the behaviour of the jet in the atmosphere will alter. As noted previously, transverse velocity fluctuations, associated with turbulent eddies at the air/water interface, will cause lateral motion of fluid elements and, if surface tension is overcome, the jet will disperse, Ervine and Falvey [42]. Similar to the establishment of a submerged jet, disintegration in the atmosphere is postulated to occur when the turbulent shear layers spread to the jet centre line and the solid inner core has hence decayed. If the outer edge is spreading in the manner indicated, Equation (2.87), then the inner core must be reducing in size in a predictable fashion. Referring back to Fig. 2.39(b), Ervine and Falvey [42] extended their jet spread model to estimate when the solid inner core would completely decay. Assuming negligible velocity change over a short distance of the high velocity jet, continuity between sections 1 and 2 of Fig. 2.39(b) gives :

$$Uodo^2 \approx Uodo^2 + (P_1/100)\, Uo\, (do^2 - d^2) + (P_2/100)\, Uo\, (de^2 - do^2) \qquad (2.103)$$

where P_1 is the percentage probability of encountering water in the δ_1 region and P_2 is the percentage probability of encountering water in the δ_2 region. Ignoring second order terms, the ratio of the magnitude of inner core decay to the outer jet spread is given by :

$$\delta_1/\delta_2 = P_2/(100-P_1) \qquad (2.104)$$

Equation (2.104) is valid only for the case of a high velocity jet spreading linearly in the atmosphere

An estimate for δ_1/δ_2 was obtained by Ervine and Falvey [42] from probability measurements made at the edge of typical jets. A probability probe showed that the edge of a jet follows approximately a Gaussian distribution, see Fig. 2.47. This is attributed to the turbulent fluctuations within the jet which cause the jet surface disturbances and also follow a Gaussian distribution. However, referring to the observations of Hoyt and Taylor [56], the probability distribution of encoutering water at the edge of the jet may derive more from the helical motion of the flow downstream of the outlet, as shown in Fig. 2.42.

Initial estimates of δ_1/δ_2 from probability data by Ervine and Falvey [42] for high velocity jets with negligable contraction due to gravity revealed a value of approximately 1/5 to 1/7. Thus the angle of jet core decay may be as small as 15−20% of the angle of lateral spread, ignoring core contraction due to gravity. For a typical outer spread δ_2/x of 3−4%, corresponding to a turbulence intensity U'/U of 5−8%, the inner core decay (δ_1/x) could then be as small as 1/2−1%. If the jet begins to break−up or to disintegrate when the inner core decays completely, the jet break−up length (LB) is given approximately for rough turbulent jets by:

$$\delta_1/x \approx 1/2\text{-}1\% = (do/2)/LB \qquad (2.105)$$

or

$$LB/do \approx 50\text{-}100 \qquad (2.106)$$

This empirical estimate of the break−up length of circular jets agrees with previous experimental data for rough turbulent jets; Ervine, McKeogh and Elsawy [69].

It is apparent from the above that the initial turbulence intensity (Tu) is the most important factor in determining the jet break−up length. This is because the initial turbulence intensity determines the degree of lateral jet spread and by continuity controls the rate of inner core decay of the jet, which in turn determines the eventual break−up of the jet. For flows more applicable to prototype behaviour, values of break−up length between 50−100 outlet diameters have been indicated as a rough estimate.

During the present research a simple model has been formulated to determine the point of core diminishment of a circular jet falling vertically through the atmosphere. Considering the turbulence level at the outlet and a Gaussian probability distribution of encountering water between the solid core and the nominal outer edge of the plunging jet, determined by projectile theory, a value of break−up length can be obained. A more detailed description of this procedure will be included in a later chapter.

It cannot be emphasised too strongly how significant the jet break−up

condition is to the plunge pool floor pressure level. Whatever means is used to estimate jet break–up length, and various methods have been outlined, it is a most important parameter in describing the condition of the jet as it impinges on the plunge pool. Clearly, if the jet plunge length (L) is near the jet break–up length (LB) then the jet spread at impact will be maximised and the mean pressures on the plunge pool floor minimised. This is the condition which is being sought in impinging jet spillway design. As it happens, air entrainment is also maximised at plunge lengths near the break–up length which again assists in reducing mean floor pressures, as will be seen in the following section.

Thus, the real diameter of the jet at the point of impact with the pool will depend on the jet surface disturbances which in turn depends on the ratio of L/LB, the ratio of the plunge length over the jet break–up length. When L/LB $\longrightarrow$ 0, we approach the submerged jet case, whereas when L/LB $\longrightarrow$ 1 we approach the optimum condition of jet diffusivity. For maximum spillway efficiency the key is to design for L/LB $\simeq$ 1. Essentially this comes down to ensuring as high turbulence as possible in the issuing jet and as small as possible discharge Q in each jet combined with the jet drop length L being as large as possible.

2.6.3 Plunge point entrainment

Research into break–up lengths has also included, in some instances, work on air entrainment of plunge pools due to free jet impingement. McKeogh and Ervine [46], with studies already mentioned, determined the effect of jet condition on air entrainment rates. It was found that the maximum entrainment rate was reached when the jet had disintegrated. After this point the jet broke up into discrete droplets, lost momentum to the surroundings and entrained less air. An empirical relationship was determined to predict the rate of air entrainment by considering air being carried along in surface disturbances of the jet and in a boundary layer surrounding the flow, Fig. 2.48. The jet surface undulations where found to increase with fall height and turbulence level, until at break–up point they were equivalent to the jet radius. The best fit for all results gave the following expression for air–water ratio (Q_A/Q_W) :

$$Q_A/Q_W = 1.4 \left[(\epsilon/r)^2 + 2(\epsilon/r) - 0.1 \right]^{0.6} \qquad (2.107)$$

where ϵ = surface disturbance on jet surface.

This relationship is not practical for use, however, as ϵ/r is not known at a given point.

Bin [70] has correlated experimental data for circular jet air entrainment from van de Sande [38], Cumming [71], Ervine et al. [69], Henderson et al. [72], Kumagai and Imai [36] and van de Donk [49]. For vertical jets the air–water flow rate was given by :

$$Q_A/Q_W = 0.04\ Fri^{0.56}\ (L/Do)^{0.4} \qquad (2.108)$$

where $Fri = Ui/\sqrt{(gDo)}$.

The correlations are shown in Fig. 2.49 and the test parameters for each author are given in Table (2.2). Equation (2.108) gives satisfactory agreement provided L/Do $\leqslant$ 100 and the nozzle length $\geqslant$ 10 outlet diameters.

Most of the jets in the data correlations are of relatively small scale, and thus viscous and surface tension forces must influence not only the nature of the surface of the plunging jet but also the inception condition for entrainment. Presumably it can be argued that the parameter (L/Do) reflects growing jet surface roughness and break–up. Initial turbulence intensity is also omitted, but Bin [70] indicates the sensitivity of the data correlations to the length of the jet nozzle, which in turn reflects the development of turbulent boundary layers within the jet at the point of entering the atmsophere.

As the velocity and turbulence level of the jet increases, the air entrainment mechanism changes. At low velocity air is supplied from surface disturbances and an air boundary layer, Fig. 2.48. At higher velocity the air entry becomes more continuous from an air layer above the jet surface, and in some cases from within the jet itself. The mechanism for a high velocity wall jet is shown in Fig. 2.50.

Considering that Froude models tend to underestimate prototype air–water ratios, due to non–simulation of turbulence scales and pertinent forces, Ervine [63] investigated the effect of increasing velocity and geometric parameters to find

a more relevant air entrainment expression. With increase in impact velocity (Ui) it had been found, from previous experiments, that the functional dependency of the air entrainment rate into the pool altered. Holding fall height and jet dimensions constant, at low velocity the air entrainment rate (Q_A) was found to vary with Ui $\uparrow$2 $\longrightarrow$ 3, while at higher velocity, it was better correlated with Ui $\uparrow$1 $\longrightarrow$ 2. For constant velocity and fall height, the air entrainment was found to be independent for jet thickness or diameter > 20mm or Re > $5x10^4$, depending on the initial jet turbulence level. The effect of jet break-up was incorporated, from research by McKeogh [39], to obtain an expression for the air entrainment rate, where the dimensions were substantial. For circular jets :

$$Q_A = K\ do\ Ui^n\ (L/LB)^{0.7 \longrightarrow 0.8} \qquad (2.109)$$

where $n = 2 \longrightarrow 3$ at low velocity
$n = 1 \longrightarrow 2$ at high velocity

From the generality of the above expression it is obvious that a great deal more research into plunging jets, particularly at larger scales and velocities, is required to utilise this form of analysis.

However, it is clear from the most relevant work by Thomas [73], Sene [53] and Ervine and Elsawy [74] that the ratio of air to water ($\beta = Q_A/Q_W$) for a plunging jet varies with plunge length (L) in the form :

$$\beta \propto \sqrt{(L/do)}.f(Tu) \qquad (2.110)$$

where do is the nozzle diameter, and Tu the jet turbulence level. All of these authors above have suggested constants of proportionality to substitute for the turbulence function. For circular jets of high turbulence :

$$\beta \approx 0.3\ \sqrt{(L/do)} \quad (\text{valid for } L/do<100) \qquad (2.111)$$

For circular jets of very low turbulence :

$$\beta \approx 0.15\ \sqrt{(L/do)} \quad (\text{valid for } L/do<400) \qquad (2.112)$$

From the range of applicability of the above expression it can be seen that the upper limit of β at the impact point is approximately 3 for circular jets plunging vertically.

A practical example of utilising the break– up process and air entrainment is shown in work by Mason [75]. Investigations took place into the effectiveness of splitter teeth on dam overspill crests, Fig. 2.51. Impact forces on the pool floor are minimised due to this arrangement by splitting the spillway flow and causing interaction in the atmosphere, at optimum operating condition. This process helps to break– up the concentration of the falling flow, increases the turbulence level, and entraps a substantial amount of air. The remaining flow falls as disseminated spray onto the pool below. Mason [75] cites Victoria Dam as an example of pressure reduction using this system. Here mean impact pressures on the pool apron were only 30% of the potential head.

2.7 PRESSURE FLUCTUATIONS AT HYDRAULIC STRUCTURES

2.7.1 Introduction

Over the last 20 to 30 years there has been a large increase in unit discharges q ($m^3/s/m$) carried by spillways and hence stilling basins. This has resulted in larger quantities of energy to be dissipated from high head dams, higher turbulent fluctuations in the dissipation process and higher pressure fluctuations in the hydraulic structures concerned. This has led in a few cases to severe damage of the structure as in the case of Granget Dam in the U.S.A. where, with $q = 40 m^3/s/m$, blocks of concrete and debris weighing more than 10 tons were moved out of the basin. Discussion of the damage sustained and repairs required are given in reference [76]. Further examples include Malpaso Dam in Mexico where the action of pressure fluctuations resulted in displacement and transport of floor slabs 12m x 12m x 2m in size that weighed 720 tons. The basin was damaged extensively and about 46% of the floor had to be reconstructed. Extensive damage was also noted by Bowers and Toso [77] at the Karnafuli Dam spillway in Bangladesh. Inspection of the spillway revealed damage to the chute floor over an area about 600 ft. wide and 75 ft. long and was attributed to the pressure fluctuations generated in the hydraulic jump stilling basin.

Causes of failure have been two fold :

(i) The concrete base (or wall) slabs, subject to large pressure fluctuations, often have joints, or cracks or weep holes in the concrete slab which allows transmission of the large fluctuating pressures to the underside of the slab as shown in Fig. 2.52. This action could result in uplift of the stilling basin base slabs. For instance, large peak pressure fluctuations may be transmitted to the underside of the slab by the stated methods and, due to the finite time difference between application of load to either side of the slab, may coincide with a minimum fluctuation on the upper side of the slab, Fig. 2.52. The net effect of this differential pressure application may be an upward instantaneous pressure on the slab which may cause substantial uplift if the weight of the base slab and the tailwater head is overcome. If the reinforcement and anchorage is insufficient the slabs may be damaged or even dislodged from the stilling basin. Also, continuous and repeated loading of a fluctuating nature may cause vibration, fatigue and eventual break– up of the stilling basin base slabs.

When the structural integrity of the stilling basin is undermined in this way the damage can readily become substantial as the dislodged elements of the base slab are carried within the highly turbulent flow and act as further abrasive elements during energy dissipation.

(ii) The other cause of failure has been pressure fluctuations giving minimums in instantaneous pressure in the cavitation range of −9m to −10m head of water. Cavitation is the name for a change of phase in water from liquid to vapour by the formation of small voids. If the void is filled with water vapour it is known as vapourous cavitation. Correspondingly, if the void is filled with gases coming out of solution then the process is callled gaseous cavitation. Vapour cavitation is often the more serious and happens when the pressure locally is reduced to the vapour pressure of water, which at 15°C —> 20°C is around 0.2m head of water absolute or −10.1m gauge. Problems with gaseous cavitation, on the other hand, generally occur with lower velocities and high free gas content.

In hydraulic structure the occurance of cavitation is associated with local areas of low pressure such as flow separations, e.g. local uneveness on a concrete surface. With severe fluctuations in pressure at hydraulic structures, the minimum instantaneous head may reach vapour pressure and hence create vapourous

cavitation risks.

The mechanism of cavitation is still not fully understood, but is illustrated schematically in Fig. 2.53. For example, at the point of separation in a high velocity flow, eddies and vortices form with low pressure cores ; with local pressures reaching as low as vapour pressure. When the cavitation bubbles move to an area of higher pressure they begin to collapse. The voids represent small pockets of great potential energy and, when they collapse near a solid boundary, water cannot enter the void as easily from the boundary side as from the other side. Therefore, the collapse is not symmetric, so water entering from one side forms a micro–jet of such intensity that it can cause damage to materials as durable as stainless steel.

Numerical analyses and high speed photographs have shown that the cavity bubble collapse has similar characteristics to water hammer phenomena. The resulting dynamic pressures on the boundary being similar in magnitude to water hammer pressures, and the micro–jet velocities being of the order of 100 to 1000 m/s. The micro–jet velocity impinging on the solid boundary appears to be closely related to the sonic velocity, in the sense that a 1% by volume of air injection reduces cavitation dramatically in a similar relation to the reduction in the velocity of sound. Cavitation has not been a problem in plunge pools because the large air concentrations present have effectively eliminated the damage. An air concentration of 7% near the solid boundary is sufficient to remove the risk of cavitation completely.

Pressure fluctuations are derived in the main from turbulent velocity fluctuations and large eddy behaviour. A typical example is shown in Fig. 2.54 of a stilling basin, where the floor has been lined with sensitive pressure transducers to pick up the fluctuations. The transducer indicated will pick–up low frequency fluctuations from the large eddy shown and will also pick up random turbulence, possibly down to the micro scale, depending on the area and sensitivity of the measurement instrument. This point will be discussed in the following chapter. A typical trace of the pressure fluctuations with time from such a device is sketched in Fig. 2.55.

With the mean pressure defined as $\bar{P}$ and the fluctuating component as $\underset{\sim}{P}$, the instantaneous pressure is given, similar to the instantaneous velocity, by :

$$P = \bar{P} + \underset{\sim}{P} \tag{2.113}$$

and the root mean square of all the values of $\underset{\sim}{P}$ fluctuating about the mean is denoted by P', the R.M.S. fluctuating component. Thus :

$$P' = \sqrt{(\underset{\sim}{P}^2)} \tag{2.114}$$

If the pressure fluctuations were all due to random turbulence the distribution of $\underset{\sim}{P}$ would naturally be Gaussian normal. However, with recent experiments on a hydraulic jump model, Toso [78] has revealed that this is not exactly the case. A typical distribution is shown in Fig. 2.56(b). From the figure it can be seen that the data fits the Gaussian distribution fairly well for about two standard deviations but thereafter an extreme value distribution (Type I) provided a better fit for the large pressure fluctuations. These large pressure fluctuations are of the order of seven to ten standard deviations from the mean. The normal distribution cannot provide an estimate of probability in this region. To adequately describe the probability density function of such non-Gaussian behaviour further statistical information, including the distribution skewness and kurtosis, is required. This point will also be discussed in the following chapter.

According to Toso [78], water cascading down the face of the jump and large eddies travelling through the jump caused the positive fluctuations to be dominant at this measurement point. In other words, the large scale motions superimposed on to the random turbulence produced maximum fluctuations well in excess of that expected from a Gaussian distribution.

Returning to the definition of the pressure fluctuations, the R.M.S. pressure fluctuations are normalised by dividing with the kinetic pressure head ($1/2\rho U_i^2$) to give :

$$Cp' = \frac{P'}{1/2\rho U_i^2} = \frac{h'}{U_i^2/2g} \tag{2.115}$$

Typical values of the pressure coefficient Cp' for various hydraulic structures are given in Table (2.3). The following section will introduce some simple turbulence-pressure fluctuation relationships for these structures.

2.7.2 Turbulence and pressure fluctuations at hydraulic structures

Work on the relationship between turbulence and pressure fluctuations has been carried out for hydraulic structures where the flow conditions are more amenable to analysis. For example, a pure boundary layer type flow, such as an open channel chute spillway, may be estimated accurately. Nezu et al. [79] have shown the velocity fluctuations at the channel bed (normal to the flow) to be of the order :

$$V' \simeq 1.23\ U_* = 1.23\ \sqrt{(f/8)}.\bar{U} \qquad (2.116)$$

where f = Darcy-Weisbach friction factor
$\bar{U}$ = mean flow velocity
U_* = shear velocity $\sqrt{(\tau_0/\rho)}$

Typical values of Cp' for such boundary layer type flows have been measured by Minami [80] and Locher [81] to be in the region of 0.007 giving a relationship of the form :

$$Cp' \simeq 2 \text{ to } 3\ (Tu)^2 \qquad (2.117)$$

where Tu is the relative turbulence intensity defined as U'/Ui

The proportionality constant of 2–>3 is greater than isotropic, homogeneous cases (noted later = 1.4), but will be significantly less than expanding shear layer type flows, such as a hydraulic jump or a sudden expansion.

Hydraulic jump stilling basins are the most common type of energy dissipator used in hydraulic structures. The mean flow characteristics have been extensively studied, by authors such as Rajaratnam [82]. However, fluctuations in pressure originating in the free shear layer and transmitted to the flow boundaries, have only recently been investigated. The fluctuations in pressure have many undesireable effects such as fatigue damage by vibration and erosion of the downstream channel. In extreme cases, as explained, slabs can be uplifted from the stilling basin and cavitation of appurtenances, such as baffle blocks etc., can occur due to application of large instantaneous pressures. Most flow situations with regard to submerged, free and forced hydraulic jumps have been investigated

in the studies of Akbari et al. [83], Vasiliev and Bukreyev [84], Schiebe and Bowers [85], Narasimhan and Bhargava [86] and Toso [78].

It has been found, in general, that the fluctuations in pressure on the solid floor beneath the jump reduce with increase of the readily definable incident Froude number. The peak values also occur further downstream relative to the incident supercritical depth with increase in Froude number, as shown in Fig. 2.57. The location of maximum Cp' values has been found to be coincident with the maximum values of turbulence measured by Rouse et al. [87], indicating a relationship between the two. Typical values of Cp' on the solid floor beneath a hydraulic jump have been found in the range 0.02 to 0.08 (Fig. 2.57), whilst typical values of turbulence intensity in the vertical direction have been shown to be in the range 0.04 to 0.09. For hydraulic jumps this would produce a relationship of the form :

$$Cp' \simeq 10\ (Tu)^2 \qquad (2.118)$$

Both Cp' and Tu in Equation (2.118) are normalised relative to the upstream supercritical mean velocity at entry to the jump, Ui.

Care must be taken with the turbulence results of Rouse et al. [87], as the inflow condition tested was undeveloped. This has a very different turbulence structure in the jump compared with an inflow where the boundary layer has reached the free surface. However, Equation (2.118) can be tested for similar separated flows to determine its applicability. Mansoori [88], for example, has recently measured both turbulence intensities and pressure fluctuations on the walls of a sudden expansion bottom outlet for a dam. The relationship $Cp' \simeq 10(Tu)^2$ was again found to be representative for fluctuations on the side walls of the bottom outlet. Both Cp' and Tu are, in this case, normalised by the upstream velocity before the sudden expansion.

Returning to the statistical analysis of the pressure values measured at hydraulic jump stilling basins, it has been found, and shown, that the distribution of fluctuations in not Gaussian, as normally assumed. In fact, depending on the position in the stilling basin, a large skewness of the probability distribution of the pressure fluctuations has been noted by researchers such as Lopardo et al. [89] and, as previously mentioned, Toso [78].

Another interesting feature regarding hydraulic jump experimentation is the good agreement found between model results and prototype data based on Froude scaling. As the pressure fluctuations are predominantly of low frequency, the large scale flow motions are deemed to be ascendant in terms of pressure fluctuation production. Consequently, for hydraulic jump pressure fluctuations simulation, it is only necessary to reproduce primarily the macroturbulent flow in the model. The low frequency fluctuations scale as the turbulent energy in respective eddy lengths produce comparable results, see Fig. 2.58. This has been verified by Thomas and Lean [90] in a 1:50 scaled model (with $Re = 6.3 \times 10^5$). The model has no significant scale effects for frequencies down to 200 Hz ; this limit is sufficiently larger than normal frequencies in a hydraulic jump.

Considering measurements at forced hydraulic jumps, baffle blocks, provided to reduce the basin length and stabilise the jump, undergo large variations in loading. On the front face of the block, the flow is impacting normally, rather like the base of a plunge pool, and extreme pressure fluctuations are expected. Compared with the floor beneath the hydraulic jump, where the boundary is parallel to the mean flow direction, fluctuations in pressure at the baffle blocks are expected to be of much greater magnitude. Lopardo et al. [91] have measured the pressure levels at baffle blocks when studying stilling basins designed in accordance with the United States Bureau of Reclamation (U.S.B.R.) guidelines. The magnitude of Cp' will vary depending on the baffle block position and incident Froude Number, however, results have shown typical values of Cp' on the front face of baffle blocks to be between 0.15 to 0.25. This will give an indication of the magnitude of fluctuations that may be expected at the plunge pool floor, which is another case of the flow impinging normally to the solid boundary, rather than being parallel to the boundary.

Considering the likely pressure fluctuations on a plunge pool floor, it should be stated that prior to the work of this thesis, no such measurements had ever been undertaken in a systematic fashion. An order of magnitude of Cp' might be obtained by employing the over simplified relationship $Cp' = 10\ (Tu)^2$ for free shear layers, but this depends on an accurate estimate of longitudinal (axial) turbulence intensity along the jet. Such measurements of turbulence intensity had already been taken by Corrsin [12] for the case of a jet issuing submerged from a circular nozzle.

Values of the longitudinal turbulent velocities U'/Ui where taken at various distances from the nozzle, Corrsin [12]. Considering these values in the region of established flow, along the jet centre line, a relationship of the following form was developed :

$$U'/Ui = 0.84\ (Y/Di)^{-0.68} \qquad (2.119)$$

where Y is the distance into the pool and Di is the diameter of the submerged nozzle.

A comparison of the jet centre line turbulence characteristics from this work and later material by Corrsin [23], together with U'/Ui data for the case of a bounded submerged jet, Mansoori [88], and an impinging turbulent jet with low droplength and air bubble concentration, McKeogh [39], is shown in Fig. 2.59. It can be seen that, in all cases, the maximum longitudinal turbulence intensity, relative to the upstream inlet velocity (Ui), is 0.14 to 0.15. The maximum value usually occurs between 5 and 10 jet diameters downstream from the entering jet. This is presumably related to the position where the highly turbulent mixing regions ingress to the jet centre line. Utilising the expression defined earlier for shear layer type flow, Equation (2.118), and the experimental results on the turbulence characteristics of spreading jets, an estimate of the maximum r.m.s. pressure fluctuation at the plunge pool floor can be made. With a maximum centre line longitudinal turbulence intensity of 0.14 to 0.15 the corresponding value of Cp' would be expected to be between 0.19 to 0.22, located around 5 to 10 diameters downstream from the start of the jet. It is of interest to note the coincidence of this range of Cp' with the results of baffle block testing and also that these values are approximately three to four times greater than both an hydraulic jump as well as side wall measurements on a bounded jet. This represents the essential difference between parallel and normal wall fluctuations in a free shear layer. It will also be noted that the relationship between Cp' and $(Tu)^2$ gives a high constant of 10 approximately for free shear layers, whilst the constant is only 2–>3 for boundary layer flows on a flat plate.

In a spreading shear layer flow a mixture of coherent vortex structures and turbulence exist which are translated into fluctuations in pressure at the plunge pool floor. Hence, it is postulated that a relationship will exist between the turbulence level and the generated pressure fluctuations, as noted. For the even

more idealised case of isotropic and homogeneous turbulence, which rarely exists in practice, Hinze [92] quotes :

$$P' = 0.7\ \rho\ (U')^2 \qquad (2.120)$$

where P' = root mean square of pressure fluctuations. In terms of the non-dimensional coefficient Cp' $(= P'/\ 1/2\rho Ui^2)$:

$$Cp' = 1.4\ (U'/Ui)^2 = 1.4\ (Tu)^2 \qquad (2.121)$$

For most shear flows, with anisotropic and non-homogeneous characteristics, the value of 1.4 represents a gross underestimate.

2.8 MODELLING IMPINGING JET SPILLWAYS.

So far in this literature review chapter an attempt has been made to introduce the reader to the various flow phenomena associated with jet behaviour in the atmosphere and in the plunge pool, including mean and fluctuating pressures, turbulence, aeration, jet stability and break-up, jet diffusion and the influence of nearby solid boundaries.

In this section we will turn our attention to model studies which have been carried out specifically for the design of such impinging jet spillways and for the prediction of the plunge pool behaviour, whether it be concrete lined or a natural scour hole.

From the point of view of designing lined plunge pools downstream of dams, one of the most important factors is the pressure, both mean and fluctuating, which will be generated due to impact of the incoming flow on the solid boundary. The influence of a tailwater cushion above the solid boundary in dissipating some of the spillway jet energy will also be of significance, as will the condition of the impinging jet at the point of entry to the plunge pool.

As the flow field in the plunge pool comprises of a highly turbulent two-phase shear layer, the situation is not amenable to a purely theoretical treatment. Most of the limited amount of work on impinging jet spillways has

comprised of measurements made on models of proposed prototype structures. The drawback of this of course is that the results are really only applicable to the prototype being investigated. Certain general conclusions, however, can be drawn from observations made during these studies.

Model testing of this form of prototype structure has been carried out by King [93,94], Lemos and Ramos [95] and Bhargava et al.[96].

In the mid to late 1960's King [93,94] produced a recommended design for Morrow Point Dam, Colorado, U.S.A., after extensive testing and modifications to a 1:24 scale model. At the time of construction Morrow Point was the highest double curvature, thin arch concrete dam under the jurisdiction of the United States Bureau of Reclamation (U.S.B.R.). It was also the first U.S.B.R. dam to incorporate an orifice type free–fall spillway and underground powerplant. It is shown in Fig. 2.60.

The prototype spillway capacity of 1,132 m^3/s is discharged via four 4.57m square gated outlets set high up in the dam structure. Spillway jets fall approximately 107m, almost vertically, before impinging on a concrete lined plunge pool with a tailwater cushion around 20m deep. The testing programme by the U.S.B.R. (King) consisted of pressure measurement on the plunge pool floor and a pilot scheme on the frequency analysis of pressure fluctuations occuring at the pool base.

Mean pressure readings up to one third of the jet fall height were registered, along with large fluctuations of low frequency, attributed to surface waves, surging and large scale eddies within the plunge pool. Stochastic methods were employed to analyse the random pressure fluctuations, and frequency spectra were produced from the pressure records.

Considering analysis of the pressure records, the paper by King [97] presented design–orientated data on pressure fluctuations for two model stilling basins, the plunge pool type at Morrow Point Dam and a hydraulic jump at Crystal Dam (U.S.A.). The Fast Fourier Transform (F.F.T.) and the power spectrum of the pressure signal for both cases are presented. However, there is an ambiguity in the analysis of the data. The power spectrum is used to estimate both the dominant frequency of the signal and "the maximum effective

pressure head". The latter term is in question as the use of the power spectrum is limited to providing information on the frequency domain of the signal.

Certain other anomalies occured in King's work [97] with the measurements taken for spectral analysis. Firstly, a lower frequency limit of 0.5 Hz was operating due to equipment limitations. Hence, very low frequency fluctuations were completely omitted. The second point concerns the pressure measuring system of the above models. The pressure transducers were linked to the stilling basin with tubing. In checking the dynamic response of the system a resonance condition was noted, due to coincidence of the system's low natural frequency with critical ranges of measurement, creating invalid peaks in the power spectrum. This point will be further discussed in the following chapter.

Scale effects were not mentioned in the U.S.B.R. report by King but they were considered by Lemos and Ramos [95] as well as Bhargava et al. [96], mentioned previously. Both sets of work point out that Froude models of this complex impinging jet phenomena do not reproduce the forces of viscosity and surface tension which have a profound effect on jet behaviour in the atmosphere and hence the diffusion process in the plunge pool. However, their methods of addressing this problem were different.

Lemos and Ramos [95] argued that viscosity effects can be neglected, for low frequency pressure fluctuations, if the Reynolds Number in the model is greater than $5x10^4$. The influence of surface tension was investigated separately by model studies of a free overfall crest dam. It was found, during testing of a small 1:50 scale model, that individual jets between crest splitters were highly concentrated at impact, the natural water cushion was rendered inoperative, and high mean pressures and fluctuations were produced. When testing a larger 1:20 model of the spillway crest it was found that adjacent jets associated together. In other words, at the larger model, individual jets produced between the crest splitters spread laterally in the atmosphere and combined, resulting in a more diffuse impact condition. By artificially forcing lateral junction of the spillway jets in the smaller model, and therefore simultating the larger scale flow conditions more accurately, the surface tension effect of constraining the individual spillway jets was made irrelevant. The resulting values of impact pressure were greatly reduced in the 1:50 scale model. Prior to alteration of the flow conditions, the mean and maximum impact pressures were about 25m and 48m

head of water respectively. After simulation of the larger model flow behaviour these pressures reduced to 7m and 12m head.

The work of Bhargava et al. [96] concerned a more complex flow situation proposed for Lakhwar Dam. In this case, with the help of an elevated trajectory bucket supplemented with curved flow splitters, the spillway jets would interact in the atmosphere, disperse and entrap air. The jets are further disintegrated during plunge in the atmosphere, falling as a heavy spray into the plunge pool where collision with the water mass promotes further energy loss. This situation is shown in Fig. 2.61.

Bhargava decided to investigate three models of different scales to determine viscosity and surface tension influences. Measurements of pressure were taken on the solid plunge pool bed and water surfaces profiles of the spillway jets were observed for different discharges. It was noted that as the model size increased, the dispersion of the free falling nappe and air entrainment increased, resulting in reduction of impact energy. In fact, at low flows, the smallest model produced no interaction of spillway jets, whereas jet collision was marked in the largest model. Mean pressures on the plunge pool floor, as well as low frequency pressure fluctuations picked up by transducers on the pool floor, showed a reduction with increase in model size. However, the reduction was not as marked as in the work of Lemos and Ramos [95]. It was therefore concluded from this study that the modelling of such hydraulic structures would, in general, provide results that would be at least conservative. This point will be covered in more detail later in this section.

More systematic and controlled experiments were undertaken by Hausler into impinging jet spillways. In his earliest work, Hausler [29] did a study on a circular jet plunging vertically into a water cushion. Fig. 2.62 shows a sketch of the apparatus used. Mean dynamic pressures were measured at a table, representing the plunge pool floor, which could be altered in position to vary the pool depth. The height from header tank level to pool level (H) varied from 2.4 to 3.6m ; nozzles used were 40, 60 and 90 mm diameter. The depth of tailwater varied from 0 to 1.60m. Hausler produced a series of empirical equations to define the central mean pressure developed at the plunge pool floor, from a best–fit through the experimental data.

Hausler found that the full stagnation pressure ($1/2\rho Ui^2$) is maintained down into the plunge pool to a depth below the free surface Yc, the limit of the zone of flow establishment, and given by :

$$Yc = 2.32\ Di + 0.02\ H \qquad (2.122)$$

where Di is a jet diameter at the impact point, H is the total head available and Ui the theoretical jet velocity at impact point :

$$Di = \sqrt{(4Q/\pi Ui)} \qquad \text{and} \qquad Ui = \sqrt{(2gH)}$$

Hausler developed the following relationship for the central mean pressure at plunge pool depths greater than Yc :

$$\frac{\bar{P}m - \rho gY}{\rho gH} = 10^{(Y-Yc/m)} \qquad (2.123)$$

where $\bar{P}m - \rho gY$ is the mean pressure above the hydrostatic and m is an empirical value given by : $m = -0.225\ Q^{0.35}$

Equation (2.123) shows that the centre line pressure decays rapidly at depths below Yc as a power law expression which is partly dependent on the discharge rate being used.

The limiting depth (Ys) for the central pressure is given by :

$$Ys = m \log \left| \frac{-m}{2.3026\ H} \right| + Yc \qquad (2.124)$$

This is the depth required to completely dissipate the jet.

In later work, Hausler [28] derived equations based on free jet turbulence theory, confirmed by submerged jet experiments, to define the mean dynamic pressure development in a limited tailwater. This assumes that dispersion in the pool is almost linear and a core of constant velocity is formed. The following relationship was given for the mean pressure head above hydrostatic depth at the jet centre line, $(\bar{H}_m - Y)$:

$$\frac{\bar{H}m - Y}{U_j^2/2g} = \left[\frac{Ri}{C_2 Y}\right]^2 \qquad (2.125)$$

where Ri = radius at impact.

$\bar{H}m$ = total mean pressure head.

Results from the earlier work were utilised to determine the value of C_2 which was found to be approximately 0.1, although dependence on Reynolds Number was noted. The value of C_2 also defines the tangent of the angle at which the solid inner core will converge, Fig. 2.63. The core length (Yc) is therefore 5 diameters or width of the jet at impact. Up to this point the centre line mean pressure should be equal to that of the incoming jet. However, it should be noted from the results that the non-dimensional pressure head ratio of Equation (2.125) in the region of flow establishment does not equal unity but rather is centred around 80-90% of the theoretical value. At the end of this core region Hausler states that only 30% of the circular jet energy will be dissipated.

As free jet theory would only predict total dissipation at infinite pool depths, further investigation was undertaken by Hartung and Hausler [98] to find a practical limit where the jet could be said to be fully dissipated. From the previous results, Hartung and Hausler predicted that by $Y/Di \simeq 20$ the jet would be completely dispersed. A graphic description of the scour process due to the build up of hydrodynamic pressures was also included in this work [98] and it was noted that at low pool depths the outlined theory based on turbulent mixing would not be valid as a hydraulic jump would form.

A great number of questions arise from Hausler's work concerning jet "compactness" at impact. Firstly, at no time is air entrainment of the plunge pool taken into account. The cushioning effect of air bubbles, increased mixing in the diffusion zone due to air interaction and disruption of velocity and pressure profiles, as previously noted, is completely neglected. Instead Hausler suggests adjustment to the jet dimensions at impact, but no guidance is given on this point. Another problem exists with the calculation of the impact dimensions themselves. According to Hausler the tested jets all contracted under the influence of gravity during the descent. This may be true if the jets were extremely laminar and the fall height was sufficiently small, however no

information is given to justify this calculation and it seems highly unrealistic. In fact, no discussion on the transitory nature of the impact diameter was included.

The expressions, as Hausler states, would be conservative, but, if no account is taken of the jet condition on plunge pool diffusion, then the application of the derived mean values, for that part of the pressure field, would result in over–design. Unfortunately no measurements were taken of fluctuations above and below mean pressure during the studies. There is also no mention on how this would effect the structural integrity of the pool or scouring action on bedrock.

Similar tests were carried out by Lencastre [99] with 44 and 96 mm thick rectangular slot jets. Lencastre's study shows a much more rapid jet decay in the pool than previously suggested, as shown in Fig. 2.64, and also includes measurements of dynamic pressure fluctuations. Lencastre found the frequency and amplitude of the fluctuations decrease rapidly with increase in depth of the water cushion. By 15 slots widths into the pool the fluctuations were found to be practically negligible. The lateral distribution of fluctuations also shows a marked decrease when a substantial pool depth is operative. Interestingly, Lencastre concludes that the water cushion acts as a low pass filter and eliminates fluctuations above 10 Hz. During Lencastre's study some negative pressures were found at the pool base, as shown in Fig.2.65.

A more recent investigation into the processes involved in falling jet energy dissipators, and scale effects included in modelling the phenomena, has been provided by Ervine and Falvey [42]. Areas of this paper have already been extensively detailed in both Sections 2.5 and 2.6 of the literature review. The point of this particular discussion is to bring all of the previously noted aspects together.

Considering jet behaviour in the atmosphere, Ervine and Falvey [42] have produced theories, explained in Section 2.6, for the onset of free surface aeration, jet dispersion and disintegration, all dependent on parameters non–simulated by Froude models. Explanation of the fact that Froude scale models must over–estimate mean dynamic pressures compared with a prototype is therefore provided. As mentioned, in the atmosphere, the jet behaviour is considerably affected by turbulence intensity, Weber Number and Reynolds

Number, resulting in a more diffuse prototype jet at the point of impact with the plunge pool. Furthermore, a prototype jet will invariably have greater air concentrations in the shear layer in the plunge pool. Both sets of factors ensure mean prototype pressures are significantly less than model pressures. A schematic representation of the jet dispersion process and resulting plunge pool diffusion is given in Fig. 2.66.

Problems do exist with the scenario for the free falling jet produced by Ervine and Falvey [42]. Firstly, no influence of gravity was taken into account in the analysis as the test jets issued horizontally. This being the case, if the jet spread is assumed to be produced by a constant lateral (radial) velocity component, then the resulting nominal outer jet edge would be rather more parabolic for a free–falling jet than linear. Also, gravitational acceleration of the jet during its fall would tend to reduce the jet in area, from continuity, while the jet would try to diverge outwards due to the jet turbulence overcoming restraining surface tension and air entrainment. Of the two competing factors, jet divergence would be more significant with increase in the initial jet velocity. Another point regards the probability distribution of encountering water at the edge of the jet. As noted, Hoyt and Taylor [56] have suggested that this distribution derives more from helical motion of the jet downstream of the outlet rather than a symmetrical increase in the occurance of water particles between the jet outer edge and solid inner core.

As Ervine and Falvey [42] point out, the ability of the jet to spread laterally in the atmosphere, entrain air, become increasingly roughened with distance from the outlet and break–up, if the fall height is sufficient, will have a profound effect on the dissipation process in the pool and hence pressures exerted on the pool floor. To this end a comparison was made of the diffusion process in the plunge pool between jets in various conditions of "compactness" at plunge point. Submerged jet diffusion was first considered and compared with plunging jets of various turbulence levels at impact with the pool surface, taken from the work of McKeogh [39]. A plunging jet of low turbulence and entry velocity, but where no air entrainment was observed, produced a diffusion pattern strikingly similar to that of a submerged jet. When a smooth turbulent jet with low pool air concentration ($C \simeq 2\%$) was tested, however, a 50% increase in both inner core decay and outer spread angle was found. This is attributed to a large increase in turbulence level of the shear layer. Details of these comparisons are

given in Section 2.5.

Referring to Fig. 2.66, as the turbulence level of the incoming jet is further increased, conditions at impact become more irregular. According to Ervine and Falvey [42] the jet diameter at impact, if it still exists, will be oscillating in width (the indicated outer edge is only a nominal designation based on the r.m.s. turbulent component) and air may be present in the outer jet regions. Surface waves will be produced rather than well defined penetrating shear layers. In this case large air concentrations are entrained, often of the order of 40%. The outer spread angle will be greater than those previously considered and will be around 14°, as already confirmed by Sene [53]. Hence, inner core decay is expected to increase accordingly. Ervine and Falvey [42] estimated the inner core decay angle to be 7°− 9° giving Yc/Di= 4. Unfortunately this angle has not been measured due to the presence of large amounts of air bubbles.

As shown in Fig. 2.66, the outlined situation is more relevant to both prototype and large model behaviour. Therefore, in the prototype, a more diffused jet will be apparent and hence the mean dynamic pressure will be less than model predictions. Due to the presence of large amounts of air it is speculated by Ervine and Falvey [42] that the mean dynamic pressure will be reduced. Expressions are derived to determine the mean dynamic pressure with air concentration ($\bar{C}$) taken into account.. The mean centre line dynamic pressure beyond the solid inner core is given by Equation (2.86), noted in Section 2.5, as:

$$\bar{P} \propto (1 - \bar{C})\ 1/2\rho w\ Ui^2\ [16\ (Di/Y)^2] \qquad (2.86)$$

Problems exist with this formulation as it is based on submerged jet diffusion principles which have been partly refuted earlier in the review. The diameter at impact is also contentious, as has been noted, due to its transitory nature. The diameter at impact can be decaying from a jet diameter as small as the plunging jet solid inner core, $d_1 < di$, and can also be decaying from a jet diameter almost as large as the outer jet edges. No exact value can be attributed to a highly turbulent jet. This will result in an oscillating value of Yc which may be much less than 4 di and also much greater than 4 di. However, even though no data is available, as yet, to check this expression, Equation (2.86) may provide a useful first estimate for the mean centre line dynamic pressure.

An investigation of mean and fluctuating pressures at a plunge pool floor, for the case of rectangular jets, is currently under way at Hydraulics Research Ltd., Wallingford [100]. It is hoped that the H.R. Ltd. data will compliment the circular jet results from this thesis. A rig was constructed, Fig. 2.67, where rectangular jets (200mm x 67mm) fall vertically into the plunge pool below. Maximum outlet velocities tested were around 5 m/s. The spillway jets are therefore roughly equivalent to models of 1:50 to 1:80 scale. Measurements of mean and fluctuating pressures were taken at the pool floor via a bank of pressure transducers flush mounted to the pool base plate. By carrying out a systematic testing programme the ultimate aim of the H.R.Ltd. research is to determine a scaling relationship between model and prototype and therefore provide values for stilling basin design.

Initially submerged jet tests were undertaken. Typical pressure results are shown in Fig. 2.68. In this example, with a shallow pool depth (Y ≃ 470mm) relative to the submerged jet diameter, it was found that, as anticipated, the diffusing jet core produced central mean dynamic pressure head values equivalent to the entering velocity head (Ui = 3.17 m/s and 4.48 m/s). The distribution of pressure decreases fairly symmetrically from the central peak value in both directions. Also shown in the figure are the range of pressures that were noted. In this particular test only the difference between the maximum and minimum dynamic pressure heads were recorded and plotted assuming the maximum fluctuations were distributed symmetrically about the mean value. The maximum range of pressure head (Δh = maximum − mean) at the central gauge was found in this way to be approximately 470mm.

Provision has been made in the experimental rig to alter the plunge pool depth and the vertical down pipe could be shortened so that the jet would discharge at a level above the pool surface. Subsequent tests were carried out on free−falling jets. Air was therefore introduced into the pool through natural aeration. Measurements of the turbulence level of the free falling jet and the jet dimensions were taken along with pressures on the floor of the basin. Typical results are shown in Fig. 2.69 where the fall height above the pool surface (L) was around 1.715m and the pool depth (Y) was 585mm. The effect of the aeration, and the slightly increased distance travelled by the jet through the pool, can be seen by comparing the pressures shown in Fig. 2.69 with the results in Fig. 2.68 for the submerged jet. The mean dynamic pressure heads are

considerably lowered. For example, with an outlet velocity (Uo) of 4.24 m/s, a rough calculation, considering the stated fall height, indicates a pool impact velocity (Ui) of approximately 7.2 m/s (neglecting air resistance). The mean dynamic pressure head at the central gauge appropriate to this condition is only around 280mm, in other words it is only around 10% of the impacting velocity head ($Ui^2/2g$). In comparison, the central mean dynamic pressure head for the submerged jet case is roughly equivalent to $Ui^2/2g$. This indicates clearly the significant beneficial effects of the jet plunge in the atmosphere, pool air entrainment and the resulting increased pool mixing on the impact pressures at the plunge pool floor.

Although the free–falling jets produced lower mean pressures than a similar submerged jet, a larger range of pressure variation about the mean is observed. Unlike the submerged jet case, the peaks indicated in Fig. 2.69 are actual maximum and minimum values. As can be seen from these results, the maximum positive fluctuations within the jet were larger than the negative ones by a factor of about 3–4. This suggests strongly that the pressure variations do not follow a symmetrical Gaussian type of probability distribution. The maximum fluctuation above the mean at the central gauge can be seen from Fig. 2.69 to be over one metre head. This is a significantly larger pressure fluctuation than produced by submerged jet diffusion, although the distribution of fluctuations in the submerged case had already been assumed. Finally, regarding the results from spectral analysis for the fluctuations caused by the plunging jet, it was found that most of the energy was of low frequency, up to 10 Hz, with peaks of about 2–4 Hz. It was also found that fluctuations at the edge of the jet (transducer 5B – Fig. 2.69) are larger than in the centre (transducer 3B – Fig. 2.69). An example of the spectra obtained from the centre and edge transducer along with the values of the r.m.s. pressure fluctuations are given in Fig. 2.70.

Another feature of the experimental rig is that provision has been made to add air to the jet at the outlet and hence artificially aerate the jet so that this effect on impact pressures can be investigated; although no results for this condition are included in the report. The report available at this moment is only at a preliminary stage, so no correlation can be formed as yet regarding the influence of free–falling jets and the associated pool air entrainment on the limited pressure results. However, considering the important implications of the preliminary findings, a comprehensive study of this form is necessarily required to

provide information that can be utilised in the design of aprons in plunge pools.

2.9 SCOUR IN NATURAL PLUNGE POOLS.

For stilling basins below free–falling jets where no protective lining is provided, the alternative is usually to allow dissipation through formation of a scour hole. Direct impingement on the bedrock or jet dispersion in the tailwater, if provided, produces dynamic pressure fluctuations on the bed, as detailed earlier. The fluctuations are transmitted into and along fissures promoting break–up of the bedrock. Some of the eroded material is carried away by the flow to form a berm downstream, while the remainder recirculates causing further disintegration of the rock mass and degradation of individual elements. This process of erosion is continued until the ultimate scour depth has been reached. At this point the plunging jet has insufficient energy to further disrupt the bed rock or the rising currents are unable to transport material from the scour hole.

The importance of work on this area to the current research is that the parameters which determine the forces and hence extent of scour have been investigated and are used in prediction of ultimate plunge pool depth. The same parameters are therefore relevant in determining the forces exerted on a fixed boundary within the pool.

Problems arise from the action of jet diffusion in scour holes. Firstly, formation of a bar downstream can substantially increase tailwater levels and hence reduce efficiency of power production and bottom outlets. More importantly, the extent of the scouring can proceed in an unpredictable manner which may require expensive remedial work due to damage to side slopes or by causing a threat to the dam foundation. A well known example of a major scour hole is that at Kariba Dam, see Fig 2.71. Due to more regular use of the spillway at Kariba than had been originally intended, a plunge pool of large extent rapidly developed immediately downstream. By 1981, the scour hole had reached a depth equivalent to almost two thirds of the dam height.

As the pool geometry is constantly changing and the tailwater contains a mixture of water, air and bed material, a theoretical analysis of the scour proves difficult. Model simulation also runs into difficulties regarding geology

representation, however, most work in this area concentrates on experimentation and observation to determine empirical formulae to define ultimate scour depths.

Mason and Arumugam [101] reviewed the accuracy of the formulae that had been produced for scour depths by comparison with model and prototype data. The authors found that when the formulae were tested against a larger amount of data than had previously been considered, the results lost a great deal of accuracy. Also, it was found that formulae which provided good estimates for model scour depths were generally inaccurate for prototype data and vice versa.

The authors therefore produced a formulation which applied most satisfactorily to both model and prototype. The value of ultimate scour depth (De) including tailwater influence (h) was:

$$De = Kq^{x} H^{y} h^{0.15} / g^{0.3} d^{0.1} \qquad (2.126)$$

where : q = Unit discharge
H = Height from reservoir to tailwater level
d = Characteristic particle size (models)
= 0.25m (prototype)
$K = 6.42 - 3.10 H^{0.10}$
$x = 0.60 - H/300$
$y = 0.05 + H/200$

In later work Mason [43] argued that the reasons for inaccuracies in various formulations is that additional factors may not have been taken into account.

As a large variation was found amongst authors over the importance of jet fall height in scour depth calculations, Mason [43] hypothesized that this may be linked to plunge pool air entrainment. Aeration, as noted, is not only a function of fall height but of other factors such as jet dimensions, internal turbulence and impact angle. Therefore, if the effect of air entrainment is not quantified, variable results will necessarily be produced. To this end tests were carried out on a hydraulic model, shown in Fig. 2.72, where air could be introduced in a controlled manner and the volumetric air to water ratio (β), flow (q) and head drop (H) could be varied separately. Establishing the correct amounts of air to be introduced was a fundamental part of Mason's work. The most relevant

expression, similar to Equation (2.112), for sheet or rectangular jets falling vertically was of the form :

$$\beta = 0.13\ (1 - Ue/Ui)\ (H/t)^{0.446} \qquad (2.127)$$

where t is the jet thickness at impact and Ue is the minimum jet velocity required to entrain air, taken as 1.1 m/s from the work of Ervine [102].

Equation (2.127) was used to establish how much air to introduce into the plunge pool in order to simulate how much air a given jet, falling a height H, would entrain naturally. Equivalent jet thicknesses t and velocities Ui were computed in each case from the appropriate values of q and H tested. It was found that measured scour depths were dependent only on q and β with the apparent effects of H recorded in the past being possible due to associated variations of β with H. Expressions were then developed to more accurately estimate scour depths including the variable β rather than H. The resulting expression was :

$$De = 3.39\ \frac{q^{0.6}\ (1+\beta)^{0.3}\ h^{0.16}}{g^{0.3}\ d^{0.06}} \qquad (2.128)$$

Equation (2.128) was shown to apply to a wider body of model test data than previous relationships and also to prototype data. Pool air entrainment has been shown by Mason [43] in his study to be a significant variable in plunge pool scouring.

It is recognised by Mason [43], however, that Equation (2.128) is limited in the sense that the expression used in estimating β only applies to free–falling, near–vertical jets. To further refine equation (2.128), and therefore increase its applicability, the air/water ratio produced in the pool from various alternative spillway configurations, for instance flip buckets, must be considered.

2.10 SUMMARY.

Although plunge pools below overfall spillways in arch dams constitute an important category of energy dissipator, no data up to the present has been available which would enable designers to assess impact pressures on protective aprons. Certain individual aspects of turbulent jet behaviour in the atmosphere and in the plunge pool have been studied, as detailed in this review, but work is needed to unify each of these topics and reduce the subjectiveness of various investigations. Description is required of the spillway flow from outlet to tailwater level through to the plunge pool floor. In particular, there is a need for a systematic study of the magnitude, frequency and distribution of mean and fluctuating pressures generated at base slabs under plunging jets as a function of pool depth and quantity of entrained air. This will provide information to quantify these effects for design and help prevent failures due to the action of this form of loading on the structure.

Therefore, experimentation should be carried out, with apparatus detailed in the following chapter, to determine the relationship between such measured impact pressures and the characteristics of the jet entering plunge pools of various depths. To define the jet condition at impact, investigation of the turbulence propagation of the free-falling jet and the jet dimensions during the plunge is also required. Alteration of the jet condition at impact, and hence the plunge pool diffusion process, with regards to air entrainment mechanism, air concentration etc., is possible by testing a range of pertinent parameters affecting the flow such as outlet velocity, jet fall height and outflow turbulence level. To this end, provision has been made in the experimental rig to allow discharge of the jet at various levels above the pool surface and the turbulence level of the issuing jet can be altered by manipulation of the outlet configuration.

Scale effects can be investigated by testing into the prototype velocity range and with models of various sizes. As a result of the research, relations could be produced to allow estimation of prototype forces for design. The remaining chapters will define the study course, by detailing the experimental apparatus, and evaluate the results from the experimentation.

REFERENCES FOR CHAPTER 2

1. Prandtl, L., "Bericht uber untersuchungen zur ausgebildeten Turbulenz.", ZAMM 5, 136, 1925.

2. Reynolds, O., "On the Dynamical Theory of Incompressible Fluids and the Determination of the Criterion.", Philosophical Transactions of the Royal Society, Vol. 186, 1894.

3. Boussinesq, J., "Theorie de l'ecoulement tourbillant.", Mem. Pre. par. div. Sav. 23, Paris, 1877.

4. Taylor, G.I., "The Transport of Vorticity and Heat through Fluids in Turbulent Motion.", Proc. Royal Society, Vol. A135, 1932, pp. 685–705.

5. Von Karman, T.H., "Mechanische Ahnlichkeit und Turbulenz.", Proc. 3rd Int. Congress Appl. Mech., Stockholm, Pt. 1, 1930.

6. Albertson, M.L., Dai, Y.B., Jensen, R.A., and Rouse, H., "Diffusion of Submerged Jets.", Proc. A.S.C.E., Vol. 74, 1948, pp. 639–663.

7. Pai, Shih.I., "Fluid Dynamics of Jets.", Pub : Van Nostrand Co. Inc., 1954.

8. Davies, J.T., "Turbulence Phenomena.", Pub : Academic Press Inc., 1972.

9. Reynolds, A.J., "Turbulent Flows in Engineering.", Pub : John Wiley and Sons, 1974.

10. Forstall, W., and Gaylord, E.W., "Momentum and Mass Transfer in a Submerged Water Jet.", Jour. Appl. Mech., 22, 2, 1955.

11. Trupel, T., "Zeitschrift fur das gesammte Turbinenwesen.", 5–6, 1915.

12. Corrsin, S., "Investigation of Flow in an Axially Symmetric Heated Jet of Air.", N.A.C.A. Wartime Report, W–94, 1943.

13. Hinze, J.O., and Zijnen, B.G. Van der Hegge, "Transfer of Heat and

Matter in the Turbulent Mixing Zone of an Axially Symmetrical Jet." Jour. Appl. Sci. Res. A1, 1949, pp. 435–461.

14. Wygnanski, I., and Fiedler, H., "Some Measurements in the Self–Preserving Jet.", Jour. Fluid Mech., 38, 1969, pp. 577–612.

15. Schlichting, H., "Boundary Layer Theory." Pub : McGraw–Hill, New York, 6th edition, 1968.

16. Forthmann, E., "Turbulent Jet Expansion." English translation N.A.C.A, TM–789, 1936. (Original paper in German, Ing. Archiv., 5, 1934).

17. Morton, B.R., Taylor, G.I., and Turner, J.S., "Turbulent Gravitational Convection Maintained and Instantaneous Sources." Proc. R. Soc. London, A234. 1956, pp. 1–23.

18. Tollmien, W., "Berechnung Turbulenter Ausbreitungsvorgange.", Z.A.M.M., 6, 1926, pp. 468–478. (English translation, N.A.C.A. TM–1085, 1945).

19. Goertler, H., "Berechnung von Aufgaben der freien Turbulenz auf Grundeines neuen Naherungsansatzes." Z.A.M.M., 22, 1942, pp. 244–254.

20. Reichardt, H., "Gesetzmassigkeiten der freien Turbulenz.", VD1 – Forschungsheft, 414, 1942. (2nd ed., 1951).

21. Abramovich, G.N., "The Theory of Turbulent Jets.", English translation published by M.I.T. Press. Massachusetts, 1963.

22. Hrycak, P., Lee, D.T., Gauntner, J.W., and Livingood, J.N.B., "Experimental Flow Characteristics of a Single Turbulent Jet Impinging on a Flat Plate.", N.A.S.A., TND – 5690, 1970.

23. Corrsin, S., Uberoi, National Advisory Committee for Aeronautics, Technical Note 1865, 1949.

24. Liepmann, H.W., and Laufer, J., "Investigation of Free Turbulent Mixing.", N.A.C.A. Tech. Note 1257, 1947.

25. Wygnanski, I., and Fiedler, H., "Some Measurements in the Self– Preserving Jet." Jour. Fluid Mech., 38, 1969, pp. 577–612. (Ref. No. 14 Previously)

26. Levey, H.C., "The Back Effect of a Wall on a Jet.", geit. f. Angew. Math. Phys., Vol. 11, No. 2, 1960, pp. 152–157.

27. Tani, I., and Komatsu, Y., "Impingement of a Round Jet on a Flat Surface.", Proc. 11th International Congress of Applied Mechanics, Henry Goertler ed., Springer– Verlag, 1966, pp. 672–676.

28. Hausler, E., "Dynamic Water Pressures upon Floors of Stilling Basins Caused by Free Overfall Jets at Dams.", Die Wasserwirtschaft, 56. Jahrgang, Heft 2, 1966.

29. Hausler, E., "Transformation of Energy for a Free– Falling Circular Jet in a Water Cushion." Versuchsanstalt fur Wasserbau, TH Munchen, Report No. 1, Diss., 1962.

30. Poreh, M., and Cermak, J.H., "Flow Characteristics of a Circular Submerged Jet Impinging Normally on a Smooth Boundary.", Proc. of 6th Midwestern Conference on Fluid Mechanics, 1959, pp. 198–207.

31. Beltaos, S., and Rajaratnam, N., "Impinging Circular Turbulent Jets.", Jour. of the Hydraulics Division, A.S.C.E., Vol. 100, No HY 10, 1974, pp. 1313–1328.

32. Davanipour, T. and Sami, S., "Short Jet Impingement.", Jour. of the Hydraulics Division, A.S.C.E., Vol. 103, No. HY 5, 1977, pp. 557–567.

33. Cola, R., "Energy Dissipation of a High Velocity Vertical Jet Entering a Basin.", Proc. of 11th Congress of I.A.H.R., 1.52, 1965.

34. Kamoi, A., and Tanaka, H., "Measurements of Wall Shear Stress, Wall Pressure and Fluctuations in the Stagnation Region Produced by Oblique Jet Impingement.", Proc. DISA Conf., Univ. of Leicester, 1972, pp. 217–227.

35. Ciborowski, J., and Bin, A., "Investigation of the Aeration Effect of

Plunging Liquid Jets.", Inzynieria Chem. (Polish) 2, 1972, pp. 557–577.

36. Kumagai, M., and Imai, H., "Gas Entrainment Characteristics of an Impinging Water Jet.", Kagaku Kogaku Ronbunshu 8, 1982, pp. 1–6.

37. Smigelschi, O., and Suciu, G.D., "Size of the Submerged Biphasic Region in Plunging Jet Systems.", Chem. Eng. Sci. 31, 1976, pp. 1217–1220.

38. van de Sande, E., "Air Entrainment by Plunging Water Jets.", Ph.D. Thesis, Technische Hogeschool Delft, 1974.

39. McKeogh, E.J., "A Study of Air Entrainment Using Plunging Water Jets.", Ph.D. Thesis, Queen's University of Belfast, 1978.

40. Johnson, G., "The Effect of Entrained Air on the Scouring Capacity of Water Jets." 12th Int. Congress of I.A.H.R., Fort Collins, Vol. 3, Paper C26, 1967, pp. 218–226.

41. Tabushi, K., "Air Entrainment and Pressure Distribution in a Circular Tank by Plunging Liquid Jet.", 13th Congress of I.A.H.R., Tokyo, 1969, pp. 81–89.

42. Ervine, D.A., and Falvey, H.T., "Behaviour of Turbulent Water Jets in the Atmosphere and in Plunge Pools." Proc. I.C.E., Part 2, 1987, pp. 295–314.

43. Mason, P.J., "Effects of Air Entrainment on Plunge Pool Scour.", Jour. of the Hydraulic Division, A.S.C.E., Vol. 115, No. 3, 1989, pp. 385–399.

44. Auton, T.R., Sene, K.J., Hunt, J.C.R., and Thomas, N.H., "Entrapment and Transport of Bubbles by Transient Large Eddies in Multi–phase Turbulent Shear Flows.", Int. Conf. on Phy. Mod. of Multi–phase Flow, Coventry, England, 1983, pp. 169–184.

45. Haberman, W.L., and Morton, R.K., "David Taylor Model Basin Report.", 802, 1953.

46. McKeogh, E.J., and Ervine, D.A., "Air Entrainment Rate and Diffusion Pattern of Plunging Liquid Jets.", Chem. Eng. Sci., Vol. 36, 1981, pp.

1161–1172.

47. Bin, A.K., "Comments on Oxygen Transfer in Jet Mixers.", by K. Tojo and K. Miyanami, Chem. Eng. Jour., 26, 1983, pp. 255–57.

48. Bonsignore, D., Volpicelli, G., Campanile, A., Santoro, L., and Valentino, R., "Mass Transfer in Plunging Jet Absorbers.", Chem. Eng. Process, 19, 1985, pp. 85–94.

49. van de Donk, J.A.C., "Water Aeration with Plunging Jets.", Ph.D. Thesis, Technische Hogeschool Delft, 1981.

50. van de Sande, E., and Smith. J.M., "Mass Transfer in a Pool with Plunging Liquid Jets.", Int. Chem. Eng. Symposium "Multi–phase Flow Systems.", Glasgow, 1974.

51. Vigander, S., "Bubbles, Drops and Friction on the Judgement Scale.", Symposium on Scale Effects in Modelling Hydraulic Structures, Paper 5.1, Esslingen, Germany, 1984.

52. Brauer, H., "Grundlagen der Einphasen und Mehrphasen – stromungen.", Verlog–Sauerlander, Aerau und Frankfult am Main, 1971.

53. Sene, K.J., "Aspects of Bubbly Two–phase Flow.", Ph.D. Thesis, Trinity College, Cambridge, 1984.

54. Frizell, K.W., "Model – Prototype Comparison of the Pressure Fluctuations in the Boundary Layer of a High Head Tunnel Spillway.", A.S.C.E. Hyd. Div. Proc. of Int. Symposium, Colorado, 1988, pp. 210–217.

55. Novak, P. (Ed.), "Developments in Hydraulic Engineering.", Elsevier Applied Science, London, 2, Chapter 5, 1984.

56. Hoyt, J.W., and Taylor, J.J., "Turbulence Structure in a Water Jet Discharging in Air.", The Physics of Fluids, Vol. 20, No. 10, Pt. 11, 1977.

57. Mullin, T., "Chaos in Turbulent Flows.", Dept. of Physics, University of

Oxford, 1989.

58. Rayleigh, J.S.W., Phil. Mag., Vol. 34, p. 145, 1892.

59. Weber, K., Z. agnew. Math. Mech., Vol. 11, p. 136, 1931.

60. Haenlein, A., N.A.C.A. Tech. Memo., No. 659, 1932.

61. Smith, S.W.J., and Moss, H., Proc. Royal Soc., Series A, Vol 93, 1917, pp. 373–394.

62. Grant, R.P., and Middleman, S., "Newtonian Jet Stability.", A.I.Ch.E. Journal, Vol. 12, No. 4, 1966, pp. 669–678.

63. Ervine, D.A., "A Review of Bubbly and Air Pocket Flows in Civil Engineering Hydraulic Structures.", Series of Lectures Presented to the United States Bureau of Reclamation, Denver, 1985.

64. Chen, T–F., and Davis, J.R., "Disintegration of a Turbulent Water Jet.", Jour. of the Hydraulics Division, A.S.C.E., Vol. 90, No. HY1, 1964, pp. 175–206.

65. Baron, T. Tech. Rept. University of Illinois, No. 4, 1949. (Prepared under contract N–6–ORI–71, Task order No. XI, ONR Navy Dept.).

66. Horeni, P., "Disintegration of a Free Jet of Water in Air.", Byzkumny ustav vodohospodarsky prace a studie, Sesit 93, Praha – Podbaba, 1956.

67. van de Sande, E., and Smith, J.M., "Jet Break–up and Air Entrainment by Low Velocity Turbulent Water Jets.", Chem. Eng. Sci., Vol. 31, 1976, pp. 219–224.

68. McCarthy, M.J., and Molloy, N.A., "Review of Stability of Liquid Jets and the Influence of Nozzle Design.", Chemical Engineering Journal, Vol. 7, 1974, pp. 1–20.

69. Ervine, D.A., McKeogh, E., and Elsawy, E.M., "Effect of Turbulence

Intensity on the Rate of Air Entrainment by Plunging Water Jets.", Proc. Instn. Civ. Engrs., Part 2, 1980, pp. 425–445.

70. Bin, A.K., "Air Entrainment by Plunging Liquid Jets.", Symposium on Scale Effects in Modelling Hydraulic Structures, Esslingen, Germany, Paper 5.5, 1984.

71. Cumming, I.W., "The Impact of Falling Liquids with Liquid Surfaces.", Ph.D. Thesis, Loughborough University of Technology, 1975.

72. Henderson, J.B., McCarthy, M.J., and Molloy, N.A., "Entrainment by Plunging Jets.", Proc. of Chemeca'70, Melbourne, Sec. 2, 1970, pp. 86–100.

73. Thomas, N.H., "Research Report to C.E.G.B.", Department of Applied Mathematical and Theoretical Physics, Cambridge, 1978.

74. Ervine, D.A., and Elsawy, E.W., "The Effect of a Falling Nappe on River Aeration.", Proc. 16th Congress I.A.H.R., Brazil, Paper C45, 1975.

75. Mason, P.J., "Energy Dissipating Crest Splitters for Concrete Dams.", Water Power and Dam Construction, 1983, pp. 37–40.

76. Working Group, French Committee on Large Dams, "Quelques problemes particuliers poses par les deversoirs a grande capacite : tapis de protection, dissipation d'energie par deflecteurs et aeration et cavitation produite par les ecoulements a grande vitesse." 13th I.C.O.L.D., New Delhi, Q50, R38, 1979, pp. 649–673.

77. Bowers, C.E., and Toso, J.W., "Karnafuli Hydroelectric Project, Hydraulic Model Studies of Spillway Damage.", Proc. of the Speciality Conference, Hydraulics and Hydrology in the Small Computer Age, Hyd. Div./ A.S.C.E., 1985, pp. 1136–1141.

78. Toso, J.W., "The Magnitude and Extent of Extreme Pressure Fluctuations in the Hydraulic Jump.", Ph.D. Thesis, University of Minnesota, 1986.

79. Nezu, I., and Rodi, W., "Open Channel Flow Measurements with Laser Doppler Anemometer.", J. Hyd. Eng., A.S.C.E., 112, 1986, pp. 335–355.

80. Minami, I., and Aki, S., "A Consideration on the Supervision of a Concrete Arch Dam in the Flood Time.", 10th I.C.O.L.D., Montreal, 938, R8, 1970, pp. 113–190.

81. Locher, F.A., "Some Characteristics of Pressure Fluctuations on Low–ogee Crest Spillways Relevant to Flow–induced Structural Vibrations.", U.S. Army Engineers Waterways Experiment Station, Vicksburg, Contract Report No. H–71–1, 1971.

82. Rajaratnam, N., "Hydraulic Jumps.", Adv. in Hydro. Science, Vol. 4, Academic Press, (ed. V.T. Chow), 1967.

83. Akbari, M.E., Mittal, M.K., and Pande, P.K., "Pressure Fluctuations on the Floor of Free and Forced Hydraulic Jumps.", International Conf. on the Hyd. Modelling of Civ. Eng. Structures, B.H.R.A. Fluid Eng., Coventry, Paper C1, 1982, pp. 87–96.

84. Vasiliev, O.F., and Bukreyev, V.I., "Statistical Characteristics of Pressure Fluctuations in the Region of Hydraulic Jump.", Proc. of 12th Congress of I.A.H.R., Vol. 2, Colorado, 1967, pp. 1–8.

85. Schiebe, F.R., and Bowers, C.E., "Boundary Pressure Fluctuations due to Macroturbulence in Hydraulic Jump.", Proc. of Symposium on Turbulence in Liquids, University of Missouri – Rolla, 1971, pp. 134–139.

86. Narasimhan, S., and Bhargava, V.P., "Pressure Fluctuations in Submerged Jump.", Jour. of Hyd. Div., A.S.C.E., Vol. 102, No. HY3, 1976, pp. 334–350.

87. Rouse, H., Siao, T.T., and Nagaratnam, S., "Turbulence Characteristics of the Hydraulic Jump." Trans. A.S.C.E., Vol. 124, 1959.

88. Mansoori, A., "Turbulent Velocity and Pressure Fluctuations Occuring in Water at a Sudden Enlargement.", Ph.D. Thesis, King's College, London, 1988.

89. Lopardo, R.A., De Lio, J.C., and Vernet, G.F., "Physical Modelling on Cavitation Tendency For Macroturbulence of Hydraulic Jump." International Conference on the Modelling of Civil Eng. Structures, Coventry, Paper C3, 1982,

pp. 109–121.

90. Thomas, A.R., and Lean, G.H., "The Vibration of a Submerged Wall Subjected to a Jet.", Proc. 10th Congress of I.A.H.R., London, Vol. 3, 1963, pp. 89–100.

91. Lopardo, R.A., Orellano, J.A., and Vernet, G.F., "Baffle Piers Subjected to Flow–induced Vibrations.", Proc. 17th Congress of I.A.H.R., Baden–Baden, Vol. 3, 1977, pp. 445–452.

92. Hinze, J.O., "Turbulence.", Pub. McGraw Hill, New York, 1959.

93. King, D.L., "Hydraulic Model Studies for Morrow Point Dam.", U.S.B.R, Engineering Monograph No. 37, 1967.

94. King, D.L., "Supplemental Tests of Morrow Point Spillway, Stilling Basin and Powerplant Tailrace.", U.S.B.R. Report No. HYD–586, 1969.

95. Lemos, F.O., and Ramos, C.M., "Hydraulic Modelling of Free Jet Energy Dissipation.", Symp. on Scale Effects in Modelling Hydraulic Structures, I.A.H.R./D.V.W.K., Esslingen, Paper 7.6, 1984.

96. Bhargava, D.N., Rajput, A.S., and Tiagi, S., "Energy Dissipation through Diffusion of Jets and Air Entrainment – Model Simulation.", Symp. on Scale Effects in Modelling Hydraulic Structures, I.A.H.R./D.V.W.K., Esslingen, Paper 7.7, 1984

97. King, D.L., "Analysis of Random Pressure Fluctuations in Stilling Basins.", Proc. 12th Congress of I.A.H.R., Colorado, 1967.

98. Hartung, F., and Hausler, E., "Scours, Stilling Basins and Downstream Protection Under Free Overfall Jets at Dams.", International Commission for Dams, Q.41, R.3, Madrid, 1973, pp. 39–56.

99. Lencastre, A., "Free Overflow Spillways.", Engineering and Design Principles, National Laboratory for Civil Engineering Studies, Report No. 174, Lisbon, Portugal, 1961.

100. Contract No. DGR PECD 7/6/29–204/83, "Impact Pressures in Falling–jet Energy Dissipators.", Hydraulics Research Limited, Report No. SR 124, April, 1987.

101. Mason, P.J., and Arumugam, K., "Free Jet Scour below Dams and Flip Buckets.", Jour. of Hyd. Div., A.S.C.E., Vol. 111, No. 2, 1985, pp. 220–235.

102. Ervine, D.A., "The Entrainment of Air in Water.", Int. Water Power and Dam Construction, 28 (12), 1976, pp. 27–30.

CHAPTER 3

DIMENSIONAL ANALYSIS AND EXPERIMENTAL APPARATUS

CONTENTS

3.5.4 Spatial and temporal resolution.

3.5.5 Mounting the pressure transducers.

3.5.6 Calibration of the pressure transducers.

3.5.7 Signal conditioning.

3.6 DATA ACQUISITION SYSTEM

3.6.1 Introduction.

3.6.2 Acquisition hardware.

3.6.3 Data quantification.

3.6.4 Computer interface and specification.

3.6.5 Software.

3.6.6 Sampling routine.

3.6.7 Data acquisition capacity.

3.6.8 Data qualification.

3.6.9 Special routines.

3.7 DATA STORAGE AND PROCESSING

3.7.1 Introduction.

3.7.2 The Probability Density Function.

3.7.3 The Power Spectrum.

3.7.4 Graphical representation.

CHAPTER 3

3.1 INTRODUCTION

There is a lack of knowledge regarding flow behaviour at plunge pool energy dissipators, and hence the objective of this research is to investigate the fundamental flow behaviour of such dissipators by means of a physical modelling experimental programme. The main purpose of the experimental programme is to determine the magnitude and frequency range of pressure fluctuations generated at the solid floor of a plunge pool stilling basin due to the action of an impinging jet, although determination of the mean pressures is also important. Subsidiary characteristics of interest include the propagation of turbulence within free falling spillway jets, the rate of jet expansion in the atmosphere, the mechanism of jet break–up as it plunges through the atmosphere and an investigation into scale effects involved in modelling such physical situations.

To accomplish these aims, a test rig was constructed to produce water jets which would fall freely through the atmosphere and impinge on a pool below. Measurements of instantaneous velocity and pressure were required to determine the level of turbulence in the free–falling jet and the magnitude of pressure fluctuations generated at the pool base. Acquisition of the required data was facilitated by use of a microcomputer linked to measurement devices located in the floor of the plunge pool and in the plunging jet. An additional feature of this study is the software that was utilised to control the data acquisition process and assist in data analysis.

3.2 DIMENSIONAL ANALYSIS

The introduction in Chapter 1 and various sections of Chapter 2 will already have convinced the reader of the very complex nature of impinging jet spillways. The flow behaviour will be dependent to a large extent on the type of outlet device used, the flow conditions at the outlet device, conditions during the jet plunge through the atmosphere as well as conditions in the plunge pool after the point of impingement.

A list of seventeen independent parameters is given below, highlighting the

great difficulty in providing a comprehensive experimental programme, in the time available, to cover every possible scenario. A judicious choice must be made at the start of the research programme as to which are likely to be the most important parameters.

The seventeen independent parameters were chosen based on an initial physical understanding of the flow mechanisms. Between them, they will determine the magnitude and extent of dependent variables such as pressures, velocities, turbulence levels, rate of air entrainment, jet spread, jet break–up, conditions in the plunge pool and scale effects. Some of the physical parameters are shown in Fig. 3.1.

INDEPENDENT PARAMETERS

Geometry of outlet device

L_0	length of upstream nozzle
Φ_0	angle of nozzle convergence
θ_0	angle to horizontal
K_s	boundary roughness
b_0	width of opening
d_0	depth of opening

Flow conditions at outlet device

$\bar{U}_0$	velocity
ρ_w	density
μ_w	viscosity
σ	surface tension

Flow conditions in the atmosphere

L	vertical droplength
ρ_a	density ambient air
μ_a	viscosity air
g	gravity

Plunge pool

Y	plunge pool depth
B_1, B_2	plan dimensions of plunge pool

A dimensional analysis revealed that the conditions in the plunge pool could be described by the relationship,

$$[\text{Conditions in plunge pool}] = f\,[\,\underbrace{L_0/d_0,\ \Phi_0,\ \theta_0,\ K_s/d_0,\ b_0/d_0,}_{\text{upstream geometry}}$$

$$\underbrace{Re_0,\ We_0,}_{\text{flow conditions at nozzle}}\qquad \underbrace{Fr_0,\ L/d_0,\ \rho_a/\rho_w,\ \mu_a/\mu_w,}_{\text{flow conditions through atmosphere}}$$

$$\underbrace{Y/d_0,\ B_1/d_0,\ B_2/d_0\,]}_{\text{plunge pool conditions}} \qquad (3.1)$$

In view of this complexity it is important to review each parameter in turn, commenting on its relative importance, whether it should be varied or not, and which possible simplifications might be made.

Considering each non–dimensional parameter in turn:

– θ_0 refers to the angle of the outlet jet to the horizontal direction. It was decided to keep this value constant at 90^0 (vertical) for all tests. The reason for this concerned the fact that tests were carried out in the laboratory covering both the model and prototype range of velocity. Accepting that most prototype jet spillways have a horizontal (0°) outlet, restrictions on laboratory space did not permit horizontal outlet velocities in the prototype range. In any case it was felt that most jet spillways impinge on the plunge pool near vertical, so the constant vertical orientation was adopted. Vertical orientation is also convenient in the locating of pressure transducers on the plunge pool floor.

– Φ_0. It was decided initially to use gradually converging nozzles to produce the vertical jet. These will be described in detail in Section 3.3.2. The convergence

angle of the nozzles Φ_0 was kept constant at 7^0 to avoid flow separation along the length of the nozzle. Three nozzle diameters were used throughout the tests, namely 78mm, 52.5mm and 25mm.

It was generally recognised at an early stage in this research that the level of turbulence generated in the issuing jet would have a significant effect on dependent parameters such as jet spread in the atmosphere, jet diameter at the point of impact, jet break–up, air entrainment and eventually pressures in the plunge pool. It was also recognised that an orifice plate might generate greater turbulence intensities in the issuing jet than the nozzles. Thus it was decided to carry out tests with an orifice plate (diameter 25mm). This in effect is an angle Φ_0 of 90^0 (angle of convergence). Therefore two values of Φ_0 were employed, 7^0 and 90^0, representing the range of behaviour of outlet devices at a dam.

– K_s/d_0 refers to the non–dimensional sand grain roughness of the inner pipe and nozzle wall. For all experiments carried out, a smooth PVC pipe was used upstream of the nozzle or orifice, and the nozzles themselves were constructed of perspex and aluminium, ground and polished to give a K_s value near zero. Thus, the K_s value was not varied in these experiments and even though d_0 varied between 25mm and 78mm, the ratio of K_s/do was more or less constant. Tests at the U.S.B.R. in Denver, Colorado, have already shown from ramp aerators that the value of K_s affects both the turbulent velocity U' and also the boundary layer thickness δ_0. In this set of experiments the effect is negligible.

– b_0/d_0 refers to the aspect ratio of the emerging jet. In this set of experiments it was decided to keep the ratio constant at unity, for circular jets. It is clear that the aspect ratio has considerable effect on the spread of jets. This is shown in Fig. 3.2, describing the rate of spread of plunging jets at Morrow Point Dam for various aspect ratios. It appears that the rate of jet spread may be a maximum for aspect ratios of the order of 2. Also, it was known at the commencement of this research work that tests on rectangular jets were in progress at H.R. Ltd. Wallingford as well as U.S.B.R. Denver, Colorado, so it was decided to opt for the simpler circular shape.

In any case, most rectangular jets tend towards a circular shape during their plunge through the atmosphere, and at the point of impact may appear more circular than rectangular.

– L_0/d_0 refers to the non–dimensional length of the upstream nozzle and pipe system. Clearly a very long pipe and nozzle will ensure a fully developed boundary layer at the exit to atmosphere which in turn will produce greater turbulence intensities, shorter break–up length and lower mean pressures in the plunge pool. At the other extreme a very short nozzle exiting from a large tank will produce a thin boundary layer at the exit to atmosphere, a solid more laminar, inner jet core, a longer break–up length and hence higher mean pressures in the plunge pool. Prototype structures usually relate more to short nozzles and thin boundary layers.

In this set of experiments the nozzle lengths were kept approximately constant and the value of L_0/d_0 did not vary over a significant enough range. For the lower level tests with short droplength in the atmosphere, a longer length of PVC pipe was used at the upstream end of the nozzle (see Section 3.3.3) effectively ensuring that initial boundary layer thickness δ_0/d_0 was greater for the lower level tests than the higher level tests. It proved extremely difficult to separate this effect out of the test results, because it also coincided with large variations in the droplength through the atmosphere L/d_0.

– Re_0, the Reynolds Number at the exit nozzle is known to be significant and was varied in this set of experiments from approximately $6x10^4$ to $1.0x10^6$ determined from the range of diameters 25–78mm and the range of velocities from 1.5m/s to 25m/s.

The effect of Reynolds Number means that at higher Reynolds Number of flow at the nozzle/orifice, the flow becomes more turbulent, the jet has a greater angle of spread in the atmosphere, smaller eddy lengths have greater turbulent energy hence causing a more fine–grained surface structure and more free surface aeration. This is seen very clearly in photographs, Figs. 3.3 and 3.4, taken from Reference [1], showing the same jet at two different Reynolds Numbers of $4x10^5$ and $2x10^6$. Of course it should also be noted that the Weber Number of the flow has also increased in these two photographs roughly from 185 to 925, showing that the restraining influence of surface tension is relatively much less in the second photograph.

The Reynolds Number at exit is known to have significant effect on jet break–up length [2], [3], [4] and [5] and in the case of Horeni [6] is considered

to be the only significant variable.

It is also considered to have a significant effect on the core length of the jet once entered into the plunge pool [1], on the turbulent energy spectrum of eddies within the plunge pool and also the mean dynamic pressures on the plunge pool floor, as described by Hausler [7].

– We_0, the Weber Number at the exit nozzle is also known to be significant in the sense that it determines the degree of restraint on the turbulent velocities within the plunging jet, the break–up length of the plunging jet and also the degree of aeration.

In this set of experiments the Weber Number was varied over the range 50 to 450 which represents a very large variation of surface restraint. Considering the jet break–up length, for instance, Chen and Davies [8] have shown an almost linear increase in break–up length with Weber Number in the range of 50 to 250. Considering air entrainment, Pinto has shown a linear increase in aeration with Weber Numbers up to 500 albeit with the Weber Number based on jet length rather than jet thickness. Substituting typical jet lengths for Pinto's work of $L/d \approx 10$, we obtain Weber Number influence up to around 150, when based on the jet thickness.

Thus it is clear that Weber Number is significant in this work, probably up to around 150–200, which covers a significant proportion of the data.

One of the problems of incorporating the Reynolds Number and the Weber Number together in any correlation is that it is usually only possible to separate their influence by using different fluids with different values of surface tension and viscosity. The reason for this is obvious. If only velocity and jet diameter are used to vary the Reynolds Number, then the Weber Number changes as well. The process of using different fluids has not been carried out in these experimental tests.

– Fr_0, the Froude Number, refers to the influence of gravity on the jet behaviour. In the tests carried out in this experiment the Froude Number varied approximately in the range 1.7 to 50. For jets issuing horizontally, gravity affects the entire jet trajectory. This is not the case for vertical jets. For

vertical jets acceleration under the effect of gravity, the jet diameter will decrease, particularly for low turbulence jets at low velocity. Thus, gravity has a significant effect on determining jet conditions at the point of impact and thus, the Froude Number needs to be included. In fact, the Froude Number (gravitational influence) would only be excluded for vertical high velocity jets with shorter droplengths.

Further downstream, gravity may have some influence in the plunge pool as well, through the formation of free surface waves on the plunge pool surface which will be picked up by pressure transducers on the plunge pool floor as very low frequency oscillations. This phenomenon has already been reported by Danny King [9].

– L/d_0, the droplength through the atmosphere is considered to be a very significant term. Simply stated, any processes which are started at the nozzle area (such as turbulence, jet spreading, inner core decay, jet break–up, aeration, etc.) will develop (increase or decrease) during the fall length L, and hence the value of L will determine the difference between conditions at the nozzle and conditions at impact. Thus, if the parameters are referred back to the nozzle using U_0 and d_0, then inclusion of L/d_0 is imperative in determining impact conditions into the plunge pool which then determines all that happens in the plunge pool itself. In these experiments L/d_0 was varied from 10 to 100, covering most of the existing prototype range.

– ρ_a/ρ_w , represents the difference in density between the jet and the ambient surrounding atmosphere. In these tests the parameter was kept constant by using air and water at a reasonably constant temperature of 65°F.

– μ_a/μ_w, representing the different viscosities between the jet and the surrounding ambient atmosphere, again was not varied in the experimental test runs.

– Y/d_0 is the non–dimensional plunge pool depth and is perhaps the most important parameter in determining the mean and fluctuating pressures on the plunge pool floor.

The behaviour of jets in a water cushion has already been described in

detail in Section 2.4. This cited section has highlighted the importance of the zone of flow establishment where a decaying inner core is thought to exist, as well as the zone of established flow with its steady decay in velocities and hence mean pressures. The plunge pool depth (for vertically impinging jets) therefore represents how far along the zone of flow establishment, and decay, the pressure transducers are situated.

The same is true for pressure fluctuations, which stem in turn from turbulent fluctuations in the flow. In the zone of flow establishment turbulence is being transmitted towards the inner core reaching a peak, at least for the case of the jet centre line, at a point just beyond the start of the zone of established flow (Y/d approx. 5−10). Beyond this point, the centre line jet turbulence decays. It is clearly seen that the plunge pool depth will also have a major effect on the magnitude of pressure fluctuations existing.

The same argument is also put forward for the air bubble concentrations in the plunge pool. Air is entrained at the impact point and diffused in the shear layer. Each air bubble is subject to various forces such as drag force causing it to descend into the plunge pool, vorticity forces causing the air bubble to become trapped in coherent structures in the plunge pool shear layer, and also buoyancy forces causing the air bubble to return to the free surface. The first two forces decrease with depth into the plunge pool, whereas the buoyancy force remains more or less constant, thus reducing the air concentration with increasing depth into the pool.

It is clear therefore that the plunge pool depth is a most important parameter with regard to the magnitude of pressures experienced. The same argument might by advanced for the frequency of pressure fluctuations. This is based on the simple premise that the eddy mixing length increases in the downstream direction in a shear layer, proportionately to the shear layer width. Large eddies produce lower dominant frequencies and hence deeper plunge pools may reduce the frequency at which peak power is experienced.

– B_1/d_0, B_2/d_0, represent the plan dimensions of the plunge pool. In the case of these experiments B_1 remained constant at 1.22m and B_2 remained constant at 1.84m. For outlet diameter, d_0 varying from 25mm to 78mm, the values of B_1/d_0 and B_2/d_0 varied over the total range 16 to 74. The range seems large

but in fact even the smallest case of $B/d_0 = 16$ effectively represents a very large pool size compared with the jet dimension. In other words, in terms of plan area, the jet was unconfined for all tests and not subject to much influence from plunge pool walls.

At this stage we may omit from Equation (3.1) the parameters which were either not varied, or were thought to be not very significant, producing a new non-dimensional expression for conditions at the plunge pool floor in the form,

$$(\text{Condition at plunge pool floor}) = f(\Phi_0, Re_0, We_0, Fr_0, L/d_0, Y/d_0) \qquad (3.2)$$

This reveals that the main parameters to be varied are, plunge pool depth Y, jet droplength L, jet diameter d_0, jet velocity U_0 and arrangement of outlet device Φ_0. It was decided to vary all five parameters, with the jet velocity U_0 varying from the model into the prototype range.

3.3 THE EXPERIMENTAL APPARATUS

3.3.1 General layout and discharge measurement

The experimental apparatus was constructed at the University of Glasgow and is shown in detail in Fig. 3.5. In this figure access scaffolding and the supporting framework is omitted for clarity. Manometers used in flow measurement are similarly omitted. Photographs of the general layout are also shown in Figs. 3.6 and 3.7.

Basically the apparatus consists of a recirculating flow system. A high head pump delivers the flow at rates over 60 l/s (0.06 m^3/sec), to the outlet nozzles (or orifice), and at that point the flow enters into the atmosphere. The outlets tested consisted of smooth tapered nozzles of various diameters. In later tests an orifice was substituted in place of a nozzle in an attempt to produce a larger range of jet turbulence. The jets of water produced at the outlet fall vertically through the atmosphere into a tank below, which simulates the plunge pool.

Connected to the plunge tank is a sump tank which supplies flow back to the pump for recirculation.

Before reaching the outlet nozzles, the flow passes through a flow straightener to eliminate swirl in the flow produced along the pipe and particularly at the final 90^0 bend in the pipework. The flow straightener is of the tube bundle (Type C) form and is designed in accordance with B.S. 1042 [10]. Flow measurement was by means of an orifice plate with D and D/2 tappings, again designed according to the guidelines in B.S. 1042. To minimise head loss in the system the maximum diameter ratio for the orifice (0.75) was selected. To cover the range of flow rates required for testing, the associated manometer system comprised of two elements. At low flow rates a water/air manometer was employed to ensure an adequate head difference between manometer limbs while at high flow rates, mercury was utilised as the manometer fluid, thus eradicating the requirement of a large manometer system.

The physical constraints of the apparatus did not allow the required number of pipe lengths upstream and downstream of the orifice plate, as specified in B.S. 1042. Therefore, the theoretical head–discharge relationship could not be relied upon. An experimental calibration of the orifice plate was therefore carried out to obtain the actual correlation between the head difference at the manometer system and the flow through the orifice plate.

The orifice plate calibration was accomplished by taking point velocity measurements over the cross section of the various outlet jets using a 6mm outside diameter Pitot–static tube, which had been previously tested for reliability. By integrating the point velocity readings over the area of the outlet jet, the flow rate could be calculated and related to the measured head difference at the manometers. Fig. 3.8 shows the experimental calibration compared with the theoretical head–discharge relationship from B.S. 1042. The calibrated orifice was then used to determine the mean velocities at the outlet during testing. At extremely low flow rates it should be noted that an accurate head reading was not possible, even from the water manometer, and the Pitot–static tube was used directly to determine the outlet velocity into the atmosphere. The calibration equation for the orifice plate (best fit) was $Q = 0.139 \sqrt{\Delta h}$ (mercury manometer).

Flow control was attained by means of a gate valve situated just above the pump. The resulting outlet velocity ranged from 1.5 m/s up to 25 m/s, for the smallest outlet diameter tested, covering the model/prototype range. The pump itself was insulated from the laboratory floor by use of rubber packs thus reducing transmission of vibration to the tank system and ultimately to the plunge pool floor.

3.3.2 Outlet nozzles and outlet orifice

At the commencement of the research work, three conical outlet nozzles were fabricated from rolled plate. The rolled plate had been worked into tapered pieces and butt welded at the seam to produce the complete conical nozzle section. Three separate nozzles were constructed, each 500mm long, which in turn reduced from the pipework diameter of around 150mm to 75, 50 and 25mm diameter nozzles. The outlet diameters were selected in multiples to allow estimation of scale effects between small and larger scale models. At the 150mm pipe end, an eight hole flange (B.S.10: Table E) was welded to the nozzle to allow connection to the pipework.

During preliminary testing, the original outlet arrangement proved inadequate. This became most apparent when testing the smallest outlet (1"). The butt weld at the nozzle seam produced uneven flow conditions and the issuing jet was not of a uniform nature. The welding process also caused a slight deviation from the circular shape of the nozzle at the outlet. The end result was erratic behaviour of the jet as it issued into the atmosphere, also causing problems during the calibration of the flow measuring orifice plate. A totally different fabrication system was therefore required to ensure proper operation of the outlet nozzles.

It was decided to form the nozzles from solid material, at the University of Glasgow workshops. To save material, the nozzles were machined so that they could be used as extension pieces. The largest portion consisted of a tapered perspex piece from 152mm internal diameter to 78mm at the outlet. This size of outlet thus represented the largest jet tested. The remaining portions were fabricated from aluminium and acted as reducing pieces, connected in series to the perspex portion. The resulting outlet diameters were 52.5mm and 25mm. The final nozzle arrangement including dimensions is shown in Fig. 3.9. A general view of the nozzle attached to the pipework is also shown in Fig. 3.10.

Due to the machining process greater control could be exercised in the quality and finish of the completed nozzles. The inner bore was machined to a constant 7^0 taper and the internal surface finish was made as smooth as possible. Circularity was ensured and all burrs and rags were removed by fine machining. The system, when tested, proved to be very efficient. A combination of the tube bundle flow straightener upstream, the gently tapering smooth nozzle and the favourable pressure gradient produced by the nozzle resulted in a jet which was of a very smooth turbulent form, even at high velocity.

In order to investigate the effect of increasing the turbulence level of the issuing jet, an alternative outlet arrangement was designed. The solution was to provide a sudden reduction in the flow area. This was achieved by the use of a 25mm diameter orifice plate attached directly to the 152mm (6 inch) diameter pipework. Just downstream of the orifice outlet, the jet was of a glassy nature due to the restraining contraction that was formed. However, beyond this point a jet with a far rougher form than that achieved using smooth nozzles was apparent. A section through the orifice and the outlet support is shown in Fig. 3.11.

3.3.3 Pipework extension pieces

To enable a variable fall height of the jet from the outlet to the plunge pool level (and hence allow investigation of the effect of this parameter on the pressure fluctuation level), the vertical pipework section above the plunge tank had to be of adjustable length. Pipework extension pieces were fabricated and connected to the existing 90^0 bend to satisfy this requirement. This is shown in Fig. 3.5. The outlet arrangement would then connect directly to the pipework extensions. For stability, additional supports had to be provided along the vertical pipework length and a substantial connection was required at the outlet to prevent the nozzles or orifice from pulling away from the pipework, due to the large momentum change. The jets could subsequently be discharged at a large fall height, with the outlet situated just after the pipework bend, or alternatively, with the extension pieces, at a small distance above the pool. Knowing the precise fall height and the average outlet velocity, an estimate of the impact velocity at plunge pool level can be made. For vertical jets, only a small discrepancy will be incured by neglecting air resistance in this calculation. Thus, the jet impact velocity is approximated as $Ui = (Uo^2 + 2gL)^{1/2}$.

Without pipe extensions, the maximum droplength was available and was determined by the plunge pool depth and the nozzle outlet under consideration. For the 25mm nozzle outlet, the maximum drop length was around 2.5m, giving the largest droplength to outlet diameter ratio (L/Do) of approximately 100. The purpose of providing such a large droplength, relative to the outlet diameter, is that the impinging jet will be wither partially or fully disintegrated during the fall, depending on the turbulence level and outlet velocity. As the maximum amount of air is entrained into the pool when the impinging jet is in this condition, then the greatest effect of air bubble action can be evaluated.

The maxium reduction in fall height was made possible by utilising all three extension pieces. The pieces were each 500mm long and when assembled together the total fall height was reduced by 1505mm, including gaskiets. When fitted, the smallest ratio of fall height to outlet diameter tested was approximately 9. Therefore, the range of most prototype jet conditions, with respect to full height, were largely covered.

Although little is known of the pressure fluctuations produced due to submerged jet diffusion, results for a fall height of zero were not considered. This was one area where a great deal of research had been carried out into mean flow characteristics but, as has been pointed out, its application was limited with respect to impinging jet dissipators. Zero fall height would correspond more closely to submerged bottom outlets from dams.

3.3.4 Base plate arrangement

The purpose of the base plate was to provide a floor to carry the flush-mounted pressure transducers. The transducers will be described in detail in Section 3.5. This section will detail the base plate arrangement. Fig. 3.12 shows a plan and section of the base plate which was situated in the plunge tank to simulate the stilling basin floor. Due to the axi-symmetric nature of the diffusion pattern, it was necessary to take pressure measurements only along one plane radiating from the jet axis. The central measurement point was located below the jet centre line and the remaining pressure transducer positions emanated in a row from the central location. The distribution of pressure on the level base plate surface could then be determined from the readings at the

various locations, each 100mm apart, in the radial direction. Pressures values were registered by pressure transducers that were flush–mounted to the base plate through a stainless steel insert piece.

To prevent resonance conditions developing due to the pressure fluctuations generated at the pool base, all of the base plate components were carefully designed. The choice of one inch thick marine plywood for the base plate itself is an example. Rigidity of the base system was ensured by supports below the plate not readily apparent in Fig. 3.12 (Plan). The base plate was supported at the edges with 25mm diameter steel rods and was propped at the central portion to the tank floor by a framework of 20mm square hollow stainless steel sections attached to the underside of the plate.

The support system had two purposes. Firstly, to allow movement of the base plate thereby achieving proper alignment with the impinging jet, and secondly, to ensure when fully clamped that the plate would not vibrate due to the impacting jet action. Base plate alignment was required, as it proved very difficult to ensure that the jet impinged exactly orthogonally on the plunge pool surface and exactly on the centre of the central pressure transducer. If the jet trajectory deviated from the vertical by even a minute angle, then over a large jet fall height this could account for a discrepancy between the actual impact position and the theoretical plumb point at the centre of the central pressure transducer. This discrepancy was accounted for by observations during preliminary testing of each outlet. The actual jet impact point at the base plate was located and the base plate was accurately positioned over the edge supports so that the centre of the impact point would coincide with the central measurement transducer. Once this was successfully carried out, the base plate was clamped rigidly in place at the supports. Levelling feet on the vertical legs of the central framework ensured that any disparity in the tank floor could be accomodated, and provided a direct support to the base of the plunge tank.

The natural frequency of the base plate set–up was therefore much higher than envisaged for the dominant frequencies of pressure fluctuations in the plunge pool and hence the possibility of a resonant condition for the base system was eradicated. This was checked by measurement of base plate movement under loading conditions.

3.3.5 Plunge pool depth measurement

The plunge pool depth (Y) above the level surface of the base plate was set during testing operation by means of an outlet valve at the bottom of the sump tank and a water level indicator at the corner of the plunge tank. A small stilling box was constructed around the inlet to the tapping of the pre–calibrated water level gauge, to damp out waves and variations in the pool surface, and to prevent air bubble entry. A view of the water level indicator is given in Fig. 3.13. The water level indicator gives a value of the mean pool depth above the plunge pool floor. The plunge pool depth was varied from 0–500mm, in four increments, to simulate a range of tailwater values. The maximum ratio of plunge pool depth to outlet diameter (Y/Do) tested was 20. Considering circular submerged jet diffusion, a value of pool depth around 20 impact diameters is thought sufficient to fully dissipate the incoming energy, Hausler [11]. Therefore, the maximum value of (Y/Do) tested should fully define the range of impact pressures generated at the pool floor.

Some problems emerged with the water level measurements during testing. As the indicator was set at the corner of the plunge tank, then the recorded plunge pool depth was not exactly equal to the actual water depth at the jet impact point. For example, with a shallow pool depth of 100mm set by the depth recorder gauge and with a large diameter and high velocity jets, then the water cushion was made ineffectual at the impact point. A radial hydraulic jump was formed and the jet impacted directly with the base plate. In other words at the impact point the pool depth was actually zero.

As another example, under specific flow conditions, the tank boundaries would effect the impact region and surface vortices would form. This caused a drawdown of the water level at the impact point which was not registered at the indicator.

These problems were alleviated by observing the impact conditions during testing and rectifying the value of pool depth measured at the gauge.

3.3.6 Measurements taken

A typical test run involved a wide range of measurements which had to be

recorded and stored by micro–computer. The range of measurements included:–

(i) Discharge measurement by the orifice plate meter as described in Section 3.3.1. The value of discharge then determined the mean outlet velocity Uo at each nozzle (or orifice). Values of outlet velocity up to 25m/s were tested.

(ii) The plunge pool depth (Y) measurement was carried out as described in Section 3.3.5.

(iii) The jet plunge length (L) from the outlet of the nozzle, or orifice, to the plunge pool free surface was measured.

(iv) The behaviour of the jet in the atmosphere was thought to be very dependent on the initial turbulence levels within the jet as well as the subsequent development of turbulence within the jet as it plunged through the atmosphere. It was decided therefore to carry out a testing programme of turbulence measurement within the plunging jet. This involved the designing and testing of a turbulence probe described in some detail in Section 3.4.

Longitudinal turbulence intensity values (U'/Uo) were measured within the plunging jet, both across the width of the jet and also along the length of the jet in the axial direction. To permit these measurements, a traverse system was developed which provided movement and accurate positioning of the turbulence probe in both directions. The measurements were restricted, however, to the inner jet core and the initial jet length, thus avoiding the problem of intermittency at the jet edges and drop out due to air bubble entrainment into the jet far downstream from the outlet.

(v) Jet diameter at impact point:

A set of high–speed photographs were taken during each test to permit determination of the rate of jet expansion and the resulting jet impact diameter at the plunge pool. Direct physical measurement of the jet diameter was also carried out at pool level to further define the value of jet impact diameter computed from the photographic technique. At low outlet velocities the jets contracted under the accelerating influence of gravity, and this proved far more amenable to direct measurement than at high flow rates. When the outlet velocity increased the jet would overcome surface tension restraint and contracting

effects. The resulting jet at pool level would be rather more irregular, sometimes accompanied with spray, and hence measurement of the jet diameter was more difficult. A method was developed to determine the jet diameter at the pool impingement point by calculation based on the turbulence level of the issuing jet and the fall height. This method was employed to compare with values of jet impact diameter determined from photography and direct measurement, and is detailed in Chapter 6.

(vi) Pressure measurements on plunge pool floor:

On entering the plunge pool the large amounts of air entrainment meant that turbulence measurments were no longer possible. It was decided to take measurements of the impact pressures produced at the plunge pool floor, this being an area where very little data was available. A line of pressure transducers were flush–mounted on the pool floor, capable of picking up instantaneous pressures along a radial arm of the pool floor.

A detailed description of the pressure transducers is given in Section 3.5 and the subsequent data acquisition and analysis system in Section 3.6.

3.3.7 Test procedure

For each outlet type, the pool depth was set, as previously described, and the resultant fall height was calculated knowing the fixed distance between the outlet and the surface of the base plate. The outlet velocity was arranged by use of the gate valve and the orifice plate calibration. Velocities were selected and tested over a large range, and the readings of impact pressure on the pool floor or, at a later date, turbulence values within the jet were directed to a computer system for storage and analysis.

With the variation in pool depth, jet fall height, outlet form and velocity, an extensive series of results were obtained. Table (3.1) shows the range of parameters which were tested and gives an indication of the thorough investigation of each influence on the dissipation process. For the largest diameter outlet, Figs. 3.14 and 3.15 show the range of jet conditions in the atmosphere that could be obtained and Figs. 3.16 and 3.17 indicate the forms of plunge pool dissipation that were observed.

3.4 INSTRUMENTATION - THE TURBULENCE PROBE

3.4.1 Introduction

A schematic diagram of the nozzle outlet arrangement of the experimental equipment and the measurement instrumentation is shown in Fig. 3.18. The instrumentation comprised of a turbulence probe which was used to determine the turbulence level of the plunging jet, and an array of flush-mounted pressure transducers, used to pick up impact pressures generated at the pool floor due to the impinging jet action.

As the turbulence probe caused interference to the flow pattern downstream of the measurement device, the turbulence testing was carried out independently of the floor pressure measurements. To allow direct comparison, however, turbulence readings were taken with the same outlet conditions which were operating during acquisition of the impact pressures at the pool floor. The following sections describe the detailed design and calibration of the turbulence probe, whilst the pressure transducers will be described in detail in Section 3.5.

3.4.2 The turbulence probe concept.

Turbulence measurements of jets in air have successfully been carried out by hot wire anemometry at velocities above 200m/s, provided that the flow was free from contaminants. For liquids, hot film probes are preferred due to their increased rigidity and resistance to contamination. One method of operation is constant temperature anemometry. The probe is heated at the tip and in turn the heat is transferred to the flowing fluid at a rate proportional to the flow velocity. The time-history of the velocity is then determined by measurement of the probe current feedback. Alternatively, if the supply remains constant, the probe resistance can be measured, and again the flow velocity is obtained. The main advantage of the anemometry system is that the probes are very small and therefore, pocesses a high frequency response and also cause minimum flow disturbance during measurements.

However, above 10 m/s the technique is unsuitable for liquids, even with hot film probes, due to lack of sensitivity and excessive heat transfer. One

alternative method of turbulence measurement is to use a Laser Doppler Anemometer (LDA). This method was used successfully by Ervine [1] for a circular jet in the atmosphere, but measurements were only possible at a region just at the jet outlet point, with the attachment of a small piece of circular arc perspex. The small piece of perspex remained in contact with the edge of the jet and was large enough to allow the laser beams to pass through with the minimum of surface disturbance.

The (LDA) method is restricted only to a few limited measurements at the nozzle outlet, simply because the "noise" picked up by the laser beams crossing the free surface is too excessive, and too distorting to produce good turbulence data from the jet. This method was not attempted, as it could not be used along the length of the plunging jet.

A simple, effective and reliable method was therefore required which would be sufficiently robust to take measurements in high velocity liquids and is economical in the sense of materials and construction. The solution adopted was to take turbulence measurements by means of a total pressure probe based on a design of Arndt and Ippen [12]. The system comprised of a total head tube leading to a pressure transducer as sketched in Fig. 3.19. As the transducer was of the flush mounted type, an adaptor was required to connect the tube to the brass housing which formed a mount for the measurement device. During testing, readings of pressure were taken and converted to velocity to allow determination of the internal turbulence level of the free falling jet.

Details of the transducer operation and capabilities will be given in later sections on pressure measurement while Section 3.4.3 below will cover the turbulence probe design.

3.4.3 Turbulence probe design.

Two objectives determine the design of any turbulence measurement device, namely spatial and temporal resolution. In other words, the size of the probe (the aperture at the tip of the tube, see Fig. 3.19) must be small enough to resolve the spatial extent of the turbulent disturbances, and secondly, the probe must have an adequate frequency response. (The response time must be smaller

than the micro scale divided by some characteristic velocity). In the case of a total head tube, the frequency response is proportional to the tube diameter so the two requirements of spatial and temporal resolution are in opposition to each other.

A schematic representation of the system in question is shown in Fig. 3.20. The transducer is represented by a spring loaded piston, the spring stiffness being based on the average deflection. For a clamped circular membrane the spring constant (Kd) is given by:

$$K_d = \frac{16\,\pi}{rd^2} \; \frac{E\,h^3}{(1-\eta^2)} \qquad (3.3)$$

where rd = transducer diaphragm radius
E = Young's Modulus of the diaphragm
h = transducer diaphragm thickness
η = Poisson's Ratio

For such a system, with a single degree of freedom, the natural frequency (fo), according to Ippen and Raichlen [13] is:

$$fo = \frac{1}{2\,\pi} \sqrt{\frac{Kd}{A_1\,L_1}\left[\frac{A_1}{A_2}\right]^2} \qquad (3.4)$$

provided the following simplifications were made:

$$L_2 \ll (A_2/A_1)\,L_1 \qquad (3.5)$$

and

$$(\,dz/dt\,)^2 \approx 0 \qquad (3.6)$$

where A_1, A_2, L_1, L_2 and Z are shown in Fig. 3.20.

Without detailing the dynamics of the system, refinements to the formula are

undertaken which allow expression of the natural frequency of the instrument (fo) in terms of quantities which are readily available. It should be stated at this juncture, however, that there will be less than 10% distortion in the turbulence signal for frrequencies below 75% of the natural frequency, with an instrument designed in accordance with Equations (3.3) and (3.4).

As a commercially available transducer is used in the system, the only useful data that is given is the size of the transducer and its natural frequency (fd). The natural frequency of the instrument must, therefore, be in terms of these and other known quantities, and is given by:

$$f_0 = 1.11\, fd^{3/2} \left| \rho d/\rho\ A_1/L_1 \right|^{1/2} \left| \frac{\rho d(1-\eta^2)}{E} \right|^{1/4} \qquad (3.7)$$

where ρd = density of diaphragm.
ρ = density of test fluid

and fd is the diaphragms natural frequency quoted by the manufacturer (10 KHz).

Selecting an operational frequency range (75% of natural frequency), Equation (3.7) was used to determine the dimensions of the total pressure probe. A check on the computed frequency and the required degree of damping was then carried out experimentally.

The probe was constructed using a tube of 2mm inside diameter and 3.2mm outisde diameter which was connected to a brass housing. The housing was machined to provide a shock chamber and a mount for the pressure transducer. Considering the natural frequency selected, the total length of the tubing from the shock chamber to the probe tip was determined from Equation (3.7). The resulting tube length was 115mm, which was sufficient to measure jet centre line turbulence readings in the largest diameter jets without causing undue interference to the flow pattern. Fig. 3.19 shows the final design of the turbulence probe, including dimensions of the total head tube and shock chamber.

Initially the assembled instrument was tested without damping to ensure that the natural frequency (fo) was in fact that which was selected from Equation (3.7). It was decided to test the response of the probe to a sudden decrease in pressure, facilitated by a "bursting balloon" method developed by Arndt and Ippen. The pressure trace was recorded and displayed on a fixed–image oscilloscope. The time period between peaks of the resulting trace was measured to determine the natural frequency of the complete instrument. After a number of tests the average value of natural frequency was found to be around 200 Hz to 210 Hz. A typical example of the undamped trace is given in Fig. 3.21. The value of (fo) was considerably less than had been used in Equation (3.7) to determine the probe dimensions initially. This was due to the overly optimistic value quoted by the manufacturer (10 KHz) for the natural frequency of the transducer. However, as will be explained later, the frequency response was still sufficient to determine the turbulence activity in the free–falling jet.

The instrument was damped to ensure a flat response over the frequency range. In other words, to achieve minimum distortion to the signal due to resonant conditions. The frequency response, F(f), of such a system to a sinusoidally varying pressure (P) is well known and given by:

$$F(f) = \frac{Z_m}{PoA_2/Kd} = \frac{1}{[(1-(f/fo)^2)^2 + 4(\beta_D/fo)^2(f/fo)^2]^{1/2}} \qquad (3.8)$$

where $P = Po \sin 2\pi ft$

Zm = maximum membrane deflection.

f = frequency.

and β_D is the damping factor defined by:

$$\beta_D = \frac{C}{4\pi \rho A_1 L_1} \left(\frac{A_1}{A_2}\right)^2 \qquad (3.9)$$

where C = damping coefficient

Critical damping is obtained when $B_D/fo = 1.0$. It can be shown that for a given natural frequency, fo, the flattest frequency response is obtained when:

$$\beta_D/fo = 1/\sqrt{2} = 0.707 \qquad (3.10)$$

Equation (3.8) then reduces to:

$$F(f) = \frac{1}{(1 + (f/fo)^4)^{1/2}} \qquad (3.11)$$

Experimentally, this means that once the natural frequency has been established, the instrument is damped until a trace is obtained from the oscilloscope that agrees with the theoretical response of a single degree of freedom system damped to 70.7% of critical. The response of the instrument to the instantaneous reduction in pressure must be such that the resultant membrane oscillations die away at a rate dictated by Equation (3.10).

Fig. 3.22 shows the comparison between the spectral distribution of energy measurements in an open channel, where the bulk of turbulence was in the frequency range of 0 to 80 Hz, utilising a probe in the damped and undamped condition (fo=150 Hz). This figure clearly illustrates the advantage of damping. A pronounced resonant peak is evident at the natural frequency of the undamped probe. This distortion can amount to 50% of the total energy in the signal. The damped instrument has a flat response to a sufficiently large value of frequency and therefore no corrections are necessary to the signal.

3.4.4 Accuracy of turbulence probe.

The accuracy of the instantaneous turbulence data depends on four factors as follows:

(a) the frequency response of the probe relative to the spectral distribution of

turbulent energy.

(b) the size of the probe relative to the scale of the turbulence.

(c) the relative intensity of the turbulence.

(d) inclination of the probe from horizontal due to flow past instrument.

Elements (a) and (b) have been covered in the previous section on the turbulence probe design. The resulting effect of these conflicting factors is that the probe has a relatively low frequency response (200 Hz) and there is a lack of resolution of the micro scale. This precludes the use of the instrument in studies concerned with the details of turbulence at the high frequency end of the spectrum. However, as the turbulent eddies around the jet core increase in size with distance from the nozzle outlet, Falvey and Ervine [14], and the study was concerned only with the development of boundary layer turbulence generated at the nozzle/orifice outlet, then the instrument had sufficient detail relative to the eddy size to indicate the approximate turbulence magnitude and migration.

The effects of turbulence intensity (c) are essentially due to the fact that the probe senses total instantaneous pressure, the instantaneous value being related to both local velocity and local pressure. For a closed conduit, say, the instantaneous total pressure (P_T) sensed by the tube is:

$$P_T = \rho/2 \; (\bar{u} + \underset{\sim}{U})^2 + \bar{P}s + \underset{\sim}{P}s \qquad (3.12)$$

where $\bar{u}$ is the mean velocity, $\underset{\sim}{u}$ is any fluctuation of velocity about the mean, $\bar{P}s$ is the static pressure term (not included for jet in atmosphere), and $\underset{\sim}{P}s$ the fluctuating pressure about the mean.

Expanding (3.12) and taking the time average yields:

$$\bar{P}_T - \bar{P}s = \rho/2 \; \bar{u}^2 + \rho/2 \; U'^2 \qquad (3.13)$$

Thus,

$$\bar{U} = \sqrt{ [\; 2/\rho \; (\bar{P}_T - \bar{P}s)]} . (1 + u'^2/\bar{U}^2)^{-1/2} \qquad (3.14)$$

The static pressure term is obviously not included for a free falling jet. However, it can be seen from Equation (3.14) that the accepted relation for mean velocity is in error by an amount:

$$0.5\ (U'^2/\bar{U}^2) + \text{higher order terms} \qquad (3.14a)$$

Neglecting higher order terms, the error in mean velocity is thus only 0.5% if the turbulence intensity is of the order of 10%. An expression to corrrect the root mean square velocity term can also be obtained by expanding Equation (3.12). Without detailing the procedure, it can be shown that an error of approximately ± 5% is to be expected for turbulence measurements with an intensity around 10%. Adjustments must therefore be made to the velocity readings to ensure correct values of turbulence are obtained.

(d) To prevent probe inclination and deflection due to the momentum of the oncoming flow, the probe support was designed to ensure that the tube tip would be at right angles to the issuing jet. Radial and longitudinal movement was made possible by the traverse system to provide a range of data over various jet cross–sections, but, during measurements, the support arrangement was clamped rigidly in place to prevent vibration under the dynamic force of the fluid. The probe and probe support is shown in Fig. 3.23. The plunging jet in this figure is issuing from the orifice plate outlet.

Dynamic calibration of the turbulence probe was carried out by correlating the output voltage from the time–history of the turbulence probe readings with average velocity measurements from a Pitot–static tube. The average velocity readings were taken at the same location and under the same flow conditions that were operating during turbulence probe measurements, but obviously not at the same time period. Fig. 3.24 shows a typical calibration curve for the turbulence probe showing the voltage–velocity relationship. Problems encountered during the turbulence probe calibration were also applicable to the transducers used for pressure measurement in the plunge pool and hence will be detailed in Section 3.5 dealing with floor impact pressures.

Finally, testing comprised of measurement of the longitudinal turbulence intensity within the plunging jet, both in the radial and streamwise direction, to determine the propagation of internal jet turbulence. The results of these tests

and their application will be discussed in a later chapter.

3.5 INSTRUMENTATION - THE PRESSURE TRANSDUCERS

3.5.1 Introduction to pressure transducers.

The most important aspect of the work in this thesis is the measurement of instantaneous pressures on the floor of a plunge pool basin. The results are recorded, stored and analysed to produce mean pressures, R.M.S. fluctuating pressures, instantaneous peak pressures and instantaneous minimum pressures.

In order to measure the pressures generated at the plunge pool floor (due to the impinging jet action) pressure transducers were flush-mounted on the plunge pool floor surface. Pressure transducers themselves represent only a small part of the measurement system. The measurement system converts the continuous electrical signals from each transducer into physical results through the processes of amplification, signal conditioning and digitisation. These processes will be covered in Section 3.6 while the transducer aspects will be detailed below.

For the three available transducers, five locations were chosen each 100mm apart, arranged in a row at the plunge tank base plate. This is sketched in Fig. 3.12. Therefore, the value of total pressure at any measurement point and the distribution of pressure along a radial line from the impinging jet centre line could be evaluated.

To ensure correct operation of the pressure measurement device meant that several requirements had to be satisfied as follows:

(i) the transducer must be adequately robust to resist high dynamic forces and a large pressure range, including negative pressures.

(ii) the transducer diaphragm area must be small enough to prevent integration of the turbulence micro scale (spatial resolution).

(iii) the transducer response must be sufficient to measure the high frequency fluctuations (temporal resolution).

(iv) the device should cause minimum disturbance to the flow.

(v) the noise level of the output signal and non-linearity of amplification stages, must be kept to a minimum to prevent data distortion.

The five points outlined above will be discussed in more detail at various stages throughout this section, and each point should be carefully considered before choosing a pressure transducer.

3.5.2 The range of pressures expected.

The most fundamental consideration in the choice of a pressure transducer is the full working pressure range it is expected to operate over. This corresponds to item (i) above. The transducer should have sufficient capacity and sensitivity to allow measurement of the full loading range which may be expected during the testing programme.

As the tailwater depth was varied from 0 - 500mm, the highest mean loading would obviously occur when the jet impacted directly with the transducer diaphragm at zero plunge pool depth. Considering the jet to be intact at impact, the largest mean pressure would result from the highest velocity jet tested falling through the maximum drop height available. For an outlet velocity of 25m/s and a fall height of approximately 2.5m, the mean pressure head developed at the impact point would be around 34m head of water. Due to the large fluctuations in pressure generated at the impact point, the maximum instantaneous pressure could be assumed to be much larger than the mean pressure head. At this stage no general information was available on the value of maximum instantaneous pressure above the mean, as this in fact was one of the purposes of carrying out the research. Hence, an estimate had to be made of this value. Referring to previous literature, it was assumed that the maximum instantaneous pressure would be about twice the mean value. The transducer therefore had to have a measurement range up to 68m head of water and as a factor of safety, have an over-pressure capacity which was twice the rated value.

At the opposite extreme, assuming fluctuations below the mean pressure head were sufficient to reduce the instantaneous head beneath zero, the transducer had

to be capable of measuring negative pressure heads. This might involve pressures as low as −10m head of water.

In the case of direct jet impact on the transducer diaphragm, it should be noted that if, during testing, the fluid was not clean and free from foreign elements, pressures could be generated which were greater than indicated above and hence damage could be sustained to the transducer device. To preclude this occurance, the pipe−work was constructed completely from P.V.C and the tanks were sealed with a durable non−corrosion paint. Water quality was monitored constantly to ensure that no degradation of the flow had appeared during operation of the system.

3.5.3 Choice of pressure transducer.

Following detailed consideration of the five points outlined in Section 3.5.1, it was decided to choose a range of transducers of the flush−mounted variable resistance type, manufactured by Western Sensors Limited (WS−5000). These instruments have a diaphragm diameter of 19mm and can measure pressures up to 100 p.s.i (approximately 70m head of water). A similar transducer had been incorporated in the total pressure probe, used for jet turbulence readings which has been described in Section 3.4.

A full−bridge (4 arm) foil strain gauge is bonded to the transducer diaphragm and is excited by a constant 10 volts. Fig. 3.25 shows a schematic diagram of the strain gauge arrangement. Output from the transducer is determined by the resistance of the strain gauge bridge and with application of load, the diaphragm deflects and the resistance is altered. Hence, the output voltage will be altered and can be related to the load causing deflection, by accurate calibration. In other words, operation of the device is by means of a change in capacitance resulting from deflection of the flexible transducer diaphragm under load.

As the maximum output voltage from the transducer was only ± 20mV for the constant 10 volt supply, amplification was required of the small magnitude signals. The transducer supply and amplification was provided by a signal conditioning unit, manufactured by Micro Movements Limited, which allowed

monitoring of each transducer on a digital display, and outputed the amplified voltage for interfacing with the remaining elements in the data acquisition system.

Before each test run, to maximise the resolution of the data, the gain on the transducer output was adjusted so that the full plus or minus 10 volt extent of the acquisition equipment was utilised. As mentioned, each element of the data acquisition system will be discussed in Section 3.6.

3.5.4 Spatial and temporal resolution.

Items (ii) and (iii) in Section 3.5.1. indicate that a good pressure transducer will have a small enough plan area to pick–up fluctuations at small eddy length scales without a great deal of area averaging, as well as ensuring the fastest frequency response possible.

These two demands are often in conflict with each other, and have been discussed in a little detail already in Section 3.4, dealing with the turbulence probe design.

In the case of pressure measurements on a plunge pool floor, however, spatial and temporal resolutions are tackled in a slightly different manner. The transducers are designed to be operated with a diaphragm flush–mounted to the plunge pool floor. This arrangement ensures that the maximum frequency response will be available, but, with the full diaphragm area facing the incoming flow, there is a possibility of integration of the small scale turbulent fluctuations over the full diaphragm area. One solution is to place the transducer head in a chamber with a pin–hole leading to the plunge pool floor measurement surface. As there is a finite time period required for the pressure at the gauge to adjust to a change at the measurement surface, spatial resolution is achieved at the expense of temporal response. Another method is to connect the pressure tappings to the transducer through flexible tubing. This enables sampling of more than one position with a single transducer by connecting the tapping tubes one by one to the measurement transducer. However, with long tubes, the dynamic response of the system may be severely reduced and there is a possibility of excessive damping of the pressure fluctuations. Akbari et. al. [15], found (during preliminary experiments on hydraulic jump stilling basins) that the maximum

length of plastic tubing beyond which the results were affected adversely by damping was only 1.0m. When studying aerated flows as in the case of this study, these methods also have a disadvantage in that they can become partly filled with air, or an air bubble gets trapped at the entrance to the flexible tubes completely distorting any pressure reading.

Flush surface mounting of the pressure transducers on the plunge pool floor was therefore adopted as the most satisfactory arrangement. This completely overcame any problems of disturbance to the flow outlined in item (iv) (Section 3.5.1) and eliminated any problems of chamber mounts and tubing connections. It also ensured the fastest possible frequency response to pressure fluctuations and also ensured that trapped air bubbles did not interfere with any of the pressure measurements. It quickly became clear that flush–mounted transducers are much more likely to produce reliable pressure fluctuation data, than data taken using other systems. The only question which remained concerned the diameter of the pressure transducer used.

The diameter of pressure transducer used was 19mm. This was the commercial diameter readily available for the pressure gauge concerned (–10m to +70m head). It was also the same size as that adopted by a parallel study at H.R. Ltd. Wallingford, and a little larger than the pressure transducers used by Toso [16] in the University of Minnesota study. It did give a little cause for concern, considering the micro scale of turbulence is of the order of fractions of a millimetre in eddy length scale.

Justification of the use of a larger, less expensive transducer is as follows:–

– Similar studies have shown that larger scale pressure fluctuations are the most important in stilling basins and plunge pools.

– The dominant range of these fluctuations is of the order of 5 to 10 Hz, Toso [16], Lencastre [17] and King [9].

– The relative turbulence intensity of fluctuations in a submerged jet is anything up to $U'/\bar{U} = 0.15$, and is typically $U'/\bar{U} = 0.1$.

– With mean velocities between 2.5m/s and 25m/s, we have turbulent velocities $U' = 0.25$m/s and 2.5 m/s.

– The inter–relationship between turbulent velocity, frequency and eddy length is $u' = \ell'/\text{time} = \ell' f$, where f is frequency in Hertz.

– For a frequency f = 1 Hz, $\ell' = u'/f$ = 0.25 to 2.5m diameter.

For dominant frequency f = 10Hz, ℓ' = 0.025m to 0.25m diameter.
For high frequencies f = 50 Hz, ℓ' = 0.005m to 0.05m diameter.

– Thus a diaphragm of 19mm diameter (0.019m) will produce reasonably accurate results right up to 50Hz, which is well beyond the range of the turbulent spectrum which is thought to be significant for this type of pressure fluctuations.

– Consultations with various experts suggested that any errors in area averaging should be less than 5%, provided values above 50 Hz were not included.

3.5.5. Mounting the pressure transducers.

The only remaining problem concerned the mounting of the line of pressure transducers at the base of the plunge pool. With the transducers being totally submersed, they had to be carefully water–proofed before connection to the underside of the base plate. The transducer diaphragm fitted through a 19mm diameter hole in the metal base plate insert and was held in place by a specially fabricated mounting ring, see Fig. 3.26. Extraneous forces were eliminated by fabricating the insert plate from solid aluminium material to prevent pinching of the transducer head due to deformation of the housing under load. Connection of the transducers to the underside of the base plate, via the mounting ring, was carefully carried out to prevent additional stress building up on the instrument and causing zero–ing errors.

3.5.6 Calibration of the pressure transducers.

To ensure the accuracy of results from any measurement instrument, careful and regular calibration must take place. In this case, with the large pressures expected up to 70m head, calibration over the full range of loading precluded the

use of water columns alone. A method was therefore developed to determine the response of each transducer over its entire capacity. First, a pressure cell was machined from solid brass and the transducers were located inside the housing with a connection similar to the in situ arrangement for pool pressure testing. The set–up is shown in Fig. 3.27. Pressure was supplied to the transducer through an air/water chamber, and was evenly distributed over the diaphragm within the brass pressure cell. The transducer output was noted both from the digital display on the signal conditioning unit, and from the mean value determined by a computer. Methods of acquiring and statistically processing the transducer output by computer will be detailed in Sections 3.6 and 3.7. A schematic diagram of the calibration rig is shown in Fig. 3.28. Pressures were applied in increments, both increasing and decreasing load, up to 6.5 bar (approximately 94 p.s.i.). As a result, for each transducer, a linear relationship between the amplified output voltage and the applied pressure, converted to metres head of water, was obtained with a typical example shown in Fig. 3.29.

The process was repeated several times for each pressure transducer to confirm that the calibration relationship was as initially determined. With the transducers located in the base plate, the calibration was checked at the lower end of the range by relating the static head of water above the diaphragm (measured using the water level indicator) with the value given from the amplified transducer output. Amplification gain was increased at such low pressure head levels to utilise the full voltage range of the acquisition elements and this ensured that downranging, i.e. error in measurement of small pressure values relative to the transducer capacity, should be reduced. However, during preliminary testing, it was found that the transducer response was not as straightforward as had first been imagined and it required more extensive treatment to be certain that the pressure results were reliable.

3.5.7 Signal conditioning.

Calibration of the transducers was accomplished by relating the water pressure, applied via the set–up described earlier, to the output voltage. However, when the transducers were located at the plunge pool floor, and fully under water, they produced results that were not exactly equivalent to the actual static head above the transducer diaphragm. This was because the transducers

were sensitive to temperature change and, if the applied water head was not of a similar temperature to the test fluid, then a discrepancy would be produced. To achieve a proper calibration of the transducers, the pressure head had to be applied to the transducers as it would be insitu. Therefore, the fluid in the whole pressure cell/transducer assembly had to be at the same temperature as the test fluid.

With changes in temperature of the pool fluid, there was a slight change in the calibration coefficient. This temperature effect was incorporated in the data processing, using the appropriate calibration relationship for the monitored fluid temperature. Once temperature effects had been taken into account, the located transducer output could be checked with the applied static head. Doubts regarding the temperature sensitivity of the transducers meant that calibration had to take place before and after each set of tests, by the methods described above.

Other sources of doubt concerning the transducer operation included signal drift, electrical noise, signal dropout and loss of output. Similar problems were encountered with the turbulence probe and called into question some of the specifications quoted by the manufacturers for the device. However, due to budget limitations, the instruments had to be persisted with and both on–board and off–board signal conditioning was required to eliminate spurious or degraded data signals from the measurement device.

After a long period of time, for instance, a static reading from the transducer would tend to drift from the correct value. To minimise this effect, a stabilising circuit had to be added to the amplifier unit and, during testing, simultaneous readings were taken from the instruments to ensure that they were operating under exactly the same conditions. By testing, the minimum time period required to fully define the output signal was also determined and this was found to be much less than the time drift effect with the compensating circuitry.

Electrical noise was partially eliminated by shortening the length of cable from the measurement device to the amplification unit. Extra shielding was also required to reduce the noise portion of the amplified signal to a minimum. As noise is usually in the high frequency band (50 Hz), filtering can be incorporated to reduce this element of the signal, but the risk is that some higher frequency pressure fluctuations may be neglected. Frequency filtering and minimum sample times will be addressed later in this chapter in Section 3.6.

Finally, signal dropout and loss of signal due to transducer malfunction was detected by visual inspection of the data. When this was occasionally apparent, the test run had to be repeated until the proper signal form was obtained. Hence, with the additional signal conditioning that has been mentioned, the values of total pressure from the transducers could be taken with more confidence.

The following section (3.6) will describe the elements included in the collection of data from the measurement instruments and detail the processes involved in controlling the data acquisition system.

3.6 DATA ACQUISITION SYSTEM (D.A.S.)

3.6.1 Introduction.

Prior to the late 50's, many characteristics of turbulent flow situations remained hidden or were inadequately explained due to lack of instrumentation that could probe them. With the subsequent introduction of high response pressure transducers and anemometry, description of pressure fluctuations in the fluid could be obtained. Originally, readings from the sensor were recorded on magnetic tape. The method commonly used to analyse the voltage output of the instrument was then to playback the recording into analog equipment to give estimates of the magnitude and frequency characteristics of the signal. For visual inspection of the results, the output could be displayed by a chart recorder or on a oscilloscope screen.

By the late 60's, as computers became more readily available, they could be used to analyse the tape recorded output, once it had been digitised. Computers had the advantage of increasing the speed, accuracy and ease of manipulation of the data. With further developments in electronics, it became possible to both acquire and analyse data adequately, first on mini computers and then more recently by a micro computer. Currently, technology in data acquisition and analysis with micro computers had advanced so rapidly, in terms of memory capacity and processing speed, that the system used in this research is already slightly outdated even after only a three year period. However, the general method remains the same, and micro computers offer a fast, inexpensive and

accurate means of obtaining, processing and presenting data.

The system utilised in the present research study consisted of various elements. Fig. 3.30 illustrates the method of data collection that was used. Analog voltage signals from the sensor (either turbulence probe or pressure transducers), representing the flow behaviour at the instrument, were amplified, conditioned, digitised and either stored or processed directly on a micro computer using a program developed from software which was specifically obtained for the task.

3.6.2. Acquisition hardware.

Amplification and signal conditioning operations have already been mentioned in the previous sections. Linearity is achieved in all amplification stages by considering the difference between static and dynamic calibration of the measurement device. It can then be determined if all signals are amplified equally without regard to frequency. This procedure was carried out before testing was commenced. Signal conditioning, as has been pointed out, was by both physical means, e.g. extra cable shielding and additional circuitry, and also by visual inspection of the resulting data. Using these methods, factors effecting the accuracy of the results are reduced to a minimum.

This section, however, will concentrate on the hardware that was used in the data acquistion process. The hardware consisted of printed circuit boards. Each board performed a specific task which will be detailed below.

Hardware was furnished by the Burr–Brown Corporation (PCI – 20000) and comprised of a termination panel, a analog input module and a carrier card. These elements were accessed with the micro computer via the specialised software. Each of the hardware components and the computer interface are shown in Fig. 3.31. The signal termination panel provided convenient screw terminal connections between the internal electronics and the external field readings. Board space was also provided for passive signal conditioning, including extra earthing options.

As all data is represented digitally in the computer, the amplified analog

signals from the measurement device had to be converted to digital form for computer manipulation. Therefore, readings from each active channel in the termination panel were passed through a analog input module which performed the analog to digital (A/D) conversion. Because such converters are expensive, a number of input signals are multiplexed to use the same converter. The multiplexer switches several input signals or channels one at a time into the A/D converter.

3.6.3 Data quantification.

The relationship of the digital value produced by the conversion of the input signal level depends on the resolution, or number of binary digits (bits), of the converter as well as the input voltage range. In this case, for a 12-bit converter with a ± 10 volt input range, there are 4096 (2^{12}) possible values of the digital result and a voltage range of −10 volts to +10 volts, covering a span of 20 volts. This means that the value of each bit of the A/D result is:

1 bit = 20 Volts/4096 = 4.883 mV (approx.)

Therefore, the actual voltage corresponding to any converted value, for a converter with a straight binary code, is:

Voltage = A/D result.(4.883 mV) (approx.)

The resulting relationship between the binary code and the relative voltage is:

Voltage = [A/D result. (20 / 4096)] - 10 (3.15)

The voltage scale must be corrected by dividing by the gain of all amplification stages, including any off-board amplification, as well as any on-board amplifier. Errors, involved in representing the infinite number of levels in the continuous analog data by the fixed number of binary digits available, are negligible, compared with other sources in the data acquisition and processing procedures.

3.6.4 Computer interface and specification.

The main circuit board in the system is called a carrier, and it inserts into one of the expansion slots in the back of the host micro computer. Interfacing with the internal bus of the micro computer's central processing unit is through the carrier card. It also provides power and a physical mounting for the instrument module. The carrier is functionally programmed by the plug–in instrument module, in this case an analog input device. Communications between the computer and the converter are through the carrier card. This is shown in Fig. 3.31.

Considering the micro computer itself, certain facilities were required to adequately perform the tasks of data acquisition, processing and storage. A I.B.M. X.T. personal computer was selected as this had proved to be a reliable and relatively inexpensive piece of equipment with the capabilities to accomplish the work. The specifications of the system are:

(i) standard I.B.M. PCXT system unit with 640 Kb of R.A.M.
(ii) enhanced keyboard
(iii) one floppy disc drive with 360 Kb capacity and one hard disc with 20Mb capacity
(iv) I.B.M. mono display monitor
(v) Hercules compatible graphics card
(vi) 8087 maths co–processor
(vii) disc operating system (version 3.2)
(viii) Epson FX–80 dot matrix printer

Illustration of the system set–up in the laboratory is given in Fig. 3.32.

3.6.5 Software.

As noted before, the computer could read the sensor signal once it had passed through various peripheral units including an analog to digital converter. The sixteen channel A/D board was installed on the carrier card which was connected to the computer. Each of the channels of analog to digital input were assigned a memory address. In order to read or sample the output of a sensor

linked to a channel, the memory address assigned to the channel had to be accessed by the computer. This was accomplished by creating a computer program or software.

The computer program was fundamental to the collection of data through hardware control, and provided a method to process the readings once they had been acquired. Apart from channel selection, the program was responsible for initiation of conversions, synchronisation of events and data pre-processing. Pre-processing involved converting the digitised data (voltage) to physical units (pressure, velocity). This step was carried out according to the previously determined calibration equation which was included in the program.

The computer program was written in Asyst (version 1.56); a software package which was purchased specifically for this research project. Basically, Asyst is a sophisticated high-level language utilising words or phrases (commands) which perform particular functions. A program is generated by sequential combination of these commands. Hence, the language can be customised to suit the requirements of the operator. When executed, the program will carry out the specific operations that have been stipulated by the commands. The advantage of using this software is that it provided extensive capabilities for manipulation and reduction of large amounts of data in one step by a single command.

Together with providing the program structure, the basic functions of the Asyst software are statistical analysis and graphical representation of the data. To interface between the Asyst language program and the system hardware, software support had to be added (PCI-20046S - 4). The software support consisted of assembly language sub-routines which included all instructions for the major hardware operations. When the software support instruction is called, program control is passed from Asyst to the PCI routines. Once the operation has been completed, the software support is designed to return to the Asyst language program. The status of the operation is monitored during any sub-routine instruction and in the event that an error occurs, the program will again return to Asyst, this time with feedback on the cause of the problem.

By combining the Asyst structured program with hardware control routines, a method was developed which could automatically acquire data from any transducer

and then process the resulting array of instantaneous readings.

The instrument sampling routine was therefore defined by the computer program, but, as will be detailed in the following sections, it must satisfy certain requirements to ensure that the resulting measurements are representative of the actual flow phenomenon. A listing of the Asyst language sampling routine, for the pressure transducers located at the plunge pool floor, is given in Appendix A. The particular example given is heavily commented to explain each of the events in the program.

3.6.6 Requirements of sampling routine.

Digitisation of the continuous signal from the sensor means that it is converted to a digital form by sampling at discrete inervals. The problem is defining the instantaneous points at which the data values are to be observed.

Sampling for digital data processing is usually performed at equally spaced intervals, Fig. 3.33(a). The aim is then to determine the appropriate sampling interval which will fully define the signal. On the one hand, sampling at points which are too close together will yield correlated and highly redundant data, and this unnecessarily increases the labour and cost of calculations. On the other hand, sampling at points which are too far apart will lead to confusion between the low and high frequency components in the original data. This problem is called "aliasing" and will be explained below.

The sample rate is dictated by the frequencies in the signal to be sampled. To adequately define the signal with discrete points in time at least two samples per cycle are required. Taking the time period between samples to be t, the highest frequency which can be defined by sampling at a rate of 1/t samples per second is 1/2t cycles per second (c.p.s.). Frequencies in the original data above 1/2t c.p.s. will be folded back into the frequency range, from 0 to 1/2t c.p.s., and will be confused with data in this lower range, Fig. 3.33(b). This cutoff frequency (fc = 1/2t) is called the Nyquist frequency or folding frequency and this point is shown in Fig. 3.33(c).

There are two methods to avoid the aliasing problem. The first method is

usually used when the frequency range of the acquisition equipment is limited. Prior to sampling, the data is filtered so that information above one half of the maximum sample rate is removed. Therefore, no data will exist above the cutoff frequency. With a low pass filter, this method has the advantage that it may reduce the noise portion of the signal. However, there is a possibility that a substantial contribution to the results may be omitted by neglecting the higher frequency elements.

The second method is to choose the sample period sufficiently small so that there is no possibility for data to exist above the cutoff frequency. This means choosing the sample frequency to be at least two times greater than the maximum frequency in the flow that is being investigated.

The second method was adopted in the sample routine to prevent any high frequency omissions from the signal. During preliminary testing, the signal was sampled at the highest rate possible supported by the software which was around 230 Hz. By inspection of the signal analysis it was found that the spectrum of frequencies due to the pressure fluctuations at the pool base, and in the plunging jet, were concentrated well below 50 Hz. This assessment has also been noted in previous research work. The minimum sample rate for the experiments was therefore 100 Hz, at least twice the maximum observed. Signal analysis will be dealt with in later sections.

3.6.7 Data acquisition capacity.

Directly accessible memory was limited in the IBM PCXT computer. After accounting for application programs, the disc operating system, and other necessary items needed for basic operations, the set-up had enough memory to store approximately 24,000 points of data. At 100 samples per second from one transducer this memory would be filled in around four minutes. The data would then be processed or dumped from the computer memory to disc storage for later evaluation. Software was used to maximise data storage space and to speed up the dumping process. With use of the software it was possible to dump the 24,000 point data set to disc storage in ten seconds.

A further requirement of the sampling routine was the need to read more

than one transducer record, and further to sample the transducers simultaneously. This was needed to ensure that the instruments in the plunge pool would be operating under exactly the same conditions. Correlations were not required as the spatial extent of the plunging jet action was well defined. To accomplish the requirement of simultaneous readings, data buffers were constructed for each of the three transducer channels and these were filled in sequence by operation of a program loop. As has been mentioned, the program controlled which transducer to sample, the sample rate, and called an assembly language routine which carried out the sampling. The end result was a sampling routine which allowed a variable rate, above 200 samples per second if required, from any of the transducers with a small time lag between records of different channels. It should be noted that the maximum sample rate for multiple transducers was not limited by the hardware, which only took 76 microseconds for acquisition, conversion and multiplexer settling time, but rather by the restraints of the computer program operation. As stated previously, the program structure is shown in Appendix A.

With the data sets of plunge pool pressure values including nearly simultaneous records from three transducers at a sample rate of 100 Hz, the total 24,000 point buffer would hold an eighty second record. A three minute record length had two ten second breaks while the two eighty second data sets were dumped to disc. This method was utilised to sample the instruments in the plunge pool once the sample duration had been found to be adequate. The adequacy of the sample duration will be discussed in the following section.

3.6.8 Data qualification.

In order to interpret the data it is necessary to know something about its basic characteristics. The three most important of these characteristics are:

(i) the stationarity of the data

(ii) the normality of the data

(iii) the presence of periodicities in the data

Point (i) will be covered below while points (ii) and (iii) will be investigated in the data processing discussion in Section 3.7.

The stationarity of the data may be accepted if the basic physical factors which generate the phenomenon are time invariant. In the plunge pool, the random data represents pressure fluctuations at the pool floor due to the impact of a turbulent free shear layer. If the flow is constant and the boundary is fixed, it would be reasonable to assume that the resulting pressure data is stationary. Although this argument is correct, it is slightly over–simplified. Therefore, the stationarity of the data must be evaluated by studies of the sample time history records. The minimum sample duration may then be determined for which the results may be said to be independent of time.

The time of integration (or averaging time) has been found to vary from 5 seconds to 2 hours depending on the investigation (Refs. 18–26); although the majority have been short run times of around 60 seconds. Akbari et al. [15], for example, suggested that the duration of pressure recordings should not be less than one minute for reliable and consistent analysis. In the present study, as a further requirement of the sampling routine, experiments were carried out to determine the length of time necessary to find no significant difference in the mean and standard deviation of the results. In order to accomplish this an additional special routine was written.

3.6.9 Special routines.

To evaluate the stationarity of the results, a program was written, again using the Asyst software and hardware support instructions, which could acquire data for different input sample durations. For each stipulated duration, several sets of data were taken. The difference between results from the data in successive runs was determined and compared with the average value. The time period was then increased until it was found that there was no significant difference between results, in terms of the data mean and standard deviation. It was found that a sample time of around 20 seconds was sufficient to define the signal. The actual sample duration was therefore adequate in terms of the average value and variance of the data set. Fig. 3.34 shows a typical example of the results obtained from a stationarity test and Appendix B includes a listing of the program used.

It has been argued that since there is a given amount of energy entering the

pool there is a nominal upper limit to the maximum pressure fluctuations. By sampling for a long time period it is postulated that this limit can be determined.

Another routine was developed to obtain only the maximum and mean value of the pressure fluctuations after each 60 seconds of a continuous test run. A similar process was carried out for the minimum fluctuations. After the test run, the cumulative maximum and average mean values were determined. The program had a total duration of 24 minutes, but well before this time it could be seen, by observing the mean values, that drift was effecting the results.

However, in the initial period, where the mean data was consistent, it could be seen that the maximum value did approach a limit, as shown in Fig. 3.35. Although longer than the time period required to fully define the mean and standard deviation, the time period adopted for each test run (3 minutes in total) was found to be adequate to define this limiting value. A listing of the program used for these experiments is also given in Appendix B. The examples in Appendix B are for one transducer channel only, in this case the centrally located device.

3.7 DATA STORAGE AND PROCESSING

3.7.1 Introduction.

Values of the instantaneous pressure head as well as values of the instantaneous velocity that had been generated during each test run from each instrument, now required to be stored on data file. Each file contained details of the appropriate experimental conditions, including comments on transducer location, flow rate, pool depth and jet fall height, in addition to the raw data time history. Processing of the raw data either took place directly after each test run or, at a later date, by calling the data file back from disc storage.

Due to the random nature of turbulent flow processes, description by means of an analytical explicit time function is not possible. However, there are good ways of characterising random phenomena, in a quantitative manner, by a statistical analysis. The power spectrum and probability density function are the most suitable methods in this case. Once stationarity is ensured, the turbulent

fluctuations in the flow can be considered mathematically as a stochastic, steady process, whose magnitude and frequency is described by these density functions. For each data record, the amplitude characteristics can be derived from the probability density function, while information concerning the signal distribution with respect to frequency can be obtained from the power spectrum. Each of these methods of processing the raw data will be detailed below.

It is very common to assume that the normality of turbulent fluctuations is valid. In other words, the fluctuations in pressure, generated by the turbulent flow behaviour, will fit the Normal of Gaussian distribution. Using this assumption, an estimate can be made of the maximum, and minimum, load which may occur with the mean and the standard deviaiton of the signal as the only data requirements. Knowing the mean and standard deviation, pressure levels with a very low probability, such as one percent, are applied with a safety factor to estimate maximum conditions for design. However, it has been found by Toso [16] and Lopardo et al. [27], for example, that pressure fluctuations at hydraulic structures, which are produced by coherent vortex structures and random turbulence, do not fit this simple and convenient designation. To adequately define the amplitude characteristics of the signal, the actual probability density function must be obtained.

3.7.2 The Probability Density Function.

The probability density function indicates the amount of time the signal spends at a given amplitude and may be described numerically by its moments. For practical purposes, the first four moments are adequate. These are commonly known as the mean, standard deviation, skewness and kurtosis, repsectively, and are shown in Fig. 3.36. The mean and standard deviation terms have been mentioned previously and are the basic measures of central tendency and dispersion which fully define the Normal distribution. The third and fourth moments provide more information on the deviation, if any, of the distribution from the classical "bell" shape. For the Normal distribution, skewness is equal to zero (symmetrical about mean) and kurtosis is equal to three (standard shape).

A data processing routine was written to compute the above amplitude

characteristics as well as the minimum and maximum values for each pressure record. Therefore, with the transducers located at various positions in the pool base, the distribution of fluctuations at a point and over the area of the floor could be computed. Once the amplitude characteristics were obtained, they could be printed out and stored in the data file along with the raw material and the test condition information. A listing of the processing program is given at the end of the sample routine in Appendix A.

The moments of the probability density function were calculated in the following manner for the stationary random digital data. The sample mean value is given by:

$$\text{mean, } \bar{H}m = \frac{\Sigma h}{N} \qquad (3.16)$$

where h = pressure head at given time interval
N = total number of time intervals
Σ = all summations from 1 to N

The sample standard deviation is given by :

$$\text{standard deviation, } h' = \frac{(\sum(h-\bar{H}m)^2)^{1/2}}{N^{1/2}} \qquad (3.17)$$

The third and fourth moments are given as follows:

$$Sk = \frac{\Sigma (h-\bar{H}m)^3}{N h'^3} \qquad (3.18)$$

$$Ku = \frac{\Sigma (h-\bar{H}m)^4}{N h'^4} \qquad (3.19)$$

Equation (3.17) along with the maximum and minimum pressure heads were converted to non-dimensional coefficients by division with the theoretical jet incident pressure level. The generalised pressure head coefficient is therefore given by:

$$Cp = \frac{\Delta h}{Ui^2 / 2g} \qquad (3.20)$$

where Δh = pressure head deviation from mean (m)

Ui = pool level impact velocity of the jet (m/s)

The mean pressure head is also converted to a non-dimensional form in a similar manner to the above.

3.7.3 The Power Spectrum.

The second type of statistical information of interest is that involving the frequency of occurrence of events. This information can be presented in the form of a power spectrum. The power spectrum is first developed by means of the fast implementation version of the discrete Fourier transform. By taking the fast Fourier transform (F.F.T.) of the raw data directly, it is decomposed into its intergal frequency components. Squaring the magnitude of the data's F.F.T. will result in the power spectrum which will define the frequency composition of the data. As it is a symmetrical function, only one half of the spectrum need be considered, up to the previously defined cut-off frequency. One of the applications of the power spectrum is that periodicities in the data can be detected. This is useful as detection of the dominant frequency of the fluctuations from the spectrum will provide information for the structural design in order to prevent resonance conditions.

Principally any sample size N can be handled, but practically, records are usually $N = 2P$ in length, where P is the term number. A 2048 point transform was therefore utilised. For each instrument, 7 ensembles of data resulted in a relatively smooth and constant spectrum. This is equivalent to using approximately 143 seconds of data. With use of the software, it was simple to obtain and plot the power spectra.

3.7.4 Graphical representation.

One of the main advantages of the software was that complicated statistical procedures could be carried out in very simple steps with individual instructions. The raw data was first called back from disc storage and was plotted directly for visual inspection of the waveform on the computer monitor. Figs. 3.37−3.40 show typical wave forms for a ten second excerpt from the central pool pressure transducer operating under various conditions. Considering segments of the raw data, the power spectrum was easily obtained and plotted using the software. Seven spectra were produced in this way for each particular pressure and velocity record. The averaged power spectra are shown in Figs. 3.41−3.47 for the central pressure transducer operating under the same conditions as the waveform examples and other operating conditions. It can be seen from these figures that under all operating conditions shown, the dominant fluctuations occur in the low frequency range (3 to 10 Hz) with little contribution above this level. In many cases this corresponds to larger eddy lengths, usually of a size larger than the impinging jet diameter. A listing of the program used to obtain and plot the power spectra and waveforms is given in Appendix C. This program differs from the previous examples in that only Asyst language commands are used.

REFERENCES FOR CHAPTER 3

1. Ervine, D.A. and Falvey, H.T., "Behaviour of Turbulent Water Jets in the Atmosphere and in Plunge Pools.", Proc. I.C.E., Part 2, 1987, pp. 295–314.

2. Weber, K., Z. angew. Math. Mech., Vol. 11, 1931, p. 136.

3. Grant, R.P., and Middleman, S., "Newtonian Jet Stability.", A.I.Ch.E. Journal, Vol. 12, No. 4, 1966, pp. 664–678.

4. Baron, T., Tech. Rept. University of Illinois, No. 4, 1949.

5. Miesse, C.C., Ind. Eng. Chem., Vol. 47, 1955, p. 1690.

6. Horeni, P., "Disintegration of a Free Jet of Water in Air.". Byzkumny ustav vodohospondarsky prace a studie, Sesit. 93, Praha–Padbaba, 1956.

7. Hausler, E. "Dynamic Water Pressures upon Floors of Stilling Basins Caused by Free overfull Jets at Dams.", Die Wasserwirtischaft, 56. Jahrgang, Hefte 2, 1966.

8. Chen, T–F., and Davis, J.R., "Disintegration of a Turbulent Water Jet.", Journal of the Hydraulic Division, A.S.C.E., Vol. 90, No. HY1, 1964, pp. 175–206.

9. King, D.I., "Supplemental Tests of Morrow Point Spillway, Stilling Basin and Powerplant Tailrace.", U.S.B.R. Report No. HYD – 586, 1969.

10. B.S. 1042 "Measurement of Fluid Flow in Closed Conduits.", Section 1.1, 1981.

11. Hartung, F., and Hausler, E., "Scours, Stilling Basins and Downstream Protection Under Free overfull Jets at Dams.", International Commission for Dame, Q.41, R3, Madrid, 1973, pp. 39–56.

12. Arndt, R.E.A., and Ippen, A.T., "Turbulence Measurments in Liquids using

an Improved Total Pressure Probe.", Jnl. of Hydraulic Research, No. 2, 1970, pp. 131–158.

13. Ippen, A.T., and Raichlen, F., "Turbulence in Civil Engineering: Measurements in Free Surface Streams.", Proc. A.S.C.E., Paper 1392, 1957.

14. Falvey, H.T., and Ervine, D.A., "Aeration in Jets and High Velocity Flows.", A.S.C.E. Int. Symposium on Model–Prototype Correlation of Hyd. Structures, Colorado Springs, 1988, pp. 25–55.

15. Akbari, M.E., Mittal, M.K., and Pande, P.K., "Pressure Fluctuations on the Floor of Free and Forced Hydraulic Jumps.", International Conf. on the Hyd. Modelling of Civil Eng. Structures, B.H.R.A. fluid Eng., Coventry, Paper C1, 1982, pp. 87–96.

16. Toso, J.W., "The Magnitude and Extent of Extreme Pressure Fluctuations in the Hydraulic Jump"., Ph.D. Thesis, University of Minnesota, 1986.

17. Lencastre, A., "Free Overflow Spillways.", Engineering and Design Principles, National Laboratory for Civil Engineering Studies, Report No. 174, Lisbon, Portugal, 1961.

18. Schiebe, F.R., and Bowers, C.E., "Boundary Pressure Fluctuations due to Macroturbulence in Hydraulic Jump.", Proc. of Symposium on Turbulence in Liquids, University of Missouri, Rolla, 1971, pp. 134–139.

19. Abdul Khader, M.H., and Elango, K., "Turbulent Pressure Field Beneath a Hydraulic Jump.", Jnl of Hyd. Research, Vol. 12, No. 4, 1974, pp. 469–489.

20. Narsimham, S., and Bhargava, V.P., "Pressure Fluctuations in Submerged Jump.", Jnl. of Hyd. Division, A.S.C.E., Vol. 102, No. HY3, 1976, pp. 339–350.

21. Vasilliev, O.F., and Bukreyev, V.I., "Statistical Characteristics of Pressure Fluctuations in the Region of Hydraulic Jump.", Proc. of the 12th Congress of I.A.H.R., Vol. 2, Fort Collins, Colorado, 1967, pp. 1–8.

22. Bowers, C.E., and Tsai, F.Y., "Fluctuating Pressures in Spillway Stilling Basins.", Jnl. of Hyd. Div., A.S.C.E., Vol. 95, No. HY6, 1969, pp. 2071–2079.

23. King, D.L., "Analysis of Random Pressure Fluctuations in Stilling Basins.", Proc. of 12th Congress of I.A.H.R., Vol.2, Fort Collins, Colorado, 1967, pp. 210–217.

24. Lesleighter, E.J., "Pressure Fluctuations in Large Energy Dissipation Structures.", Fourth Australasian Conference on Hydraulics and Fluid Mechanics, Melbourne, 1971, pp. 434–440.

25. Lopardo, R.A., Orellano, J.A., and Vernet, G.F., "Baffle Piers Subjected to Flow–Induced Vibrations.", Proc. of 17th Congress of I.A.H.R., Vol.4, Baden–Baden, 1977, pp. 445–452.

26. Narayanan, R., "Pressure Fluctuations Beneath Submerged Hydraulic Jump.", Jnl. of Hyd. Div., A.S.C.E., Vol. 104, No. HY3, 1978, pp. 1331 – 1342.

27. Lopardo, R.A., De Lio, J.G., and Vernet, G.F., "Physical Modelling on Cavitation Tendency for Macroturbulence of Hydraulic Jump." International Conf. on the Hyd. Modelling of Civil Eng. Structures, B.H.R.A. Fluid Engineering., Coventry, Paper C3, 1982, pp. 109–121.

CHAPTER 4

EXPERIMENTAL RESULTS OF MEAN PRESSURES IN PLUNGE POOL AND PLUNGING JET TURBULENCE MEASUREMENTS

CONTENTS

CHAPTER 4

4.1 INTRODUCTION

Chapter 4 presents the measured data of the mean pressure heads experienced at the plunge pool floor, both in the radial direction and with varying plunge pool depth. The data is presented for various nozzle diameters, jet velocities, jet fall heights and for the orifice test, for direct comparison with nozzle behaviour.

The latter part of Chapter 4 presents data on the turbulence intensity within the plunging atmospheric jet, both in the radial and longitudinal directions, again for a range of jet velocities and again comparing nozzle with orifice behaviour.

During the systematic testing programme a vast amount of data was obtained. The time-history of impact pressures on the plunge pool floor was acquired and processed to evaluate the statistical properties of the raw data, including the mean, maximum, minimum and R.M.S. of the pressure trace at each measurement position. Longitudinal values of turbulence intensity were also measured across the plunging jet at several distances downstream from the outlet. As well as these results, the physical dimensions of each test run were recorded, including the jet fall height (L), plunge pool depth (Y) and jet diameter at impact with the plunge pool surface (Di). Also, knowing the average outlet velocity (Uo), at the nozzle or orifice, from flow measurements, and the pre-determined fall height (L), the jet impact velocity (Ui) could be estimated and hence lead to a value of the impact velocity head ($Ui^2/2g$) for each test run. The impact velocity, neglecting air resistance, can be estimated as:

$$Ui = \sqrt{(Uo^2 + 2gL)} \qquad (4.1)$$

and, from continuity, a theoretical jet diameter at impact for each outlet diameter (Do), based on gravitational acceleration, can be calculated by:

$$Di = \sqrt{(Uo/Ui)} \cdot Di \qquad (4.2)$$

It should be noted that this theoretical jet impact diameter was not used to normalise the data but instead the diameter at impact used in the graphical representation of the results is the external jet diameter which was measured directly during each test run, and also estimated from high-speed photographs. Only in the case of low velocity, smooth turbulent plunging jets is the jet diameter at impact roughly equivalent to the flow dimensions calculated from gravity and continuity considerations alone, as in Equation (4.2).

This chapter will briefly report on the results derived from the extensive experimental programme, first in terms of the mean pressure head developed at the plunge pool floor during jet impingement, and then, for the propagation of turbulence in the plunging jet.

The chapter following will report on the fluctuations of pressure about the mean that occured during the testing programme and the instantaneous maximum and minimum pressures. Analysis of the results will then be carried out in Chapters 6 and 7 along with comparisons with relevant results from other authors. Additionally, in Chapter 6, for each of the plunging jet conditions, a method is developed to calculate the important parameter of the jet dimensions at impact with the plunge pool surface. This allows comparison with the measured values of jet impact diameter which have, as noted above, been used to normalise the data.

Fig. 4(a) shows a sketch of the experimental apparatus including a definition of terms used in the presentation of the results. Most of the parameters shown in Fig. 4(a) are straightforward geometric dimensions and require no further explanation. The mean pressure head terms, however, used throughout this chapter, require some further definition and explanation.

The total mean pressure head, at any pressure transducer on the plunge pool floor, is defined by the term $\bar{H}m$ and is illustrated in the sketch overleaf. $\bar{H}m$ is the time-averaged total mean head at the pressure transducer.

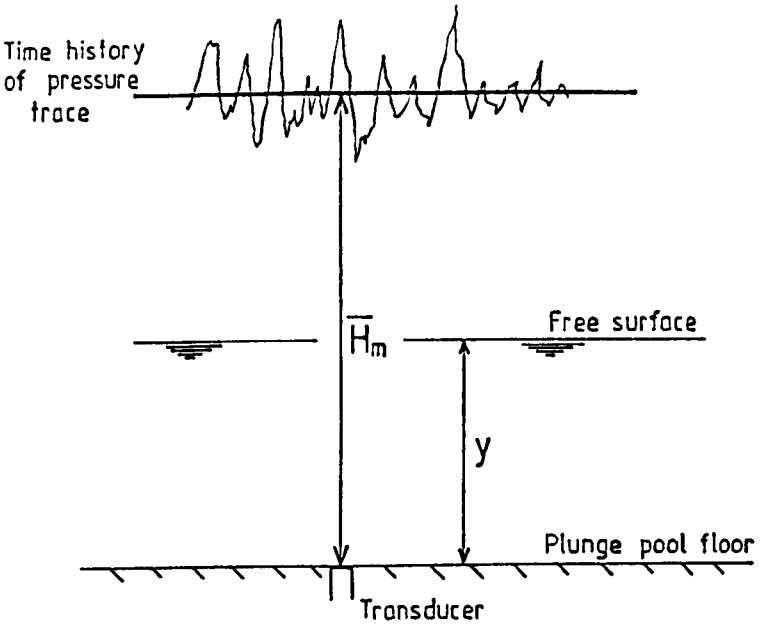

Furthermore, the mean dynamic pressure head is therefore defined as the total mean head minus the hydrostatic head of water in the plunge pool. In other words, the mean dynamic pressure head at the plunge pool floor is given by $\bar{H}m - Y$.

Actually, this is not a precise evaluation of the mean dynamic pressure head as the effect of air entrainment on the pool static head (Y) is not taken into account. Also, as mentioned in Chapter 3, at high impact velocity and low submergence ratio (Y/Di) the tailwater definition is rendered inoperative by the formation of a radial hydraulic jump. The, this definition of the mean dynamic pressure head is only roughly true for a jet of low impact velocity and where the tailwater depth is large relative to the impacting jet diameter. However, as no measurements of the pool air concentrations were available or were readily calculable, the expression ($\bar{H}m - Y$) is taken as indicative of the mean dynamic pressure head for all of the results in this chapter.

Throughout this chapter, both of these terms ($\bar{H}m$ and $\bar{H}m - Y$) are made dimensionless by division with the calculated impact velocity head $Ui^2/2g$ to produce mean pressure head coefficients. A similar process is carried out in Chapter 5 to express the fluctuations of pressure around the mean head, as well as the instantaneous maximum and minimum pressure head fluctuations, in terms of dimensionless coefficients.

4.2 RADIAL DISTRIBUTION OF MEAN PRESSURE HEADS IN PLUNGE POOL.

Experience at the United States Bureau of Reclamation had shown that the design of a plunge pool should be based primarily on a knowledge of the variation of plunge pool pressures with depth. It was also recognised that the variation of plunge pool pressures with radius is an important parameter in the sense that it will determine the plan dimensions of the plunge pool. In other words, a rapid decay of plunge pool pressures in the radial direction would lead to the design of smaller plunge pools. At Morrow Point Dam (previously detailed in Chapter 2 and shown in Fig. 2.60), this is compounded by the fact that up to four plunging jets can be operating simultaneously. Hence the radial distribution of pressure will provide information on the overlap of one jet pressure with the adjacent jet, and how far apart such jets should be placed.

It was clear from the initial literature search, that the variation of mean pressures on the plunge pool floor in the radial direction was already well understood. Thus it was decided in this study to devote only a few tests to variations in the radial direction, and these tests were confined to the nozzle of diameter 78mm. The results are summarised in Fig.4.1 to Fig. 4.4(i).

As detailed in Chapter 3, the axi-symmetric nature of the diffusing circular jet required measurements only along a line emanating from beneath the flow centre line to define the distribution of mean and fluctuating pressures radially on the plunge pool floor. Therefore, the array of flush mounted pressure transducers were located at the pool base in a row with the first transducer positioned at the theoretical centre line of the diffusing jet. Each of the transducers were 100mm apart, the distance being dictated by the size of the transducer housing and intermediate supports. Due to this relatively large distance between individual pressure transducers on the plunge pool floor, the best representation of the radial distribution is given for the largest jet diameter tested (Do = 78mm). This is the condition for the first set of figures that will be investigated.

Figures 4.1 and 4.2 show the radial distribution of the total mean pressure head ratio at the plunge pool floor. The total mean head ($\bar{H}m$), is made dimensionless by the impact velocity head $Ui^2/2g$. The radial term (Rp= distance

from centre line on pool base) is made dimensionless by the outlet diameter in Figure 4.1, and the measured impact diameter in Figure 4.2. The jet fall height in this case is 725−1125mm, depending on the plunge pool depth. Each of the diagrams in Figures 4.1 and 4.2 are for a particular outlet velocity and for the four plunge pool depths tested, namely Y = 100mm, 200mm, 350mm and 500mm

The following observations can be made from Figures 4.1 and 4.2:

(i) The highest total mean pressure heads occur along the plunging jet centre line in the pool, corresponding to the stagnation point (Rp= 0).
(ii) The jet centre line values decrease with increasing plunge pool depth as would be expected. This phenomenon is less marked at the highest jet velocities.
(iii) The total mean head decays rapidly in the radial direction with values being very small at about three jet diameters out from the centreline. This pattern fits broadly the existing relationships for radial decay, for example, as shown in Fig. 2.24 from the work of Hrycak et. al. [1]. An expression for this form of radial decay of the mean head produced by Beltaos and Rajaratnam [2] is given by:

$$\bar{h} / Ui^2/2g = 50\ (Di/Y)^2\ \exp.^{-114(Rp/Di.Di/Y)2} \qquad (4.3)$$

It should be noted that the expression above has been derived for submerged jet diffusion and is only applicable at pool depths larger than the solid core extent.

(iv) The value of plunge pool depth has a marked effect on the total mean head ratio. This can be seen in Figs 4.1(a) and (b) for instance. For higher jet velocities, the effect of plunge pool depth has much less effect, (Figs 4.1(e) and 4.1(f)). For high jet velocities, a radial hydraulic jump or free surface vortex formation with drawdown, is more likely, rendering the tailwater cushion partly inoperative.

(v) The decay of mean heads in the radial direction is most marked at the smallest plunge pool depth (Y =100mm, Y/Do = 1.28). The reduction with radius is least marked at deepest plunge pool depths. This phenomenon is a function of the diffusion of the jet within the plunge pool, which produces a much more uniform spread of pressures with increased depth, as sketched overleaf.

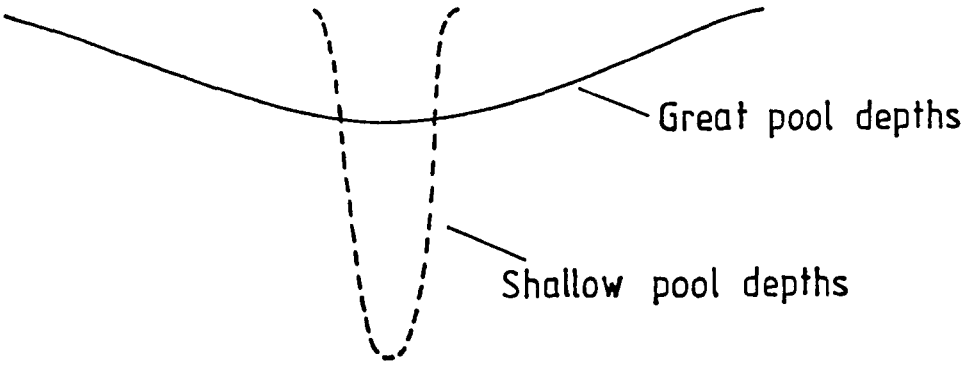

It can be noted from comparision of Figures 4.1 and 4.2 that, at low outlet velocity, the ratio Rp/Do is smaller than Rp/Di. This means that, as anticipated, the jet is contracting during its plunge at low outlet velocity. However, at higher outlet velocities (e.g. Uo ≈ 13 m/s) the ratio Rp/Do is larger than Rp/Di. This is because the falling jet is expanding to some degree from the outlet at higher outlet velocities. Plotting the pressure values with Do as a parameter means that the effect of the jet plunge is not included. By plotting the data values with the measured jet diameter at impact Di, more representative results are obtained, as this parameter partly takes into account the jet behaviour in the atmosphere. One problem with this method however, is that measuring the jet conditions and diameter at impact proves difficult, particularly for high velocity, rough turbulent plunging jets. This point will be investigated in later results sections.

Figures 4.3 and 4.4 show the radial variation of the mean dynamic pressure head. This is determined by subtracting the hydrostatic plunge pool head (depth) from the total mean head. The following observations can be made:

(i) The pattern is similar to Figs. 4.10 and 4.2 showing highest pressures along the jet centre line, the most rapid decay with the shallowest pool depths, etc.

(ii) There is one major difference, however, and that concerns the possibility of obtaining negative mean dynamic heads. The reason for small negative dynamic pressures in Figs. 4.3 and 4.4 is sketched below. The submerged jet spreads radially at the plunge pool floor stagnation point, forming a radial submerged jet which eventually moves in the upward direction forming submerged rollers.

Negative mean dynamic pressure occurs at the points where the jet flow direction is away from the pressure transducer and not towards it. This occurs about 2 to 3 net diameters away from the jet centre line.

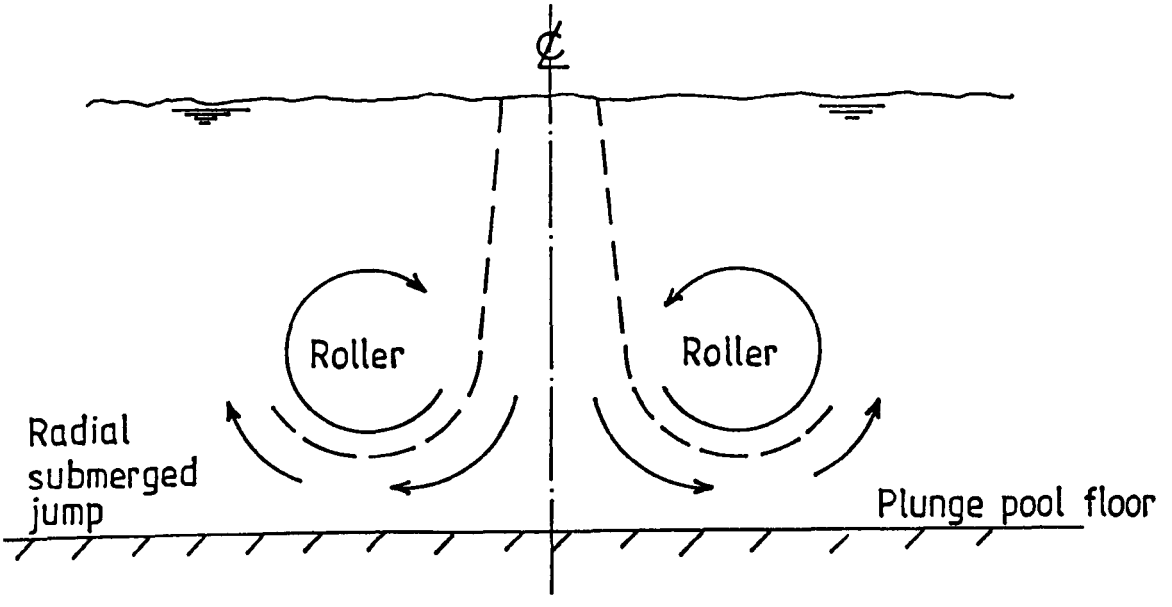

(iii) For the case of the lowest velocity and submergence, the centre line mean dynamic pressure head is roughly equivalent to the entering velocity head ($Ui^2/2g$). As the velocity increases the centre line value is reduced slightly, because of a more diffuse impacting jet, and the cushioning effect of increased air entrainment into the pool.

Fig. 4.4(i) shows a summary of all the mean dynamic pressure head ratios with radial distance, made dimensionless by the impact diameter. The figure illustrates the general trend of the results, reducing from the centre line maximum value with an asymptotic approach to zero, at a distance of Rp/Di between 2 and 3. Beyond this location the pressure is equal to the ambient hydrostatic pressure or slightly negative due to upward velocity components in the main roller as described in the sketch above.

4.3 CENTRE LINE MEAN PRESSURE HEAD VARIATION WITH PLUNGE POOL DEPTH.

4.3.1. Introduction

Perhaps the most significant and least understood aspect of plunge pools is the influence of the depth of the water cushion on both the mean and fluctuating pressures. This section will investigate the variation of plunge pool depth on the value of mean pressures obtained. This process will be carried out along the jet centre line ONLY. The reason for this is that the most significant plunge pool mean pressures are along the centre line as demonstrated already in Section 4.2.

The results for this section are all contained within Figs. 4.5 to 4.23, covering a range of jet diameters, velocities, fall lengths and the orifice test to compare with the nozzles.

Each of the nozzle outlets (Do = 78, 52.5 and 25mm) were tested at two different levels above the plunge pool floor. The distance between the two levels was approximately 1505mm. With alteration of the drop height of the jet above the plunge pool surface, a range of plunge lengths (L/Do) between 9 and 97 could be obtained. This would allow estimation of the influence of the jet fall height parameter on plunge pool dissipation, and cover most of the range encountered at dams. An orifice plate outlet (Do = 25mm) was also tested to investige the effect of a plunging jet with a higher internal turbulence intensity on the dissipation process, and, therefore, impact pressures. The pool depth (Y) was varied from 100 to 500mm (in increments) to qualify the effect of different tailwater levels on the plunge pool pressures. The range of Y/Do tested was from approximately zero, when a hydraulic jump formed, to a maximum value of 20, where the flow was deemed to be fully dissipated.

From the previous section it has been verified that the highest mean pressures are generated beneath the theoretical plunging jet centre line. Therefore, for each outlet, fall height, and jet velocity, the centre line pressure measurements were recorded and analysed specifically, for the range of pool depths mentioned above. Evaluation of the centre line mean pressure head variation with pool depth could then be made under all test conditions.

The mean pressure heads $\bar{H}m$ and $(\bar{H}m - Y)$ were made dimensionless, in the same way as described in Section 4.2, by division with the estimated impact velocity head $Ui^2/2g$. Variation of the centre line values with plunge pool depth were plotted for two instances.

(a) For the case of non-dimensional plunge pool depth Y/Do where Do is the nozzle or orifice diameter.
(b) For the case of non-dimensional plunge pool depth Y/Di, where Di is the measured impact diameter.

Organisation of the centre line mean pressure head results is as follows. Each outlet is considered in turn, firstly for the smallest fall height, range tested, (the precise fall height being dependent on the plunge pool depth), and then for the larger fall height range.

For each fall height range the total mean pressure head ratio $(\bar{H}m)/(Ui^2/2g)$ variation with pool depth is plotted followed by the variation of the mean dynamic pressure head ratio $(\bar{H}m - Y)/(Ui^2/2g)$. After each set of results for the particular outlet have been illustrated in this way a graph is shown of the comparison of results between the two fall height ranges (L/do).

4.3.2. Experimental data for the 78mm diameter nozzle.

Figs. 4.5(a) and (b) show the centre line total mean pressure head results obtained under conditions of a nozzle diameter of 78mm and jet fall length L in the range 725mm-1125mm, depending on the plunge pool depth. The plotted results relate to the jet centreline values of the pressure distribution (Rp= 0). The following observations can be made from comparison of Figs. 4.5 (a) and (b):

(i) A better correlation is achieved by plotting the total mean pressure head ratio with Y/Di, Fig. 4.5(b)

(ii) In Fig. 4.5(b) there is data spread for each of the outlet velocities tested, but the general form is quite clear with reduction in total mean pressure head with increased pool depth, relative to the impact diameter.

Figs. 4.6(a) and (b) show the corresponding variation in the mean dynamic pressure head ratio. The following points can be made regarding these figures:

(i) The best correlation of all is achieved for the mean dynamic pressure head ratio plotted with Y/Di where the results show evidence of collapse onto a narrower band of behaviour.

(ii) The collapse of results in Fig. 4.6(b) is to be expected as the pressures generated at the pool base by the impinging jet are of a purely dynamic nature and, therefore, the static component should not be included in the velocity head relation. The term ($\bar{H}m - Y$) is therefore a more appropriate parameter for the pressure head value. Normalisation of the pool depth by Di is also more appropriate as this parameter partly takes into account the jet condition at the pool surface.

(iii) The mean dynamic pressure head reduces from a value slightly below the full impact velocity head with increase in pool depth relative to the diameter at impact. This can be attributed to the reduction in longitudinal velocity of the diffusing jet flow with distance into the pool, as described by Albertson et. al. [3] for submerged jets.

(iv) Theoretically, as a solid jet core would still exist at the pool surface for these smooth turbulent jets at low droplength, it is anticipated that entrained air will not affect the centre line pressure head results for small pool depths. The mean dynamic pressure head should, therefore, equal the full velocity head as shown below.

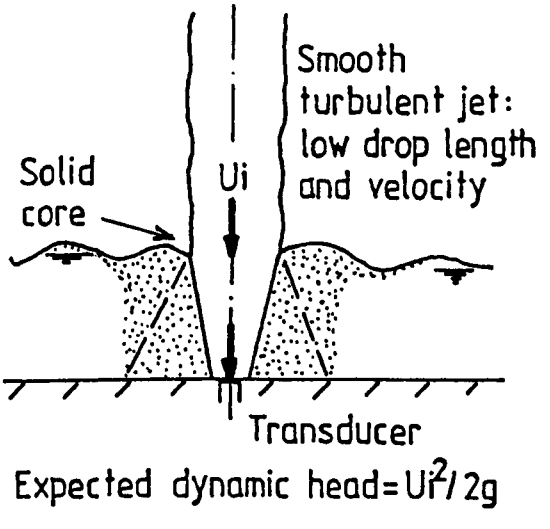

Yet it can be seen, in general, from Fig. 4.6(b) that the mean dynamic pressure head ratio does not equal unity for even low submergence (Y/Di) and outlet velocity. This may be attributed to the actual jet motion in the atmosphere. If the jet has an axial helical swirl during its plunge, as described by Hoyt and Taylor [4], and shown in Fig. 2.43, then the centre of the plunging jet will not at all times impact with the pool surface at a point vertically below the nozzle. The flow position at impact will be oscillating laterally due to the imparted swirl. Therefore, as the centre of the impacting jet will not always be directly above the central transducer, the measurement device will not be subjected to the full centre line velocity head continuously, and hence the measured pressure will not attain the theoretical core value. This phenomena has been verified to a lesser extent in a recent U.S.B.R. testing programme, particularly at larger droplengths.

(v) The beneficial effect of the turbulent plunging jet on the mean pressure development can be seen by considering some of the values in Fig. 4.6(b). For example, at a submergence of Y/Di = 6, the mean dynamic pressure head ratio is around 0.48 to 0.62. When this is compared with Albertson's work [3] on submerged jets, assuming the diameter at impact Di is equivalent to a submerged nozzle diameter, the submerged jet would still theoretically have a solid inner core which would produce a centre line ratio of 1.0.

So, even for a low turbulence plunging jet, produced from a gently tapered nozzle, and for a small fall height relative to the outlet diameter (L/Do = 9 to 14), the mean dynamic pressure is only around 55% of the submerged jet case. This illustrates the advantage of enhanced velocity decay and air entrainment on mean pressures due to the jet plunge through the atmosphere.

(vi) The variation of the mean dynamic head with velocity in Fig. 4.6(b) is such that the largest decay with depth is seen for the case of the lower velocities. The difference in decay rates, however, is not highly significant.

Figs. 4.7 and 4.8 show similar results for the same outlet diameter but for the much larger jet fall height between 2230mm and 2630mm. This corresponds to L/Do from 29 to 34. Due to the larger jet contraction or expansion over this fall height, the pressure results cover a slightly more extensive range of Y/Di than the previous examples. The following points can be noted:

(i) The minimum spread of results is seen again for the mean dynamic pressure head ratio correlated with Y/Di, as in Fig. 4.8(b).

(ii) In Fig. 4.8(b) the maximum centre line value of the mean dynamic pressure head ratio of around 0.8 to 0.9 occurs between Y/Di of 1 to 3 with a rapid reduction after this to a value of around 0.15, for the lowest velocity case, at Y/Di $\approx$ 10.

Fig. 4.9 shows the variation of the total mean and mean dynamic pressure head ratio with plunge pool depth for both jet fall height ranges. In this diagram it should be noted that similar conditions for the velocity head are included. Therefore, the results for the lowest velocity case at the fall height range of 725–1125mm and the highest velocity case of the larger fall height range of 2230–2630mm are ommitted for the purpose of direct comparison between the two cases.

The following initial comments can be made about Fig. 4.9(b):

(i) There is no significant change in the mean dynamic head comparing a drop length of L/Do $\approx$ 10 to L/Do $\approx$ 30. This is because the graph has been normalised using the actual jet diameter at impact and the actual jet velocity at impact.

It is also because smooth turbulent jets, as in this case, take a L/Do of around 300 to completely break–up. Therefore the change of L/Do from 10 to 30 is not very significant in terms of changes of jet structure. This is also true for the variation of plunge point air entrainment rates which again may not alter significantly when normalised by the impact velocity $Ui^2/2g$.

(ii) Fig. 4.9 also reveals that the mean pressures along the jet centre line remain constant for 3 to 4 jet diameters into the plunge pool. This is significantly less than the 6.2 diameters quoted for submerged jets, and reveals significantly shorter jet core lengths for plunging jets compared with submerged.

(iii) Fig. 4.9 also reveals that the mean dynamic head ratio never reaches unity as supposed in the jet core region. At first it was thought that this was a measurement error in the centre line pressure transducer. This was checked and

re– calibrated to reveal no significant errors. Vertical plumb lines were also used extensively to check the alignment of nozzles and centre line pressure transducer with no significant errors revealed. The range of possible reasons include

– air bubbles in the impinging jet.
– axial swirl and instability in the jet meaning that the jet did not always impact exactly on a point vertically below.
– diameter of pressure transducer too large.
– poor alignment of jet centre line to pressure transducer.

The most likely reason is helical jet swirl predicted by Hoyt [4] combined with air bubbles in the jet core.

4.3.3. Results for 52.5mm diameter nozzle outlet.

The same organisational sequence of results (Figs. 4.10– 4.14) follows for the next nozzle outlet in terms of magnitude (Do = 52.5mm). Obviously the smaller nozzle size will produce larger values of Y/Do and Y/Di than previously considered for the same test conditions. This allows investigation of the pressure decay at greater submergence. Fig. 4.10 shows the variation of the total mean pressure head ratio at the jet centre line with pool depth. In this case, the fall length is from 620mm to 1020mm giving L/Do in the range 12 to 20. The small difference between this range of droplengths and the previous values for the larger diameter outlet is that (as detailed in Chapter 3) the smaller 52.5 mm nozzle acts as an extension piece. The taper nozzle portion with a 52.5mm outlet connects directly onto the larger diameter counterpart, thus producing a smaller fall height for the same pool depth.

Considering Fig. 4.10, it can be seen that, at the lowest outlet velocity tested, an anomaly occurred going against the general trend of the results. That is, at the highest submergence Y/Di≈12, the total mean pressure head can be seen to increase. This can be explained by the correlation of the mean dynamic head with pool depth, shown in Fig. 4.11.

At low outlet velocity and fall height, the impact head is relatively small and, due to contraction during its fall, the jet diameter at impact is a mimimum for this set of tests. Only a minimal amount of air is entrained into the pool

under these conditions and, as the submergence is increased, a larger portion of the measured pressure is comprised of the hydrostatic head. With the highest submergence (Y = 500) and the low impact velocity head, a large proportion of the total mean pressure head ratio is due to the hydrostatic component. It is precisely this situation, with low entrainment and large pool depth, where a more accurate evaluation of the actual pressure generated by the impacting jet is given by subtraction of the full plunge pool depth from the total mean pressure head ($\bar{H}m - Y$).

By considering the same point in both Figs. 4.10 and 4.11, it can be seen that the deviation from the general trend of the results is due to the hydrostatic component in the total mean pressure head at high submergence and for a low impact velocity head. This effect is even more apparent for the smallest nozzle diameter tested at low droplength, which will be covered later in this section. It can be concluded from the above that the best correlation will be found by relating the pressure head above hydrostatic with the impacting velocity head, however, only in the specific cases mentioned is evaluation of the hydrostatic component as simple as deduction of the full plunge pool depth from the total mean pressure head.

The influence of the greater jet fall length (L/Do = 40 to 48) is shown in Figs. 4.12 and 4.13. In Fig. 4.12 the effect of the static head in the total mean pressure head is not noticeable. This is because the greater fall height (L = 2126 – 2526mm) in this example produces a larger impact velocity head and hence the hydrostatic component is a smaller proportion of the total mean pressure head. The best correlation is again obtained by plotting the estimated mean dynamic pressure head ratio with Y/Di, shown in Fig. 4.13(b). Compared with the previous diagram for the larger diameter outlet, the general trend is very similar, with a rapid reduction in pressure head for increase in pool depth after an initial peak value of around 80–90% of the impact velocity head. This is because the impact condition is taken into account for both outlets. However, extra information can be obtained due to the smaller nozzle size. For example, it can be seen from Fig. 4.13(b) that the mean dynamic head is still around 10% of the velocity head at a plunge pool depth of Y/Di = 15, approximately.

Fig. 4.14 shows the direct comparison of total and dynamic mean heads at both ranges of droplength (L/Do = 12 to 20 and L/Do = 40 to 48) for the

nozzle of 52.5mm diameter. The following points can be noted:

(i) The pattern is very similar to Fig. 4.9 for the 78mm nozzle.
(ii) There is no discernible difference for both jet droplengths provided the graph is normalised by jet diameter at impact D_j and jet velocity at impact Ui.
(iii) Again the mean centre line pressure remains constant for approximately 3 to 4 jet diameters into the plunge pool, and the values of head are significantly less than the submerged jet case.
(iv) Again the pressures in the jet core do not reach values as high as $Ui^2/2g$, probably for similar reasons as before, such as helical jet swirl in the atmosphere and air entrainment into the jet core in the plunge pool.
(v) Again there was no significant variation in mean dynamic head ratio with varying jet velocity, at least where the jet velocity at impact point Ui is used as the parameter.

4.3.4 Results for 25mm diameter nozzle outlet

The smallest nozzle outlet tested was 25mm in diameter, and Figs. 4.15 to 4.19 present the centre line pressure head results obtained for this diameter. For the lowest jet fall length range (L= 513− 913mm or L/Do= 20 to 36) the effect, mentioned earlier, of the hydrostatic component on the total mean pressure head is most pronounced, Fig. 4.15(b). At larger pool depths this effect influences the results up to an outlet velocity of approximately 5m/s. Fig. 4.16 shows the correlation of the more appropriate mean dynamic pressure head with pool depth. By testing at large pool depths relative to the jet diameter, as shown in this figure, an estimation can be made of where the diffusing jet can be said to be fully dissipated. A nominal designation of this condition can be gained by inspection of the figure to determine where the mean dynamic pressure head is, say, only approximately 5% of the impacting velocity head. Considering Fig. 4.16(b), it can be seen that this condition in roughly satisfied at a ratio of Y/Di around 18. This value is in general agreement with that quoted by Hartung and Hausler, referenced in Chapter 2 [98], of Y/Di equal to 20 for complete dissipation. It should be noted, however, that the diameter at impact in Hartung and Hauslers example is calculated purely on the basis of gravity and continuity considerations. It should also be noted that, even if the jet diameter at impact with the pool surface could be estimated for a particular prototype spillway

configuration, a plunge pool depth of this magnitude for complete dissipation in terms of mean pressure would be highly uneconomical. A lined pool plunge with a smaller depth would be supplied ensuring a greater mean pressure application to the base slab.

Figs. 4.17 and 4.18 represent the results obtained at the upper level of testing (L= 2018− 2418mm) for this nozzle outlet. This corresponds to the range of L/Do from 81 to 97. The largest fall length to outlet diameter ratio is therefore manifested for this test condition. In this case the maximum droplength is almost 100 outlet diameters above the plunge pool surface (when Y = 100mm) which is about the upper range of many prototype spillways. The results plotted against the pool depth to outlet diameter, Figs. 4.17(a) and 4.18(a), show a distinct trend with the pressure head ratio increasing with outlet velocity for a constant Y/Do value. This trend is not apparent, however, when the values were plotted with Y/Di as the dimensionless parameter, Figs. 4.17(b) and 4.18(b). The best form for the data points is again obtained by plotting the results as shown in Fig. 4.18(b). It can be seen from this figure that the flow could again be said to be completely decayed, in terms of the mean pressure exerted at the pool floor, at around Y/Di of 18. Comparison of the results for both ranges of droplength (L/Do= 20 to 36 and L/Do= 81− 97) is included in Fig. 4.19. Fig. 4.19 shows that, in general, there is no significant difference between the results for the larger and smaller jet droplengths for the 25mm nozzle, apart from at the larger pool depths where it appears that the total pressure head values for the smaller droplengths are slightly larger than the upper level values. Again this effect is due to the hydrostatic component in the total mean head at the low impact velocities which were produced for the smaller jet droplengths. The difference, therefore, is not significant in the mean dynamic heads in Fig. 4.19(b).

Figs. 4.20 (a) and (b) are significant diagrams for the design of plunge pools. This is especially true for Fig. 4.20(b) which shows the non− dimensional mean dynamic head against the plunge pool depth for three different nozzle diameters 25mm to 78mm, a range of jet droplengths from L/Do= 10 to 100 approximately, and a range of jet velocities at impact from 3m/s to 20m/s approximately, covering the model and part of the prototype structure range. The only parameter which is not varied significantly here is jet turbulence. All three nozzles produce essentially smooth turbulent jets, and hence it is premature

to use Fig. 4.20(b) for more highly turbulent prototype structures.

The results show a good collapse, especially in Fig. 4.20(b) where the effect of the hydrostatic component is negated. From this figure it can be seen that the highest value of mean dynamic head is around 0.85 of the impact velocity head at low plunge pool depths (Y/Di= 1− 3). After this there is a rapid, almost exponential decay in the mean head with pool depth. For example, at Y/Di = 8 the average mean dynamic pressure head ratio has reduced to about 0.4. At Y/Di equal to between 18− 20 the mean dynamic head is only a small proportion of the impact head, and hence, can be said to be virtually insignificant. In Chapter 6 a best fit curve will be produced for this general trend and the presentation of the results in this form will be compared with data from other relevant work in this field. Clearly if a jet diameter at impact can be calculated, then a good design tool for the mean pressure head is likely from this work.

4.3.5. Results for 25mm diameter orifice outlet

The 25mm diameter orifice outlet was incorporated to allow testing of a plunging jet which possessed a much higher turbulence than those previously encountered with the nozzles, and to produce a flow structure similar to that of a sluice gate type outlet in a dam structure. Measurements of the actual intensity and propagation of turbulence within the plunging jets will be dealt with in Section 4.4. The following will consider the mean pressure values in the plunge pool beneath the centre line of the jet produced by the flow issuing from the orifice outlet. Details of the orifice outlet design have been given in Section 3.3.2.

The structure of the falling jet issuing from the orifice was different in comparison with the jets issuing from the nozzle outlets. Just downstream from the orifice outlet a noticeable contraction formed where the flow area was reduced to around 65% of the original area. This is a Vena Contracta region. Local acceleration occurred at the Vena Contracta and made estimation of the impact velocity Ui much more difficult. In the end, this effect was ignored and the impact velocity was calculated purely on the basis of free− falling flow. At the contraction, the jet also had a glassy nature, caused by suppression of the

internal turbulence. It was not until the jet had travelled further downstream that the flow appeared to roughen and expand laterally. The rate of jet expansion was seen to be dependent primarily on the outlet velocity. At the impact point in the plunge pool, and especially with the larger velocities tested, the rough turbulent impacting jet had a highly diffused character, more akin to a prototype than the previously tested smooth turbulent jets. This was precisely the condition that was hoped for, but it proved difficult to estimate the jet diameter at impact (Di) as the flow was much more irregular in nature. Therefore, an average value had to be taken from a series of photographs and physical measurements to indicate the jet impact diameter. Taking into account these problems, regarding the jet impact velocity and diameter, the mean pressure results will necessarily not be normalised as accurately as in Figures. 4.1 to 4.20 for the nozzle behaviour.

The orifice outlet was tested for only one range of fall heights (L= 1020– 1420mm) or an L/Do ratio between 41 and 57. At larger fall heights, definition of the jet conditions at impact would prove to be even more difficult. Fig. 4.21 shows the variation in the total mean pressure head ($\bar{H}m$) ratio with pool depth normalised with both orifice diameter and jet diameter at impact. Fig. 4.22 illustrates the variation in the mean dynamic pressure head ($\bar{H}m - y$) ratio. Most of the salient points that have been covered in the previous description of such diagrams are applicable for Figs. 4.21 and 4.22. The general trend is similar to that produced by the smooth turbulent jets with mean pressure reducing rapidly from a peak value with pool depth. The best form of the results is found in Fig. 4.22(b), covering the range of velocities tested through the orifice outlet.

Fig. 4.23(b) is perhaps the most significant graph so far. This is a plot of the mean dynamic head against plunge pool depth for both nozzles and orifice plate, across the range of diameters, velocities and droplengths (L/Do up to 100) tested. The following points can be noted:

(i) The data from the orifice plate collapses on to the same curve as the nozzle data despite the fact that the turbulence level in the orifice (Section 4.4) is typically 5% and in the nozzles is typically less that 1% i.e. the jets from the orifice plate are much more diffused at the point of impingement on to the pool surface.

(ii) The mean dynamic head remains constant for 3–4 jet diameters into the plunge pool for both orifice and nozzle jets.

(iii) There appears to be no significant variation on Fig.4.23(b) for either varying jet velocity or varying jet droplength.

(iv) There is now some confidence that Fig. 4.23(b) can be used as a design curve. This will be explored further in Chapter 6, in case of a coincidence of jet break–up lengths or air entrainment rates which may have colluded to produce this collapse of data over such a wide range of parameters.

4.4 MEASUREMENT OF TURBULENCE IN THE ATMOSPHERIC PLUNGING JETS

4.4.1. Introduction

Measurements of longitudinal turbulence intensity U'/U, were taken within the plunging nozzle and orifice jets, at various points across each jet radius and at various points along the length of the plunging jet.

It should be noted that the turbulence measurement which would have been more valuable was V'/U, in the lateral direction, determining jet spread. This was not physically possible using the turbulence probe, described in detail in Section 3.4.3, and would only have been possible with laser measurement (LDV). Laser measurements were also ruled out because of a rough and uneven jet free surface.

There were three major reasons noted below for carrying out the jet turbulence measurments:

(a) To determine the jet diameter at impact.

It is already clear from Sections 4.2 and 4.3 of this chapter that the best correlations of plunge pool pressures are for the case of parameters normalised by the velocity at impact Ui and, more importantly, the jet diameter at impact Di.

The latter parameter is difficult to determine in rough turbulent spreading jets, but turbulence measurements may help in the calculation.

The idea proposed by Ervine and Falvey [5] suggests that particles of fluid near the edge of the jet, issuing from nozzle or orifice, have two velocity components acting. These are the longitudinal component U and the lateral turbulent velocity V'. These act to produce a resultant velocity for the edge of the jet which makes an angle θ, where $\theta = \tan^{-1}(V'/U)$. Water particles on this course form a parabolic trajectory under the influence of gravity as shown below. If V' and U are known then the jet diameter at impact D_i can be determined. This will be discussed further in Chapter 6.

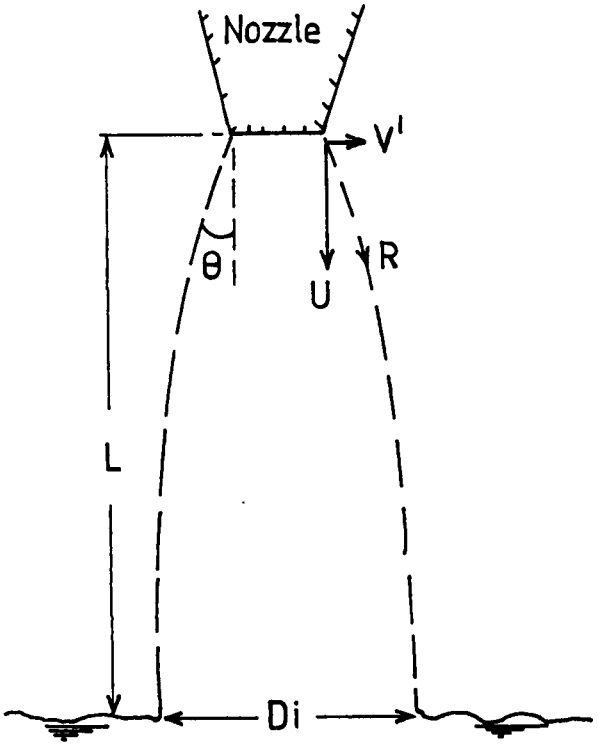

Thus turbulence measurements at the jet outlet would provide a strong indication of this parameter, if the jet diameter can be determined simply from a knowledge of turbulence, combined with continuity and gravitational considerations.

(b) Jet turbulence measurements are also useful in understanding the process of jet disintegration and break–up. This is similar to (a) above, and concerns

estimates of the jet break-up length which will be discussed in some detail in Chapter 6. The break-up length is assumed to be a function of Reynolds and Weber Number, or alternatively, may be expressed as a function of turbulence intensity, velocity and jet diameter when dealing with a water/air system.

Large turbulence intensity jets tend to have short break-up lengths of the order of L/Do≈ 50 to 100 whereas low turbulence intensity jets have break-up lengths of the order L/Do≈ 300-400. It is therefore important to have an idea of the degree of disintegration of each of the jets tested in this thesis, even though the fall length (L) in the experiment was not sufficient to measure the actual break-up length (LB) accurately.

(c) Jet turbulence measurements are useful in determining approximately how much air is entrained by the jet at the point of impact. This is because undulations on the jet surface are a function of the turbulence acting within the jet, and the rate of entrainment of air is a function of the size of the jet undulations. Ervine [6] has produced simple approximate relationships for the rate of air entrainment by plunging circular jets of the form:

$$\beta i = f\,(Tu_0)\surd\,(L/Do) \qquad (4.4)$$

which might approximate to $\beta i \approx 0.3\surd\,(L/Do)$ for rough turbulent jets and $\beta i \approx 0.15\surd\,(L/Di)$ for smooth turbulent jets. Thus it was decided to carry out a programme of turbulence measurements with the specially designed instrument described in Section 3.4, with the results presented in Figures 4.24 to 4.35.

The results are presented in the following way. For each outlet (excluding the 52.5mm nozzle), the radial distribution of the longitudinal turbulence intensity U'/Uo is plotted first with the values normalised relative to the outlet conditions, i.e. Uo and Ro where Uo and Ro are the outlet velocity and radius respectively. Subsequent radial distributions are plotted with the r.m.s. component of velocity U' and the radial distance to the measurement point from the jet centre lines made dimensionless with the local parameters U and Rj. The local parameters being the mean velocity and the jet radius at the measurement point respectively. Each figure applies at a specific distance downstream from the outlet and covers a range of tested outlet velocities. Following this, the longitudinal variation of the turbulence values is presented for each radial position but varying in the

downstream direction. Similar to above, the first version is made dimensionless with the outlet conditions and the second relative to the local conditions.

Certain restrictions applied to the radial and longitudinal extent of the measurement positions within the plunging jet. Radial measurements were kept away from the jet edge to ensure that intermittency at the jet outer surface and air bubbles would not effect the results. Measurements along the jet length were limited to the initial portion of the jet length to prevent aeration, if any, influencing the reulsts. A brief discussion of the turbulence results will be included in the following sections.

4.4.2 Results for 78mm diameter nozzle outlet

Figs. 4.24 and 4.25 show the variation of the longitudinal jet turbulence in the radial direction for various distances from the outlet. The range of initial velocities covered is 7 to 13 m/s. There is not much difference between the two figures as the condition of the plunging jet from the 78mm diameter nozzle had not changed much over such a small distance from the outlet. Considering Figures. 4.24 and 4.25 it can be seen that:

(i) The values of turbulence intensity are under 1% which represents a low turbulence intensity jet. This was made possible by the combined use of a tube bundle and a smooth tapered nozzle.

(ii) Values of turbulence intensity increase with jet velocity. This is due to the increase of Reynolds Number which almost doubles, from $5x10^5$ to $1x10^6$

(iii) Values of turbulence intensity increase with radial distance out towards the jet edge. This is due to a thin boundary layer forming along the nozzle, which occupies only a small thickness (relative to the jet diameter) at the outlet. This is sketched below.

(iv) The thickness of the boundary layer increases with distance along the jet L/Do. This is seen when comparing graphs (a), (b) and (c) which reveal the high turbulence levels at the jet edge moving towards the jet centre line as we move downstream.

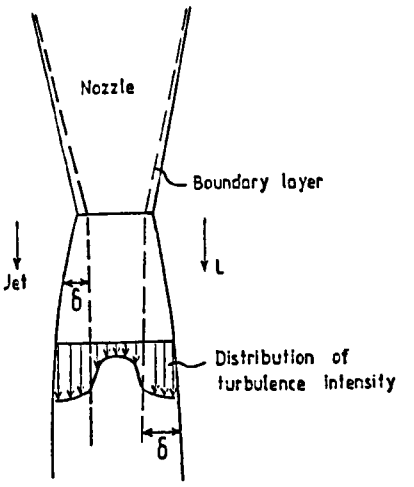

$$\frac{\delta}{L} = \frac{K}{Re_L^{0.2}}$$

where $Re_L = \frac{UL}{\nu}$

(v) The preceding point is also noticeable when considering the longitudinal variation of the jet turbulence in the downstream direction at given radial positions, as shown in Figs. 4.26 and 4.27. The centre line (rj/Ro= 0) and intermediate radial positions show fairly constant values, however, near the jet edge, Fig. 4.26(c), the turbulence intensity is seen to increase as the distance from the outlet is increased. This is attributed to the development of the turbulent boundary layer into the body of the plunging jet.

(vi) Another point regards the use of the turbulence results to estimate the jet condition at impact point. Values of the longitudinal turbulence intensity near the jet edge may be used to estimate lateral values (v'/u) and hence allow calculation of the jet dimensions with fall height. This is achieved by assuming that surface tension is overcome by the estimated lateral turbulent velocity component and the jet spreads laterally in the atmosphere. The procedure has been detailed in Chapter 2, and is augmented in Chapter 6 to include gravitational considerations, to allow calculation of the jet diameter at impact for comparison with the measured values.

The same sort of pattern in the 78mm diameter outlet results was also produced for the 52.5mm nozzle results. To allow investigation of turbulence in the plunging jet at greater ratios of l/Do, for approximately the same fall heights, the results for the 25mm nozzle outlet will be considered below.

4.4.3. Results for 25mm diameter nozzle outlet.

From Figs. 4.28 and 4.29 it can again be seen that the level of turbulence is very small. In fact, the results are even less than the core values for the

78mm diameter nozzle outlet. This is to be expected as the Reynolds Number in the 25mm nozzle is in the range of $2x10^5$ to $4x10^5$, which is only 40% of the 78mm nozzle value. It can be noted that for l/Do=17.2, Fig. 4.28(c), the turbulent boundary layer is much thicker. At this distance relative to the outlet diameter, the boundary layer had diffused further towards the jet centre line so that it is now occupying almost half of the jet radius. Figs. 4.30 and 4.31 also show the increase in turbulence near to the jet edge with distance from the outlet, due to boundary layer ingress towards the jet centre line. It is postulated that one of the major pre-conditions for eventual jet break-up is that the internal jet turbulence be diffused right to the jet centre line. This will be considered in detail in a later chapter.

4.4.4. Results for 25mm diameter orifice outlet.

It was thought that the much rougher condition of the plunging jet issuing from the 25mm orifice outlet would manifest itself in the magnitude of the jet turbulence readings. This is shown to be the case in Figs. 4.32 to 4.35. Due to the more irregular nature of these jets several runs were taken to obtain consistent results, and also the plunge length was investigated at several more downstream positions than the corresponding smooth turbulent nozzle jets. Hence, with the larger volume of results, both Figs. 4.32(i) and 4.32(ii) represent the radial variation of turbulence at given positions along the jet length relative to the outlet condition, while Figs. 4.33(i) and 4.33(ii) represent the results relative to the local velocity and jet magnitude.

From the turbulence readings at the contraction, produced just downstream of the orifice (Figs. 4.32(i)(a) and 4.33(i)(a)), the glassy nature of the flow is indicated by the small magnitude of the longitudinal jet turbulence values. Increases in jet fall length beyond the contraction produce a turbulence level which is greatly increased, especially at higher outlet velocities. Thus at l/Do=17, the jet turbulence reaches 6-7%. The increase in jet turbulence beyond the contraction was noticeable in the visual inspection of the jet condition.

The results are much more irregular than those previously considered, however, it can be seen that at the larger fall lengths and velocities, the

maximum turbulence values are displaced from the jet edges into the central portion of the flow. This is particularly true for l/Do= 17, Figs. 4.32(ii)(e) and 4.33(ii)(e) where it is seen that the variation with velocity (or Reynolds Number) is also much more significant.

The final diagrams in this chapter, Figs. 4.34 and 4.35, show the longitudinal variation of the turbulence results for a given jet radius. It can be seen in these figures the difference in the turbulence structure for the jet issuing from the orifice compared with the nozzle outlets. The centre line (rj/Ro= 0) (Graph (a)) turbulence intensity increases for greater jet fall lengths and at higher velocity, indicating migration of the boundary layer into the central portion of the jet. Near the jet edge, Graph (c), the turbulence reaches a maximum before reduction with further distance from the outlet. The maximum occurs at l/Do≈15 as shown on Graph 4.34(c). With these large values of internal jet turbulence, and re– distribution of the turbulence to the jet centre line, it is obvious that the jet condition at impact would be far more diffused than the corresponding smooth turbulent jets. This was the condition that was noted during jet impact with the plunge pool surface.

REFERENCES FOR CHAPTER 4

1. Hrycak, P., Lee, D.T., Gauntner, J.W., and Livingood., J.N.B., "Experimental Flow Characteristics of a Single Turbulent Jet Impinging an a Flat Plate.", N.A.S.A., TND–5690, 1970.

2. Beltaos, S., and Rajaratnam, N., "Impinging Circular Turbulent Jets.", Jour. of the Hyd. Division, A.S.C.E, Vol. 100, No. HY.10, 1974, pp. 1313–1328.

3. Albertson, M.L, Dai, Y.B., Jensen, R.A., and, Rouse, H., "Diffusion of Submerged Jets.", Proc. A.S.C.E., Vol. 74, 1948, pp. 639–663.

4. Hoyt, J.W., and Taylor, J.J., "Turbulence Structure in a Water Jet Discharging in Air.", The Physics of Fluids, Vol. 20, No. 10, Pt.11, 1974.

5. Ervine, D.A., and Falvey, H.T., "Behaviour of Turbulent Water Jets in the Atmosphere and in Plunge Pools.", Proc. I.C.E., Part 2, 1987, pp. 295–314.

6. Ervine, D.A., "The Entirainment of Air in Water.", Water Power and Dam Construction, 28, No.12, 1976, pp. 27–30.

CHAPTER 5

EXPERIMENTAL DATA OF PRESSURE FLUCTUATIONS AT THE PLUNGE POOL FLOOR

CONTENTS

CHAPTER 5

5.1 INTRODUCTION

It is clear from Chapters 1 and 2 that most of the problems stemming from energy dissipation in plunge pools and stilling basins derive from pressure fluctuations rather than high values of mean pressure. It is therefore apparent that an investigation into the magnitude and frequency of such fluctuations is as important in the design of a hydraulic structure, as any consideration of mean pressures acting. It follows that the results presented in this chapter should provide considerable insight into plunge pool behaviour in general, both in terms of likely vibration loading to the structure from the fluid, the likely uplift forces acting on the underside of a concrete slab, as well as the range of fluctuations which might induce scour in unlined pools.

Definition of the magnitude and distribution of the random pressure fluctuations at each measurement point on the plunge pool floor was carried out by recording and statistically analysing the sample set of instantaneous pressure head results obtained over a suitable time period. As generally detailed in Chapter 3, the statistical parameters included the sample mean head, standard deviation and the maximum and minimum instantaneous pressure head values. To test the normality of the data, the skewness and kurtosis of the results was also calculated. Normalisation of the statistical information regarding the magnitude of the pressure head fluctuations was carried out using the estimated impact velocity head ($Ui^2/2g$) at the pool surface, producing various pressure head coefficients.

These terms are expressed as follows:
The root mean square (r.m.s.) pressure head coefficient (Cp') is given as:

$$Cp' = h' / Ui^2/2g \qquad (5.1)$$

where h' is the standard deviation of the sample set. The maximum (Cp^+) and minimum (Cp^-) instantaneous pressure head coefficients are expressed relative to the mean pressure head, as:

$$Cp^+ = (Hmax - \bar{Hm}) / Ui^2/2g \qquad (5.2)$$

and

$$Cp^{-} = (\bar{H}m - Hmin) / Ui^2/2g \qquad (5.3)$$

where, Hmax is the maximum instantaneous pressure head measured during the sample period, and Hmin is the minimum instantaneous pressure head measured during the sample period. It should be noted that if the results are normally distributed, then, by definition, the values of Cp^{+} and Cp^{-} should not generally exceed three times the r.m.s. pressure head coefficient. Therefore, as well as the skewness and kurtosis parameters, a rough check can be made on the probability density function of the results by investigating this relationship. Cp+ can be referred to as peaks above the mean, and Cp^{-} can be referred to as minimum peaks below the mean.

Further information, especially useful for design, can be gained by considering the instantaneous peak and instantaneous minimum pressure head. Again these are normalised with the entering flow conditions at the pool surface by division with the impact velocity head ($Ui^2/2g$). The peak and minimum head ratios can be expressed as:

$$Hmax / Ui^2/2g \qquad (5.4)$$

$$Hmin / Ui^2/2g \qquad (5.5)$$

As before, the corresponding instantaneous dynamic peak and minimum values can be roughly determined by subtraction of the plunge pool depth from the measured (total) values. Hence, the dynamic peak and minimum pressure head ratios are given respectively by:

$$(Hmax - Y)/ Ui^2/2g \qquad (5.6)$$

$$(Hmin - Y)/ Ui^2/2g \qquad (5.7)$$

The format of the chapter will be a presentation of the various pressure head ratios (noted above) for a range of jet velocities, droplength in the atmosphere, plunge pool depth, jet diameter, comparison of nozzles and orifice as well as a brief study (below) on the variation of fluctuations in the radial direction. The parameters varied are the same as those already described in Chapter 4, covering the usual model range and also part of the prototype range,

at least in terms of velocity. It is thought that this is the first rigorous experimental study of pressure fluctuations on a plunge pool floor with free falling jets, although comparable studies have been carried out in hydraulic jump stilling basins, submerged bottom outlets of dams as well as boundary layer fluctuations on a chute spillway.

5.2 RADIAL DISTRIBUTION OF PRESSURE FLUCTUATIONS ON THE PLUNGE POOL FLOOR.

It was felt at the start of this research that the maximum values of pressure fluctuation would not necessarily occur along the jet centre line, even though the highest mean pressures occur along this line. This was speculated because pressure fluctuations are caused by turbulence, which is usually at a peak in jets some radial distance from the jet centre line. It was decided to carry out a brief investigation on the effect of varying radial distance at the plunge pool floor.

The results are presented in Figures 5.1 to 5.6, for one jet diameter only (78mm) and for one droplength only (L= 725− 1125mm). Pressure transducers are placed at the jet centre line, and at 100mm spacings radially along the plunge pool floor. The results are presented first for the r.m.s. pressure head coefficient Cp' and subsequently for the maximum and minimum pressure head fluctuation about the mean value, Cp^+ and Cp^-. For each of these terms the radial distance to the point of measurement from the jet centre line (Rp) is made dimensionless, initially by the outlet diameter Do, and then with the measured jet impact diameter Di. In each figure the individual diagrams (a− f) refer to a particlular outlet velocity and each diagram includes all of the plunge pool depths tested from 100mm to 500mm.

Figs. 5.1 and 5.2 show the radial variation of the r.m.s. pressure head coefficient (Cp'). The following points can be noted:

(i) Generally the trend of the results can be considered separately for the small pool depths (Y = 100 and 200mm) and larger pool depths (Y = 350 and 500mm). This is particularly apparent when the outlet velocity is around 7m/s and 9m/s in Figs. (c) and (d). For the small pool depths at these velocities, the maximum value of Cp' is found to occur at the intermediate measurement point

or even at the furthest radial extent shown. At larger pool depths, the maximum value of Cp' occurs along the jet centre line. Large pool depths give a rapid decay of C_p' with radius.

(ii) At the furthest radial position shown (Rp = 200mm) the r.m.s. pressure head coefficient is roughly similar for all depths (Cp' = 0.025 – 0.05). Beyond this point (Rp = 300 and 400mm) the values of Cp' remain relatively small, consistent with values where the flow is parallel to the solid surface rather than normal to it. The side walls of the plunge tank seem to have no effect on the results at the extreme radial positions as the tank dimensions are much larger than the extent of measurement.

(iii) The observations in (i) and (ii) above can be explained in the context of turbulence development in the plunge pool. This is sketched below and has been detailed in Chapter 2. It has been found from measurement that at low submergence, the maximum level of longitudinal turbulence is located outwith the jet core, in the centre of the mixing region at point A sketched below. Correspondingly, at low pool depths relative to the jet diameter, the maximum level of fluctuations will be radially situated outside the centre line of the diffusing jet. With increase in submergence some distance beyond the jet core, the maximum longitudinal turbulence is found to be at the jet centre line. Therefore, at the larger pool depths, the maximum fluctuations will be along the jet centre line.

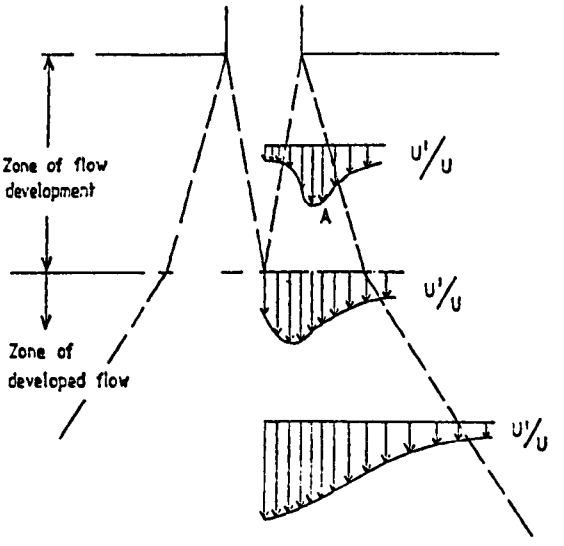

It can be seen in Figs. 5.1(f) and 5.2(f), however, that at higher velocities, the radial displacement of the highest turbulence level is true even at a plunge pool depth of 350mm, corresponding to a Y/Do of almost 5. This means that along the jet centre line in the plunge pool, turbulence intensity is increasing with depth in the core region and even slightly beyond the core region until a peak is reached. Thereafter the turbulence decreases with greater depths. This may true for pressure fluctuations as well.

The only other anomaly from the general trend is for the lowest velocity case (Uo $\approx$ 3 m/s), Fig. 5.1(a), at the pool depth of 200mm, where the maximum value of Cp' occurs along the jet centre line. This occurs at a value of Y/Do of 2.56 and implies a very short core length for such a low velocity jet.

(iv) Regarding the overall magnitude of the r.m.s. pressure head coefficients obtained during this series of tests, the largest values generally occured along the jet centre line. For the case where the pool depth was set at 500mm, the value of Cp' at the jet centre line was found to be between 0.13 and 0.19, depending on the outlet velocity. A centre line Cp' of 0.21 was recorded at a pool depth of 350mm, or Y/Do of 4.49. At the intermediate radial measurement point of those shown (Rp= 100mm), the maximum value of Cp' never exceeded 0.12.

Turning attention to the maximum and minimum fluctuations, it is clear that if the pressure fluctuations at each measurement point followed a normal distribution curve, as would be expected for the case of random turbulence, then the results for the maximum and minimum fluctuations about the mean would be equal and have a value which would be approximately three times the corresponding magnitude of Cp'. The results would be of this form as the normal distribution is symmetrical and usually truncated at three standard deviations from the mean value. That is, the probability of encountering values above, or below, three standard deviation from the mean is remote.

By referring to Figs. 5.3 and 5.4, which show the radial distribution of the maximum pressure head coefficient (Cp^+), and Figs. 5.5 and 5.6, which show the radial distribution of the minimum pressure head coefficient (Cp^-), it can be seen that the situation is similar, but not as clearly defined as Figs. 5.1 and 5.2. Generally the division of the results into two pool depth groups still holds true, with lower values at low submergence along the jet centre line, increasing with

depth along the centre line. Again in the jet core region highest values occur at a radial distance from the centre line. In certain circumstances however, the pattern is not exactly as anticipated, assuming the fluctuations fit a normal distribution curve. For example, comparing the maximum pressure head coefficient Cp^+, with the r.m.s. head Cp', it can be seen that for the lowest outlet velocity and where the pool depth is 500mm (Y/Do = 6.41), Cp^+ at the centre line is more than five times Cp'. Similarly, in the same diagram, Cp+ at the intermediate radial position where the depth is 200mm (Y/Do = 2.56) is again more than five times Cp'. Considering the minimum pressure head fluctuations at an outlet velocity of approximately 5m/s, Fig. 5.5(b), the centre line value of Cp^-, when the depth is 200mm, is around 4.7 times the value of Cp'. Many more examples can be cited but it should already be apparent that although the results have been taken under the same operating conditions, the extremes in loading are not always distributed normally about the mean head at a point on the plunge pool floor. This is the first indication that a normal distribution is not necessarily applicable for plunge pool pressure fluctuations.

Comparing the maximum and minimum fluctuation values, Cp^+ and Cp^-, it can also be seen that the values are not evenly distributed about the mean head. The centre line maximum pressure head coefficient for the largest pool depth regularly exceeds 0.6 (Uo≈ 3−9m/s) Fig. 5.3 while the minimum pressure head coefficient, under the same operating conditions, never attains this value, as seen in Fig. 5.5. In an extreme case (Uo ≈ 3 m/s and Y = 350mm) Fig. 5.3(a) the maximum pressure head fluctuation above the mean at the jet centre line is over 90% of the impacting velocity head whereas the corresponding value of Cp− is only around 0.57. This apparent asymmetry of the probability distribution at the measurement point is a further confirmation that normality cannot be assumed and that the fluctuations are not generated purely by random turbulence. The pattern emerging corresponds more towards the phenomenon of coherent vortex structures. The statistical parameters that have been included (in addition to the more usual mean and standard deviation) such as maximum, minimum, skewness and kurtosis values, are therefore warranted to fully define the magnitude and distribution of the pressure fluctuations at a point on the plunge pool floor.

Although the plunging jet may produce lower mean pressures than a corresponding submerged jet, as already seen in chapter 4, it is obvious from the magnitudes of the limited amount of data so far presented, that very large

fluctuations in pressure about the mean head are produced. These have reached 0.9 $Ui^2/2g$ above the mean and 0.6 $Ui^2/2g$ below the mean. It is precisely this type of loading which may violate the structural integrity of the plunge pool through either low frequency, high amplitude vibration or from differential pressure application to either side of the base slab.

A note about the remainder of the pressure fluctuation measurements.

From this point onwards in Chapter 5, all the pressure fluctuation measurements will refer to the jet centre line. This was a decision taken during the experimental programme despite the fact that at low plunge pool depths (in the zone of flow establishment), the maximum fluctuations do not occur at the jet centre line. They tend to occur at a radial distance of around one jet diameter. The justification is given as follows:

(i) The amount of fluctuation data taken would prove to be too much if every radial distance is to be investigated. Even the jet centre line measurements proved very time consuming, covering variations in velocity, diameter, type of outlet, plunge pool depth, jet fall height in the atmosphere, etc.

(ii) The maximum pressure fluctuations occur along the jet centre line at all depths except the shallow depths in the zone of the flow establishment. Most plunge pools would not be built as shallow as this, because practically no energy dissipation occurs until depths greater than the zone of established flow (i.e. Y/D $\approx$ 5 to 20). Thus, from a practical point of view, most plunge pools will experience maximum fluctuations at the jet centre line, on the plunge pool floor.

(iii) The highest values of mean pressure head always occur at the jet centre-line, as established in Chapter 4. There is a rapid tail-off in mean pressure with radius. Combining the mean pressure with the fluctuating components, the largest total loadings are along the jet centre line. This is the most destructive part of the jet, and therefore warrants the most detailed investigation.

5.3 PRESSURE FLUCTUATIONS ALONG THE JET CENTRE LINE IN THE PLUNGE POOL.

5.3.1. Introduction

The structure of this section is similar to the comparable section in Chapter 4 where the results are presented with a different section devoted to each nozzle outlet diameter (78mm, 52mm, and 25mm) and a further section devoted to the 25mm diameter orifice outlet.

Each outlet diameter is sub-divided into the two ranges of jet fall height tested, with each graph showing the variation of pressure head fluctuation with non-dimensional plunge pool depth. This depth parameter is made non-dimensional both by outlet diameter (Do) and also the measured jet impact diameter (Di). Each graph also shows the variation of pressure fluctuation with varying jet velocity in the same manner as chapter 4. Usually a range of six different velocities is given.

This chapter is different from the previous in the sense that seven different non-dimensional fluctuation ratios are presented. The fluctuations are considered firstly for the r.m.s. pressure head coefficient Cp' followed by the maximum and minimum pressure head coefficients, Cp^+ and Cp^- as previously defined. Absolute values, in terms of the maximum instantaneous peak and minimum head ratios Hmax / $Ui^2/2g$ and Hmin / $Ui^2/2g$, as well as the peak and minimum dynamic fluctuations are also plotted, giving a total of seven non-dimensional pressure fluctuation ratios.

As well as the magnitude of fluctuations, more statistical information is presented in the form of the variation of skewness and kurtosis values along the jet centre line, and the actual probability density function of the results at the measurement point. Comparison can then be made with the normal distribution, which only requires the mean and standard deviation to be fully defined, and has formerly been assumed to be applicable in describing the range of pressures that may be produced.

5.3.2 Centre line pressure fluctuations using the 78mm diameter nozzle.

5.3.2.1 Shorter droplength (L).

The first figures in this section (Figs. 5.7– 5.11) refer to the centre line results under the same test conditions as shown in the radial distribution results (Do = 78mm, L = 725– 1125mm) in Section 5.2. Fig. 5.7 shows the variation of the centre line r.m.s. pressure head coefficient with pool depth. As already seen in Chapter 4, a better trend is achieved by plotting the results with the pool depth made dimensionless by the measured jet impact diameter, although the relationship of Cp' with Y/Di is not as tight a correlation as with the mean pressure head values in chapter 4. The lack of "tightness" in Fig. 5.7(b) is due primarily to the sensitivity of Cp' to the incoming velocity. Larger velocities delay the increase in centre line turbulence to greater and greater Y/Di ratios. This may be a function of increased length of zone of jet developement. Another initial point to be made is that these results refer only to the largest diameter and thus cover only a limited range of non– dimensional pool depths.

From inspection of the measurement points shown in Fig. 5.7(b), it seems that the highest values of r.m.s. pressure head coefficient are around 0.2, and occur around 5 to 6 jet impact diameters into the plunge pool. Referring to chapter 2, where turbulence data for submerged, bounded, and smooth impinging jets was considered, this location coincides approximately with the maximum values of longitudinal turbulence intensity (U'/Ui) along the jet axis of around 0.14– 0.15. The relationship between Cp' and the turbulence intensity is therefore approximated by $Cp' \approx 10\ (Tu)^2$ as derived in Chapter 2 from results for shear layer type flows. Furthermore, the substantial Cp' values of 0.2 compare favourably with results from baffle block testing (Lopardo et al. [1]) and are approximately three to four times greater than both wall measurements on a bounded jet and floor measurements beneath a hydraulic jump, but these latter two cases represent flows parallel to the boundary rather than impinging normally on the boundary. The early indication is that normal impinging flows produce much larger fluctuations on a solid boundary than parallel flows.

The spread of data in Fig. 5.7(b) is due primarily to the variation of velocity, which at the impact point varies from 5m/s to 14m/s. According to jet

theory in general, the angle of diffusion/spread of a jet is practically independent of the velocity, and hence any core length in the zone of establishment should be approximately constant. For submerged jets this is around 6 diameters. For plunging jets, Chapter 4 has implied 3 to 4 jet diameters. This implies that the data in Fig. 5.7(b), which is for one jet diameter only, should collapse onto one curve as in chapter 4, although this has not occured. The reasons which might give rise to this spread of data include:-

(i) The variation in jet Reynolds Number from Re = 2.3×10^5 to Re = 1×10^6. This might have the effect of extending the zone of establishment and hence delaying the increase in Cp' at higher velocities, because of longer core lengths.

(ii) The variation of jet Froude Number at the impact point which has significant effect on the degree of air entrainment. It is not yet known how increased quantities of air affect pressure fluctuations. It should be noted however that the quantities of air entrained in Fig. 5.7(b) will vary by a factor of 2-3 over the range of velocity quoted. The effect of air entrainment will be investigated in Chapter 6 and 7.

(iii) The variation of jet velocity produces a significant variation of jet break-up length in the atmosphere. This will also be pursued further in Chapters 6 and 7. In general, low velocities produce short break-up lengths in the atmosphere and hence the low velocity jets in this test may be more substantially broken-up at the impact point compared with the higher velocity jets. This would mean that the more broken-up jets might have a less defined, or even, zero core length in the pool and hence increase in Cp' immediately. Intact jets at the impact point would have the opposite effect. It is interesting to note however, that no matter which value of Y/Di the Cp' value begins to increase from, the peak values are all around 0.2 irrespective of velocity.

Fig. 5.8 presents the maximum (highest recorded) instantaneous pressure head above the mean value while Fig. 5.9 shows the minimum (lowest recorded) instantaneous pressure head below the mean, both normalised to the jet inlet values (Graph (b)). Although the peak values of Cp^+ are not reached for some of the test conditions, extrapolating data points in Fig. 5.8(b) reveals maximum instantaneous fluctuations typically as high as 0.8 $Ui^2/2g$ head above the mean. In one instance the value of Cp^+ is over 0.9. Generally the maximum

fluctuations are four to five times greater than the root mean square value Cp' given in Fig. 5.7(b). On the other hand, the values of Cp^-, Fig. 5.9(b), seem to reach a peak at much shallower depths within the plunge pool and do not attain the same magnitude as the maximum fluctuations. From Fig. 5.9(b) it can be seen that the minimum instantaneous heads reach almost 0.6 $Ui^2/2g$ below the mean and this occurs at a depth of 4 to 5 diameters into the pool. However, as noted, cavitation is not a significant risk in such plunge pools because of large air concentrations. It should be realised that results of the form mentioned above would not be achieved if the distribution of the fluctuations at the centre line measurement point was of a Gaussian nature.

Even though the mean pressure development at the plunge pool floor may be reduced by air entrainment, the highly agitated nature of the tailwater during jet impingement, means that large fluctuations in pressure about the mean head may be produced (e.g. $Cp^+ = 0.8$, $Cp^- = 0.6$). This phenomenon is sketched diagrammatically below,

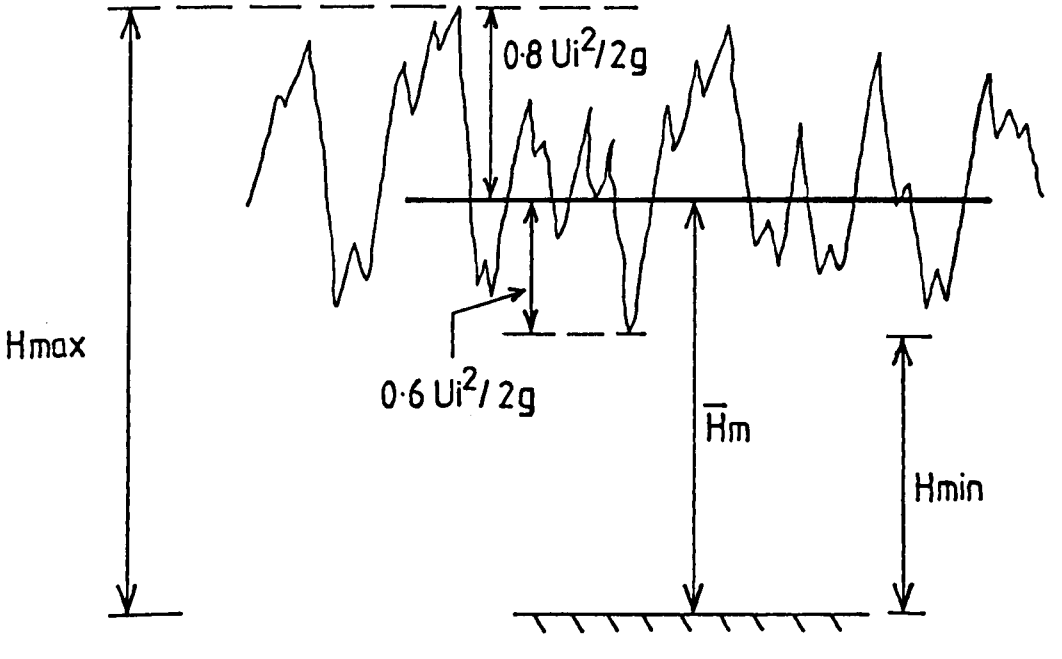

revealing the possibility of huge instantaneous swings of head from ($\bar{H}m + 0.8Ui^2/2g$) to ($\bar{H}m - 0.6Ui^2/2g$) which in practice might mean a change from around 1.6 to 1.7 $Ui^2/2g$, at the peak, to a head which can be slightly negative at the minimum. This form of loading is highly dangerous to the plunge pool as the fluctuations may be transmitted to the underside of the concrete floor, through joints and cracks, and hence generate sizeable differential pressure on the base slab due to the large variation in instantaneous values. Therefore, investigation must take place of these extreme values.

Addition of the total mean pressure head $\bar{H}m$, (Chapter 4), with the maximum and minimum fluctuations described previously, results in head values in terms of the instantaneous total peak head (Hmax) and instantaneous total minimum head (Hmin), sketched above. Similarly, addition of the mean dynamic head defined in Chapter 4 with the maximum and minimum fluctuations results in the instantaneous dynamic peak head and instantaneous dynamic minimum head. The results for the variation of the instantaneous peak and minimum value of the total pressure head with pool depth at the jet axis are shown in Fig. 5.10 while the dynamic counterparts are shown in Fig. 5.11. It should be noted that the data points on the upper part of these Figures refers to the peak pressures whereas the lower data points refer to the minimum pressures. This is sketched below to allow a clearer interpretation of the maximum and minimum values.

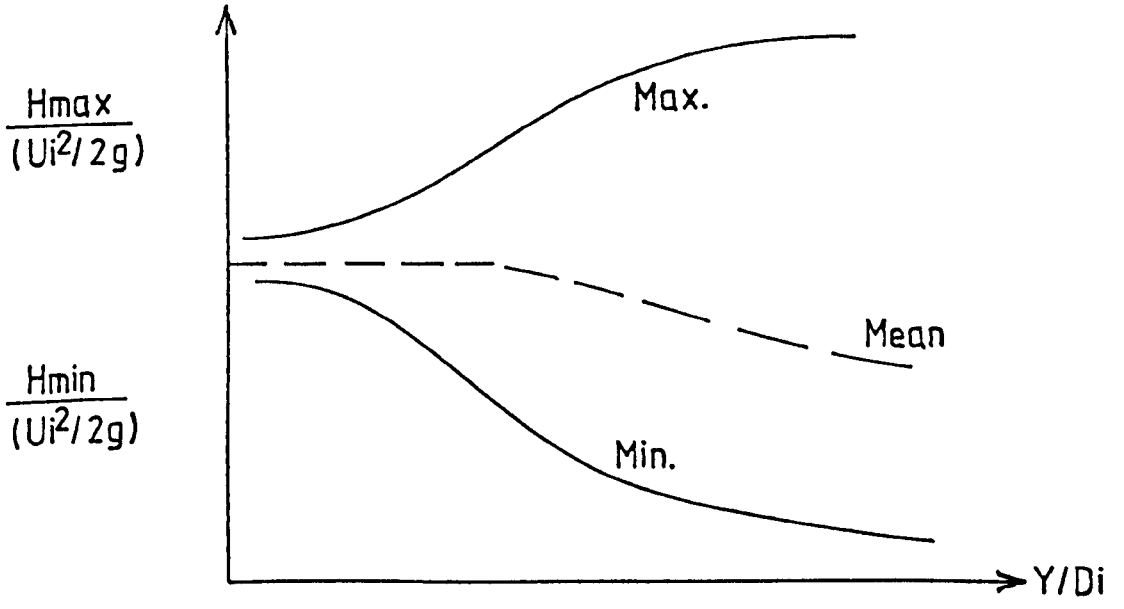

It can be seen in Fig. 5.10(b), which shows the absolute extremes in pressure including the hydrostatic component, that, at low pool depth relative to the jet diameter, the peak and minimum heads are of a similar magnitude at least up to Y/Di = 2. However, with increase in plunge pool depth, it can be seen that combination of the steadily reducing mean head with the previously detailed fluctuations, means that the difference between instantaneous values of peak and minimum head increases dramatically. At around Y/Di = 5 − 6, the total peak head reaches a ceiling well above $Ui^2/2g$ for all test cases while the total minimum head is less than 40% of this value.

Again Fig. 5.10(b) shows considerable spread of data with jet velocity. This is not so much true for the minimum pressures but more true for the maximum pressures which give higher ratios at lower velocities. This is particularly true for the 3 m/s jet which gives an instantaneous maximum in excess of $1.6Ui^2/2g$. The limited range of data in this graph prohibits generalisation at this stage.

A small but noticeable increase in the minimum head occurs for tests at low outlet velocities ($Ui^2 \approx 3$ and 5 m/s) and for the large pool depths. This is attributable to the hydrostatic component (depth of water) mentioned in Chapter 4. This situation is clarified with consideration of the instantaneous values of the dynamic peak pressure head and dynamic minimum pressure head shown in Fig. 5.11. Subtraction of the plunge pool depth (estimated as representative of the hydrostatic component) from the highest and lowest recorded pressure heads produce the dynamic results in Fig. 5.11. The maximum peak values are reduced to around 1.1 to 1.2 $Ui^2/2g$, while the minimum are also reduced, in fact down to $-0.12\ Ui^2/2g$, in one case. These sort of figures highlight the extremes in instantaneous loading that may be generated under the same flow conditions at the plunge pool floor. Magnitudes have been found from well above the theoretical mean head at pool impact $Ui^2/2g$, down to possible negative values. Loading of this form must be taken account of in design to prevent damage.

5.3.2.2 Longer jet droplength.

Figs. 5.12 to 5.16 shows the results obtained during testing of the same nozzle outlet (Do = 78mm) but where the jet droplength was considerably larger

(L = 2230 – 2630mm). Due to the larger fall heights the range of Y/Di is marginallly bigger than the previous, because of smaller values of Di at impact.

Fig. 5.12 shows the variation of the centre line r.m.s. pressure head coefficient with pool depth. Inspection of the data points in graph (b) of this figure, reveals a small peak at the lowest submergence with a larger secondary peak at Y/Di≈ 6. These observations can be explained initially by considering the jet diffusion process in the pool. At low plunge pool depths, the jet impacts directly with the plunge pool floor and being of a more diffuse or broken–up nature than the jets which fall through a smaller drop length, produce the first peak in the r.m.s. pressure head coefficient. The second, and more important, peak occurs beyond the diffusing jet core Y/Di ≈ 6 where the mixing regions have penetrated to the jet centre line. This is the situation which produces the maximum fluctuations at the jet axis. The magnitude of the highest values of Cp' seem to exceed the corresponding values obtained with the smaller fall height range. This point will be discussed below, when the results for each group of fall heights are compared.

The values of the maximum pressure head coefficient Cp^+ are shown in Fig. 5.13. When plotted with Y/Di, the results do not reach a peak, but in some instances values above 0.8 will obviously be attained. In general, the results are again much greater than three times the value of Cp', suggesting that coherent vortex structures mix with the normally distributed random turbulence in generating the fluctuations at the plunge pool floor. Again the results show a smaller and less significant peak at the lowest pool depth tested, in the general region of Y/Di = 1 to 2. On the other hand, the initial peak is not apparent for the centre line minimum pressure head coefficient variation with pool depth as shown in Fig. 5.14. In this case Cp^- typically reaches a value of 0.6 at Y/Di of around 5 to 6, although one value of Cp^- over 0.7 was also obtained when testing at the lowest outlet velocity.

Fig. 5.15 shows the results for the centre line maximum peak and minimum pressure head ratio for the longer jet droplength case. Fig. 5.16 shows the centre line dynamic peak and minimum pressure head ratios. In Fig. 5.15(b) the total peak values show a large spread, especially at low pool depths, accounted for by the wide range of jet velocity used. In comparison, the total minimum head is far more consistent throughout all of the pool depths tested. In Fig.

5.16(b) a few negative values are noticeable for the instantaneous minimum dynamic pressure head ratio when Y/Di = 6 − 10. The dynamic peak values on the other hand are, in all cases, maintained above the full velocity head averaging 1.1 $Ui^2/2g$

5.3.2.3 Comparison of the two jet droplengths

The final graphs in this section deal with comparison between the results obtained by testing the same nozzle diameter at two different fall height ranges. The figures are plotted for roughly comparable impact velocity head conditions ($Ui^2/2g$) and hence the results for the low velocity case at the small fall heights and the highest velocity case at the larger fall height range are omitted. Fig. 5.17 shows the variation in the centre line pressure head coefficients with pool depth while Fig. 5.18 shows the variation of the total and dynamic extremes in loading with pool depth. In all cases the pool depth is made dimensionless by division with the measured jet diameter at impact as this condition produces the best representation of the results from the measured geometric quantities.

It can be seen in Fig. 5.17 that the general trends for both fall height ranges are similar, but the values obtained from the larger drop height appear to be slightly bigger. Even though the actual jet diameter at impact is taken into account, it is thought that, the jets which have fallen through the greater droplength will be slightly more diffused and broken−up and hence generate larger fluctuations. Regarding the magnitude of these reasults, the highest value of the r.m.s. pressure head coefficient, graph (a), is around 0.2 to 0.22 at a plunge pool depth of Y/Di ≈ 6−8. The maximum pressure head coefficient, graph (b), seems to reach the highest values at larger Y/D_i with magnitudes in the range of 0.8 to 0.9. The highest value of the minimum pressure head coefficient, graph (c), is around 0.6 at Y/Di ≈ 5 − 6. As noted previously, the variation of these data points with Y/Di is not as definite as the mean pressure head examples in Chapter 4, and hence the conclusions drawn from these results are provisional until the wider range of experimental points are discussed for the other nozzle and orifice diameters.

Fig. 5.18 shows the combination of the maximum and minimum instantaneous fluctuations for both fall heights. There is virtually a constant value

of the peak instantaneous pressure head over this range of Y/Di, remaining in a fairly narrow band above $Ui^2/2g$. The instantaneous minimum pressure head, on the other hand, reduces rapidly with Y/Di and, for the dynamic component, reaches negative values in quite a few instances. Negative values here represent below atmospheric pressure. Design orientated information of this nature is most useful for estimating extremes in loading.

5.3.3 Results from testing of 52.5mm diameter nozzle outlet

Experimental data for the shorter jet droplength

Figs. 5.19 to 5.23 represent the results obtained for the pressure head fluctuations at the plunge pool floor centre line when testing the nozzle outlet of 52.5mm diameter and where the fall height above the pool surface (L) was between 620mm and 1020mm, constituting a shorter jet fall length. A larger range of Y/Do and Y/Do is covered compared with Section 5.3.2 simply because of the smaller nozzle diameter. This means that a wider picture of plunge pool behaviour can be obtained with values of Y/Di up to around 12.

The initial diagram, Fig.5.19, shows the variation of the r.m.s. pressure head coefficient with plunge pool depth for a range of jet velocities similar to the 78mm diameter nozzle. It can be seen that there is a spread in the results, due to velocity variations, but it can be seen, especially in Fig. 5.19(b), that the underlying trend is quite clear, particularly at the higher outlet velocities tested. The value of Cp' increases rapidly with Y/Di initially, reaching peak values again up to 0.2 at Y/Di $\approx$ 6– 8, whereafter the magnitude reduces, at a slower rate, with further increases in plunge pool depth. This pattern is strikingly similar to the results obtained from other authors [2] and [3] when testing the stilling basin floor beneath a free hydraulic jump. As described in Chapter 2, the results of fluctuations under a hydraulic jump show a relationship with the incident Froude Number ($V_1/\sqrt{gY_1}$), as expected for this gravity type of flow, but nevertheless the value of Cp' increases to a peak with longitudinal distance into the jump, $X/Y_1 \approx$ 10 to 20, before slowly reducing with further increase in distance from the start of the jump. Obviously the magnitude of the fluctuations in pressure beneath the hydraulic jump (Cp' $\approx$ 0.05) are only a fraction of those obtained at the plunge pool floor due to the orientation of the solid boundary relative to the

main flow direction. It is encouraging, however, to have such a good agreement between the trends in the results for both of these shear layer type flows.

Fig. 5.20 shows the corresponding variation in the maximum pressure head coefficient $C_{\bar{p}}^{+}$. The results, graph (b), in general follow the same trend as the preceding figure, but the peak values of Cp^{+} seem to occur at larger plunge pool depths ($Y/Di \approx 7 - 10$) also with a noticeably greater spread of data. At these approximate depths the highest values of the maximum pressure fluctuations are, as noted in Section 5.3.2, around $0.8\ Ui^2/2g$ above the mean head. Again some values of Cp^{+} are much more than they would be expected considering the values of Cp' and assuming the fluctuations at a point on the plunge pool floor follow a normal distribution pattern. For example, at the largest pool depth ($Y/Do \approx 9.5$), the value of Cp^{+} is around 0.67 when the outlet velocity is approximately 5m/s while Cp' under the same conditions is only approximately 0.082. Therefore, the maximum fluctuation about the mean is more than eight times the corresponding value of the r.m.s. fluctuation. This is an unexpected result assuming the distribution of fluctuations at the measurement point to be of a Gaussian nature. Similarly, at the same pool depth, the value of Cp+ (when the outlet velocities are around 7 and 9m/s) is over six times the value of Cp'. Results of this form indicate a large positive skewness in the probability distribution of pressure head fluctuations at the measurement point on the plunge pool floor under these test conditions. This phenomenon has already been alluded to by Toso [4] in his work on hydraulic jumps.

The minimum pressure head fluctuations below the mean, shown in Fig. 5.21, have a very tight relationship with Y/Di, increasing rapidly with pool depth until reaching a peak at a plunge pool depth around $Y/Di \approx 5 - 6$. The peak values of Cp^{-} are around 0.6, as would be expected considering the r.m.s. pressure head fluctuations are around 0.2. At greater plunge pool depths values of Cp^{-} again slowly reduce. Although Cp^{-} is approximately three times greater than Cp^{-} at the peak points, implying normal distribution, this is certainly not always the case at other plunge pool depths. For example, at a pool depth of 200mm ($Y/Do \approx 3.8$) and when the outlet velocity is approximately 11m/s, the value of Cp^{-} is almost seven times the value of Cp'. This result infers that under these test conditions the probability density function of fluctuations at the centre line measurement point is negatively skewed. Negative and positive skewing will be discussed in more detail in Section 5.4 and Chapter 7.

The observations regarding the magnitude of the extreme fluctuations in relation to the r.m.s. pressure head results clearly illustrate the need to obtain the actual probability density function of instantaneous pressure head values to fully define the range of generated pressures at the plunge pool floor. This entails, in statistical terms, determining the skewness and kurtosis of the pressure record for comparison with the Gaussian distribution values. These terms will be investigated in Section 5.4 along with an example of the actual distribution of instantaneous pressure head values at the central measurement position.

Fig. 5.22 shows the extremes in measured pressure; both instantaneous peak and minimum values. These values are relative to atmospheric pressure head. There is a large spread in the data values, particularly for the measured peak head results, but with the increased range of Y/Di, the general pattern is more clearly defined than in Section 5.3.2. Inspection of the data points reveal that initially, at small Y/Di. the peak head is consistently high (above $Ui^2/2g$), reaches a maximum level of 1.4 $Ui^2/2g$ around 6 to 8 jet diameters in pool depth and then eventually reduces with further increases in pool depth. The measured minimum heads on the other hand do not exhibit as much data spread, and reduce rapidly with Y/Di, reaching the lowest values again where the pool depth is equivalent to between 6 and 8 jet impact diameters. Beyond this depth range there is an increase in the total minimum head, especially at the low outlet velocities tested. This is caused by inclusion of the hydrostatic component in the measured value of minimum head. Therefore, as detailed with the mean head values in Chapter 4, a better representation of the results is obtained by plotting the estimated dynamic head terms, as shown in Fig. 5.23.

In Fig. 5.23 the dynamic peak values reach a maximum value of between 1.1 and 1.4 $Ui^2/2g$ before reducing beyond this location. For example, at Y/Di $\approx$ 12, the dynamic peak head has reduced to only 60% of $Ui^2/2g$ for the lowest outlet velocity tested. At around the same pool depth where the maximum peak values are produced Y/Di $\approx$ 6, the minimum head results reach the lowest level and some negative values are obtained. Beyond this point the dynamic minimum head remains virtually constant at a very small percentage of $Ui^2/2g$ or even slightly negative. It is obvious from this sort of figure that, if the jet conditions at pool impact can be estimated, the tailwater arrangement for encountering extremes in loading is to have a pool of 6 to 8 jet diameters in depth. In fact this range of depth is often chosen as designers want to go beyond the initial jet

core length but still keep the plunge pool as shallow as possible for economic reasons.

Experimental data for the larger droplength (L = 2126 – 2526mm)

Fig. 5.24 shows the variation of r.m.s. pressure head coefficient with non–dimensional pool depth at this larger jet droplength. For the higher outlet velocities the value of Cp' reduces initially with Y/Di before increasing to a peak at a pool depth between 6 and 9 jet impact diameters. The peak values reach almost 0.25 in this case, and seem to be slightly higher than those obtained when testing the 52.5mm outlet at the smaller fall height. The comparison between results for both fall height ranges will be clarified in Fig. 5.29. There is also considerable data spread in Fig. 5.24 (b), certainly more than the shorter droplength case.

The maximum fluctuations about the mean are shown in Fig. 5.25. There is a large spread of data at the lowest values of Y/Di for each of the outlet velocities tested, but at more sizeable plunge pool depths, the results seem to collapse, until at Y/Di $\approx$ 8 – 10 the peak value of Cp^+ around 0.9 is achieved. In comparison, the fluctuations in minimum pressure heads below the mean Fig. 5.26, have a good correlation with Y/Di throughout the entire range. The value of Cp^- increases steadily up to a peak of 0.6 to 0.7. This is approximately 20% lower than the highest level of the maximum fluctuations, indicating again a positive skewness. The depth of plunge pool to this minimum peak is also smaller at Y/Di $\approx$ 5 – 6, as opposed to a Y/Di of 8 to 10 for the maximum peaks.

The range of extreme instantaneous pressure head is shown in Figs. 5.27 and 5.28. The values of peak head have a large spread at the lowest pool depths, associated with the spread in Cp^+, which diminishes with increase in Y/Di and where the pattern of results is far better defined. Considering the magnitude of the instantaneous pressure heads, it is not until Y/Di > 10 that the peak values begin to reduce below the full mean velocity head. At this location the minimum head, in comparison, is only a small percentage of $Ui^2/2g$ or in some cases reach negative values.

Comparison of the two fall height ranges

Comparison of the results obtained when testing the 52.5mm outlet at both fall height ranges is presented in terms of the pressure head coefficients in Fig. 5.29, and for the extreme pressure values in Fig. 5.30. In both cases the results are plotted for roughly the same impact velocity conditions. The general pattern of the results is similar at both fall height ranges for the pressure head fluctuations, Fig. 5.29, but it seems that the highest values of Cp', Cp^+ and Cp^- are all slightly larger at the longer fall height range between 2126 – 2526mm. Also, the location of the highest values for the upper level of testing seem to be shifted slightly to a larger pool depth relative to the impacting jet dimensions. This observation is substantiated in Fig. 5.30 where the peak and minimum heads are marginally more extreme for the longer jet fall lengths due to the increased magnitude of both the maximum and minimum fluctuations. The reason for this is likely to be connected to a combination of at least two factors:

(i) Longer jet fall lengths produce a more disintegrated jet at the impact point, even for identical conditions at the nozzle. This is likely to produce more turbulence within the plunge pool and hence higher pressure fluctuations. It is not clear at this point why the higher turbulence might be produced at deeper plunge pool depths in Figs. 5.29 and 5.30 as the opposite would be expected i.e. disintegrated jets might penetrate less into plunge pools compared with non–disintegrated jets. This will be analysed in Chapter 7.

(ii) Longer jet lengths also produce greater rates of air entrainment at the impact point, for identical conditions at the nozzle outlet. This has been demonstrated by Ervine [5] in the relationship for air/water ratio in the form $\beta \propto$ / (L/Do). It is not known at this stage if the presence of air bubbles reduces or increases pressure fluctuations. Certainly Johnson [6] has shown that air bubbles decrease the mean plunge pool pressure, and numerous authors have shown that the presence of air bubbles reduces cavitation damage considerably, although the latter is related more to reductions in the sonic velocity in water. Lopardo [7] has shown as a general rule that the presence of air bubbles reduces pressure fluctuations, although Frizell [8] has shown that at certain low frequencies the presence of air bubbles can excite pressure fluctuations. On balance, it is thought that greater jet break–up will produce more turbulence but greater air entrainment might produce less turbulence. This will be analysed further in Chapter 7 also.

5.3.4 Results from testing of 25mm diameter nozzle outlet.

Experimental data for the shorter jet fall-length (L).

Figs. 5.31 to 5.35 represent the results obtained when operating the 25mm nozzle outlet and when the fall height was set between 513 and 913mm. By virtue of the smaller outlet diameter, these and the succeeding figures for the upper level of testing, provide the widest variation so far of the non dimensional plunge pool depth Y/Di and the non dimensional fall length L/Do. The centre line r.m.s. pressure head fluctuations are plotted against plunge pool depth and shown in Fig. 5.31. An extremely good relationship is obtained when the pool depth is made dimensionless by division with the measured jet impact diameter at the pool surface, as seen in Fig. 5.31(b). A good correlation is seen despite the wide range of jet velocities. Cp' increases rapidly with Y/Di until reaching a peak where the highest values of Cp' around 0.2 are developed about 6 to 9 jet diameters into the plunge pool. As noted before, this coincides approximately with the location of the highest values of longitudinal turbulence intensity along the diffusing jet axis. The peak values certainly occur some distance beyond any solid inner core length, which from Chapter 4 would appear to be only 3−4 jet diameters into the plunge pool. The highest values of longitudinal turbulence intensity, around 0.14 to 0.15, relate to the highest values of Cp' via the expression $Cp' \approx 10\ (Tu)^2$, as detailed earlier. Beyond the peak values, as with the turbulence results, Cp' reduces at a slightly slower rate until at larger pool depths (Y/Di > 12) the r.m.s. pressure head coefficient in only around 0.025 to 0.050, a small percentage of the peak value.

A good correlation is also obtained for the centre line maximum pressure head coefficient with Y/Di, Fig. 5.32(b). The values of Cp^+ follow the same trend as the preceding Cp^+ results but, in comparison with other results obtained using the larger diameter nozzle outlets, the peak values are generally smaller. At Y/Di ≈ 6−10 the peak values are only around 0.6, which is considerably less than the 0.8 to 0.9 found for the two larger diameter nozzles. This data set provided a lower bound for the highest level of maximum fluctuations obtained so far. Beyond this pool depth the maximum fluctuations reduce until at Y/Di> 12, Cp^+ is only between 15 to 30% of the peak value. The variation of Cp^+ with jet velocity is not a significant feature for this case.

The fluctuations in minimum pressure heads below the mean are correlated reasonably well with Y/Di, as shown in Fig. 5.33(b). Again the results show slightly smaller peak values than the other nozzle outlets tested. The highest value of Cp^- is around 0.5 to 0.6, reducing to between 0.05 and 0.15 at Y/Di > 12. The variation with jet velocity is more appreciable in this case.

The total peak and minimum head coefficients (relative to atmospheric pressure) are shown in Fig. 5.34. Here it is seen that the peak values just exceed $Ui^2/2g$ whereas, with larger nozzles, the values have often been around 1.2 to 1.4. Also there is an apparent increase in coefficients for large plunge pool depths. As already discussed, this is due to inclusion of the hydrostatic component in the value of Hmax and Hmin. However, it can be seen clearly in Fig. 5.35, plotting the dynamic peak and minimum heads, that this spurious trend is removed by subtracting the hydrostatic head. This figure also shows that from a maximum level of between 1.0 and 1.2 $Ui^2/2g$ (at Y/Di $\approx$ 2 – 6), the peak head reduces fairly rapidly as the value of Y/Di is further increased. At Y/Di > 12, the peak dynamic head results are less than 40% of the mean velocity head. The difference between extremes in pressure head is also small at these higher levels of submergence. It is clear that it is again possible to have slightly negative instantaneous heads.

Experimental data for the larger droplength

The experimental results for the greater fall length of between 2018 – 2418mm (L/Do $\approx$ 81 – 97), for the pressure fluctuations produced at the plunge pool floor along the jet centre line, are shown in Figs. 5.36 – 5.40. It should be noted that the velocity range shown for this set of tests is higher than all of the previous examples reaching over 15m/s at the nozzle. The r.m.s. pressure head coefficient variation with pool depth is shown, in Fig. 5.36, for this larger velocity range. Cp' increases initially from a relatively high value to a peak of around 0.2. In one particular instance, Uo$\approx$ 7m/s, the highest value of Cp' is almost 0.22 at Y/Di $\approx$ 8. With increase in Y/Di beyond this point, Cp' reduces until at a pool depth of around 14 jet diameters the r.m.s. pressure head coefficient is virtually insignificant compared to the highest values.

Fig. 5.37 represents the variation of the peak (highest recorded) instantaneous heads above the mean (normalised to the jet inlet values) plotted against pool depth. Again the fluctuations increase from a high initial value to a

peak at Y/Di ≈ 6 – 9 before reducing. The peak values are above 0.6 $Ui^2/2g$ but only in one instance is a value of 0.8 $Ui^2/2g$ attained; where Uo ≈ 5m/s. As an aside, this condition (Uo ≈ 5m/s) is considered in more detail by comparing the Cp^+ results at each pool depth with the corresponding value of Cp'. At the lowest pool depth (Y/Do = 4), Cp^+ is around 0.5 while Cp' is approximately 0.168, a three fold increase as predicted assuming that the fluctuation at a measurement position follow the Gaussian distribution. However, when the plunge pool depth was 200mm (Y/Do = 8, Y/Di≈ 10.2) the value of Cp^+ is more than five times Cp'. Further increase in pool depth also provides unexpected results. For example, at a pool depth of 350mm, Cp^+ is almost 5.5 times Cp' while at the largest pool depth tested (Y = 500mm) Cp^+ is approximately eight times greater than C_p'. For this particular nozzle, fall height and outlet velocity, it seems that, beyond a certain plunge pool depth, coherent vortex structures produced by the flow supplement the turbulence from the diffusing jets to induce positive fluctuations in pressure far greater than expected. This effect also seems to increase with plunge pool depth, relative to the impacting jet diameter.

The variation of the minimum (lowest recorded) instantaneous pressures below the mean head is shown in Fig. 5.38. It can be seen in this figure that the minimum pressure head coefficients reach the highest level at a smaller value of Y/D_j (≈ 4) than the peak pressure coefficients, and also reduce much more rapidly from the peak. Also, it is clear that the highest values (≈ 0.7) are considerably higher than the shorter droplength results in Fig. 5.33(b). Carrying out the same exercise as before, by comparing the values of Cp^- with Cp' where Uo ≈ 5m/s, it can be seen that only in one instance (Y = 100mm) does the minimum pressure head coefficient exceed three times Cp'. This implies that under this particular test condition random turbulence generated pressure fluctuations play a bigger role than coherent vortex structures in determining the minimum instantaneous pressures. The domination of random turbulence for the minimum in pressure may well be a function of the very long jet droplengths in this case, of L/Do ≈ 100, giving an extensively broken–up jet at impact.

Fig. 5.39 shows the peak and minimum measured instantaneous pressure heads recorded at the plunge pool floor along the jet centre line, while Fig. 5.40 shows the dynamic peak and minimum pressure heads, both varying with plunge pool depth. Apart from a slightly more extreme pressure range, the pattern of

results is similar to the values obtained from testing of the same outlet at the shorter fall lengths. Little effect of the hydrostatic component is seen in comparing Figs. 5.39(b) and 5.40(b). This is due to the increased jet velocity head values, $Ui^2/2g$, relative to the plunge pool depths.

Comparison of the two fall height ranges.

A comparison between results for the two different fall lengths is shown in Figs. 5.41 and 5.42. The coefficients in Fig. 5.41(a), (b) and (c) follow the same general trend but seem to be slightly higher for the larger fall heights. This is likely to reflect the greater degree of jet break-up for the longer fall length. The location of the highest values is roughly the same for C_p', however, for the longer droplength results, it seems to be at a larger value of Y/D_i for Cp+ and is developed at a smaller depth for Cp^-. With a similar mean pressure profile (Chapter 4), the larger magnitude fluctuations result in more extreme values of instantaneous peak and minimum heads for the longer jet fall length, as seen in Fig. 5.42. The greatest difference between dynamic peak and minimum heads, graph (b), is at $Y/Di \approx 6 - 8$ while at $Y/Di > 12$ the range of fluctuating pressure heads is small in comparison.

5.3.5 A comparison of all three nozzle diameters

A full comparison of the pressure coefficients for all three nozzle diameters, for the full range of velocity and the two ranges of droplength, is given in Figs. 5.43 and 5.44. The following brief points can be made:

(i) The spread of data is much greater than the data for mean heads (in Chapter 4). This spread appears to be due to both the variation of jet velocity and the variation in droplength. The variation with velocity indicates that lower velocity jets are more broken-up at impact than higher velocity jets (for the same fall length) and hence have a less significant zone of flow development in the plunge pool. The pressure fluctuations increase significantly even for low plunge pool depths, whereas with high velocity jets the increase in fluctuations is delayed until greater pool depths are achieved.

(ii) The variation in droplength indicates that longer droplength jets produce greater pressure fluctuations within the plunge pool, for comparable conditions at the nozzle. The droplength also has significance in the value of Y/Di where the pressure fluctuations reach a maximum. Again we are faced with a conclusion that more broken–up jets produce greater turbulent peaks within a plunge pool and this may be related to the "unevenness" of the jet at impact, or even the degree of air entrainment involved.

(iii) Variation of the pressure fluctuations with depth does, however, show a reasonably similar trend for all six scenarios plotted in Figs. 5.43 and 5.44. It should be remembered that these graphs are for the jet centre line only, and all are normalised relative to jet conditions at the impact point Ui and Di.

The r.m.s. pressure head coefficient, Fig. 5.43(a), increases rapidly with Y/di, reaching a maximum at a pool depth between about 6 and 9 jet diameters, of approximately 0.2. The Cp' values reduce after this location till, at a pool depth of around 12 – 14 diameters, the r.m.s. pressure head fluctuations are generally less than 0.05 $Ui^2/2g$. Maximum pressure head coefficients, Fig. 5.43(b), also increase to a peak value but with a large spread in Cp^+ at the lower values of Y/Di. Peak values of the maximum fluctuations up to 0.8 $Ui^2/2g$ are attained at Y/Di ≈ 7 – 10, although some larger values still exist beyond this location. Cp^+ in general reduces to a small percentage of the peak values at Y/Di > 14. Finally, Fig. 5.43(c) shows the variation of the minimum pressure head coefficient with Y/Di and seems to give the best correlation, with the highest level of Cp– around 0.6, at Y/Di ≈ 5 – 6. Beyond this pool depth, the value of Cp^- reduces, more rapidly than Cp' or Cp^+ coefficients, until around Y/Di > 12, Cp^- is consistently below 0.1.

Combination of the maximum and minimum fluctuations with the total and dynamic mean head is shown for all of the previous results in Fig. 5.44. The minimum heads show a very consistent trend with Y/Di (at all velocities and droplengths) compared with the peak heads. The minimum head values reduce from approximately 0.8 $Ui^2/2g$ at small pool depths, down to negative values at Y/Di ≈ 8 and staying consistently low after this location. Peak heads, on the other hand, have a large spread at low pool depths, staying well above the full mean velocity head (≈ 1.2 $Ui^2/2g$) before reducing in general at Y/Di ≈ 10. The maximum difference of around 1.0 – 1.3 $Ui^2/2g$ between the peak and

instantaneous heads occurs at a pool depth of 6 to 8 jet diameters until at Y/Di > 14 the difference in the range of dynamic pressures is only about 30% of the mean velocity head.

On the whole it can be seen from these figures that the worst case for stilling basin design under this form of free-falling jet is to provide a plunge pool between 4 and 10 jet diameters in depth due to the magnitude of fluctuations and associated extreme pressure heads that would be encountered.

5.3.6 Experimental data from the 25mm diameter orifice outlet

It is now evident from the jet turbulence measurements in Chapter 4, that a jet formed by an orifice plate contains within it much greater turbulence than a smooth nozzle generated jet. Values of longitudinal turbulence intensity U'/U reached 5% to 7% in the orifice jet, but only up to 1% in the smooth nozzle jets. The result of this variation in internal jet turbulence is a much more pronounced jet spread in the atmosphere for the orifice jet. This in turn ensures that the jet is more broken-up at the impact point, although it also ensures that a physical measurement of the jet diameter at impact is much more unreliable because of the very diffuse nature of the jet. For this reason the orifice jet was tested in the shorter droplength range (L = 1020mm to 1420mm) only. Testing at the longer droplength range would have given a totally broken-up jet at impact whose real "diameter" would have been impossible to measure. Certainly some difficulty was encountered in measuring Di even at the shorter droplength range, accounting for additional spread of data compared with the nozzle results. The results are reported briefly below.

Fig. 5.45 shows the variation of the centre line r.m.s. pressure head coefficient with pool depth. As before, Cp' increases to a peak value between 0.2 and 0.23 at a pool depth of 5 to 8 jet diameters. This is slightly greater than most of the nozzle data. Beyond this peak, Cp' reduces steadily until at Y/Di > 16 the value of the r.m.s. pressure head is around 10-20% of the highest level. Again there is more data spread at the lower pool depths than at higher pool depths where the points collapse onto one curve.

The centre line maximum pressure head fluctuations are shown in Fig. 5.46, increasing from a substantial initial value to a peak at a pool depth of between 6

and 10 jet diameters. This is comparable to data from the nozzle with large L/Do value. Typically the maximum fluctuations are four to five times greater than the root mean square values, producing fluctuations as high as 0.8 $Ui^2/2g$ head above the mean. At Y/Di > 16 the maximum fluctuations are less than 20% of the peak values.

The centre line minimum pressure head fluctuations are shown in Fig. 5.47. In this case no maximum is achieved, or at least it is likely to occur at an extremely low plunge pool depth. The results reduce immediately from highest recorded values of around 0.7 $Ui^2/2g$ to a consistently small value where Y/Di > 14. The trend of these results is slightly different from any considered previously, except perhaps the 25mm nozzle outlet results at the longer jet fall length (L/Do ≈ 100), and may be accounted for by the higher degree of jet broken–upness at the point of impact at the pool surface.

The maximum and minimum instantaneous fluctuations are shown in Figs. 5.48 and 5.49. The location of the highest values of Cp^- ensures that the minimum heads remain low throughout the entire range of Y/Di. Unlike the previous results, the peak heads do not have a plateau at small pool depths and reduce immediatley from a value of around 1.4 $Ui^2/2g$. This value is higher than most of the nozzle data. At Y/Di > 20, the difference between extreme dynamic pressure heads, Fig. 5.49, is almost insignificant.

The final figures in this section concern the comparison between results for the nozzles and orifice outlet. Fig. 5.50 shows the pressure head coefficients while Fig. 5.51 shows the extreme pressure head ratios. It is clear from Figs. 5.50 and 5.51 that the general trends of the nozzle and orifice data are reasonably consistent despite the different natures of both jets at the impact point.

The main difference between the nozzle and orifice data is that the latter tends to give slightly higher pressure fluctuation coefficients and a slightly greater range of fluctuation in Fig. 5.51. The orifice data L/Do≈ 50 gives comparable data to a nozzle jet with L/Do ≈ 100, indicating that the degree of jet break–up at impact is likely to be the most significant parameter in determining the trend of pressure fluctuation within the plunge pool.

As a rough guide, it can be seen in Fig. 5.50 that:–

– the highest values of Cp' are approximately 0.2 and occur at a plunge pool depth of 6 to 7 jet diameters.

– the highest values of Cp^+ are around 0.8 and occur at a plunge pool depth of 8 to 10 jet diameters

– the highest values of Cp^- are around 0.7 and occur at a plunge pool depth of 4 to 6 jet diameters.

From Fig. 5.51 it can be seen that the maximum instantaneous peak heads can reach up to 1.6 $Ui^2/2g$. The minimum instantaneous head can be slightly negative (sub–atmospheric) around $-0.1\ Ui^2/2g$. This is not likely to produce cavitation damage because of the large quantities of air bubbles present and also the value of Ui would require to be greater than 40 m/s. Any problems are more liable to be caused by the extreme instantaneous swings from $+1.6\ Ui^2/2g$ to $-0.1\ Ui^2/2g$

5.4 PROBABILITY DISTRIBUTION OF PLUNGE POOL FLOOR PRESSURE HEAD FLUCTUATIONS.

In the previous sections, results of the form of the pressure head fluctuation magnitudes at the plunge pool floor have been reported. These results indicate, by comparing the extreme pressure head fluctuation ranges with the corresponding r.m.s. values, that the distribution of fluctuations at a particular point on the plunge pool floor beneath the diffusing jet is not necessarily of a Gaussian nature, or normally distributed, as would be the case if they were generated purely by random turbulence.

This section will briefly report on the characteristics of the distribution of pressure head fluctuations at the central measurement position, including investigation of skewness and kurtosis values as well as an example of the actual probability density function.

Statistically, the standard deviation of the pressure fluctuations illustrates only

the second moment of the probability density function. More information may be gained from the third moment, the skewness, and the fourth moment, the kurtosis. (The normal or Gaussian distribution is defined with only the first two, the mean and the standard deviation. For normal distribution the skewness is equal to zero and kurtosis is equal to three). For each test run, the raw pressure head data was analysed to determine the skewness and kurtosis magnitudes for comparison with the normal distribution values.

Fig. 5.52 represents just one example of the general behaviour of these moments for the centre line pressure fluctuations with plunge pool depth. It can be seen that the skewness values are initially negative at low plunge pool depths indicating dominance of negative values over positive. As the pool depth is increased, large positive values are evident and the situation is reversed. These features can be recognised, as noted, in the individual pressure fluctuation figures already discussed in this chapter, by comparing the maximum and minimum values (Cp^+ and Cp^-)with the r.m.s. component (Cp'). The kurtosis values are generally greater than three throughout the entire range of pool depths tested.

For practical purposes many investigators have assumed that pressure fluctuation at a point follow the Gaussian distribution. Fig. 5.52 and the previous fluctuation results illustrate the inaccuracy of this assumption. The most graphic description of this point is achieved by comparing the actual probability density function of pressure fluctuation results with the Gaussian distribution, as shown in Fig. 5.53. This is one single example but typical of most of the data collected.

In this figure, the probability f(p) is plotted versus the pressure head, as seen in graph (a). An increase in the kurtosis value is obvious at the peak probability level, while, at the tails of the distribution, indication of the distribution skewness can be noted. It is difficult to evaluate the fit in this region using linear scales, so the positive half of this figure is replotted on graph (b) with a semi– log scale, Log f(p) versus pressure head. It can be seen that the data departs from the normal distribution and is much more extreme for the large positive pressure head fluctuations. At this pool depth, the maximum fluctuations are dominant and are of the order of six to seven standard deviations from the mean. The normal distribution cannot provide an estimate of probability in this region and hence the evaluation of maximum loading for design cannot be determined by assuming this function. The actual extremes in loading

must be obtained to satisfy design requirements. Extreme value theorems may be more useful in this context.

5.5 A SUMMARY OF THE MAIN POINTS.

(i) Power spectra obtained from the plunge pool floor were presented in Chapter 3. Typically, the spectra showed that dominant fluctuations occured in the 3 to 10 Hz frequency range, which has also been noted by other workers in the field. In most cases this corresponds to larger eddy lengths, usually of a size larger than the impinging jet diameter. For design, the natural frequency of the plunge pool arrangement should be outwith the range stipulated above to prevent resonant conditions and therefore reduce vibration of the structure due to this type of impinging spillway flow.

(ii) Mean pressure head results were detailed in Chapter 4 along with jet turbulence results. Considering the distribution of mean pressure heads at the plunge pool floor, it was found that the largest magnitude was consistently along the impinging jet centre line and hence this condition was studied in more detail. The centre line mean pressure head variation with pool depth was therefore presented for all test conditions. These results showed a good correlation with plunge pool depth when normalised by the measured jet impact diameter Di reducing, almost exponentially, from a peak of around 0.85 $Ui^2/2g$ at $Y/Di \approx 1-3$ to very small magnitudes at $Y/Di \approx 18-20$. Due to the jet plunge through the atmosphere and pool air entrainment, mean pressure heads were produced which were much less than predicted by submerged jet principles.

(iii) This chapter has presented experimental data in terms of the pressure fluctuations generated at various locations on the plunge pool floor. First, the radial distribution of fluctuations over the surface of the pool base was considered, and it was found that, for moderate to large tailwater depths, the worst condition, in terms of extremes in loading, was again along the impinging jet axis. Secondly, the magnitude of pressure fluctuations at the jet centre line for the range of pool depths was considered. When the pool depth was made dimensionless with the jet impact diameter, reasonable correlations were obtained over the range of parameters tested. The largest value of the r.m.s pressure head coefficient, Cp', was found, for the particular test conditions, to be 0.2 –

0.25 at Y/Di ≈ 6−7 while the largest values of Cp+ were around 0.7 − 0.9 at Y/Di ≈ 7−10 and 0.5 − 0.7 for Cp^- at Y/Di≈ 4−7. Location of the maximum value of Cp' was found to be at a plunge pool depth intermediate between the peaks of the positive Cp^+ and negative fluctuations Cp^-. The maximum difference between instantaneous pressure heads occured at Y/Di ≈ 6−10 from peak values of around 1.4 $Ui^2/2g$ to minimum values of approximately −0.1 $Ui^2/2g$.

(iv) The magnitude of fluctuations indicated that they do not necessarily follow the Gaussian distribution. This was confirmed by investigating the statistical moments of the instantaneous pressure head values obtained at the central measurement position. To fully define the extremes in pressure head (which are the most important in terms of design) the mean and standard deviation of the pressure head time history are not sufficient. The actual limit of minimum and maximum pressure heads must be ascertained to provide useful design criteria. A extreme value probability function may be of more use.

(v) Jet break−up condition at the impact point may well prove to be the most important factor in determining the magnitude and distribution of pressure fluctuations within a plunge pool.

REFERENCES FOR CHAPTER 5

1. Lopardo, R.A., Orellano, J.A., and Vernet, G.F., "Baffle Piers Subjected to Flow Induced Vibrations.", Proc. XVII I.A.H.R Congress, Baden– Baden, Vol. 3, 1977, pp. 445– 452.

2. Akbari, M.E., Mittal, M.K., Pande, P.K., "Pressure Fluctuations on the Floor of Free and Forced Hydraulic Jumps.", Proc. Int. Conf. on Hydraulic Modelling of Civil Engineering Structures, B.H.R.A., Coventry, 1982, Paper C1, pp. 87– 96.

3. Narasimhan, S., and Bhargava, V.P., "Pressure Fluctuations in Submerged Jump.", Proc. A.S.C.E., Jour. of Hyd. Div., Vol. 102, No. HY3, 1976, pp. 339– 350.

4. Toso, J.W., "The Magnitude and Extent of Extreme Pressure Fluctuations in the Hydraulic Jump.", Ph.D Thesis, University of Minnesota, 1986.

5. Ervine, D.A., "The Entrainment of Air in Water.", Water Power and Dam Construction, 28, No. 12, 1976, pp. 27– 30.

6. Johnson, G., "The Effect of Entrained Air on the Scouring Capacity of Water Jets.", 12th Int. Congress of I.A.H.R., Fort Collins, Vol. 3, Paper C26, 1967, pp. 218– 226.

7. Lopardo, R.A., "Stilling Basin Pressure Fluctuations.", A.S.C.E., Proc. of Int. Symp., Model– Prototype Correlation of Hydraulic Structures, Colorado Springs, 1988, pp. 56– 74.

8. Frizell, W., "Model/Prototype Comparison of the Pressure Fluctuations in the Boundary Layer of a High Head Tunnel Spillway.", A.S.C.E., Proc. of Int. Symp., Model– Prototype Correlation of Hydraulic Structures, Colorado Springs, 1988, pp. 210– 217.

CHAPTER 6

ANALYSIS OF MEAN DYNAMIC HEADS IN THE PLUNGE POOL.

CONTENTS

CHAPTER 6

6.1 INTRODUCTION

Chapter 6 sets out to analyse the mean presure head values reported in Chapter 4, and to set the results into a framework where they might be used in the design of plunge pools in general. Pressure fluctuations are not considered in this chapter and will be analysed in the next.

Chapter 6 contains a brief analysis of the mean pressure head values in the radial direction, but primarily deals with the distribution of mean pressure heads along the jet centre line with increasing plunge pool depth. The reason for concentrating on the jet centre line, is that highest mean heads are found along that line.

A good deal of this chapter will be given over to analysing the results shown in Fig. 4.23(b) where the mean dynamic head ($\bar{H}m - Y$) normalised by the impact velocity head $Ui^2/2g$, is plotted against plunge pool depth Y normalised by the measured jet diameter at impact Di. The result shows an unexpected collapse of data for a range of nozzle diameters, for an orifice outlet with higher turbulence, for a range of jet fall lengths through the atmosphere and for a wide range of impact velocities almost up to the prototype range.

Before Fig. 4.23(b) can be used as a design curve, the following questions must be satisfactorily answered:—

(i) Is the collapsed data in Fig. 4.23(b) simply a result of the narrow range of experimental parameters used in this research, or is it indicative of a wider range of behaviour ?

(ii) How does Fig. 4.23(b) compare with previous measurements of mean dynamic heads in a plunge pool ?

(iii) How can Fig. 4.23(b) be used in practice when the jet diameter at impact (Di) is unknown, being a function of jet acceleration as well as jet dispersion in the atmosphere. In other words, can Di be calculated ?

(iv) How can such a data collapse be possible given that the jets at impact encapsulated a large range of air entrainment rates into the plunge pool, a range of jet "broken–upness", as well as a substantial range of Reynolds Number at the impact point ?

These questions will be investigated in detail in this chapter, but the answers must be understood in the context of a conceptual framework outlined below.

6.2 A CONCEPTUAL FRAMEWORK.

For a water jet plunging through the atmosphere, the first part of the conceptual framework is that the jet will eventually disintegrate or break–up. This is true for both laminar and turbulent jets and is due to initially small instabilities in the flow, being magnified during the plunge. This means that the jet at impact will be disturbed from its initial shape at nozzle or orifice, the degree of disturbance being very dependent on the length of fall through the atmosphere, as well as the degree of turbulence inherent in the jet itself.

Considering large scale turbulent jets, such as used in this experiment, there are three possibilities concerning the growth of surface disturbances:

(i) The first is sketched in Fig. 6.1, and has been advocated by Sene [1] and later by Falvey and Ervine (1987). This is based on the premise that turbulent jets have a lateral turbulent velocity V' which causes an instantaneous dynamic force $1/2\rho(V')^2$ on the surface of the jet. This causes a surface bulge of a size dependent of the eddy length ℓ'. The restraining surface tension causes a stress $2\sigma/R$, where R is the radius of curvature of the disturbance. At some point the value of $1/2\rho(V')^2$ may be greater than $2\sigma/R$ and cause the jet to spread laterally. Droplets and particles of water are ejected from the main flow, following a parabolic trajectory and defining the outer edge of the jet, as shown by the dashed curve in Fig. 6.1.

(ii) An alternative way of describing this is to consider the jet in the atmosphere to be analogous to jet diffusion in the plunge pool, as shown in Fig. 6.2. In other words, a shear takes place between the water jet and ambient air forming vortices in the same way as a submerged jet. In this case the vortices

form at the air/water interface and take the form of surface rollers which bend back akin to breaking waves. Like submerged jets, the size of the surface rollers increases linearly in the downstream direction $\ell = Kx$. This idea has been postulated by Hecker (1988).

(iii) A third possibility has been proposed by Hoyt [4] and is shown in Fig. 6.3. This idea accepts that surface disturbances may be caused by lateral turbulent components V', as well as surface vortices due to shear at the free surface, as shown in Fig. 6.2, but this is also combined with a helical swirl which increases in diameter in the downstream direction. The reason for this (not given by Hoyt) is most likely to be connected with natural flow circulation caused by the earths rotation and evident very obviously in draining tanks.

A plunging jet may contain all three elements noted above and hence at the point of impact with the plunge pool surface will be a pulsating chaotic mixture of water and air, with the remnants of a solid jet core partly remaining, but with the remainder of the flow outside the solid core, intermittent in nature, right down to an occasional water droplet at the jet extremeties.

However chaotic the jet becomes during the plunge through the atmosphere, an analysis of Fig. 4.23(b) is only possible by some idealisation of the nature of the jet at impact. The idealisation used in this work is based on jet measurements carried out at the United States Bureau of Reclamation, revealing the intermittent jet edge to be Gaussian in distribution. That is, the probability of encountering water is normally distributed from 100% in the solid core region to zero at the jet edge, (which is deemed to be approximately three standard deviations in radial distance out from the solid core region). This is sketched in Fig. 6.4, defining the regions of the solid inner jet core (dc) as well as the outer jet extremes (di).

It can be seen from the sketch (Fig. 6.4) that the region outisde the solid inner core is a complex mixture of air and water where the outer edge (di) simply represents the outer limit of jet surface distrubances. The intermittent region from dc to di can therefore be considered like a pseudo−fluid of density $\rho = \rho_w(1-\alpha)$, where α is the local air concentration going from 0 at the edge of the solid jet core to 1 at the outer limits.

It follows from Fig. 6.4 that the ratio dc/di is a measure of how much the atmospheric jet is broken–up at impact, and also how much air will be entrained into the plunge pool.

If a means can be found to calculate di and dc for a plunging jet, then the degree of jet disruption and air entrainment rate may be characterised at the impact point. This is one of the tasks to be attempted in this chapter, in Section 6.3.4 and Section 6.3.7.

The next step in the conceptual framework is to consider the behaviour of the chaotic jet on entering the plunge pool. For submerged single phase jets, a zone of flow establishment occurs which is about six diameters in length containing a core where the velocity remains unaffected by the surrounding shear layer and remains at the same value of velocity as at the initial cross section.

For impinging turbulent jets, Sene [1] has shown that the shear layer is initially more turbulent than the submerged jet case, producing a greater spread angle α_2 in the shear layer, of the order of 14^0. This larger angle of spread can be combined with a simulation of various levels of air concentration in the shear layer to provide estimates of α_1, the inner core decay angle as sketched in Fig. 6.5. This has been carried out by Ervine and Falvey [2] revealing an estimated core length of 4dc when large air concentrations are present. Hausler [5] has suggested that impinging jets have core lengths of the order of five diameters into the plunge pool.

In either case, it may be possible to conceptualise a zone of flow establishment with an inner core of length four to six inlet diameters. The problem which remains is which diameter to accept as the real jet diameter, dc or di ?

The minimum value of core length would appear to be 4 times dc, where dc is the solid, intact part of the impinging jet. The largest core length possible would be 6 di (after Albertson et al.), with the real value varying between these two extremes.

Using this conceptualisation, it is clear that any mean pressure head measurements along the jet centre line will remain constant along the length of

the core, and decay thereafter, with the maximum value in the core being $Ui^2/2g$ or a coefficient of unity. Inspection of Fig. 4.23(b) reveals that the centre line head remains constant for values up to 4 di approximately, which is greater than the 4 dc estimate but also significantly less than 6 di. It is still to be clarified in this chapter if 4 di is a universal core length, or just pertinent to this data set.

Early thoughts on this matter indicate that a core length of 4 di would not be universal, especially when considering very long jet droplengths in the atmosphere. Previous research by Ervine, McKeogh and Elsawy [6] has shown that very smooth turbulent jets do not disintegrate until about 300– 400 diameters in length, whereas very rough turbulent jets may disintegrate after 50 diameters droplength. If a jet has already disintegrated at the impact point, then by definition there will be no solid inner core remaining. This means that the impinging jet will be intermittent and may not exhibit ANY core in the pool, using conventional criteria. The absence of a solid inner core may well imply velocity and pressure head decay along the centre line, right from the point of impact, although it should be noted that this phenomenon has not been measured in practice by any previous experimenters.

It is apparent, however, that the interpretation of the mean head values in the plunge pool cannot be carried out without an understanding and analysis of the jet behaviour in the atmosphere. This includes the physical process of jet spread in the atmosphere, estimates of di and dc at the impact point as well as estimating the degree of jet break– up at the impact point.

A further point of interest in the conceptual framework concerns the presence of air bubbles in the plunge pool. Their presence ensures that the density of the plunge pool flow is less than the equivalent submerged jet case. This in turn implies that the dynamic mean head is also less than the submerged jet case, the amount of reduction being dependent on the quantity of air in the pool.

As a rough guideline, the ratio of the impinging jet dynamic head to the submerged jet dynamic head will be of the order of $(1-\alpha)$, where α is the local air concentration along the jet centre line. The air concentration was not measured in this work, but it can be inferred by estimating the rate of air

entrainment at the impact point, and using a simplified model of the rate of air concentration reduction with pool depth to estimate α at each plunge pool depth.

The final conceptualisation in this chapter is the assumption that impinging jet diffusion in the plunge pool has analogies with the submerged jet diffusion case. In the latter, a zone of flow establishment is followed by a zone of established flow where the centre line velocity decays linearly with distance. Albertson [7] has estimated the centre line velocity decay to be $Um/Ui \approx 6.2(Di/Y)$. This would imply that the mean dynamic pressure ratio would be proportional to $(Um/Ui)^2$ and hence $(Di/Y)^2$.

The concept of separate zones is borne out in the comparison of all the mean dynamic head values plotted on the same graph as the submerged jet case in Fig. 6.6.

6.3 JET CONDITIONS IN THE ATMOSPHERE.

6.3.1 Introduction

Although most of the measurements in this thesis were carried out at the plunge pool base, a sufficient volume of data was gathered from the jet in the atmosphere to enable some analysis of the jet at the point of impact. Measurements in the atmospheric jet included mean velocity at the nozzle (or orifice) outlet, turbulent velocities U' in the longitudinal and radial direction in the jet, photographs of the rate of jet spread in the atmosphere, as well as measurements of the jet "diameter" at impact di.

Analysis of these measurements will be used to provide some insights into the mean dynamic heads on the plunge pool floor, and in particular will be used to provide answers to the following questions,

- Can the jet diameter at impact (di) be predicted ?

- Can the degree of jet break-up at the impact point be predicted ?

- Can the degree of air entrainment into the plunge pool be predicted ?

6.3.2 A note on outlet conditions and jet spread.

A typical arrangement for an impinging jet spillway is shown in Fig. 2.60 for the case of Morrow Point Dam, Colorado, U.S.A. with its concrete lined plunge pool. Fig. 2.71 shows the arrangement for Kariba for the case of an unlined plunge pool. In both cases the jet emerges from an orifice or nozzle type arrangement and plunges through the atmosphere, impinging on the plunge pool and thereafter returning to the river downstream of the dam. The jet does not have to emerge from a closed conduit structure, but can instead be a free surface overflow weir with ski–jump or flip–bucket to ensure the jet impingement point is well clear of the base of the dam. This type of arrangement is shown in Fig. 1.2 for the case of Crystal Dam, Colorado, U.S.A. The work in this thesis concentrates more on the case of the orifice/nozzle type outlet.

The outlet structure for Morrow Point Dam is shown in more detail in Fig. 6.7 for the case of the sluice gate closed. When the sluice gate is fully open, the flow from the reservoir enters what is effectively a short tube, and similar in nature to the nozzles used in this work. When the sluice gates are partially open, the flow passes under the sluice gates to the atmosphere and the effect is more like that of an orifice plate, or at least, the upper portion of the flow is subject to orifice plate like conditions. This is similar to the orifice set of experiments in this work.

For the case of short–tube or nozzle type outlet, the flow enters to nozzle from a large reservoir volume (Fig. 6.7) and boundary layers grow from the entrance of the outlet structure. The shortness of the nozzle ensures thin boundary layers at the exit to the atmosphere and hence a substantial core of undisturbed flow in the inner part of the jet. The large undisturbed inner core is not a desirable feature as it will produce less spreading of the plunging jet in the atmosphere and higher pressures in the plunge pool. This is the purpose of nappe deflectors and crest splitters; to disturb the jet near its origin, and hence to obtain a diffused jet at the impingement point. Even when the sluice gate is fully open (Fig. 6.7), the gate slot will act as a turbulence generator and at the very least will disrupt the growth of the boundary layers producing greater turbulence intensities at least near the edges of the emerging jet. A partially closed sluice gate also acts as a turbulence generator by causing flow separation

in the upper part of the flow, internal shearing and hence greater turbulence which in turn is transmitted under the sluice gate with the emerging jet. This is sketched in Fig. 6.8.

It will be recognised immediately that the thickness of the boundary layer and the degree of turbulence at the point of jet emergence into the atmosphere will depend on the length of the tube/nozzle Lo, the outlet water velocity Uo, its opening size do, the boundary roughness size of the concrete structure Ks, and whether or not there is disruption to the flow, as in the case of a sluice gate. For the purposes of analysing these experimental results, the latter parameter may be expressed as the angle of nozzle convergence, Φo, which was of the order of 7^0 for most of the tests, but suddenly increased to 90^0 for the case of the orifice. Thus Φo represents the type of outlet structure.

Another important parameter governing initial jet conditions is the outlet width bo. This is seen clearly in Fig. 3.2, showing prototype data from Morrow Point Dam of the angle of jet spread for various openings of the sluice gate. The greatest spread and probably the greatest jet turbulence occurs at an aspect ratio bo/do around 2. The reason for this is not immediately apparent, because it is also mixed in with increasing Reynolds Number, as well as increasing Weber Number of the flow, both of which cause greater jet spreading i.e. higher Reynolds Number produces higher turbulent energy in the smaller eddy length scales, and higher Weber Numbers reduce the degree of restraint of surface tension on the free surface of the plunging jet. It is speculated by the author, that an aspect ratio of 2 often produces the strongest secondary cells, with a double cell structure operating.

It is apparent therefore that short smooth nozzles will produce jets of very low internal turbulence, but will contain greater turbulence at the jet edges in the region of the boundary layer. This has been confirmed by turbulence measurements reported in Chapter 4. For short nozzles, the boundary layer thickness will be thin at the outlet point, and will vary with the Reynolds Number according to the relationship

$$\delta/L = K.\ Re_L^{-0.2} \qquad (6.1)$$

Measurements in Section 4.4 have shown the boundary layer to increase in

width in the downstream direction. This behaviour pattern may be closest to an outlet from a reservoir with the sluice gates fully open.

It is also apparent from Fig. 6.8 that jets from an orifice plate will exhibit much greater internal turbulence because of flow separation upstream of the orifice plate. This has also been verified in Chapter 4 with turbulence intensities of the order of five times that of a smooth nozzle. This behaviour pattern may be closest to an outlet from a dam with the sluice gates only partially open.

In both of the flow cases outlined above, the initial conditions have significant effect on the degree of jet spread in the atmosphere. This is illustrated graphically in Fig. 6.9, showing data from high speed photographs measuring the half angle of jet spread in the atmosphere with varying jet velocity, for three different outlet conditions.

It is clear from Fig. 6.9 that the angle of jet spread in the atmosphere increases with jet velocity and also the degree of turbulence in the jet at the outlet point. The worst case concerned an orifice jet with no upstream tube bundle flow straightener, giving spreads of 4%. The least spread was the smooth nozzle with upstream flow straightener with outer spread less than 0.5%, with the jet only spreading at velocities greater than 10m/s. In all cases, the half angle of jet spread was approximately 40% of the measured longitudinal turbulence intensity value.

Although not shown in Fig. 6.9, testing larger jet diameters also increased the degree of jet spread in the atmosphere at any given outlet velocity. This means that jet spread increases with both velocity and diameter, and hence with increasing Reynolds Number ($Uodo/\nu$) and also with Weber Number $(\rho Uo^2 do/\sigma)^{1/2}$. This is to be expected as an increase in Reynolds Number increases the turbulent energy in smaller eddies in the jet, whilst an increase in Weber Number reflects a relatively reducing surface tension effect. Both these effects work in concert to increase jet spread, but the effects are difficult to separate when using just one fluid.

Jet spread in the atmosphere can therefore be characterised by the type of outlet used, as well as the Reynolds and Weber Numbers at the outlet. It follows, therefore, that the degree of jet break-up and the degree of air

entrainment at the impingement point, will also be a function of these parameters, as well as the length of fall through the atmosphere.

6.3.3 Comparison of measured and predicted jet diameters at the impact point.

The use of Figures 4.20 and 4.23 as a design tool for predicting mean dynamic heads in a plunge pool, will be possible only when the diameter of the jet at impact point Di, can be predicted. The experimental data in Chapter 4 refers to a measured diameter at impact, therefore a simplified method of predicting the impact condition would be a useful step forward.

According to Ervine and Falvey [2], the outer jet spread angle for a jet is proportional to the lateral component of turbulence intensity V'/Uo. For vertically plunging jets, to estimate the outer flow profile, the spreading effect must be combined with the contracting influence on the jet from acceleration due to gravity. If this is possible, a simple model can be produced to estimate the jet diameter at impact with the plunge pool surface.

The jet spreading concept is sketched in Fig. 6.10 and the preliminaries for calculation of the jet spread are as follows. From the jet turbulence measurements in Chapter 4 at each tested distance from the outlet (of which a sample is shown in Figs. 4.24 to 4.35), the value of longitudinal turbulence intensity is selected at the extreme radial measurement position (rj) which is thought to be representative of the jet edge value. Knowing the mean jet velocity at this location, the R.M.S. longitudinal velocity component (U') can be obtained which is then converted to a lateral (radial) value (V') from the approximate proportionality relationship. Ervine and Falvey [2] postulated a relationship for high velocity horizontal jets in the form:

$$V' \approx 0.38\ U' \qquad (6.2)$$

Hence, to define the extremes in the jet spread, a valve of $3V'$ would be utilised in the calculation. This is based on a Gaussian distribution of lateral turbulence of which V' is the standard deviation.

Once the lateral velocity component has been established, the outer spread

angle of the jet can be calculated. At the jet edge, the particles are deemed to travel radially at a rate dictated by this lateral velocity component. As the jet is accelerating during its fall, the lateral spread is not linear but rather parabolic. Using simple projectile theory, and knowing the vertical droplength from the turbulence readings to the pool surface, a value of the external jet diameter, due to jet spreading only, can be established.

It should be noted at this juncture that, as the turbulent velocity varies with time, it follows that the actual lateral jet spread, which is deemed to be dependent on a statistical designation of the magnitiude of the jet turbulence, must have a transitory nature. Therefore, the jet diameter at impact, as well as the solid inner core (which will be discussed later) can not be defined explicitly but rather as a nominal designation. The greater the degree of turbulence, the larger will be the oscillations of the jet dimensions at the pool surface. This has been found when testing the jets issuing from the orifice plate outlet, where the condition at impact was much more irregular than the corresponding jets from the nozzle outlets.

It should also be noted that if the jet outer edge is spreading as described, the solid inner jet core must be reducing in size in a predictable fashion. At various distances from the outlet and considering continuity (conservation of mass) of the plunging jet, the calculated outer edge from the jet turbulence results and the probability distribution of encountering particles between the solid inner core and the outer edge, the core dimensions can be obtained. It is postulated that once the solid core has completely diminished the jet will break-up into droplets. This procedure will be detailed in Section 6.3.4.

Returning to the jet diameter calculation, the influence of the acceleration due to gravity is to promote contraction of the flow. This effect must be combined with the jet spread model above to provide a good estimate of the jet dimensions at impact. If the turbulence is very small, the jet will contract during the plunge. The calculation for the diameter at impact is as follows:

(i) For a jet falling vertically, the velocity at impact with the plunge pool surface (Ui), neglecting air resistance, is given by:

$$Ui = \sqrt{(Uo^2 + 2gL)} \qquad (6.3)$$

Novak [8] has shown that air resistance is only significant above 18 m/s approximately.

(ii) By continuty, for a jet contracting due to gravitiational acceleration, the diameter at impact (D_{iG}) is given by:

$$D_{iG} = \sqrt{(Uo/Ui)}.Do \qquad (6.4)$$

(iii) The time taken for the jet to fall from the outlet to the pool surface (t) is given by:

$$t = \frac{Ui - Uo}{g} \qquad (6.5)$$

(iv) The radial turbulent component (V'') is given by:

$$V'' = K\,U' = \frac{K\,Tuo\,Uo}{100}\ (m/s) \qquad (6.6)$$

where Tuo is the percentage longitudinal turbulence intensity normalised to the outlet condition.

(v) Considering the turbulence readings at the outlet, for simplicity, the total radial distance travelled by the outer jet edge due to spreading only is given by:

$$V''.\,t = K\,Tuo\,Uo.10\ (mm/s).\ \frac{Ui - Uo}{g} \qquad (6.7)$$

where, in this case Ui is based on the full fall height (L). At other turbulence measurement positions downstream of the outlet, the calculation above would be modified.

(vi) The jet diameter at impact for jet spreading (Dis) is then given by:

$$Dis = 2\,(V''.\,t + rj) \qquad (6.8)$$

where rj is the radial distance to the turbulence measurement from the theoretical jet centre line.

(vii) Combining the conflicting effects of jet spreading and contraction, the diameter at impact can be stated as:

$$Di = (Dis - Do) - (Do - D_{iG}) + Do$$

$$\therefore \quad Di = Dis + D_{iG} - Do \qquad (6.9)$$

The above principles were modified to define the outer edge of jets issuing from outlets other than vertical and by assuming the turbulence intensity. The procedure is similar to the above but the projectile theory is more involved.

At low velocity, for the vertical plunging jets, it can be seen from Equation (6.9) that when the turbulence is very small ($V'' \rightarrow 0$) and taking $r_j = Ro$, the result for Di would be:

$$Di = D_{iG}$$

In other words, at low turbulence, the jet diameter at impact would be for a jet contracting purely under the influence of gravity.

To speed-up calculation and prevent errors, the expanded expression derived from Equation (6.9) was mounted on a micro-computer. With input of the outlet diameter and velocity, fall height, distance from turbulence measurements to the pool surface and the actual jet turbulence magnitude and radial location, the calculated jet diameter at impact with the plunge pool surface was obtained.

The calculated external jet diameter at impact with the plunge pool surface was then compared with the results obtained from direct physical measurements and high-speed photographs. This is shown in Fig 6.11 for the case of each test run using the nozzle and orifice outlets. It can be seen from Fig. 6.11 that the comparison is extremely good with exact agreement in some instances.

Comparison with the plunging jet dimensions from the orifice outlet are not as precise as with the smoother jets. There are various reasons for this occurence.

(i) At the Vena Contracta, the turbulence is suppressed and hence using the lateral turbulent velocity component from the measurements at this location, consistently underestimates the measured jet impact dimensions.

(ii) As the downstream turbulence level is larger than the nozzel case, measurement of the jet diameter at impact proved much more difficult, as the jet structure was quite irregular at the pool surface.

However, when utilising the jet turbulence results downstream from the Vena Contracta, where the turbulence is better developed, and accepting that the measured dimensions are estimated, correlation between the calculated and measured values of Di was satisfactory. This is shown clearly in Fig. 6.11.

Therefore, if the turbulence intensity of the issuing jet is measured, or can be estimated, the diameter at impact can be calculated, as detailed above for a vertical circular jet. The fitted trend for the data shown in Fig. 4.23 can then be used in design to determine the mean dynamic pressures generated at the pool floor for the selected pool depth.

6.3.4 Estimation of jet inner core dimension at impact and its relation to the jet break-up length.

(i) It is postulated in this section that, if the outer edges of the jet are spreading laterally, as calculated in Section 6.3.3, then the inner solid core of the jet (dc) is going to diminish in size with plunge length. Diminishment of the solid core due to ingress of disturbances towards the jet centre line should not be confused with the growth of the turbulent boundary layer, as advocated in Equation (6.1), with distance from the outlet.

(ii) It is postulated that the diameter of the inner solid core can be calculated at any point during the jet plunge by an extension of the model in 6.3.3.

(iii) It follows, from the determination of the core diameter at impact, that the ratio of dc/di at impact will represent the degree of jet break– up at that point.

(iv) It is also postulated that when the inner solid core of the jet has decayed to zero over long plunge lengths, then the jet will be considered to have broken– up. This droplength will be referred to as the jet break– up length LB. The validity of this concept is achieved by comparring measured break– up lengths with the calculated break– up length based on zero core diameter. (Section 6.3.5).

(v) It follows from (iv) that the ratio L/LB, the actual jet droplength over the jet break– up length, will also represent the degree of jet break– up at impact, much in the same way as dc/di.

It can be suggested that:

$$L/L_B \longrightarrow 1 \qquad \text{when} \quad dc/di \longrightarrow 0$$

$$\text{or} \quad L/LB \propto 1 - (dc/di) \tag{6.10}$$

A sketch of the parameters noted above is given in Fig 6.12. A summary of the theory used to predict dc at any point and LB, the break– up length, is as follows:–

Referrning to Fig 6.12 and considering continuity of the water flow rate, it can be stated, that at any distance from the outlet:

$$Qo = Q_1 + Q_2 \tag{6.11}$$

where Qo is the outlet water flow rate, Q_1 is the flow in the core region and Q_2 is the flow in the diffused region between the jet core and the outer jet edge. In the diffused region, according to Ervine and Falvey [2], the probability of encountering water is of a Gaussian form. This is shown in Fig. 6.13 along with the notation for the following theoretical treatment.

Expanding Equation (6.11), the continuity relationship at any section L_1 for a circular plunging jet is given by:

$$\pi Ro^2\ Uo = \int_0^{rc} 2\pi r U.dr + \int_{rc}^{R} 2\pi r\ P(r)U.\ dr \qquad (6.12)$$

where $U = f(Uo, L_1)$, R is the external radius determined from the method outlined in Section 6.3.3, and P(r) is the probability of encountering water between rc and R.

The probability density function P(r) is given, normalised to produce unity at $r = rc$, as:

$$P(r) = \exp. \left[- \frac{(r - rc)^2}{2\sigma^2} \right] \qquad (6.13)$$

Integration of the core region simply produces:

$$Q_1 = \pi\ rc^2\ U \qquad (6.14)$$

Integration to determine the flow in the difused region is much more difficult due to the probablity density function. The procedure will be detailed later in this section, when considering the Gaussian distribution to be across the entire jet width, along with proof of the integration technique. For the moment, calculation of the flow over the annulus between rc ($\sigma = 0$) and R ($\sigma = 3$) produces:

$$Q_2 = 2\pi/9\ U\ (\ R^2 + 1.8\ Rrc - 2.8\ rc^2\ ) \qquad (6.15)$$

Equation (6.15) satisfies the condition that $Q_2 = 0$ when $rc = R$ and also indicates that when $rc = 0$ the flow in the diffusion region is $Q_2 = 2/9\pi\ R^2\ U$. This last point can be achieved by integration, as will be detailed below.

Combining Q_1 and Q_2, the overall flow at a section downstream is given by:

$$Q_1 + Q_2 = 2\pi/9\ U\ (R^2 + 1.8\ Rrc + 1.7\ rc^2) \qquad (6.16)$$

when $rc = R$, $Q_1 + Q_2 = \pi\ rc^2\ U$, while when $rc = 0$, $Q_1 + Q_2 = 2/9\pi\ R^2 U$

Hence, once the external radius (R) has been calculated at the prescribed distance from the outlet, Equation (6.16) can be equated to the outlet flow condition to determine the core dimensions. The solution for rc is in the form of a quadratic equation.

It should be noted here that the model is based on jet spreading. If the turbulence is insufficient, the jet will contract and the external radius will equal rc. This is shown by considering one of the limiting conditions of Equation (6.16), where the core dimensions will be calculated simply from gravitational acceleration. Contracting jets have a bearing on the break-up calculation, as will be shown.

Once the solid core has diminished to zero at the jet break-up point, then the Gaussion distribution is assumed to be across the entire jet cross section as shown in Fig. 6.14. The flow in the diffused region is then given by:

$$Q_2 = 2\pi\ U \int_0^R P(r)\ r.\ \partial r \qquad (6.17)$$

Incorporating the P.D.F, Equation (6.17) is given as:

$$Q_2 = 2\pi\ U \int_0^R \exp.\ -9/2.\ r^2/R^2.r.\ dr \qquad (6.18)$$

Substituting $z = r^2/R^2$ and the differential dz, Equation (6.18) becomes:

$$Q_2 = \pi\ UR^2 \int_0^1 \exp.\ -9/2.\ z\ dz \qquad (6.19)$$

Integrating Equation (6.19) and re-substituting gives:

$$Q_2 = -\ 2/9\ \pi\ U\ R^2 \left[\exp.\ -9/2.\ r^2/R^2 \right]_0^R \qquad (6.20)$$

therefore:

$$Q_2 \simeq 2/9\ \pi\ R^2\ U \qquad (6.21)$$

Equation (6.21) has previously been developed from Equations (6.15) and (6.16) for the case of rc = 0. Equating the flow at the downstream location with that of the outlet and expanding gives:

$$Uo\ Ro^2 = 2/9\ \surd\ (Uo^2 + 2gL_1).\ \left[R = f(Uo, Do, Tu, L_1, g)\right]^2 \qquad (6.22)$$

which can be solved for $U = \surd(Uo^2 + 2gL_1)$ and hence $L_1 = L_B$.

Two methods can be employed to determine the break-up length:

(i) An iterative technique can be employed to solve Equations (6.11) and (6.16) for the core dimensions at steadily increasing distances downstream from the outlet. Once the core diameter approaches zero (within stipulated range) the final cumulative length increment can be taken as the break-up length. A graphical representation of the core diameter calculation is shown in Fig 6.15 and a listing of the program developed to carry out the iterative technique is given in Appendix D.

(ii) Equation (6.22) can be solved directly by using Cardan's method, or similar, for cubic equations.

Both methods (i) and (ii) were employed to act as a cross-check, and in general produced very good agreement. Thus a method is provided to determine not only the inner jet core dimension in the conceptual model, but also the jet break-up length.

It was thought that a check on the authors method of calculating the flow in the diffused jet region would be if the same method could be applied to other situations where the flow pattern was governed by the Gaussian distribution and the solution was known. The example chosen was that of the classical submerged jet diffusion pattern, where the form of the velocity profile at any cross-section is known (Albertson [7]) but could now be compared with the method above. If successful, this would provide proof of the integration technique employed in

determining the jet core dimension and hence the break- up length.

For submerged jet diffusion in an unlimited tailwater, it can be said that the momentum flux is conserved. Expressed matheimatically:

$$\frac{M}{Mo} = \frac{\int_0^{\infty} U^2 \, dA}{Uo^2 \, Ao} = 1 \qquad (6.23)$$

According to Albertson et al [7] the velocity profile in the established flow region is given by:

$$U/Um = \exp.^{(-r^2/2\sigma^2)} \qquad (6.24)$$

where the standard deviation (σ) is a simple linear relationship in the form:

$$\sigma = 0.081y \qquad (6.25)$$

Thus Equation (6.24) becomes:

$$U/Um = \exp.^{-(r^2/0.0131y^2)} \qquad (6.26)$$

$$U/Um = \exp.^{-76.2(r^2/y^2)} \qquad (6.27)$$

Squaring Equation (6.27) gives the momentum flux velocity profile as:

$$U = Um^2 \exp.^{-152.4\,(r/y)^2} \qquad (6.28)$$

The momentum flux in the established flow region can then be expressed as:

$$M = 2\pi\, Um^2 \int_0^{\infty} \exp.^{-152.4(r/y)^2} r.dr \qquad (6.29)$$

Substituting $z=(r/y)^2$ and the differential ∂z, in a similar manner to Equation (6.18), gives:

$$M = \pi\, Um^2\, y^2 \int_0^1 \exp.^{-152.4} z.dz \qquad (6.30)$$

$$\therefore M = -\frac{\pi\, Um^2\, y^2}{152.4} \left[\exp.^{-152.4(r/y)^2} \right]_0^{\infty} \qquad (6.31)$$

$$\therefore \quad M = \frac{\pi \, Um^2 \, y^2}{152.4} \tag{6.32}$$

Using Equation (6.23), the downstream momentum flux can be equated to the intial value as:

$$Um^2 \, y^2/152.4 = Uo^2 \, Ro^2 \tag{6.33}$$

$$\therefore \quad Um^2 \, / \, Uo^2 = 152.4 \, Ro^2 \, / \, y^2 \tag{6.34}$$

$$\therefore \quad Um/Uo = 12.34 \, (Ro/y) \tag{6.35}$$

Which provides the solution for the centre line velocity decay in the established flow region as:

$$Um/Uo = 6.17 \, (Do/y) \tag{6.36}$$

According to Albertson et al [7] the actual solution for circular jet diffusion is given by:

$$Um/Uo = 6.2 \, (Do/y) \tag{6.37}$$

Therefore, the integration technique used previously in determining the flow in the diffused jet region has proved to be applicable by providing a correct solution to another situation where the flow pattern is governed by the Gaussian distribution.

6.3.5 Comparison with previous experiments on the jet break-up length.

In Section 6.3.3 a method was proposed to determine the jet diameter at impact Di of a plunging turbulent jet. A good correlation was produced with measured value of Di.

In Section 6.3.4 a method was proposed to determine the inner solid core dimension at impact dc, as well as the jet break-up length where dc $\longrightarrow$ 0.

There are no physical measurements of the core diameter at impact in the literature, and hence convincing evidence of the proposal in Section 6.3.4 can only be achieved by comparing the estimated break–up lengths of the jet in Section 6.3.4 with previously measured values of jet break–up length in the literature.

It is clear that if the authors method of estimating L_B is accurate, then the ratio L/L_B (actual fall length / jet break–up length) could be used to describe how much the plunging jet has broken–up at the point of impact. It might be described as a coefficient of jet disruption or jet break–up.

A lot of experimental data on break–up lengths relate to horizontally issuing jets. For instance, the expression produced by Horeni [9] relates to a horizontal rectangular jet, and is given by:

$$L_B = 7.8\ Reo^{0.319} \qquad (6.38)$$

For vertical jets, the influence of gravity is to accelerate the flow and hence promote contraction. Therefore, with laminar jets, the jet will decrease in diameter with distance from the outlet. There are also diameter changes due to velocity profile relaxation and surface tension forces. It was supposed that gravity would not effect the jet break–up length considerably, and this has been supported by small scale jet evidence. However, theoretical and experimental data of Takahashi and Kitamura [10] reveals that the effect of gravity in the case of vertical, laminar jets is pronounced, mainly in a contraction of the jet, which in turn influences its break–up length. From a theoretical investigation into the growth of jet surface disturbances and by testing horizontally and vertically issuing jets, it was found that the break–up length of a contracting jet is larger than that of a cylindrical jet at the same initial conditions. Furthermore, the larger the nozzle diameter, the greater the difference in the break–up length between these two types of jets. Takahashi and Kitamura [10] correlated their experimental data for laminar jets with the following semi–empirical equation:

$$L_B/Do = 18\ Weo^{8/7}\ Fro^{-2/7} \qquad (6.39)$$

When Equation (6.39) was imputed with the present experimental test conditions, however, inordinately high values of L_B were obtained. More realistic results are

produced with the expression by Iciek [11], in a similar form to Equation (6.39), and given as:

$$L_B/Do = 11.5\ Weo^{0.62} \qquad (6.40)$$

An empirical expression of this nature may be more appropriate at the lower outlet velocities and extremely low turbulence levels tested in the experimental programme, where the jets contracted during the plunge and the theoretical model would not suffice.

In the turbulent region of the break-up length curve, shown in Fig. 2.45 various expressions have been developed. For instance, Chen and Davis [12] produced:

$$L_B/Do = 1.15\ Weo + 30 \qquad (6.41)$$

while Baron [13], using dimensional analysis, expressed the break-up length us:

$$L_B/Do = 537.6\ Weo\ /Reo^{5/8} \qquad (6.42)$$

Equations (6.41) and (6.42) produce widely varying results as the magnitude (and development) of the jet turbulence is not taken into account. Mckeogh et al. [6] managed to measure the turbulence in a vertical plunging circular jet and demonstrated that the break-up length is strongly dependent on this parameter. The break-up length was correlated with discharge of water from the tested circular nozzles (Do = 6 mm to 25 mm) and the expression for break-up length was related to the water discharge rate in the form,

$$L_B = C\ Qw^n \qquad (6.43)$$

where the power exponent of Qw was found to be dependent on the turbulence level in the jet and independent of the nozzle diameter. The values of C and n are given in Table 2.1.

As expected (from the jet spreading calculations), an increase in jet turbulence intensity will reduce the jet break-up length, for a constant flow. That is, with increase in turbulence intensity, the jet will spread more expansively

and hence the inner core will decay at a shorter droplength.

It was decided to compute jet break–up lengths for a diameter of 25mm and for a range of outlet velocities using the the authors method, Section 6.3.4, to compare with some previous experimental and empirical relationships from the literature.

A typical plot is shown in Fig. 6.16 showing correlations of Chen and Davis, Baron and Mckeogh (0.3%, 1% and 3% jet turbulence), and these are compared with the authors "zero core" method also at 0.3%, 1% and 3% jet turbulence levels.

The following points can be made from Fig. 6.16:

(i) The jet break–up length increases with both velocity at the outlet, and also the diameter of outlet, although the latter point is not shown in Fig 6.16.

(ii) The jet break–up length decreases with increasing jet turbulence levels.

(iii) The comparsion of the authors zero core method and Mckeogh data [6] is quite good, especially at the lower turbulence levels.

(iv) Baron's correlation [13] is relevant mainly to high turbulence jets more like the orifice plate jets in this research.

(v) Chen and Davis work [12] gives a reasonable correlation at lower velocities but poorer correlation at higher velocities.

(vi) Fig. 6.16 serves to show the enormous influence of the outlet flow structure (initial turbulence level) even for a given Reynolds and Weber Number of the flow (Uo, Do constant).

(vii) A curve showing the average of five different methods in the turbulence range (0.3% to 1%) is shown in Fig. 6.16. This is the range of the nozzle tests in the work.

An analysis of the nozzle jets in this work, averaging over the FIVE

methods in Fig. 6.16 and also carrying out the calculations for all three diameters 25mm, 52.5mm and 78mm respectively, produced an estimated jet break-up length of the order,

$$L_B \simeq 41.2\ Uo^{0.625}\ Do^{0.9} \qquad (6.44)$$

This expression is relevant to turbulence levels under 1% only and hence has no relevance to the orifice jets.

Fig. 6.17 shows the variation of the non-dimensional break-up length L_B/Do plotted for a range of initial turbulence intensities using the authors model, and is compared with Baron's relationship [13] as well as experimental data from Mckeogh [6]. Mckeogh's data represents a constant nozzle velocity but for three different nozzle diameters. The larger diameter nozzles produce the lowest non-dimensional break-up ratios.

It is clear from Fig. 6.17 that the authors model agrees with Baron's proposal at moderate to large turbulent intensity jets, such as those found in prototype structures. For the smooth turbulent nozzle jets in this work, with $U'/Uo < 1\%$, Baron's relationship would not be adequate giving a gross under-estimate of break-up length.

It is also clear from Fig. 6.17 that the authors method of calculating L_B is independent of scale, and hence would correspond to Mckeogh's data devoid of any jet size scale effects. The pattern of variation with turbulence intensity is comparable with Mckeogh's as is the pattern of variation with jet diameter.

6.3.6 Estimates of the degree of jet break-up for the nozzles and orifice used in this work.

The authors model of estimating jet break-up length and inner jet core diameter, would appear to be at least as accurate as any previous scale dependent measurements in the literature.

It would be also reasonable to assume that the ratio of L/L_B would be the most suitable non-dimensional ratio to describe the degree of jet break-up at

the point of impact. L is the droplength to the impact point and L_B, the theoretical break-up length. Clearly small values of L/L_B would indicate a substantially intact jet at impact whilst values of L/L_B near unity would indicate a greatly dispersed jet at impact.

Having established a method of determining L_B, we can now provide estimates of the range of L/L_B used in the these experiments. This is necessary in interpretation of the mean dynamic head data.

The estimates of L/L_B are given in Table 6.1 (Vol.II) covering the range of diameters, droplengths and outlet velocities tested. Break-up lengths for the jets issuing from the nozzle outlets have been calculated using Equation (6.44) while the corresponding break-up lengths of the orifice plate jet have been determined from Mckeogh's [6] expression for a jet turbulence of 3% ($L_B = 16.1\ Uo^{0.31}Do^{0.62}$).

6.3.7 Estimates of the degree of air entrainment into the plunge pool.

The rate of air entrainment by plunging circular jets in plunge pools, has been measured by numerous authors including Henderson et al [14], van de Sande [15], Cumming [16] and Mckeogh et al. [6] to name but a few. The relationship by Ervine [17], however, has been validated by Mason [18] and Kobus [19] and was therefore accepted as an estimate of the initial ratio of air flow to water flow entering the plunge pool, (βi)

The relationship was used in the form,

$$\beta i = K\ (L/do)^{1/2}\ (\ 1 - Umin/Ui) \qquad (6.45)$$

where K varies with the turbulence level in the jet from 0.2 approximately for very smooth turbulent jets to about 0.4 for very rough turbulent jets.

L is the jet plunge length

Ui is the impact point velocity

Umin is the minimum velocity to entrain air and has been found by Mckeogh et al. [6] to be a function of the relative turbulence of the jet.

Equation (6.45) above contains the term K which is a function of the outlet type, L/do which is a function of the growth of surface disturbaces along the jet length, and (1− Umin/Ui) which is a scale effect term. That is, jets of moderate turbulence (3%) do not entrain air at velocities below 1m/s approximately.

The air/water ratios computed from Equation (6.45) were converted into initial air concentration values by the relationship:

$$Ci = \beta i / (1+\beta i) \qquad (6.46)$$

this being a measure of the initial mean air concentration just at the impact point near the pool surface.

The estimates of initial mean air concentration are given in Table 6.2 (Vol. II) for the range of diameters, droplengths and velocities tested. Tables 6.1 and 6.2 are simply presented at this juncture. The influence of the tabulated parameters on plunge pool presure will be considered in later sections of this Chapter (6.4.4 and 6.4.5) and in Chapter 7.

6.4 FLOW CONDITIONS IN THE PLUNGE POOL

6.4.1 Introduction

The purpose of Section 6.3 was to find ways of characterising a turbulent, uneven jet at the point of impingement with a plunge pool surface. This included a conceptual impact diameter Di, a remnant core diameter dc, a jet break− up coefficient L/L_B, as well as the degree of aeration entering the plunge pool Ci. It is hoped that these parameters will be of use in interpreting the mean and fluctuating pressures on the plunge pool floor.

The purpose of Section 6.4 is to analyse the mean dynamic pressure on the plunge pool floor both in the radial and depth directions. It is hoped that when the mean pressure heads are related to the degree of jet break− up and aeration at the plunge point, a more general framework of model and prototype pressure distributions will evolve.

6.4.2 Mean dynamic pressure head variation with radius.

Figures 4.3 and 4.4 show the radial variation of mean dynamic pressure heads at the plunge pool floor. The radial distance (Rp) is normalised by the nozzle outlet diameter (Do) in Fig 4.3 and the measured jet impact diameter (Di) in Fig. 4.4. The results in Figs 4.3 and 4.4 can be compared with other data considering plunging jet diffusion to determine if the same magnitude of mean dynamic pressures has been found in other testing programmes. Fig. 6.18 plots the variation of mean dynamic head in the radial direction, and shows the comparison of the present research results (Refer Fig. 4.3(b)) with that of Lencastre [20] and Hydraulic Research Ltd. [21]. In this figure it should be noted that the radial distance from the jet centre line is normalised by the jet outlet width (b) in each of the cited sources, as no guidance on the impact diameter dimensions was provided. The data from this present work is therefore normalised by the nozzle outlet diameter to remain consistent.

It can be seen from Fig. 6.18 that the comparsion of the magnitude of the present results with that of the other sources is very favourable. However, no expressions have been developed in the studies mentioned above to describe the mean dynamic pressure head distribution. Other sources must therefore be investigated to determine if any pertinent correlations are avaliable, including submerged jet diffusion studies.

The magnitude of the mean dynamic pressures at the jet centre line are generally less in the plunging jet case than the corresponding submerged jet case. This is due to an uneven and dispersed jet at impact, as well as aeration, both of which combine to reduce mean pressures. It is surprising therefore when the two types of jet are compared, that the pattern of radial variation of the mean dynamic pressure heads is strikingly similar in both cases. This can be seen in Fig. 6.19, comparing the radial variation of mean dynamic pressure heads for the case of a low velocity plunging jet (Fig. 4.4(b)), with that of a submerged jet, from the data of Hrycak et al. [22]. The radial distance (Rp) in this figure is normalised by the measured jet diameter at impact assuming this is equivalent to the diameter of a submerged nozzle. It is thought that, as the patterns in Fig. 6.19 are similar, the substantial theoretical treatment of submerged jet diffusion may provide expressions to describe the plunging jet pressure head distribution in the radial direction.

Considering Fig. 6.19 it can be seen, for both cases, that the maximum value of mean dynamic head at each pool depth is obtained along the jet centre line (Rp= 0). The centre line values reduce with increased pool depth. In the radial direction, the value of mean pressure reduces from the centre line value with the most rapid decay at the smallest pool depth. At radial values of Rp/Di $\geq$ 2, the dynamic pressure is considered negligable.

For the submerged jet case, the mean pressure head radial distribution at pool depths less than the theoretical core length (e.g. Y/Di $\leq$ 4), can be described by an expression based on free jet principles derived by Hausler [5]. The expression is independent of pool depth and is given by:

$$\frac{\bar{H}m - Y}{\bar{H}s} = \frac{\bar{H}m - Y}{Ui^2/2g} = \exp. - 2(Rp/Di)^2 \qquad (6.47)$$

where $\bar{H}s$ is the mean dynamic pressure head at any section along the jet centre line. Thus $\bar{H}s$ is equal to $Ui^2/2g$ only in the specific region of jet core but not beyond.

Comparing Equation (6.47) with Hrycak's values for a submergence of Y/Di= 4 in Fig. 6.19, the fit is most satisfactory. Once the dynamic pressure heads have been correctly normalised relative to the centre line value $\bar{H}s$, it is expected, at the lower pool depths (Y= 100mm and 200mm), that an equation in this form would be applicable to the present study. This point will be investigated later in this section.

Equation (6.47) cannot, however, be extended to larger pool depths (Y= 350 and 500mm – beyond the jet core) as, like the velocity profile development, the various regions of flow require their own particular treatment. In the case of the boundary pressure distribution beneath a submerged jet, three regions can be established, advocated by Beltaos [23], namely:

(i) small depth impingement $0 \leq Y/Di \leq 6$.

(ii) transition $6 \leq Y/Di \leq 8$.

(iii) large depth impingement Y/Di ≥ 8.

The region can be seen by comparing the radial pressure head values at various pool depths as show in Fig. 6.20. The data comes from Hrycak et al. [22], Kamoi and Tanaka [24] for a slot jet together with data from the present study. Fig. 6.20(a) shows the radial distribution of pressure with the radius made dimensionless by the jet impact diameter while Fig. 6.20(b) shows the pressure head values with the radius normalised by the pool depth. In both figures the dynamic pressure head is made dimensionless by the pressure head scale, in this case, the dynamic pressure head at the jet centre line. Consequently, the pressure head ratio for all pool depths at the jet centre line is equal to unity.

When normalised by the submerged jet nozzle diameter, Fig. 6.20(a), it can be seen that the non-dimensional pressure head reduces most rapidly in the radial direction at the smallest pool depths. On the other hand, when plotted with Rp/Y (Fig. 6.20(b)) the decay with radius of the mean dynamic pressure head ratio was most pronounced at the larger pool depths. Comparing the location of the data values from Fig. 4.4 with these general trends provides an estimation of the region of pressure development outlined above.

Technical reasons dictated that the minimum distance between measurement instruments on the pool floor was 100mm. Therefore, the minimum ratio of Rp/Di was around 1.15 (Dimax = 87mm). Similarly the minimum ratio of Rp/y was 0.2 (Ymax = 500mm). However, even with this limitation, it can be seen from Fig. 6.20(a), when the data is plotted in this form, that at Y/Di = 1.15 to 1.48, the results seem to fall in the small depth impingement designation while for Y/Di = 6 to 6.44 the transition designation is more appropriate.

Comparing the data values with the trends for various submergence ratios in Fig. 6.20(b) it can be seen that at Y/Di = 4.1 to 5 the appropriate designation would be that of short depth impingement while at Y/Di = 6 to 7 the region, as noted above, is that of transition. If separate equations were valid for each of the pressure development regions then expressions for the plunging jet pressure distribution could be obtained.

By plotting the experimental results of Beltaos and Rajaratnam [25] and Poreh and Cermak [26] in a similar form to Fig. 6.20, with the pool depth

replaced by a length scale, it has been found [25], for submerged jets at large pool depths, that the dimensionless pressure head profiles are similar. For Y/Di > 21 (Region (iii) above), the dynamic pressure head rate can be defined by the expression:

$$\frac{\bar{H}m - Y}{\bar{H}s} = \exp.^{-0.693\,(Rp/bp)^2} \qquad (6.48)$$

where bp is the radial distance to the point where the dynamic pressure is one half of the centre line value.
At the plunge pool floor it has been found by Beltaos and Rajaratnam [25] that bp = 0.078Y and hence Equation (6.48) can expressed as:

$$\frac{\bar{H}m - Y}{\bar{H}s} = \exp.^{-114(Rp/Y)^2} \qquad (6.49)$$

where, for the submerged jet case, $\bar{H}s = Ui^2/2g.\ f(Y/Di)$.

This expression produces approximately the same values as the case of Y/Di = 20 in Fig. 6.20(b) and is shown in Fig 2.23.

Extending this concept of similarity, which has only been proven strictly true for submerged jet diffusion rather than impinging jet action, and applying the principle to each of the pressure profiles shown in Fig 6.20b, which are taken as indicative of each region defined above, equations can be developed for the other zones of impingement and which may be applied to the data values shown in Fig 4.4.

For <u>short depth</u> impingement (considering the pressure head curve at Y/Di = 4 in Fig. 6.20), the radial length scale, bp, where $\bar{H}m - Y/\bar{H}s = 0.5$ is found to be approximately 0.15Y. Substituting this value in Equation (6.48), the following expression can be developed:

$$\frac{\bar{H}m - Y}{\bar{H}s} = \exp.^{-30.8\,(Rp/Y)^2} \qquad (6.50)$$

where, for the case of submerged jet diffusion, $\bar{H}s = Ui^2/2g$.

Equation (6.50) is an alternative version of Equation (6.47) with the jet diameter term replaced by the plunge pool depth term in the relationship.

In the transition region (Y/Di = 7−8 in Fig. 6.20(b)), the following expression can similarly be developed (bp ≈ 0.11):

$$\frac{\bar{H}m - Y}{\bar{H}s} = \exp.^{-57.3\,(Rp/Y)^2} \qquad (6.51)$$

where $\bar{H}s = Ui^2/2g.\ f(Y/Di)$

The expressions developed above for each region can be used to provide a fit for the data values presented in Fig 4.4. This is shown in Figs. 6.21(a) and 6.21(b). The ratio of Rp/Y is large for the small pool depths (Y= 100mm and 200mm) and hence the best representation for the data at the transducer located at Rp= 100mm from the jet centre line is by applying Equation (6.47), Fig 6.21(a), and plotting the dimensionless dynamic pressure head with R/Di. It can seen from Fig. 6.21(a) that the measurements were slightly above those predicted by Equation (6.47). The expresion was therefore modified to produce a more precise correlation and is given by:

$$\frac{\bar{H}m - Y}{\bar{H}s} = \exp.^{-1.6\,(Rp/Di)^2} \qquad (6.52)$$

Equation (6.52) is also shown in Fig. 6.21(a) and the fit for the limited data is satisfactory. At Rp/Di ≥ 2 the mean dynamic pressure is approximately zero. In other words, the mean pressure approaches the hydrostatic head.

At the larger pool depths (Y= 350mm and 500mm), the designations found for the present data in Fig. 6.20(b) are applied to select the appropriate expression from Equations (6.49) to (6.51). Therefore, Equation (6.50) fits the limited data most satisfactorily for Y/Di = 4.1 to 5 while Equation (6.51) is adequate as a lower bound for Y/Di= 6.7, as shown in Fig. 6.21. To produce a more precise fit for the experimental data at Y/Di = 6 − 7, Equation (6.51) was modified to produce:

$$\frac{\bar{H}m - Y}{\bar{H}s} = \exp.^{-47.5(Rp/Y)^2} \qquad (6.53)$$

At Rp/Y $\geq$ 0.35, the mean dynamic pressure is practically negligable when compared with the centre line value.

As detailed above, to determine the radial variation of the dimensionless mean dynamic head, the submergence (Y/Di) must first be assesed. The correct equation can then be selected to determine the pressure head value, relative to the centre line head, at the particular radial position.

For the submerged jet case, the variation of the dynamic head scale ($\bar{H}s$) with pool depth is already well known, as noted after Equations (6.49) to (6.51). On the other hand, for the impingement of a plunging jet, the variation of the pressure head scale has not, as yet, been defined. Therefore, to ascertain the magnitude of the mean dynamic pressure head values in the radial direction, the variation of the pressure head scale must be determined. In other words, for the previous equations to be useful, an expression for the variation of the centre line mean dynamic head with pool depth must be developed. This process will be carried out in the following section.

6.4.3 Mean dynamic head variation with plunge pool depth.

The variation of the jet centre line mean dynamic head with plunge pool depth data is presented in Figs. 4.5 to 4.23 of Chapter 4. In this series of results, the most significant diagrams are Fig. 4.20(b), which shows a good data collapse for all three nozzle outlets, range of droplength and jet velocity, and Fig 4.23(b), which contains the same material as Fig. 4.20(b) but also includes the results for the orifice plate test. The data collapse is achieved, to some extent, by normalising the measurements of mean dynamic head and pool depth with the jet conditions at impact with the plunge pool surface. The mean dynamic head ($\bar{H}m - Y$) is made dimensionless by the estimated pool impact velocity head $Ui^2/2g$ while the pool depth is divided by the measured jet impact diameter.

In both Figs. 4.20(b) and 4.23(b) it can be seen that the centre line mean dynamic pressure head attains a plateau of around ($0.86\ Ui^2/2g$) for 3 to 4 jet diameters into the plunge pool. Thereafter, the mean dynamic pressure head reduces dramatically with increase in pool depth. At Y/Di = 20, the values of mean dynamic head are negligable.

The intention in this section is to compare the results with that of data from other experimental sources (to ensure the validity of the results) and also to produce a best fit for this trend shown in Fig. 4.23(b). The influence of parameters such as jet "compactness" and air entrainment rates on the pool diffusion process and their contribution to the data collapse in Figs. 4.20(b) and 4.23(b) will also be investigated, in subsequent sections.

(A) Comparsion of mean dynamic pressure head results with previous studies.

The main differences between submerged diffusion of a water jet and that of turbulent plunging jet diffusion are, that at entry into the quiescent fluid, submerged jet conditions are well defined and no air is entrained into the pool. The rate of longitudinal deceleration in the case of the single–phase flow will, therefore, be lower than the plunging jet case, as less turbulence is generated in the diffusion process, and the cushioning effect of air bubbles on floor pressures, along with other effects such as surface wave formation, will not be apparent. Hence, values of mean dynamic pressure, in the case of submerged jet diffusion will always provide an upper bound to the mean pressures generated by plunging jet impingement. The mean dynamic pressures presented in Fig. 4.23(b) will therefore be compared first with submerged jet diffusion to ascertain if this is the case, and also to find out if the established submerged jet theory can be applied directly or, in modified form, to the impinging jet case.

The centre line velocity decay of a submerged jet in an infinite medium has been analysed by Albertson et al [7], Rajaratnam [27] and Abramovich [28] to name but a few. Their work can be used to estimate the centre line mean dynamic pressure developed at a boundary due to orthogonal impingement of a submerged jet on this solid boundary.

Within the flow establishment region the centre line velocity (Um) is, by definition, equal to the in initial velocity (Ui) while, beyond this point (Y> Yc) the centre line velocity has been shown to decay with distance from the pool surface as:

$$Um/Ui = Yc/Y \qquad (6.54)$$

where, according to Albertson [7] Yc (core length) = 6.2 Di

The principle used to develop an expression for the dynamic pressure at a surface below the submerged jet, due to this form of velocity decay expression, is to assume that the pressure developed at the boundary would be equivalent to the velocity head at the same pool depth if no boundary was present. That is, for $Y \leq Yc$:

$$\frac{Um^2}{Ui^2} = \frac{\bar{H}m - Y}{Ui^2/2g} = 1 \qquad (6.55)$$

while for $Y > Yc$:

$$\frac{Um^2}{Ui^2} = \frac{\bar{H}m - Y}{Ui^2/2g} = 38.44\ (Di/Y)^2 \qquad (6.56)$$

This principle is not strictly true as the boundary will affect the centre line velocity development within the vicinity of the surface. However, it provides a good initial estimate of the variation of centre line mean dynamic pressure with depth, and the form of the expressions above have been proved by experimental evidence.

For example, Beltaos and Rajaratnam [25], when testing submerged jets at large distances from a solid boundary, produced the expression:

$$\frac{\bar{H}m - y}{Ui^2/2g} = 50\ (Di/Y)^2 \qquad (6.57)$$

while Poreh and Cermak [26] produced the expression:

$$\frac{\bar{H}m - Y}{Ui^2/2g} = 60.4\ (Di/Y)^2 \qquad (6.58)$$

It can be seen that the only difference between Equations (6.56), (6.57) and (6.58) involve the constant which varied from 38.44 to 60.4. This may be traced to the length of the jet core which is indicated to have ranged from 6.2 Di to

7.8 Di in the cited cases or may be due to the mentioned boundary affects. Albertson's [7] expression will be used for comparison with the present experimental results as it produces the lowest values of mean pressure out of all the submerged jet cases detailed above.

Fig. 6.6 shows the comparison of results from Fig. 4.23(b) with that of a submerged jet, assuming that the measured jet diameter at impact is equal to the submerged outlet magnitude. It can be seen immediately from Fig. 6.6 that the submerged jet results do indeed provide an upper bound to the experimental results. The centre line values of mean dynamic pressure head are equal to the initial velocity head ($Ui^2/2g$) up to around 6 jet diameters into the pool for the submerged jet case, whilst it can be seen that the present results remain constant at around 0.86 $Ui^2/2g$ for approximately 3 to 4 jet diameters into the plunge pool. The centre line values are less than those of the submerged jet case in the jet core region due to reasons outlined in Chapter 4 but, more importantly, the fact that the results are only constant for 3 to 4 jet diameters into the pool proves that the diffusion process occurs much more rapidly in the impinging jet case. After the initial peak region, the experimental results are still significantly smaller than those predicted by submerged jet theory, apart from at large pool depths relative to the impact diameter. This is probably due to a disrupted jet at entry as well as the effect of air entrainment. Therefore, submerged jet theory would have to be modified to provide any suitable expressions for the impinging jet action.

Actual data of mean dynamic pressures generated by plunging jet impingement produced a good comparsion with the experimental results shown in Fig. 4.23(b) as seen from the work of Hausler [5] and Lencastre [20] and shown in Figs. 6.22 and 6.23. Hausler carried out an experimental programme to determine the mean dynamic pressure development at a stilling basin floor due to impingement of a circular plunging jet. The set−up is shown in Fig 2.62. Nozzle outlets were used which were 40mm, 60mm and 90mm in diameter. The fall height (L) was 1.3m and the pool depth was varied from 0 to 1.6m. The apparatus was similar to that used in the present research. However, some basic differences were evident. The fall height was kept constant, the type of outlet device was not altered and, most importantly, only mean pressure measurements were presented. The mean pressure results are useful for comparison however, especially as the parameters mentioned above did coincide in some instances with

the present experiments.

Fig 6.22 shows the comparsion of Hausler's [5] results for the centre line mean dynamic pressure head, with those of Fig. 4.23(b). It should be noted that the diameter at impact in the case of Hausler results has been calculated on the basis of contraction of the plunging jet due to gravitational acceleration only and also, since the results showed some variation with Reynolds Number, only the upper and lower limits are plotted in Fig. 6.22. It can be seen from Fig. 6.22 that the agreement between both sets of data is extremely good. The expressions developed by Hausler were based on submerged jet principles, which have been detailed previously, and no new treatment were forthcoming.

Lencastre [20] tested rectangular plunging jets and the comparsion with the present experimental results is shown in Fig 6.23. Lencatre tested slot jets where the outlet width varied from 44mm to 96mm. As no information was provided on the jet turbulence level, the pool depth in the case of Lencastres data is normalised by the slot width. It can be seen from Fig 6.23 that a good comparsion is again achieved with the authors data.

Hydraulics Research Ltd. [21] are undertaking similar tests to Lencastre but, at the time of writing this thesis, only one submergence has been tested. The result in Fig. 6.23 is lower than the authors data when normalised by the outlet slot width.

In Fig. 6.23 field data from Morrow Point Dam is also incorporated. Location of the data points is as follows. Considering the maximum discharge per gate opening at Morrow Point Dam and the sluice gate size, an estimate of the maximum outlet velocity can be established. Converting the square opening into an equivalent diameter, and with knowledge of the jet droplength at Morrow Point Dam (L= 110m), the theoretical jet impact diameter Di and velocity Ui can be obtained (assuming acceleration due to gravity only). Hence, the measured head at Morrow Point Dam (39m– 47m) can be normalised with the estimated impact head and the pool depth plotted relative to the impact diameter for comparsion with the experimental results. It can be seen in Fig 6.23 that the Morrow Point Dam values fall below the experimental data. This would be expected because of very large Reynolds and Weber Numbers at Morrow Point, but it may also be due to the non– rectangular shape of the Morrow Point

plunge pool which was shaped to fit the surrounding rock formation.

Overall the comparsions with other sources have been satisfactory, in the sense that:—

(i) The experimental results lie below the submerged jet case which, as explained, acts as an upper bound for the developed mean pressure. Submerged jet theory must, therefore, be modified for the impinging jet case.

(ii) When the magnitude of the variation of centre line mean dynamic pressure head is compared with the limited data on plunging jets, the outcome was generally very successful.

(iii) As would be expected for the results of a large scale structure, the mean dynamic pressure at the Morrow Point prototype lies below the experimental results.

Therefore scale effects should be assesed, but, as a first estimate, utilisation of the experimental results in this work will provide a slightly conservative estimate.

(B) An emprical fit for the authors data.

At least—squares fit was produced for the experimental results of Fig. 4.23(b) and is shown in Fig. 6.6. Although the magnitude of mean dynamic pressure heads due to the plunging jet are less than the submerged jet case, at low submergence (Y/Di) the pressure head ratio is similarly a constant and for Y/Di $\leq$ 4, the average value is given by:

$$\frac{\bar{H}m - Y}{Ui^2/2g} \approx 0.86 \qquad (6.59)$$

Beyond this depth, analysis by the author has produced a best fit given by the following exponential function:

$$\frac{\bar{H}m - Y}{Ui^2/2g} \quad \exp.^{-[\,0.1919\,(Y/Di) - 0.6084]} \qquad (6.60)$$

Almost all data points for Y/Di = 4−24 are within 10% of the value predicted by Equation (6.60) as seen in Fig. 6.6. A similar accuracy in the region Y/Di = 5−20 can be achieved by expressing the mean dynamic head in a slightly different form, closer to the free jet theory, and given by:

$$\frac{\bar{H}m - Y}{Ui^2/2g} = -2.92\,(Y/Di)^{-2} + 5\,(Y/Di)^{-1} - 0.2 \qquad (6.61)$$

The above expressions are useful to define the results in terms of the variation of the centre line mean dynamic pressure head with pool depth. Equations (6.59) to (6.61) are also a definition of the pressure head scale ($\bar{H}s$) that was used to normalise the pressure head distribution in Section 6.4.2. In other words, the term ($\bar{H}m - Y$) at the jet centre line was defined previously as $\bar{H}s$. The appropriate equation, considering the plunge pool depth, can therefore be substituted into the profiles detailed in Section 6.4.2 to predict the radial variation of mean dynamic heads (Fig. 4.4) in terms of the impact velocity head. The previously derived expression, when combined with Equations (6.59) or (6.60), provides good agreement at the measurement location of 100mm from the jet centre line. At the other measurement location outwith the centre line (Rp= 200mm), the expressions predict approximately zero dynamic head, which was generally the case.

6.4.4 Mean dynamic pressures and the degree of jet break−up at impact.

Section 6.3.4 provided a method by the author of determining the break−up length of an impinging vertical jet. It is an idealised concept based on lateral outward spread of a jet in the atmosphere due to turbulence, and by continuity of water flow, a decay in the width of the inner solid jet core with jet plunge length. A jet might be considered to have broken−up (L/LB ≈ 1) when the inner solid jet core has zero width so that jet surface disturbances can "meet in the middle" thus providing a possible definition of the break−up point.

Section 6.3.5 shows with some clarity that this concept is not too far removed from reality, with such a theoretical estimate of break−up length LB,

being mirrored closely by experimental data (albeit at small scale) of jet break– up lengths.

Section 6.3.6 therefore recognises the tentative nature of the concept of jet break– up length by producing estimates of LB which are an ensemble average of both theoretical and experimental estimates of LB, both for nozzle and orifice tests.

This means that the ratio L/LB, the actual jet plunge length over the ensemble mean estimate of jet break– up length, will be a measure of the degree of unevenness of the edge of the jet surface at impact. Values of L/LB are shown in Table 6.1 for the range of nozzle/orifice diameters, velocities and drop lengths tested in this research. By and large, the range of L/LB tested in this research is concentrated in the 0.04 to 0.4 range, although a limited number of tests were done with L/LB > 0.4, as shown in Table 6.1.

Perhaps one criticism of this work is that some tests were not carried out for the L/LB$\longrightarrow$1 condition. In many ways this criticism is valid, but it would have meant using a smaller diameter jet of the order, 10–15mm diameter, at a lower velocity, which would have produced significantly lower Reynolds Number $UoDo/\nu$ and significantly lower Weber Number $(\rho Uo^2 Do/\sigma)^{1/2}$, and hence would have introduced scale effects in the form of greatly reduced jet turbulence and damped surface effects.

There is no evidence at the moment, but it is felt intuitively that for plunge lengths or associated conditions which are sufficient for the jet to be broken– up before impact with the pool surface, the mean dynamic pressure generated at the plunge pool floor will be less than shown in Fig. 6.6. If the jet disintegrates before impact, it will break– up into discrete particles, lose momentum to the surrounding air and fall as disseminated spray into the pool. Hence, this mechanism will necessarily produce lower mean dynamic pressures than a corresponding intact jet.

Nevertheless, the range of L/LB shown in Table 6.1 was thought to be wide enough to detect any variation of mean dynamic head (with plunge pool depth) with the degree of jet break– up (L/LB) at impact, at least up to the jet break– up condition.

The correlation is shown in Fig. 6.24 for all the experimental tests in this work. The mean dynamic head along the jet centre line is shown plotted against the non-dimensional plunge pool depth Y/Di, for two ranges of L/LB. The "X" symbol represents all tests with L/LB < 0.2 and the "O" symbol represents all test runs with 0.2 < L/LB < 0.6.

Fig. 6.24 shows that there is no correlation of mean dynamic head with the degree of jet break-up at impact. This is perhaps one of the most significant non-correlations of this work, because it reveals that normalisation of the plunge pool depth by the ACTUAL jet dimension at impact, goes some considerable way in minimising the differences due to the degree of jet break-up at impact.

By implication, Fig. 6.24 might then be treated as a universal description for all vertical impinging circular jets, irrespective of the ratio of L/LB up to unity, provided the jet velocity at impact can be determined (Ui) as well as the actual jet diameter at impact Di, the latter procedure having been described in detail in Section 6.3.3.

Justification for the non-correlation of the results with L/LB is achieved by considering mean pressure values obtained when testing a thin, impinging rectangular jet, as carried out by Castillo [29]. This work has only recently been contained, and is more extensively investigated in Chapter 7. For the moment, it can be stated that the tested jets were substantially broken-up (i.e. L/LB = 0.65 – 0.85) and therefore provide an extension to and confirmation of the present experimental data.

As shown in Fig. 6.25, the mean dynamic pressure head values from Castillo [29] are normalised by the impact velocity head and plotted relative to the pool depth normalised by the impacting jet width. It can be seen in Fig. 6.25 that when the results are compared with values obtained considering velocity decay of a submerged slot jet (Albertson [7]), the difference between the two cases is similar to the pattern observed with comparison between the present experimental results and values predicted for circular submerged jet diffusion (Fig. 6.24). Therefore, up to the jet break-up condition, the universality concept seems to be justified, provided the jet conditions at impact can be defined.

The only other justification for this universality is the fact that other

experimental data from a circular vertical jet produces values in the same domain, for instance from Hausler [5], as shown in Fig. 6.22. Experimental data for a rectangular jet from Lencastre [20], where the velocity decay in the plunge pool was much more rapid than that of Albertson's work, has also provided comparable values with the present results, as shown in Fig. 6.23.

Returning to Fig. 6.24 with its non–correlation between mean dynamic head and L/LB ratio, it is important to offer some explanation, however tentative, regarding this figure. Certainly all the evidence to be revealed in Chapter 7, point firmly to a strong variation of the pressure FLUCTUATIONS (as characterised say by Cp') with the break–up ratio L/LB. Larger L/LB ratios produce larger fluctuations along the plunge pool centre line. This is because the unevenness of the jet edge, transmits or produces extra turbulence in the pool shear layer, which in turn manifests itself as extra pressure fluctuations.

By implication, greater turbulence in the plunge pool at larger L/LB ratios, should lead to shorter pool core lengths, faster decay of velocity with plunge pool depth and hence lower values of the mean dynamic head. This is shown not to be the case in Fig. 6.24. The higher break–up ratios appear to have no effect on either the core length ($Y/Di < 4$) or the rate of decay thereafter. Non–variation of mean pressures with L/LB is explained briefly as follows.

It should be recognised from Table 6.1 that the main device for increasing the ratio L/LB was to reduce tha jet velocity at nozzle or orifice. Such a reduction in velocity, reduces.

(i) the Reynolds Number of the flow ($UoDo/\nu$)
(ii) reduces the internal turbulence level in the jet (see Section 4.4)
(iii) reduces the degree of air entrainment into the plunge pool. (See Table 6.2)

All three of these effects will work to <u>increase</u> the mean dynamic head in the plunge pool.

Therefore, it might be postulated that the mean dynamic head shows little variation with break–up ratio L/LB, even though higher L/LB ratios produce greater turbulence in the pool and should produce faster decay of mean velocities. This may be a function of the fact that the L/LB ratio was often increased by

decreasing the velocity of the jet, which in turn reduced turbulence, air entrainment and Reynolds Number.

Even the use of a smaller jet diameter to increase L/LB, (see Table 6.1) also has the effect of reducing jet turbulence and Reynolds Number as shown in Figs. 7.31(a) and (b). Reductions in turbulence have the opposite effect of increases in L/LB and hence the two effects may be cancelling each other out. This conclusion is somewhat tentative at this stage but does represent a conflict between using velocity and diameter reductions to increase the L/LB ratio (Table 6.1) whilst at the same time reducing air entrainment and natural turbulence within the impinging jet.

6.4.5 Mean dynamic heads and the degree of air entrainment at impact.

Section 6.3.7 describes one method of determining the degree of air entrainment by an impinging circular jet into a plunge pool. The relationship by Ervine [17] has been verified by other authors and can be used with some degree of confidence. Equation (6.45) simply predicts the initial rate of air entrainment at the impact point, but makes no predictions of the variation of air concentration on entering the plunge pool.

However, it is felt intuitively that an increase in air entrainment in the plunge pool will reduce the mean dynamic head measured at the plunge pool floor. This is because air is 800 times less dense than water, and hence the mean density of the air/water mixture in the plunge pool must be less than solid water with no air content. As a first guess, the air/water mixture might be characterised as a pseudo-fluid with mean density $\rho w(1-C)$. (ρw is water density and C the local air concentration at any point). This would imply that the pressure head along the plunge pool centre line might be characterised by:

$$\frac{\text{mean dyn. head}}{Ui^2/2g} = \rho w\ (1-C)\ Ps \qquad (6.62)$$

where Ps might be the mean centre line pressure head when no air is present. An estimate of this value might be made for the greatly idealised case of a submerged jet in an infinite plunge pool where the inner core length is given by:

$$Yc \approx 6.2\ Di \tag{6.63}$$

from Albertson's work [7]

At points beyond the inner core, the velocity may decay linearly according to the relationship,

$$Us/Ui = 6.2\ Di/Y \tag{6.64}$$

and because mean pressure head is proportional to velocity squared, $Ps \propto Us^2$, then from (6.64).

$$\text{mean dyn. head } /Ui^2/2g \approx \rho w(1-C)\ 38.4\ (Di/Y)^2 \tag{6.65}$$

for values of Y/Di > 6.2.

This relationship is plotted in Fig. 6.26 for the initial air concent ration Ci = 0^0 (solid curve) and Ci = 0.2, 0.5 and 0.7 shown as dashed curves. These values of Ci correspond to air concentrations estimated in Table 6.2 for all the experimental test runs in this work.

Perhaps the most significant finding in Fig. 6.26 is that all the experimental data points for the mean dynamic head fit the predicted range of Ci from 0.2 to 0.7, when applied to Equation (6.65) above. This finding is important because it provides a ready–reckoner for the mean dynamic head at any plunge pool depth greater than 6.2, provided the initial air concentration at impact may be found, Ci. This latter value may be estimated from Equation (6.46).

The experimental data points in Fig. 6.26 have been subdivided in three, representing three bands of impact air concentration. It is clear from Fig. 6.26 that for pool depths less than Y/Di<10 say, there is no clear correlation between mean dynamic head and air concentration.

On the other hand, for pool depths Y/Di>10, the picture changes completely with the highest air concentrations producing the lowest mean dynamic heads and the opposite for low air concentrations. In fact, a closer inspection of Fig. 6.26 reveals that the experimental points fit Equation (6.65) almost exactly

for pool depths Y/Di> 10, revealing that submerged jet theory can be used with great confidence at larger pool depths.

The problems with pool depths from Y/Di between 4 and 10, is that there is no strong dependence on either L/LB (previous section) or the initial air concentration Ci. This makes the mean dynamic head very difficult to predict in this region and resort must be made to the data fit presented in Equation (6.60) in Section 6.4.3. Pool depths shallower than Y/Di= 4 produce a constant mean dynamic head, around 0.86 $Ui^2/2g$.

The reason for no correspondence between air concentration and mean dynamic head for shallower pool depths is that in the core region, and beyond, to some extent, air bubbles in the shear layer have not yet reached the jet centre line. Values of mean dynamic pressure will therefore not be affected by pool air entrainment at shallow depth, but rather by any air bubbles that have been entrained into the jet during its plunge through the atmosphere.

REFERENCES FOR CHAPTER 6

1. Sene, K.J., "Aspects of Bubbly Two–Phase Flow.", Ph.D. Thesis, Trinity College, Cambridge, 1984.

2. Ervine, D.A., and Falvey, H.T., (1987), "Behaviour of Turbulent Water Jets in the Atmosphere and in Plunge Pools.", Proc. I.C.E., Part 2, pp. 295–314.

3. Hecker, (1988), Private Communication, Alden Laboratories, Mass., U.S.A.

4. Hoyt, J.W., and Taylor, J.J., "Turbulence Structure in a Water Jet Discharging in Air.", Physics of Fluids, Vol. 20, No. 10, Pt. 11, 1977.

5. Hausler, E., "Dynamic Water Pressures Upon Floors of Stilling Basins Caused by Free Overfall Jets at Dams.", Die Wasserwirtschaft, 56. Jahrgang, Heft 2, 1966.

6. Ervine, D.A., McKeogh, E., and Elsawy, E.M., "Effect of Turbulence Intensity on the Rate of Air Entrainment by Plunging Water Jets.", Proc. I.C.E., Part 2, Vol. 69, 1980, pp. 425–445.

7. Albertson, M.L., Dai, Y.B., Jensen, R.A., and Rouse, H., "Diffusion of Submerged Jets.", Proc. A.S.C.E., Vol. 74, 1948, pp. 639–663.

8. Novak, P. (Ed), "Developments in Hydraulic Engineering.", Elsevier Applied Science, London, 2, Chapter 5, 1984.

9. Horeni, P., "Disintegration of a Free Jet of Water in Air.", Byzkumny ustav vodohospodarsky prace a studie, Sesit 93, Praha–Podbaba, 1956.

10. Takahashi, T., and Kitamura, Y., "Stability of a Contracting Liquid Jet.", Memoirs of the School of Eng., Okayama University, Vol.7, 1972, pp. 61–84.

11. Iciek, J., "The Hydrodynamics of Free, Liquid Jets and their Influence on Direct Contact Heat Transfer – Hydrodynamics of a Free Cylindrical Liquid Jet.", Int. Jour. Multiphase Flow, Vol. 8, 1982, pp. 239–249.

12. Chen, T−F., and Davis, J.R., "Disintegration of a Turbulent Water Jet.", Proc. of A.S.C.E., Journal of the Hydraulics Division, Vol.90, No. HY1, 1964, pp. 175−206.

13. Baron, T., University of Illinois Technical Report 4 (Prepared under Contract N−6−ORI−71, Task Order No. XI, ONR Navy Dept.)

14. Henderson, J.B., McCarthy, M.J., and Molloy, N.A., "Entrainment by Plunging Jets.", Proc. of Chemeca,'70, Melbourne, Section 2, 1970, pp. 86−100.

15. van de Sande, E., "Air Entrainment by Plunging Water Jets.", Ph.D. Thesis, Technische Hogeschool, Delft, 1974.

16. Cumming, I.W., "The Impact of Falling Liquids with Liquid Surfaces.", Ph.D. Thesis, Loughborough University of Technology, 1975.

17. Ervine, D.A., "The Entrainment of Air in Water.", Water Power and Dam Construction, 28, No.12, 1976, pp. 27−30.

18. Mason, P.J., "Effects of Air Entrainment on Plunge Pool Scour.", Jour. of the Hydraulics Division, A.S.C.E., Vol.115, No.3, 1989, pp. 385−399.

19. Kobus, H.E., "An Introduction to Air−Water Flows in Hydraulics.", Eigenverlag des Instituts fur Wasserbau der Universitat Stuttgart, Heft 61, 1985.

20. Lencastre, A., "Free Overflow Spillways.", Engineering and Design Principles, National Laboratory for Civil Engineering Studies, Report No. 174, Lisbon, Portugal, 1961.

21. Hydraulics Research Limited, "Impact Pressures in Falling−Jet Energy Dissipators.", Report No. SR 124, 1987.

22. Hrycak, P., Lee, D.T., Gauntner, J.W., and Livingood, J.N.B., "Experimental Flow Characteristics of a Single Turbulent Jet Impinging on a Flat Plate.", Lewis Research Centre, N.A.S.A., TDN−5690, 1970.

23. Beltaos, S., Discussion on "Short Jet Impingement.", Proc. of A.S.C.E.,

Journal of the Hydraulics Division, No. HY12, 1977, pp. 1504–1506.

24. Kamoi, A., and Tanaka, H., "Measurements of Wall Shear Stress, Wall Pressure and Fluctuations in the Stagnation Region Produced by Oblique Jet Impingement.", Proc. of D.I.S.A. Conference, University of Leicester, 1972, pp. 217–227.

25. Beltaos, S., and Rajaratnam, N., "Impinging Circular Turbulent Jets.", Proc. of A.S.C.E., Journal of the Hydraulics Division, Vol.100, No. HY10, 1974, pp. 1313–1328.

26. Poreh, M., and Cermak, J.E., "Flow Characteristics of a Circular Submerged Jet Impinging Normally on a Smooth Boundary.", Con. on Fluid Mechs., 1959, pp. 198–212.

27. Rajaratnam, N., "Turbulent Jets.", Developments in Water Science, No.5, Pub: Elsevier Scientific, New York, 1976.

28. Abramovich, G.N., "The Theory of Turbulent Jets.", Pub.: M.I.T. Press, Massachusetts, 1963.

29. Castillo, L., "Metodologia Experimental Y Numerica Para La Caracterization Del. Campo De Presiones En Los Disipadores De Energia Hidraulica.", Ph.D. Thesis, University Politechica de Catalunye, Barcelona, 1989.

CHAPTER 7

ANALYSIS OF PRESSURE FLUCTUATIONS IN A PLUNGE POOL

CONTENTS

CHAPTER 7

7.1 INTRODUCTION

Experimental data for pressure fluctuations in plunge pools has been presented in detail in Chapter 5.

The purpose of this chapter therefore, is to provide a convincing argument for the magnitude and distribution of fluctuations measured in the plunge pool; to offer possibilities as to the mechanisms of pressure fluctuations; to compare with other authors data on plunge pool fluctuations; to compare with data from similar types of hydraulic structures such as bottom outlets, hydraulic jumps and chute spillways; to investigate the influence of jet turbulence, air entrainment and jet disruption at the impact point on pressure fluctuations; and to provide a general critique on the usefulness of this research in the design of plunge pools in general.

The core of this chapter is to be found in two sections, namely Section 7.2.2 dealing with the mechanism of pressure fluctuations in a plunge pool; and more importantly Section 7.4.2 which provides an explanation for the variation of pressure fluctuations with plunge pool depth. The latter in particular seems to look in a new way at how pressure fluctuations are influenced by jet conditions at impact, including the turbulence of the jet at impact as well as its degree of break–up, reflecting the surface instabilities of the impinging jet.

7.2 MECHANISMS OF PRESSURE FLUCTUATIONS

This section is in some ways a speculative note on the causes, magnitude, and distribution of pressure fluctuations in hydraulic structures. The note will commence with hydraulic jump situations, where much more evidence is available, and conclude with plunge pools, where the evidence is sketchy. Most plunge pool research has concentrated on one sub–section of behaviour, and none to date, including this work, have measured pressure fluctuations together with velocity distributions, turbulent velocity distributions and air concentrations.

7.2.1 Pressure fluctuations in hydraulic jumps.

The RMS pressure fluctuation coefficient Cp' is shown in Fig. 7.1 for the case of a hydraulic jump, at a upstream Froude Number of 5.98. This graph was produced by Toso [1] and shows a distinct peak of pressure head fluctuation $Cp' \simeq 0.05$ when the distance into the jump is around $X/Y_1 \simeq 12$. The pressure fluctuation measurements were recorded on the hydraulic jump floor.

It is felt, intuitively, that such pressure fluctuations on the jump floor, must be related to the magnitude of turbulent velocities on the floor, especially the vertical components of turbulent velocity V'. By coincidence Rouse et al. [2] have measured the RMS turbulent velocity fluctuations along a hydraulic jump floor, also at a upstream Froude Number of 6. The vertical components are denoted by V'/U_1 and the longitudinal components by U'/U_1. These are presented in Fig.7.2 plotted against X/Y_1. (Some interpretation was required here for Rouse's data was plotted in the form X/Y_2. However, Y_2/Y_1 for $Fr_1 = 6$ is approximately 8, and hence a conversion factor of 8 was used to translate from X/Y_2 to X/Y_1).

It is clear from Fig. 7.2 that the pattern of vertical turbulent velocities V'/U_1 is very similar to the pattern of RMS pressure fluctuations $P'/\frac{1}{2}\rho U_1^2$, in Fig. 7.1, both peaking at a distance of $X/Y_1 = 12$, when the upstream Froude number is 6. This provides initial evidence of a link between the pressure fluctuation p' and the RMS velocity fluctuation V'.

For idealised, isotropic and homogeneous turbulence, in the absence of macro–turbulence from coherent vortex structures,

Hinze quotes $$p' = K \rho (v')^2 \qquad (7.1)$$

where the value of K is quoted as 0.7.

Applying the same formulation to an hydraulic jump in the presence of macro–turbulence, we obtain a value of K around 5; when $X/Y_1 = 12$, $v'/u_1 \simeq 0.06$ to 0.07 and $Cp' \simeq 0.04$ to 0.05. In other words:

$$p' \simeq 5 \rho (v')^2 \qquad (7.2)$$

$$\text{or} \quad \frac{p'}{\frac{1}{2}\rho u_1^2} = Cp' \simeq 10 \left(\frac{v'}{u_1}\right)^2 = 10\,(Tuv)^2 \qquad (7.3)$$

The constant of proportionality is several times greater than that quoted by Hinze [3] and may reflect the highly sheared nature of the flow in a hydraulic jump, the large scale vortex structures in the jump, as well as the undulating surface roller.

The equations above assume that pressure fluctuations are caused by fine scale turbulence produced in the highly sheared flow in the jump, but ignores larger scale flow structures and pressure fluctuations due to the undulating roller at the jump free surfacs. Concerning larger scale flow structures such as sketched in Fig. 7.3, it is clear that these can occupy the full flow depth and produce low frequency fluctuations.

Points A and C in Fig. 7.3 will correspond to minimum pressure fluctuations because of the direction of the passing roller. This would be indicated by assuming a constant streamline energy ($p/\rho g + v^2/2g$). Point B on the other hand might operate like a stagnation point, giving a maximum pressure pulse at that point. This type of behaviour is different from pure turbulence, with its random eddies of varying size, magnitude and direction, but is much more a definite larger scale secondary flow pattern which is superimposed on the finer scale turbulence, producing different magnitude and frequency of pressure fluctuations.

An approximate analysis of the likely range of fluctuations in boundary pressure due to large vortex structures can be attempted by appealing to Toso's [1] power spectra plots. These are shown in Fig. 7.4 for $X/Y_1 = 7.4$, $X/Y_1 = 10.4$ and $X/Y_1 = 17.2$. This is the range of highest pressure fluctuations in Fig. 7.1. It is seen from Fig. 7.4 that the peak fluctuations occur at 1 to 3 Hz. If we assume this peak is due to large vortex structures, then an estimate of the recirculation velocity Vr (Fig. 7.5) can be made. It is argued for a circular orbit that:

$$Vr \simeq \pi\, Y / T \qquad (7.4)$$

where T is the period, which is between 0.30 secs. to 1 sec., say averaging 0.5 secs. at the highest fluctuation range at $X/Y_1 \simeq 12$.

Also from Fig. 7.5, the difference in pressure head between points 1 and 2 must be approximately $Vr^2/2g$, and this might represent the range of head fluctuation due to the large flow structures, but excluding pure turbulence.

Thus the pressure head fluctuation magnitude between points 1 and 2 might be given by

$$\underline{h} \simeq \frac{Ur^2}{2g} \simeq \frac{\pi^2 y^2}{2gT^2} \qquad (7.5)$$

and hence the non-dimensional fluctuating head coefficient

$$\underset{\sim}{Cp} = \frac{\underline{h}}{U1^2/2g} \simeq \frac{\pi^2 y^2}{U_1^2 T^2} \qquad (7.6)$$

Substituting typical Toso values for U_1, y and T gives a non-dimensional pressure coefficient $\underset{\sim}{Cp}$ approximately equal to 0.1 to 0.3. This is a substantial head fluctuation coefficient, considerably greater than the RMS value of 0.05 for Cp'.

However, values of 0.1 to 0.3 are much more in line with the instantaneous maximum and minimum fluctuations Cp^+ and Cp^- measured by Toso and shown in Fig. 7.6. These represent the peak extremes measured, and show non-dimensional coefficients around 0.4. That is, the peaks are approximately $0.4\ U_1^2/2g$ above the mean, and the minimum's are approximately $0.4\ U_1^2/2g$ below the mean, although both situations do not coincide at the same distance into the jump as seen in Fig. 7.6.

It is becoming clear from the crude analysis above that such extremes of pressure fluctuation may be due mainly to large vortex structures rather than random turbulence. This is clear from the magnitude of the estimated pressure fluctuations due to large flow structures being in the same range as the extremes of head fluctuation actually measured. Furthermore, purely random turbulence would ensure that Cp^+ and Cp^- graphs were co-incident in Fig. 7.6 which is not the case.

One key question involves the reason why, from Fig. 7.6, the positive fluctuations peak at a distance of $X/Y_1 = 8$ into the jump, whereas the negative fluctuations peak at a point much deeper into the jump around $X/Y_1 = 18$.

The fluctuations are positively skewed in the initial stages of the jump and negatively skewed in later stages. Toso [1] explains this by the statement "Water cascading down the face of the jump to the toe causes positive fluctuations to be dominant near the toe, and negative pulses to be dominant further downstream".

This can now be amplified by considering two different situations sketched in Fig. 7.7.

The first situation, Fig 7.7(a), is a droplet of water falling on a flat surface. A sensitive pressure transducer will pick−up a pressure pulse as sketched. Compared to the ambient mean pressure, a continuous stream of drops will produce positively skewed pressure pulses, because the large positive pulses are more dominant than any negative "rebound" pulses which might be generated.

The second situation, Fig. 7.7(b), concerns flow expansion, with intense vortices generated in the shearing zone and larger recirculating eddies formed in the semi−stagnant region behind the shearing zone. This situation is almost the "opposite" of the falling droplets, where, in this case, the whole thrust of the flow is attempting to remove fluid from the region marked A, off in the downstream direction. This not only has the tendency to produce negative mean pressures but also negatively skewed pressure fluctuations (Lopardo[4]), which in turn can lead to cavitation when pressures reach −8.5m to −10m head.

Returning to the case of an hydraulic jump sketched in Fig. 7.8, the author proposes the following mechanisms for positive skewing in the earlier part of the jump and negative skewing later.

Upstream of point A (Fig. 7.8), the solid boundary feels only boundary layer type pressure fluctuations, where the RMS value of Cp' is less than 0.01 and usually around 0.007 according to Minami [5].

In the region AB, the solid boundary feels the remnant of the boundary layer fluctuations from the upstream flow, fluctuations from the turbulence production in the shearing region, fluctuations from the recirculating roller above the shear zone, as well as surface disturbances on the free surface, boiling and collapsing and transmitting pressure to the base. The spectrum of pressure fluctuation will therefore be a mixture of all these. Fig. 7.6 shows in this

region that both positive and negative fluctuations are increasing, but the positive at about twice the rate of the negative. The reason for this is most likely to be the downward roller direction in this part of the jump, combined with collapsing and ejected fluid particles plunging towards the base as sketched in Fig. 7.8.

The maximum possible positive pulse from a falling droplet of fluid would be $Ui^2/2g$, where Ui is the impact velocity as shown. Furthermore, the value of u_i cannot be greater than $\sqrt{[2g(Y_2 - Y_1)]}$. Hence, the maximum instantaneous pulse must be less than

$$\underset{\sim}{h} < \frac{Ui^2}{2g} < \frac{[\sqrt{(2g\,(Y_2 - Y_1))}]^2}{2g} = Y_2 - Y_1$$

$$\text{and } \underset{\sim}{Cp} = \frac{\underset{\sim}{h}}{U_1^2/2g} < \left[\frac{Ui}{U_1}\right]^2 < \frac{Y_2 - Y_1}{(U_1^2/2g)} \qquad (7.7)$$

For a Froude Number of 6 as in Fig. 7.6, the ratio $(Y_2 - Y_1)/(U_1^2/2g)$ is approximately 0.4, giving an upper bound to fluctuations of this type.

Beyond point B in Fig. 7.8, the flow is expanding with a slight upward net direction in this region. This also coincides with maximum turbulent convection, according to Rouse et al. Maximum convection occurs about $X/Y_2 \simeq 2$, or for a Froude Number of 6, at $X/Y_1 \simeq 16$, as $Y_2/Y_1 \simeq 8$. Maximum convection produces the largest sudden increases in the longitudinal velocity (e.g. increases in Ur) and hence the largest reductions in instantaneous pressure, from Bernoulli.

The author would speculate that a combination of diverging/expanding flow, together with highest turbulent convection, produces the significant negative skewing of pressure fluctuations as evident in Fig. 7.6 at $X/Y_1 \simeq 16$ to 18.

7.2.2 Pressure fluctuations in plunge pools.

The question of mechanisms is now extended to fluctuations in a plunge pool, where an impinging jet (much more diffused and aerated than the hydraulic jump) impinges normally. At this stage it is not clear what parallels exist

between normal impinging jet fluctuations and parallel hydraulic jump fluctuations. Perhaps a hydraulic jump visualised vertically, with the floor of the jump representing the line of symmetry of the plunge pool jet, might be the best comparison.

The RMS pressure fluctuation coefficient Cp' is shown in Fig. 7.9 for the case of all the tests carried out in this thesis. This covers the full range of jet diameters, jet droplengths, jet velocities up to the prototype range, incorporating smooth nozzles as well as the orifice tests. The graph shown in Fig. 7.9 is a mean value from all these tests, already shown in Fig. 5.50(a). This graph is the jet centre line RMS pressure fluctuation, showing a peak at a plunge pool depth of 6 impact diameter (Y/Di = 6). It is of great interest to note from Fig. 7.9 that the highest RMS values in the jump occur at $X/Y_1 = 12$, which shows a strong coincidence for an assumption that $Di = 2\ Y_1$.

In any case, a peak of RMS pressure fluctuations at Y/Di = 6 shows that the jet centre line turbulence may not peak until this value. Chapters 4 and 6 have shown conclusively that the impinging jet initial core region is not greater than 4 D_j, and hence the largest RMS fluctuations do not occur until some distance beyond the end of the core region.

It is felt appropriate at this stage to compare the Cp' graph in Fig. 7.9 with turbulence measurements along a jet centre line. It was not possible to obtain turbulence measurements in this work because of large concentrations of air bubbles, but some turbulence work had been done by Corrsin [6] for submerged jets, by Mansoori [7] for a submerged bounded jet, and by McKeogh [8] for an impinging jet with low concentrations of air bubbles (C < 2%). These turbulence measurements are shown in Fig. 7.10. None of the data from Fig. 7.10 are exactly comparable to the high velocity impinging jets in this thesis, but nevertheless they do provide some guide to the range of longitudinal turbulences to be expected.

It is clear from Fig. 7.10 that all three types of jet are remarkably similar giving the highest RMS longitudinal turbulence of 0.14 at a pool depth between 6–10 Y/Di. This value of pool depth is slightly greater than the impinging jet data for Cp' in Fig. 7.9, but this is to be expected in view of the fact that the jets in this work have a shorter core length (4 Di) compared to submerged jets

in Fig. 7.10 (6 Di). The parallel between Fig. 7.9 and Fig. 7.10 is again significant (as in the case of a hydraulic jump) revealing a close link between turbulent fluctuations and RMS pressure fluctuations.

In fact, if we take the highest value of Cp' to be 0.2 approximately, and the highest value U'/Ui to be 0.14 approximately, and we assume with Hinze that:

$$p' \propto (U')^2$$

$$\text{then,} \quad \frac{p'}{\frac{1}{2}\rho Ui^2} = Cp' = 10\left[\frac{U'}{Ui}\right]^2 = 10(Tu)^2 \qquad (7.8)$$

or, in other words, the constant of proportionality of 10 is exactly the same as Equation (7.3) for the hydraulic jump case, producing further evidence for a link between RMS pressure fluctuations and RMS turbulent velocity fluctuations.

Further confirmation of the reasonableness of Cp' = 0.2 is afforded by a comparison of longitudinal and vertical turbulence intensities in a hydraulic jump. Rouse [2] showed:

$$\frac{U'}{U_1} \simeq \frac{2\,V'}{U_1} \quad \text{as in Fig. 7.2}$$

for a jump, and again assuming $P' \alpha (U')^2$, then $(U_1 - Ui)$:

$$Cp' \alpha \left[\frac{U'}{Ui}\right]^2 \alpha\, 4 \left[\frac{V'}{Ui}\right]^2$$

or Cp' (jet) should be $\simeq$ 4 Cp' (jump)

which is verified as $0.2 \simeq 4\ (0.05)$. (7.9)

At this point it is useful to investigate the role of larger vortex structures in producing the important pressure fluctuations in a plunge pool. This is sketched in Fig. 7.11 in an idealised form showing a core of length (4 Di) with a shear layer where most of the large coherent structures might emanate from. Even larger scale eddies are expected outside the shear layer, being driven by impingement of the jet on a solid base with subsequent radial flow causing large

scale circulations whose dimensions are dependent on the plunge pool plan dimensions.

There are three types of larger scale structures to consider:

(i) Vortex structures whose diameter ℓ' is less than the shear layer width, and whose vertical components of instantaneous velocity might be characterised by U'. As a first approximation

$$u' \simeq \pi \ell'/T = \pi \ell' f \qquad (7.10)$$

where f is the characteristic frequency of such eddies.

Davies [9] has shown that the value of ℓ' varies approximatley linearly with plunge pool depth ($\ell' = kY$) hence from (7.10) above,

$$f \propto U'/Y \qquad (7.11)$$

Assuming that the dominant frequency in the power spectra corresponds to the point of maximum turbulence in the plunge pool, then at that point:

$$U'/Ui \simeq \text{constant} \simeq 0.14 \qquad (7.12)$$

$$\text{Then from (7.11)} \quad f \propto Ui/Y \qquad (7.13)$$

(ii) A similar argument might be applied to the next scale of eddies which occupy the full shear layer width as shown in Fig. 7.11. These eddies have a known diameter:

$$De = Di/2 + 0.25Y \qquad (7.14)$$

in view of the fact that the outer edge of the shear layer varies approximately at a slope of 1:4. When $Y >> Di$, then we can write:

$$De \propto Y \qquad (7.15)$$

The direction of these eddies alternates in both directions, but the

predominant sense is anti–clockwise as shown, transferring momentum from the centre line of the jet to the edges. This will lead to positively skewed pressure pulses along the jet centre line, at least at points beyond the end of the core region. (See Point A on Fig. 7.11).

At that point the vertical instantaneous velocity might be characterised by Ur, where:

$$Ur = \pi\ De.f = KYf \qquad (7.16)$$

and again the value of Ur is driven by the impact velocity Ui, hence it can be stated:

$$f \propto Ui/Y \qquad (7.17)$$

(iii) The third type of eddies can occupy the full plunge pool depth, hence

$$De = Y \qquad (7.18)$$

Again these eddies are driven by impingement on a solid surface and by the velocity U_i, hence their characteristic frequency might also be expressed by:

$$f \propto Ui/Y \qquad (7.19)$$

At this point it was decided to appeal to the power spectra in this research, to measure the dominant frequency, f_{DOM}, from each graph, and to relate it to Ui/Y. The result is given in Fig. 7.12 revealing a tentative relationship for plunge pools in the form,

$$f_{DOM} = 0.25\ Ui/Y \qquad (7.20)$$

This refers only to larger scale vortex structures and hence could <u>not</u> apply in the core region of the diffusing jet at values of $Y/Di < 4$.

Equation (7.20) can be used, however, to obtain estimates of the dominant eddy sizes which are causing dominant frequencies in the plunge pool.

For instance in type (i) eddies, where at the maximum point $U'/Ui \simeq 0.14$, then, from Equation (7.10),

$$U' \simeq 0.14\ Ui = (\pi)(KY)(0.25\ Ui/Y)$$

$$\text{giving} \quad K = 0.17 \tag{7.21}$$

or the dominant eddy size, $\ell' = 0.17Y$, is therefore smaller than the shear layer width $Di/2 + 0.25Y$, but still a substantial eddy diameter.

At the other extreme, the very large eddies of size $De = Y$, are likely to have recirculating velocities as low as 0.035 Ui. This is the estimate from Thomas [10] for an infinitely large plunge pool.

Then from Equation (7.16)

$$Ur \simeq 0.035\ Ui = \pi\ Y\ f$$

$$\text{giving a dominant frequency} \quad f \simeq 0.01\ Ui/Y \tag{7.22}$$

This is considerably less than 0.25 Ui/Y in Fig. 7.12, giving considerable evidence that such large eddies are not dominant in plunge pools at least at depths greater than the core length.

A further aspect of the pressure fluctuation mechanism in a plunge pool concerns the distribution of the maximum and minimum instantaneous pressure fluctuations denoted by Cp^+ and Cp^- respectively and shown in Fig. 7.13. This graph will be discussed in greater detail in later sections of this chapter, but it is clear that the minimum instantaneous fluctuations peak at $Y/Di \simeq 4$ with values up to $0.6\ Ui^2/2g$, whilst the maximum instantaneous fluctuations peak at much greater plunge pool depths $Y/Di = 8-10$, and reach much higher peak values of $0.8\ Ui^2/2g$ above the mean. It will be appreciated that the curves shown in Fig. 7.13 are mean values from the test runs shown in Figs. 5.50 (b) and (c).

It is also of interest to compare these graphs with the RMS pressure fluctuation Cp'. If fluctuations were stemming from pure random turbulence, then from Gaussian distribution analysis, the peak fluctuation coefficients would be

$3Cp'$. This graph has also been plotted in Fig. 7.13 showing a reasonable correspondence with the Cp^- graph in terms of peak magnitude, and close correspondence with the Cp^+ graph in terms of the increase in fluctuations along the first four to six diameters in length.

It would be easy to argue from Fig. 7.13 that the fluctuations in the core region Y/Di $\simeq$ 0 to 4 are caused by random turbulence because the $3C_p'$ graph is similar to the Cp^+ and Cp^- graphs. However, if this was the case then the Cp^+ and Cp^- graphs would coincide, with equal peaks below the mean as above the mean. It is clear, however, from Fig. 7.13 that the core region contains negatively skewed fluctuations which is somewhat surprising in view of the positive normal impingement of the jet.

What is the reason for negatively skewed pulses when impingement is within the core region? The first point to bear in mind is that the core region contains turbulence from the impinging jet itself, and has still not "felt" the full impact of the turbulence and large flow structures from the shear layer, which are still at some radial distance from the jet centre line.

There is a further flow mechanism however, which is sketched in Fig. 7.14 and may be responsible for negative skewing. It concerns an impinging jet and the sudden turning though 90^0 of the streamlines from the vertical to the radial direction.

If we assume that the jet centre line is the line of axi-symmetry, and the flow stream lines travel out in a radial direction, then the flow pattern may be considered analogous to flow at a sharp angled bend as sketched, with its resulting flow separation and formation of a recirculating eddy.

The recirculating eddy is driven in the direction shown, so that the stagnation point will experience a predominance of upward velocity pulses characterised by Ur. It is likely that this phenomenon occurs at all plunge pool depths, but, at distances beyond the core, the large positive pulses from the shear layer will dominate. These are discussed in more detail below.

Fig. 7.13 also shows the large positively skewed fluctuations to peak at Y/Di= 8-10. The reason for positive skewing is due to the direction of

momentum transfer, as already explained, by producing large eddies as shown in Fig. 7.15, which predominate in the anti–clockwise direction giving positive pulses at point A.

Large positive pressure pulses are felt at A, along the jet centre line, at the point of maximum turbulent CONVECTION. At this point the value of Cp^+ is of the order of 0.8 whilst the RMS fluctuation is only 0.1 to 0.15, a factor difference of 6 to 8 times. Random turbulence would produce a factor difference of only 3 times.

This means that the peak fluctuations at point A are not characterised simply by the turbulent velocity U', but velocity fluctuations of greater magnitude than U', which reflect a combination of smaller scale turbulent fluctuations, U' and larger scale structures (Ur).

7.3 PRESSURE FLUCTUATIONS IN THE RADIAL DIRECTION

Most of the measurements in this thesis have concerned pressures along the jet centre line in the plunge pool. Some measurements, however, were taken in the radial direction. The reporting of radial variation of pressure fluctuations has been carried out in Chapter 5, with results presented in Figs. 5.1 to 5.6, covering values of Cp', Cp^+ and Cp^-, as previously defined. What is the explanation for the variation of fluctuations as outlined in these figures?

Section 7.2 above has offered some ideas on the mechanisms of pressure fluctuations in plunge pools. It is clear that the highest r.m.s pressure fluctuations coincide fairly closely with the highest turbulence intensity measurements, whilst the highest peak fluctuations occur when larger shear layer flow structures produce maximum convection. The dominant eddy lengths appear to occupy a substantial proportion of the shear layer width. A rough guide line to the inter–relationship between r.m.s pressure fluctuation and velocity fluctuation can be given as:

$$Cp' = h'/(U1^2/2g) = 10\ (Tu)^2 \qquad (7.23)$$

where Tu is the longitudinal turbulence intensity.

In an explanation for the distribution of fluctuations in Figs. 5.1 to 5.6, it would be apposite to review the likely flow structures in the radial direction as well as any known turbulence measurements in the radial direction. Fig. 7.16 shows the likely flow structures, with an idealised shear layer developing from the edge of the impinging jet.

Moving in the radial direction from A to A', it is likely that an initial inner core region of lower turbulence will give way to the shear layer region of high turbulent production and developing macro–turbulence, or coherent structures. The outer region is likely to be a region of fast reducing turbulence, and may well be dominated by one large eddy of pool depth dimensions.

A similar radial traverse further downstream, may well reveal large turbulence near the jet centre line, reducing in the radial direction. Thus different patterns will emerge depending on the extent of flow establishment with pool depth.

Measurements of longitudinal turbulence intensity across a diffusing bounded submerged jet by Mansoori [7] have shown that, in the flow establishment region (Y/Di = 2.15), three distinct radial zones are apparent. The regions are shown in Fig. 7.17 and are described as follows:

(i) From the jet centre line to the outer edge of the inner jet core, which show a region of low turbulence intensity, with values of Tu ≃ 4–5%

(ii) A region of intense mixing outside the solid inner core, which shows the maximum intensity of turbulence. This is the shear layer region, with values of Tu ≃ 15%.

(iii) An outer region of jet diffusion (jet edge) which shows that the intensity decreases sharply in the radial direction, emphasising negligible turbulence production in this vicinity, and probably mainly lateral turbulent advection.

Therefore, at low pool depths, less than the inner core length, the maximum r.m.s. fluctuations should be located outside the centre line stagnation point. This observation has been confirmed by the work of Kamoi and Tanaka [11] on submerged rectangular slot jet diffusion. They have shown that when the

potential core impinges on the boundary, the r.m.s. pressure fluctuations are at a maximum at some radial distance from the centre line stagnation point. The magnitude of this highest value of Cp' is not as large as would be expected from the application of $Cp' = 10(Tu)^2$, based on Kamoi and Tanaka's values of longitudinal turbulence intensity. This is explained by the flow orientation after impingement, becoming more parallel to the boundary with radial distance from the jet centre line, thus deviating from the concept of a developing free turbulent jet.

In the established region of flow, Mansoori [7] showed that downstream of the inner jet core (Y/Di = 7.36), the longitudinal turbulence intensity is at a maximum at the centre line of the flow. This indicates diffusion or advection of turbulence towards the centre of the flow. The maximum turbulence intensity is therefore likely to be converted to maximum fluctuations at the jet centre line. In this regard, Kamoi and Tanaka [11] have shown that the maximum r.m.s. fluctuations are at the centre line stagnation point when impingement is beyond the potential core. They have also shown that the centre line value of Cp' under these conditions is larger than the highest values obtained during core impingement at any radial distance outside the centre line.

According to the above, the radial distribution of the r.m.s. pressure head fluctuations should be the of the following form:

(i) At low pool depths, relative to the jet impact diameter (say $Y/Di < 4$ as in this work) the maximum value of Cp' will be located at a radial distance from the flow centre line.

(ii) At pool depths greater than the solid inner core ($Y > 4Di$ in the case of plunging jets), the maximum value of Cp' will be at the jet centre line ($Rp = o$) and will be larger than the maximum value in (i) above. According to Mansoori [7] the maximum centre line value of Cp' for bounded submerged jets will occur at a pool depth around 6 to 7 jet diameters.

(iii) In the zone of transition, the maximum value of Cp' will be located radially somewhere between that specified for (i) and (ii) above.

This pattern is evident when considering the results for the radial distribution

of Cp' for the 78mm diameter nozzle outlet as shown in Fig. 5.1. In general it can be seen that at the lower pool depths (Y/Do = 1.28 and 2.56), the maximum value of Cp' is at the radial measurement location of 100mm from the jet centre line, while for larger pool depths (Y/Do = 4.49 and 6.41), the maximum value of Cp' is at the jet centre line. The magnitude of the maximum r.m.s. pressure head coefficient for the pool depths beyond the potential core (Cp'≈ 0.15 to 0.2) is generally greater than the maximum value at the smaller pool depths (Cp' ≈ 0.05 to 0.1). At the furthest radial location (Rp/Do = 2.56), the value of Cp' is consistently small, at values around 0.025 to 0.050.

One difficulty in interpreting the data of Figs. 5.1 and 5.2 is the sparse spacing of transducers in the radial direction. This means that the data for low pool depths in Fig. 5.1 appears to peak at values of R/Do = 1.28, whereas in practice, if more transducers were available, the peak is more likely to be found around R/Do = 0.5, this being the approximate centre of the shear layer.

Thus the pattern which emerges is likely to be as sketched in Fig. 7.18, showing distinct regimes, with the dividing line being the end of the solid inner core region.

A comparison of this data trend at the lower pool depths with data from the work of H.R. Ltd. [12], is shown in Fig. 7.19. H.R. Ltd. used a rectangular outlet which for the purposes of this comparison has been converted to an equivalent circular diameter. It can be seen from Fig. 7.19 that the results from H.R. Ltd. confirm the magnitude and trend of the Cp' values found in the present study, and also confirm the likelihood of a peak in Cp' values at a value of R/Do = 0.5 as shown in the H.R. Ltd. data. Only one data point is at variance with the general trend, that being the centre line Cp' value for Y/Do= 4.4– 4.5. Clearly in the Glasgow work this is a point just beyond the end of the inner core region, whereas in the H.R. Ltd. data it is not. This is a function of the differences in jet plunge length and degree of jet disruption at the impact point, which has some effect on the length of the inner core.

The trend for the peak positive fluctuations (Cp^+) is shown in Figs. 5.3 and 5.4, and the peak negative fluctuations (Cp^-), is shown in Figs. 5.5 and 5.6. The variation of these peaks in the radial direction at the plunge pool floor are

generally similar to those obtained for the r.m.s. pressure head coefficient (C_p'). This is to be generally expected, assuming the pressure fluctuations are at least partially randomly distributed and governed by the Gaussian distribution. If this was the case then peak values Cp^+ and Cp^- would be approximately three times greater than the value of Cp' at that point.

An inspection of Figs. 5.3 to 5.6 reveals that in some cases this general rule, and, therefore, the assumption of a Gaussian distribution of pressure fluctuations, is not valid. In other words Cp^+ and Cp^- are, under certain conditions, much more than 3 times Cp'. This is due to production of large pressure pulses by coherent vortex structures in addition to the random jet turbulence. This point will be advanced further when considering the centre line variation for pressure fluctuations with pool depth, but mean time it can be noted that Cp^+ can be as much as 6 to 8 times the corresponding value of Cp'. This is clear from Figs. 5.1 and 5.3.

Fig. 7.20 shows a typical example of the variation of the peak dynamic heads and the minimum dynamic heads plotted with the radius from the jet centre line. For the measurement locations shown in Fig. 7.20, the largest values of the dynamic peak pressure head are located at the jet centre line and, for the range of pool depths most utilised in design (ie. beyond the solid jet core), the difference between the instantaneous peak and minimum head is maximised again at the jet centre line. Therefore, the most destructive effects of jet impingement, in terms of extremes in pressure head, will be experienced at the jet centre line. It follows that the magnitude of pressure head fluctuations at the jet centre line for various pool depths is the most important criterion for plunge pool design. These values will be considered in the following sections.

7.4 PRESSURE FLUCTUATIONS ALONG THE JET CENTRE LINE AT VARIOUS PLUNGE POOL DEPTHS.

7.4.1 Comparison with other authors.

The purpose of this section is to compare the pressure fluctuation data of this work with that of previous investigators, for the case of vertically impinging

circular jets into plunge pools. The main problem is that no such data exists from other sources, so no direct comparison can be made.

Resort is therefore made to indirect comparisons of the types noted as follows:–

(i) Impinging rectangular jets into plunge pools.
(ii) Interpretation from turbulence measurements in circular submerged / impinging jets.
(iii) Investigation of other hydraulic structures with flows normal to a solid boundary.
(iv) Interpretation from other types of hydraulic structure.

(i) A study of pressure fluctuations in the plunge pool of an impinging thin rectangular jet has been carried out at the Universitat Politechnica de Catalunya, Barcelona, Spain, by Castillo [13], published November 1989. The thesis (in Spanish) reached the author by September 1990, around the time of publication of this thesis, and hence the work has not been reviewed in Chapter 2.

The experimental set–up is shown in Figure 7.21, showing a simple overflow structure similar to Crystal Dam, Colorado (Fig. 1.2), producing a thin rectangular jet plunging through the atmosphere a distance Z between 1.47m and 1.72m. The plunge pool depth in Fig. 7.21, denoted by h, was varied from 0 to 0.2m giving a range of h/B (or Y/Di) between 0 and 33. Only three discharges were investigated, namely 0.003 m^3/s, 0.006 m^3/s and 0.008 m^3/s, giving impact velocities between 5.37 m/s and 5.81 m/s.

The variation of the RMS pressure fluctuation with depth is shown in Fig. 7.22, producing the first real comparison with this research. It can be seen that the highest values of Cp' are around 0.12 to 0.16, which are less than the highest values recorded in this work, but nevertheless of the same order of magnitude.

One significant difference in these studies is the high values of Cp' at low plunge pool depths in Castillo's work. To understand or explain this phenomenon, it is interesting to note the degree of break–up of these rectangular jets. Initial calculations of Castillo's data show the ratio of jet fall length to

impact thickness z/b, to vary between 160 and 300, whilst the theoretical jet break–up lengths for these jets, Horeni [4], appear to vary between z/b = 250 – 350. This means that these jets are substantially broken–up at the point of impact with equivalent values of L/L_B around 65% to 85%. Thus Fig. 7.22 represents an impacting rectangular jet almost at the point of break–up. This is compared with the more intact circular jets of this work, with ratios of L/L_B only between 0.04 and 0.6 mainly, with an average around 25%.

The work of Castillo is therefore both a confirmation of the range of data in this work, but also an extension to the case of rectangular jets almost at break–up point.

A further comparison of the two data sets is afforded in Fig. 7.23 showing the Barcelona data (solid curves) of peak and minimum instantaneous fluctuations, Cp^+ and Cp^-, compared with the Glasgow data (dashed curves), of Cp^+ and Cp^-. The graphs of Cp^- (negative fluctuations) are most similar both peaking at $Cp^- \simeq 0.6$, although the Barcelona data is consistently high even at zero plunge pool depth. This was also true for the Barcelona RMS data shown in Fig. 7.22 which gives an average Cp' of 0.12 at zero depth and a corresponding Cp^- of 0.55. Again it might be postulated that such negative skewing of data at low plunge pool depths, or even zero plunge depth, may be due to the sudden flow divergence at impact causing separation and intense eddies near the stagnation point. This was discussed in Section 7.2.

A comparison of the Cp^+ values shown considerable difference with Glasgow values rising to 0.8 as compared with 0.4 for Barcelona, and with the Barcelona data peaking at slightly greater plunge pool depths. Section 7.2 has already established that the higher Cp^+ values are dominated by larger vortex structures in the shear layer, which give highest Cp^+ values at the point of maximum turbulent convection. It is apparent from the Barcelona data that the strength of these larger scale structures is less than the Glasgow data. This implies a less well defined shear layer, which leads back to the calculation above, showing the impinging jet to be almost broken up at the point of impact, and therefore producing a less well defined shear layer. The Barcelona Cp^+ data may well represent a lower bound data set in view of the large degree of jet break–up at impact.

The differences in the two data sets may also be attributed to rectangular and circular jet differences, the latter producing more three dimensional flow structures. Nevertheless, the comparison does confirm negative pulse skewing at low pool depths followed by positive skewing at deeper pool depths.

Fig. 7.24 shows the Barcelona data for the maximum, minimum and mean dynamic pressure envelope and its variation with plunge pool depth. This should be compared with the Glasgow data shown in Fig. 4.23(b) and Fig. 5.51(b).

It is evident from Fig. 7.24 that,

(a) At low plunge pool depths, the Barcelona data produces significantly lower maximum peaks, minimum peaks and mean pressures.

(b) At zero pool depth for instance, the maximum envelope is around 0.9 for the rectangular jets as opposed to 1.2 for the Glasgow jets. The mean head coefficients are 0.65 and 0.85 respectively for Barcelona and Glasgow, while the minimum envelope is 0.1 and 0.7 respectively.

(c) Fig. 7.24, describing the Barcelona data, behaves as if it had a zero core length, but instead, an immediate development of large fluctuations associated with shear layer behaviour, right from zero plunge pool depth. This is further evidence that the advanced degree of jet break–up at the impact point almost negates the concept of a solid inner core development region in the plunge pool, but instead produces an intense shear layer type mixing pattern with negative skewing at low depths and less significant positive skewing at greater depths.

H.R Ltd. [12] are similarly carrying out a rectangular plunging jet study, but the stipulated report includes results which are limited to one pool depth only.

(ii) Interpretation from turbulence measurements in diffusing jets.

Section (7.2) has already described a link between RMS pressure fluctuations Cp', and RMS velocity fluctuations in the form $Cp' = 10\ (Tu)^2$. In the absence of other Cp' data for circular jets it is useful to compare in some more detail the relationship between Cp' and $(U'/Ui)^2$.

Turbulence data for diffusing circular jets has been presented in Fig. 7.10 for a submerged free jet (Corrsin [6]), a smooth impinging jet (McKeogh [8]) and a bounded jet (Mansoori [7]). It can be seen from this figure that the value of centre line longitudinal turbulence intensity increases rapidly with pool depth to a peak of 0.14 to 0.15 at Y/Di between 5 and 10; beyond the theoretical core. At greater depths, the longitudinal turbulence reduces, at varying rates depending on whether the jet is freely impinging or bounded. It is expected that the data of the r.m.s. pressure head coefficient Cp', should follow a similar trend.

The longitudinal turbulence intensity values can be converted to r.m.s. pressure head coefficients by use of the approximate relationsip $Cp' = 10(Tu)^2$. A comparison can then be made between the values of Cp' predicted from this relationship and the present experimental data. This comparison is shown in Fig. 7.25 comparing the prediction of Cp' for McKeogh and Corrsin's data with actual values for this work.

It can be seen from Fig. 7.25 that the general trend of the experimental results agree quite well with the values computed from Equation (7.8) and the peak magnitude of Cp' is as predicted at around 0.2.

(iii) Hydraulic structures with flows normal to the solid boundary:

Another source of comparison concerned pressure fluctuation measurements on the front face of a baffle block in a hydraulic jump stilling basin. As seen from Fig. 7.26, the flow impinges normally onto the front face and hence has some similarities with impingement in plunge pools.

As a consequence of their ability to dissipate energy, the baffle blocks will be subject directly to the fluctuating action of the flow and dangerous depressions, especially at the areas of flow separation. This may cause cavitation, fatigue or vibrations, depending on the block and flow characteristics. Damage of this form has been detailed in various instances [15–16].

Steel linings are often used as an effective, but expensive, method to resist cavitation. However, steel linings are not very successful in the armouring of baffle blocks in stilling basins, because of large pressure fluctuations which often results in vibration of the lining and fatigue of the fasteners. Polymerised steel

fibre reinforced concrete has so far proved most erosive resistant, [17].

Due to damage of baffle blocks, as noted above, tests have been carried out to establish the magnitude of these pressure fluctuations, by authors such as Lopardo et al. [18]. This data is useful, particularly in providing values of Cp' at the front face on the baffle block, as the flow action at the front face is most like the impingement of a diffusing jet on the plunge pool floor. The results of Lopardo et al [18] are given in Fig. 7.27 and show a correlation with the incident Froude number, but generally values of Cp' around 0.19 to 0.21 have been found at the baffle block front face with an average maximum value of 0.2. As will be seen, this magnitude agrees very well with the highest values of Cp' found at the plunge pool floor. This is a more satisfactory check on the validity of the experimental data than using turbulence results as actual values of the pressure fluctuation level have been measured.

(iv) Interpretation from other types of hydraulic structure:

Studies of pressure fluctuations at alternative hydraulic structures are also useful to check the trend of the experimental data but, as the flow orientation is usually parallel to the boundary of interest, the maximum magnitude of the pressure fluctuations will obviously be much less than those obtained for normal impingement.

A great deal of work has taken place for the pressure fluctuations at the floor of stilling basins beneath hydraulic jumps, eg. Akbari et al [19] and Narasimhan and Bhargava [20]. Urgency in obtaining this sort of data was due to the extensive damage to spillways and stilling basins caused by these forces. Of special interest has been the possibility of fluctuating pressure entering the drain system and causing uplift of the concrete chute and basin floor slabs. For a free jump, the values of Cp' at the stilling basin floor have been plotted in Fig.7.28, from the work of Akbari et al. [19], to provide comparison with the present experimental results. Also plotted in this figure are the values of r.m.s. pressure fluctuations beneath a turbulent boundary layer on a chute spillway, from work of Minami [5] and Locher [21], values of Cp' on the boundary wall of a sudden expansion energy dissipator where cavitation may be a problem, from the work of Mansoori [7], and centre line values of Cp' in a bounded jet where the test surface was placed orthogonal to the flow, again from Mansoori [7]. It should be

noted that in the case of the hydraulic jump data, the distance into the jump has been normalised by the supercritical depth multiplied by two. This is carried out to locate the data values relative to a parameter equivalent to the jet diameter at impact. Similarly, the incident Froude number is based on two supercritical flow depths. It can be seen from Fig. 7.28 that:

(i) The values of Cp' for the turbulent boundary layer remain fairly consistent throughout the entire test length at around 0.006 to 0.007.

(ii) For shear layers with the main flow parallel the the boundary of interest the values of Cp', as expected for the higher level of turbulence production, are much larger than (i) above.

(iii) The hydraulic jump data is well correlated with Froude number. The trend in the data indicates that as the Froude number increases, the maximum value of Cp' decreases and the location of the maximum r.m.s. pressure fluctuation moves further downstream from the toe of the jump. The location of this maximum is coincident with that of the maximum turbulence intensities measured by Rouse et al [2]. For the low Froude number shown, the maximum value of Cp' is around 0.05 to Y/Di = 6 while, for the larger Froude number shown, the maximum value of Cp' is around 0.03 at Y/Di = 10.

(iv) As expected, the maximum value of the r.m.s. pressure fluctuations at the wall of the sudden enlargement are similar to the hydraulic jump values. However, for a large Froude number the peak is located at a smaller longitudinal distance. The maximum value of Cp' is approximately 0.06 at about Y/Di = 6. This location was just upstream of the large recirculating eddy formed at the corners of the sudden expansion.

(v) For the bottom outlet, Mansoori [7] managed to measure the value of Cp' at the centre line of the diffusing jet by inserting a probe into the flow which acted as a stagnation boundary. As anticipated, the magnitude of Cp' is much larger when the flow is normal rather than parallel to the boundary. The value of Cp' increases to a peak around 0.15 at Y/Di $\approx$ 5 with a rapid reduction beyond this point.

(vi) Regarding the present experiment results, there is a considerable scatter, but

the magnitude of Cp', as expected, is similar to the centre line values for the bounded jets. For the particular Froude numbers shown, the peak values of Cp' are around 0.19, comparable to baffle block results, at Y/Di = 5–6. This location is similar to the point where the maximum centre line longitudinal turbulence intensity is developed.

The trend of the present results is similar to those of a hydraulic jump, but the peak magnitude is around 4 to 5 times greater. This represents the essential difference between parallel and normal boundary fluctuations in a free shear layer.

The trend and magnitude of the present experiment results has been verified in the previous comparisons, but there still remains the problem of explaining the reason behind the data trend and the effect of the varied parameters on the pressure fluctuation level.

7.4.2 Variation of RMS pressure fluctuations Cp' with impact velocity Ui, droplength L and outlet type.

A good summary of all the pressure fluctuation data is given in Fig. 5.50 (a), (b) and (c), covering the full range of parameters tested including types of outlet device. It is seen from Fig. 5.50 (a), (b) and (c) that when the data is normalised by the impact velocity Ui, and the measured jet diameter of impact Di, there is a reasonable collapse of data. There is however a significant enough spread to necessitate deeper analysis of the effect of each of the various parameters tested. This is particularly relevant in the light of Castillo's [13] recently released data for rectangular jets, which produce somewhat different data from this work, but have used jets near the break–up at impact.

One of the major parameters which will produce the type of data spread shown in Fig. 5.50 is the velocity at impact. This parameter affects so much of plunge pool behaviour, of which four different aspects are noted below:–

(i) Higher values of Ui give higher Reynolds Numbers of the impinging jet, and in particular, higher turbulence intensity within the impinging jet. What effect does this have on fluctuations?

(ii) Higher values of Ui give larger jet break-up lengths L_B. Therefore for a given droplength, an increase in Ui produces a decrease in L/L_B, hence producing a less broken-up jet at impact. What effect does this have on fluctuations?

(iii) Higher values of Ui give greater air concentrations in the plunge pool (for a given plunge length and jet diameter). What effect does this have on plunge pool fluctuations? This point will considered in Section 7.4.6.

(iv) Higher values of Ui increase the ratio Ui/Y which in turn increases the dominant frequency of the turbulent fluctuations.

The first step in the quest for the relative influence of each of the parameters varied begins in Fig. 7.29 which shows the variations of the RMS pressure fluctuation Cp' with plunge pool depth. The fluctuations resulting from low velocity jets are shown by the solid curve and the high velocity jet fluctuations are shown by the dotted curve. The data is for one droplength range only L = 513 - 1125mm, and each curve is the average of all three nozzles. This graph is therefore a rough approximation to general behaviour, but does hide the effect of varying jet diameter.

Fig. 7.29 reveals, perhaps surprisingly, that irrespective of the nozzle velocity range, the highest value of Cp' (0.2) does not vary significantly with velocity, nor does the value of Y/Di where Cp' reaches a maximum. This occurs at Y/Di = 6 to 7 irrespective of velocity.

Fig. 7.29 reveals that for most of the plunge pool depth range, low velocity jets produce higher Cp' values than higher velocity jets. This is the first indication of the conflict between higher velocity (greater turbulence in jets) and higher velocity (more intact jets because of longer break-up lengths). The low velocity jets in Fig. 7.29 will have a degree of break-up (L/L_B between 0.1 and 0.3 (see Table 6.1) whereas the higher velocity jets will have a degree of break-up between 0.04 and 0.14, a factor difference of over 2. This is because higher velocity jets produce much longer intact jets, so that L_B, the break-up length, is longer and hence L/L_B, the degree of break-up is much smaller.

The same effect is produced in Fig. 7.30 which is a similar plot to Fig.

7.29, only the droplength of the jets L, is much greater, varying in the range 2.018 to 2.63m for the nozzle jets. The curves are also drawn through different values of impact velocity ($Ui^2/2g$) but nevertheless approximately in the same range as Fig. 7.29. Again the lower velocity nozzle jets produce greater fluctuations. In this case the degree of break–up for the lower velocity nozzle jets, is L/L_B = 0.3 to 0.8 (see Table 6.1), whereas for the higher velocity nozzle jets the degree of break–up is around 0.12 to 0.35, again a factor difference of 2.

Thus, the first tentative conclusion is that the degree of jet break–up at impact, expressed in the form L/L_B, is a major indicator in the magnitude of RMS fluctuations experienced. The larger the value of L/L_B, the larger the values of Cp'.

This first conclusion, that low velocities produce more broken–up jets at impact, is important, and is a dominant feature of most of the results in this work. However, it does need to be countered with an important conclusion from the jet turbulence measurements described in Chapter 4, namely, that low velocity jets are also less turbulent when plunging through the atmosphere. If this lower turbulence is transmitted right to the plunge pool, then lower fluctuations may exist, at least at very shallow plunge pool depths.

A typical example for the 78mm diameter smooth nozzle is given in Fig. 4.26(a). This graph shows the variation in turbulence intensity along the jet centre line for a range of jet velocities varying between 7m/s and 13m/s. It is clear that higher velocity jets produce greater turbulence intensities. Fig. 7.31(a) shows a plot of the resultant turbulance intensity (Tu) average for each velocity from Fig. 4.26(a), showing sharp increases in turbulence intensity at the lower velocities, with a levelling off at the higher velocities. Turbulence intensity varies almost linearly at lower velocities, eventually tailing off to give little or no variation with increasing velocity.

As a point of interest, typical jet centre line data from the 25mm diameter smooth nozzle are also shown in Fig. 7.31 (a), revealing a similar pattern but at a lower level of intensity. The most obvious correlation of this data is with Reynolds Number which is shown in Fig. 7.31(b) for the jet centre line only and for low turbulence jets only. Fig. 7.31(b) illustrates very neatly the strong

dependence on jet centre line turbulence with increasing Reynolds Number, although it should be remembered that this data is all in the jet inner core region, only a few diameters downstream from the exit and with the edge boundary layer turbulence still not transmitted to the jet centre line.

The purpose of plotting Figs. 7.31(a) and (b) is to suggest that if the plunging jet turbulence varies with jet velocity, and also that the RMS pressure fluctuation varies with turbulence, $Cp' \alpha (Tu)^2$, then an increasing velocity at impact is likely to produce larger values of Cp' at impact.

This is completely the opposite trend to increasing velocities producing intact jets at impact, with low velocities producing broken-up jets at impact.

In an effort to explore this conflict further, it was decided to carry out a more detailed analysis of the RMS pressure fluctuations (Cp') with plunge pool depth, for three specific cases which were as far removed from each other as possible. The three cases are:-

(i) The 78mm smooth nozzle behaviour for the shortest possible droplength. This is the largest diameter and smallest L/Do values. The graph is shown in Fig. 7.32 for L/Do = 9.3→14.4.

(ii) The 25mm smooth nozzle behaviour for the longest possible droplengths. This is the smallest diameter and largest L/Do values from 81 to 97. Both (i) and (ii) are low turbulence jets. (See Fig. 7.33).

(iii) The 25mm high turbulent orifice jet which produces initial values of turbulence (Tu_o) of the order of 5 to 10 times greater than the smooth nozzles. This data is shown in Fig. 7.34

Starting with Fig. 7.32 for a given diameter (78mm) and droplength (725-1125mm), the values of Cp' decrease as the velocity becomes larger. Extensive analysis by the author revealed this to be primarily a function of the degree of break-up at impact. The high velocity jet in Fig. 7.32 (Uo = 11-13m/s) has a break-up ratio L/L_B of only 0.05, which means that it behaves almost like a submerged jet, being more or less completely intact at impact. Proof of this behaviour is given in Fig. 7.35, which is a deliberate attempt to

show that this intact impinging jet gives similar fluctuations to submerged jets. The comparison in Fig. 7.35 is with Corrsin's submerged free jet case with Cp' estimated from $10(Tu)^2$, and also Mansoori's bounded submerged jet, again with $Cp' = 10(Tu)^2$. The impinging jet data comes between the two, as would be expected, because it is a partly bounded jet in a plunge pool where the walls and base have some influence.

Returning to Fig. 7.32 it is now clear from the high velocity jet that the low values of Cp' at low plunge pool depths Y/Di = 2 are simply due to the fact that the impinging 78mm jet has very low turbulence along its centre line, because the outer jet boundary layer turbulence has nowhere reached near the jet centre line. This is sketched in Fig. 7.36 showing the boundary layer width and distribution of turbulence intensity.

The low velocity jet (Uo = 3 m/s) on the other hand is much more broken up at impact by virtue of its lower velocity. The edge of the jet is therefore more disturbed generating greater fluctuations in the plunge pool as soon in Fig. 7.32.

Why does it produce larger values of Cp' at the lowest plunge pool depths if according to Fig. 7.31(a) the impacting jet has less turbulence intensity because of its lower velocity.

The reason is sketched in Fig. 7.37. The low velocity, low turbulence jet produces a large contraction during the plunge due to gravity. The smaller impact diameter is now combined with a greater boundary layer thickness to produce more turbulence at the jet centre line. The boundary layer thickness is much wider in the low velocity jet because of a lower Reynolds Number, and $\delta \alpha l/Re^{0.2}$. Thus a more uneven jet edge at impact combined with a thicker boundary layer produces greater fluctuations in the plunge pool.

This means that although L/L_B is important in determining the general level of pressure fluctuations (because of its effect on the unevenness of the edge of the jet), the ratio δ/Di is also important in determining how much the boundary layer turbulence has reached the centre line of the impinging jet.

An approximate expression for the boundary layer thickness is given by:

$$\frac{\delta}{L} = \frac{0.37}{(Re_L)^{0.2}} = 0.37 \left[\frac{\nu}{Ui\ L}\right]^{0.2} \qquad (7.24)$$

Therefore,

$$\frac{\delta}{Di} = \left[\frac{L}{Di}\right]\left[\frac{\nu}{UiL}\right]^{0.2} \cdot 0.37 \qquad (7.25)$$

For this case of $L \simeq 1$ m, $Ui = 5.35$ m/s, $Di \simeq 0.058$m then:

$$\frac{\delta}{Di} \simeq 0.3 \quad \text{or} \quad \frac{\delta}{\text{Radius}} = 0.6 \qquad (7.26)$$

Therefore, at impact, the boundary layer reaches 60% of the radius which means that considerable turbulence will already have reached the jet centre line.

Turning to Fig. 7.33 for the smallest nozzle jet diameter at longest droplengths, we investigate the patterns for L/do = 81−97. It can be seen that the low velocity jets again produce higher pressure fluctuations than the higher velocity jets. Again this can be attributed to the degree of break−up as characterised by L/L_B given in Table 6.1. For the case of Uo = 5m/s the value of L/L_B is $0.5 \longrightarrow 0.6$, whereas for the case of Uo = 13−15m/s, the value of L/L_B is $0.25 \longrightarrow 0.33$ a factor difference of 2.

The high velocity jet (Uo = 13−15m/s) in Fig. 7.33 no longer behaves like the submerged jet case in Fig. 7.32, at plunge pool depths less than Y/Di < 5. In fact it reveals large values of Cp' at impact point and very shallow pool depths. The reason for this is now clear. At a velocity of Uo = 13−15m/s, the jet has reached high turbulence values. This is combined with the fact that such a long droplength has allowed the boundary layer to reach the centre of the jet as the calculated value of δ/Radius from Equation (7.25) is now greater than 1.0. Thus the high velocity jet at high droplength can produce full boundary layer turbulence at its jet centre line at impact. This produces large pressure fluctuations at impact.

The lower velocity jet (Uo = 5m/s) on the other hand is substantially

broken up at impact with values of L/L_B around 0.5→0.6. This means that the jet free surface is very uneven at impact causing large pressure fluctuations. As well as this, calculations of the boundary layer thickness also reveal the boundary layer to have reached the jet centre line as in the case of the high velocity jets. Therefore this combination of large surface disturbances and large centre line turbulence is getting closer to the highest possible generator of pressure fluctuations.

Fig. 7.34 shows the orifice data for a droplength range L = 1020−1420mm, giving a ratio of L/Do ≃ 41→57. The orifice jet turbulence readings near the outlet device were typically in the range 3−5%, which was an order of magnitude greater than the nozzle jets.

The picture from Fig. 7.34 is more confused with the low velocity jets causing higher pressure fluctuations at very deep plunge pool depths, but lower fluctuations at shallow plunge pool depths. From Table 6.1 the low velocity jets have an L/L_B around 0.5, whereas the high velocity jets have an L/L_B around 0.3→0.4, both types of jet being relatively well broken up at impact. Following the previous arguments, the low velocity jets with higher L/L_B should produce higher fluctuations at all pool depths, which is not the case for Y/Di < 7. What is the reason for lower Cp' values at lower velocities where Y/Di < 7 ?

The answer lies in the fact that both jets are relatively well broken up at impact, and both jets have high turbulence values transmitted to the jet centre line by the impact point, BUT, the high velocity jets contain much greater turbulence. Data from Fig. 4.34(a) has been transferred to Fig. 7.38, showing the difference in the turbulence readings at two different velocities, namely 9.3m/s and 13.1m/s.

It is clear from Fig. 7.38, that there is a factor of 4 difference in the magnitude of turbulence carried in the higher velocity jet. This turbulence difference will be transmitted to the plunge pool, at least for the first few diameters into the plunge pool until shear layer turbulence becomes dominant, the latter effect being governed more by disturbances on the edge of the jet free surface.

Thus Fig. 7.34 illustrates very clearly how a more highly turbulent but less

broken-up jet can produce greater pressure fluctuations, at least at shallower plunge pool depths.

The key to interpreting all this data lies in two parameters, namely L/L_B for degree of break-up, and Tu_i (centre line), the jet turbulence intensity at the jet centre line at impact. The latter effect involves the boundary layer thickness at impact and also the Reynolds Number at impact.

Another way of analysing the data of the three cases shown in Fig. 7.32, 7.33 and 7.34 is to compare their behaviour at a constant impact velocity. This has been done in Fig. 7.39 for a constant impact velocity in the range, $Ui^2/2g = 9 \rightarrow 10$. The three extreme cases are clear, for the 78mm nozzle at shortest droplength, the 25mm nozzle for longest droplength and the 25mm orifice with its much greater turbulence intensity. The values of the degree of break-up for each case are denoted by L/L_B, ranging from 0.04 for the 78mm jet to 0.3 for the 25mm jet to $0.3 \rightarrow 0.4$ for the orifice jet.

It is of some significance that the value of Cp' varies with degree of break-up L/L_B, although it is also noted that for plunge pool depths beyond $Y/Di = 7$, there is no significant variation in Cp' for this constant impact velocity.

It is also of some significance that the value of Cp' also increases with impact turbulence intensity. Although this value has not been measured, it can be inferred from the jet turbulence results from Chapter 4, where it is clear that the 78mm nozzle, for instance, will have a turbulence level around 0.4%, whereas the orifice jet will have a turbulence level around 4%, a ten-fold difference. It is clear from Fig. 7.39 that this initial difference has negligible effect at depths beyond 6 to 8 diameters into the pool.

The same procedure has been done for a lower impact velocity, and is shown in Fig. 7.40, for the case of $Ui^2/2g = 3.3 \rightarrow 4$, which is an impact velocity around 8.5m/s. The results are more surprising in this case, with the 25 nozzle jet producing greater fluctuations than the 25mm orifice jet, at least at pool depths greater than $Y/Di > 4$. In fact Fig. 7.40 shows little significant difference in Cp' values for the three cases over the range tested, which is indeed surprising in view of the fact that both 25mm jets are substantially broken

up at impact $L/L_B \simeq 0.4 \rightarrow 0.6$, but the 78mm nozzle is only lightly disrupted, with $L/L_B \simeq 0.1$.

It is becoming clear from the discussion above that the variation of RMS pressure fluctuations with plunge pool depth do indeed show significant variation with the jet conditions at impact. The significant conditions at impact appear to be:

(i) degree of break-up of the jet at impact which is characterised by L/L_B and is a measure of the surface disturbances on the edge of the jet which are translated into turbulence in the pool shear layer.

(ii) degree of turbulence internally in the jet at the point of impact, which appears to produce much greater fluctuations in the so-called jet inner core region at least over this depth of pool, to the end of the core.

Low velocity jets enhance the jet break-up parameter L/L_B as shown in Figs. 7.29 and 7.30 often producing larger pressure fluctuations. High velocity jets depress the degree of jet break-up L/L_B, but enhance the amount of turbulence within the impinging jet as shown in Fig. 7.31. In some cases (Fig. 7.34) the enhancement of jet turbulence overcomes the decrease in jet break-up, to produce higher fluctuations at shallower pool depths. This means that the highest possible pressure fluctuations are produced by a broken-up jet $L/L_B \rightarrow 1$, with a high internal turbulence intensity at impact.

The nearest these tests have approached this condition is the high velocity orifice jet with break-up parameter $L/L_B \simeq 0.3$ to 0.4 and internal turbulence $\simeq$ 4%. This is shown as the upper graph in Fig. 7.39. An extrapolation of this graph to the worst possible case would therefore involve even higher Cp' values especially at the lowest pool depths $Y/Di < 4$.

The reader is referred to Fig. 7.22 for the Barcelona data for wide rectangular jets which in fact do approach the conditions $L/L_B \rightarrow 1$, but unfortunately involve rather small Reynolds Number flows at impact $Re \simeq 3 \times 10^4$ to 5×10^4, which means that their boundary layers may be fully developed at such large droplengths but the degree of turbulence contained within them may be small. Fig. 7.22 does nevertheless provide an insight into the pattern of Cp'

for greatly broken–up jets revealing almost constant Cp' values over the first 8–10 jet thicknesses into the pool and reducing at 12–14 jet thicknesses, to much lower values.

One of the concepts described in this section has been the growth of the boundary layers from the edge of the nozzle moving towards the centre line of the jet. An expression was given in Equation (7.25) which was based on the boundary layer thickness for flow over a smooth flat surface. This type of relationship may be satisfactory for the nozzle flow, but does it still apply when the jet is plunging through the atmosphere?

It was decided to investigate some of the turbulence measurements in Chapter 4 (Section 4.4) to produce some evidence for the growth of a boundary layer. Essentially this is spreading of turbulence from the edge of the jet in towards the jet centre line. The result of nozzle type jets is shown in Fig. 7.41(a) which shows the distribution of turbulence at L/D = 0, 2.4, 5, and 17.2. The upper three graphs are taken from data of the 78mm nozzle whilst the lower graph of L/D = 17.2 is taken from the 25mm nozzle data. Clearly these two sets of data are not directly compatible because of a large Reynolds Number difference between the 78mm and 25mm nozzles, but both combined do show very clearly a qualitative picture of boundary layer growth in Fig. 7.41(a). At L/D = 0, the higher turbulence values are confined only to the outer edges of the jet (r/Ro > 0.9). At L/Do = 5, the turbulence has spread over to (r/R_o > 0.7) whereas at L/Do 17.2, the higher turbulence has reached over to the half way mark between edge of jet and jet centre line (r/Ro > 0.5). This data is taken from the high velocity end of the range with negligible contraction due to gravity over the L/D = 17.2 range.

We can now use this concept to guess the centre line turbulence values at impact for the nozzle jets in Fig. 7.39. The 78mm nozzle, for instance, at L/Do = 9.3⟶14.4 will still retain very small turbulence at its centre line, around 0.4%. The 25mm nozzle on the other hand with L/Do = 81⟶97, will have a boundary layer which has reached the jet centre line, with a turbulence value around 1%, from Fig. 7.41(a).

The orifice data is plotted in Fig. 7.41(b) for two velocity ranges, namely 7 m/s and 13 m/s and for L/D = 2, 10, and 17. The pattern here is completely

different. At L/D = 2, the orifice flow is still in the Vena Contracta region with higher turbulence only at the outer edges of the jet. By L/D = 10, the highest turbulence is now found at the centre of the jet with the value for 7 m/s being only a small proportion of the 13 m/s value. In fact, the turbulence value for the 7 m/s orifice jet is of the same order, or even less than the turbulence value for a 7 m/s nozzle jet.

This now explains why the lower velocity orifice data in Fig. 7.40 gives smaller Cp' values than the 25mm nozzle data, considering both are substantially broken–up at impact. The orifice jet has less internal turbulence at this velocity range.

We also see from Fig. 7.41(b) why the high velocity orifice jet produces such high Cp' values in Fig. 7.39. Its turbulence value at centre line is up to 4% at L/D = 17.

Thus to conclude, it is clear from Chapter 6, that aeration has a significant effect on mean dynamic pressure in plunge pools, whereas it is now clear from Chapter 7 that the degree of jet break–up L/L_B and jet turbulence at impact are the main factors in determining the degree of RMS fluctuation in the plunge pool.

7.4.3 Variation of peak fluctuations Cp^+ with the main parameters

The peak fluctuations are the maximum instantaneous recorded peaks above the mean, normalised by the inlet velocity head $Ui^2/2g$. The variation in Cp^+ with the plunge pool depth is shown in Fig. 5.50(b) for all tests carried out in this work. The highest Cp^+ values are around 0.8 and occur at a pool depth of 8 to 9 diameters, or Y/Di = 8⟶9. At this pool depth, the corresponding RMS fluctuations Cp', are around 0.15, giving a ratio of peaks to RMS of 5 to 6 times. This is greatly in excess of Gaussian normal peaks which in all probability would be 3 times greater than the RMS values. This has been explained in Section 7.2 as a result of larger vortex structures set–up in the shear layer being responsible for positive skewness of fluctuations beyond the end of the core region. The large vortex structures dominate over smaller–scale background turbulence.

It is clear from Fig. 5.50(b), that a considerable spread of data exists in the Cp^+ graphs, and the purpose therefore of this section is again to offer some explanation for such a data spread.

As in Section 7.4.2, it was decided to investigate in some detail the three extreme cases of the 78mm nozzle – short droplength; the 25mm nozzle – long droplength; and the 25mm orifice with different turbulent structure. These are shown in Figs. 7.42, 7.43 and 7.44 respectively, with Cp^+ plotted against plunge pool depth, and with curves drawn through the data at the extreme ranges of velocity.

Fig. 7.42 is applicable to the 78mm nozzle with short droplength, L/Do = 9.31 to 14.4, with the break–up ratios L/L_B varying from 0.04 to 0.14 over the full velocity range, from Table 6.1. The variation of Cp^+ in Fig. 7.42 is very similar to the variation of Cp' in Fig. 7.32, with the lower velocity jets producing significantly higher values of Cp^+ than the higher velocity jets. The most likely explanation for this is given in Section 7.4.2, involving the greater degree of break–up of the lower velocity jet combined with the greater thickness of the turbulent boundary layer at impact.

One of the most significant features of Fig. 7.42, is that the high velocity jet (which already has been established to behave similar to a submerged jet) has a value of Cp^+ which is almost exactly 3Cp' from Fig. 7.32. This implies a Gaussian distribution which derives from random turbulence. The lower velocity 3 m/s jet on the other hand has a Cp^+ value which is 4 to 5 times Cp' in Fig. 7.32. This implies that larger vortex structures have reached the jet centre line at much shallower plunge pool depths, and that the shear layer is dominant over any inner core turbulence even at very shallow pool depths.

Fig. 7.43 shows the variation of Cp^+ with pool depth for the 25mm nozzle at the longest droplengths, L/Do = 81–97, and with break–up ratios L/L_B varying from 0.3 to 0.8 over the full velocity range, as in Table 6.1. A comparison of Fig. 7.43 with the corresponding Cp' values in Fig. 7.33 reveals a similar pattern, with the lower velocity jets producing higher Cp^+ values and the higher velocity producing almost double maxima, but mostly lower Cp^+ values.

The high velocity jets in Fig. 7.43 give Cp^+ values which range between 3

to 3.5 times that of the RMS values.

The low velocity jets give the highest Cp^+ of 0.8 when the corresponding Cp' is only 0.15, a ratio of 5.3, although it should be noted that the highest Cp' values of 0.22 in Fig. 7.33 correspond to Cp^+ values around 0.7, which is a ratio just over 3.

Fig. 7.44 shows that Cp^+ values for the orifice jets with their greater internal turbulence levels, L/Do = 41−57 and L/L_B = 0.3 to 0.6. Fig. 7.44 can be compared with Fig. 7.34, revealing a similar pattern between Cp^+ and Cp' values although Cp^+ values peak at Y/Di ≃ 10 while Cp' values peak at Y/Di ≃ 6−8.

Fig. 7.44 reveals that lower velocity jets give smaller values of Cp^+ than the higher velocity orifice jets. This was also noticed for the Cp' results and reveals a different pattern from the nozzle jets. The reason has been outlined in the previous section and concerns the fact that the 13 m/s jets have very much higher turbulence levels than the 5 m/s jets, whilst their respective L/L_B ratios are not vastly different from each other. This is a case where internal plunging jet turbulence dominates over degree of jet break−up.

Both jets in Fig. 7.44 peak at Cp^+ values of 0.75 to 0.8, at a Y/Di ≃ 10. The corresponding Cp' values in Fig. 7.34 are only 0.125 giving a ratio Cp^+/Cp' of 6 to 6.5. This is the most positively skewed distribution and indicates dominance of large vortex structures when the initial jet turbulence is high.

The 13 m/s jet with 4% turbulence, shown in Fig. 7.44, is the nearest test to a prototype structure and, with a substantial degree of break−up L/LB = 0.3⟶0.4, reveals very clearly that prototype jets are going to have substantial levels of Cp^+ around 0.7 to 0.8 for pool depths up to 12 Di, and it would require a pool depth of Y/Di ≃ 16−20 to successfully reduce peaks in pressure fluctuation.

The technique of comparing the three extreme cases at a constant impact velocity is shown in Fig. 7.45 for the case of $Ui^2/2g$ = 9 to 10. There is a significant variation in the Cp^+ values at a constant velocity, but a comparison with the variation of Cp' values in Fig. 7.39 shows a very similar pattern of

behaviour.

The highest Cp^+ values refer to the orifice jet with high jet turbulence and L/L_B = 0.3⟶0.4. The moderate Cp^+ values refer to the 25mm nozzle with centre line turbulence ≈ 1% (see Fig. 7.41) and L/LB ≈ 0.3, whereas the lowest Cp^+ values refer to the 78mm nozzle with low centre line turbulence 0.4% and low break− up, L/L_B = 0.045.

The variation of Cp^+ at a lower value of constant impact velocity is shown in Fig. 7.46, for the case of $Ui^2/2g$ = 3.3⟶4. Here it is clear that the three extreme scenarios give almost identical results at the lower velocity. A comparison with the Cp' values in Fig. 7.40 again shows a very similar pattern for the Cp' values.

First it should be noted from Fig. 7.46, that the low velocity orifice jet has a centre line turbulence less than 1% when the velocity is $Ui^2/2g$ = 3.3⟶4, or Ui= 8⟶9 m/s. The 25mm nozzle at this droplength will also have a turbulence around 1%. Both jets have almost identical L/L_B values around 0.4 to 0.6.

The surprising data, however, is the 78mm nozzle which has a lower L/L_B value and a lower turbulence value, although it is not clear where this graph will peak and recede at higher values of Y/Di.

7.4.4 Variation of minimum fluctuations (Cp') with jet parameters.

The minimum fluctuations are the lowest recorded instantaneous values of pressure head below the mean, normalised by the impact velocity head $Ui^2/2g$. The variation of Cp^- with plunge pool depth is shown in Fig. 5.50(c) covering all tests carried out in this work. Highest Cp^- values are around 0.6 to 0.65 occuring at a pool depth of 4 to 5 diameters (Y/Di = 4− 5). At this pool depth, the corresponding RMS fluctuations (Cp') are usually around 0.13, giving the ratio Cp^-/Cp' of 4.5 to 5. This ratio is in excess of extreme values compared with the standard deviation for a Gaussian distribution, which would be around 3. The reason behind negative skewness of the distribution of pressure head values at small pool depths as indicated by Cp^-/Cp' has been explained in Section 7.2 (Fig. 7.14) concerning a recirculating eddy at the pool boundary

which is predominant in producing upward velocity pulses and hence minimums in the measured pressure head. At larger pool depths, as shown in Section 7.4.3, positive pulses from the shear layer will dominate over smaller–scale background turbulence and the phenomenon mentioned above causing negative fluctuations.

There is a spread in the Cp– data, as noted from Fig. 5.50(c), but it is not as considerable as either the Cp' or Cp^+ results. The spread is sufficient, however, to merit some investigation and this is the purpose of the following discussion.

As in Sections 7.4.2 and 7.4.3, it was decided to investigate the three extreme cases of the 78mm nozzle with short droplength; the 25mm nozzle with longer droplength; and the 25mm orifice with a different internal turbulence structure. These are shown in Figs. 7.47, 7.48 and 7.49 respectively, with Cp– plotted against plunge pool depth, and with curves drawn through the data at the upper and lower values of the velocity range.

Fig. 7.47 is applicable to the 78mm nozzle with short droplength, L/Do= 9.31 to 14.4, with the break–up ratios L/LB varying from 0.04 to 0.14 over the full velocity range (Table 6.1). The variation of Cp– in Fig. 7.47 is very similar to the variation of Cp' in Fig. 7.32 and Cp+ in Fig. 7.42, with the lower velocity jets producing larger values of Cp– than the higher velocity jets. The most likely explanation for this is given in Section 7.4.2, involving the greater degree of break–up of the lower velocity jet combined with the greater thickness of the turbulent boundary layer at impact.

One significant feature of Fig. 7.47, is that the high velocity jet (already established to behave in a similar fashion to a submerged jet) has a value of Cp– which is around which is around 3Cp' from Fig. 7.32, particularly at the peak location (Y/Di= 4– 6). By implication, a Gaussian distribution which derives from random turbulence seems most relevant. The lower velocity 3m/s jet, on the other hand, has a Cp^- value which is 3.5 to 4 times Cp' in Fig. 7.32. This implies that larger vortex structures are dominant over the pool turbulence.

Fig. 7.48 shows the variation of Cp– with pool depth for the 25mm nozzle at the longest droplengths, L/Do = 81 – 97, and with the break–up ratios L/LB varying from 0.3 to 0.8, as indicated in Table 6.1. A comparison of Fig. 7.48 with the corresponding Cp' values in Fig. 7.33 shows a somewhat different

pattern, particularly at low pool depths. At this location, no double maxima is present and the high velocity jet produces slightly larger pressure fluctuations. Instead of throughout the full plunge pool depth range, the low velocity jets cause higher fluctuations only after around Y/Di= 6. The reason for this sort of pattern has been explained in Section 7.4.2 and concerns the higher turbulence level in the high velocity jet than the low velocity jet, while the respective L/LB ratios are not significantly different. This is a case where higher internal turbulence dominates over degree of break-up in causing fluctuations, at least at shallower pool depths. The difference between turbulence levels for the 25mm nozzle jets is not as marked as the orifice jets for a similar range of velocities and this is reflected in the difference between peaks in Fig. 7.48 compared with Fig. 7.34.

The high velocity jet shown in Fig. 7.48 peaks at Cp^- values of around 0.65 to 0.7, at Y/Di = 4-5. The corresponding Cp' values in Fig. 7.34 are only 0.1, giving a ratio Cp^-/Cp' of 6.5 to 7. This is the most negatively skewed distribution and indicates dominance of large vortex structures for this high velocity case.

Fig. 7.49 shows the Cp^- values for the orifice jets with their greater internal turbulence levels (at least at high outlet velocity), L/Do= 41-57 and L/LB = 0.3 to 0.6. Fig. 7.49 can be compared with Fig. 7.34, revealing a similar pattern between Cp^- and Cp' values although Cp^- values peak at Y/Di $\approx$ 4-5 while Cp' values peak at Y/D $\approx$ 6-8.

Fig. 7.49 reveals that lower velocity jets give smaller values of Cp^- than the higher velocity orifice jet at initial pool depths. This was also noticed for the Cp' results. The reason has been outlined above regarding the turbulence level of the respective jets whilst the L/LB ratios are not vastly different from each other.

The high velocity jets in Fig. 7.49 give the greatest Cp^- values of around 0.7 when the corresponding Cp' = 0.17, a ratio of 4.1, although it should be noted that the highest Cp' values of 0.225 in Fig. 7.34 correspond to Cp^- values around 0.65, which is a ratio just below 3.

The 13m/s jet with 4% turbulence, shown in Fig. 7.49, is the nearest test to

a prototype structure and, with a substantial degree of break-up L/LB = 0.3 - 0.4, reveals very clearly that prototype jets are going to have substantial levels of Cp- around 0.6 for pool depths up to 6Di (much less than the extent of large Cp+ values), and it would require a pool depth of Y/Di = 10-12 to successfully eradicate sizeable depressions in pressure.

The technique of comparing the three extremes cases at a constant impact velocity was again employed, and is shown in Fig. 7.50 for the case of $Ui^2/2g = 9-10$. There is a significant variation in the Cp- values at a constant velocity, but a comparison with the variation of Cp' values in Fig. 7.39 shows a similar pattern of behaviour.

At pool depths Y/Di < 7, the highest Cp- values refer to the orifice jet with high jet turbulence and Y/Di = 0.3 to 0.4. The moderate Cp- values refer to the 25mm nozzle with centre line turbulence ≈ 1% and L/LB ≈ 0.3, whereas, as expected, the lowest Cp- values refer to the 78mm nozzle with low centre line turbulence (0.4%) and low disruption at impact, L/LB = 0.045.

It is of some significance that the value of Cp- varies with degree of break-up L/LB and internal jet turbulence, although it is also noted that for plunge pool depths beyond Y/Di = 7, there is no significant variation in Cp- for this constant impact velocity.

The variation of Cp- at a lower value of constant impact velocity is shown in Fig. 7.51, for the case of $Ui^2/2g$ = 3.3 to 4. The 25mm nozzle data generally produces higher values of Cp- than the orifice jet. This has been explained in Section 7.4.2 and concerns the higher internal turbulence of the 25mm nozzle jet at this velocity while both are substantially broken-up at impact.

At lower values of Y/Di, the data from the 78mm nozzle is, as expected considering the respective degree of break-up and jet turbulence value, less than both the 25mm nozzle and orifice outlet. Although it is not clear where this graph will recede at higher values of Y/Di beyond around 7, the results for each cited case gives similar results.

7.4.5 Variation of total envelope with jet parameters.

Combination of the normalised mean dynamic head values (analysed in Chapter 6) with the corresponding peak and minimum fluctuations (analysed in the preceding sections) results in the peak and minimum instantaneous dynamic pressure heads. The variation in these values with plunge pool depth is shown in Fig. 5.51(b) for all tests carried out in this work. Highest values for the peak (or maximum) dynamic head and lowest values of the minimum dynamic head define the total envelope of extremes in pressure encountered during the experimental programme. The highest peak head values $[(Hmax- Y)/Ui^2/2g]$ are around 1.4 and generally occur at pool depths of 5 to 7 diameters, or $Y/Di= 5-7$, while the lowest minimum lead values $[(Hmin- Y)/Ui^2/2g)]$ are around -0.1 which appear at approximately the same location.

It is clear from Fig. 5.51(b) that a considerable spread of data exists, particularly with the maximum dynamic head, and the purpose of this section is again to offer some explanation for such a data spread.

As illustrated in Chapter 6, the effect of aeration is significant on mean dynamic pressure in plunge pools. The influence, however, is only clearly apparent after $Y/Di\approx 10$. On the other hand, pressure fluctuations are determined to a significant extent by the degree of jet break-up L/LB and jet turbulence at impact, which is most pronounced at smaller pool depths. Consequently, the variation of maximum and minimum heads will be reflected mostly by the variation in pressure head fluctuations, particularly at pool depths less than 10 jet diameters. Variation of the pressure head fluctuations with the air entrainment rate will be detailed in the following section (7.4.6).

The investigation of maximum and minimum pressure heads again considered three diverse cases of the 78mm nozzle with short droplength, the 25mm nozzle with longer droplength and the 25mm orifice with different turbulence structure. These are shown in Figs. 7.52, 7.53 and 7.54 respectively. The maximum dynamic head is plotted against pool depth with curves shown solid through the data at the extreme ranges of velocity while the minimum dynamic head is shown similarly but with dotted curves.

Fig. 7.52 is applicable to the 78mm nozzle with short droplength (L/Do =

9.31 – 14.4); break–up ratios L/LB varying from 0.04 to 0.14 overall (Table 6.1). With a similar mean dynamic pressure head over this illustrated range of Y/Di and velocity, the extreme pressure head variation simply reproduces the variation in fluctuations that have been detailed in the previous two sections (7.4.3, 7.4.4). That is, extremes in both maximum and minimum head are obtained for the low velocity jet, due to the larger pressure fluctuation contribution, explained previously by the greater degree of break–up of the low velocity jet combined with the greater thickness of the turbulent boundary layer at impact.

A similar pattern is produced in Fig. 7.53 with the variation of maximum and minimum dynamic head for the 25mm nozzle at the longer droplengths, L/Do= 81–97, and with the break–up ratios L/LB varying from 0.3 to 0.8 over the full velocity range (Table 6.1). Except perhaps at the lowest pool depths tested, where the fluctuations are comparable for both velocity cases, the low velocity jets again produce the greatest extremes in both maximum and minimum instantaneous pressure head. The influence of air entrainment on the mean dynamic pressure (and fluctuations as will be seen in the following section) is not appreciable in Fig. 7.53 due to the small variation in estimates for the initial air concentration over this velocity range (Table 6.2). The rational for such behaviour shown in Fig. 7.53 has been extensively expounded in the discussion of the variation of the corresponding pressure fluctuation values (Cp+ and Cp–).

Fig. 7.54 shows the orifice data for a droplength range L= 1020–1420mm, giving L/Do= 41–57, and with their greater internal turbulence level and L/LB= 0.3 to 0.6. The picture from Fig. 7.54 is more confused with the low velocity jets producing less extreme values of maximum and minimum head at shallow pool depths and more extreme values at very deep plunge pool depths. The reason behind this trend has been outlined in the previous sections and concerns the fact that the 13m/s jets have very much higher turbulence levels than the 3–5m/s jets, whilst their respective L/LB ratios are not vastly different from each other.

The 13m/s jets with 4% turbulence and substantial L/LB= 0.3–0.4, shown in Fig. 7.54, is the nearest to a prototype structure, revealing quite clearly that prototype jets are going to have substantial maximum dynamic head values above 1.2 $Ui^2/2g$ for pool depths up to 6 Di.

As shown in Fig. 7.54, the minimum dynamic head is consistently low for both velocity cases, due to large fluctuations below the mean head produced almost from zero plunge pool depth. This has also been found by Castillo [13] for substantially broken-up jets at the point of impact. Considering their respective values, the largest difference between maximum and minimum dynamic head, and hence most damaging effect, is generally obtained for the high velocity orifice jet at low pool depths. Even at Y/Di = 12, however, the difference between maximum and minimum dynamic head is almost 0.8 $Ui^2/2g$, a sizeable possible swing in instantaneous head to be accomodated.

Comparison of the three stipulated test conditions at a constant impact velocity was again undertaken. This is shown first in Fig. 7.55 for the case of $Ui^2/2g$ = 9-10. Similar to the variation of fluctuations for constant $Ui^2/2g$ shown in Fig. 7.45 for Cp+ and Fig. 7.50 for Cp-, the maximum and minimum heads are accentuated for the case of the 25mm orifice jet. At this velocity, the 25mm orifice data with high internal turbulence and L/LB = 0.3 - 0.4 defines the overall total envelope of pressure for Y/Di < 8. Up to around this depth, the least extreme values of maximum and minimum head refer to the 78mm nozzle with low centre line turbulence 0.4% and break-up L/LB = 0.045.

The discernable difference can be detected for the influence of air entrainment on the mean dynamic pressure head contribution to both maximum and minimum values at Y/Di > 10, due perhaps to the similarity in estimated air concentration ratios at this impact velocity condition for both the 25mm nozzle and orifice (Table 6.2).

The variation in maximum and minimum head for a lower impact velocity head of $Ui^2/2g$ = 3.3-4 is shown in Fig. 7.56. Again the picture is similar to the corresponding variation in pressure fluctuations. The 78mm nozzle produces the smallest difference between maximum and minimum head at low pool depths for this velocity while beyond Y/Di ≈ 7, the results are almost identical. At depths greater than about Y/Di > 8, these consistent results define the total envelope of pressure.

As noted above, the total envelope is defined by the high velocity orifice jet, at Y/Di < 8 approximately, due to the hgiher jet turbulence level causing

large fluctuations and hence greater extreme values. Beyond around Y/Di = 8, the lower velocity jets define the total envelope better as shear layer turbulence is dominant in producing fluctuations and this effect is governed more by disturbances on the jet edge which are pronounced for low velocity jets with larger ratios of L/LB

The influence of air entrainment can be ascertained in Fig. 7.56 as the initial air concentrations (Table 6.2) for the orifice (Ci = 0.64) was sufficiently larger than the 25mm nozzle (Ci = 0.54). At Y/Di = 12, the difference between maximum heads, and minimum heads, in these cases is much smaller than indicated by the corresponding fluctations. In fact, even though the positive fluctations (Cp+) shown in Fig. 7.46 are larger in the case of the orifice jet, the reduction in mean head due to enhanced air entrainment for this case means than the maximum instantaneous values for the 25mm nozzle are slightly larger.

7.4.6 Variation of pressure fluctuations with air entrainment rate.

A significant feature of the analysis of mean pressure heads in a plunge pool, discussed in Chapter 6, is the influence of the rate of air entrainment by the plunging jet in determining the mean pressures. So far, in the analysis of fluctuations in this chapter, interest has centred on the effect of jet surface disturbances (L/LB) in promoting additional fluctuations, as well as the degree of turbulence in the jet at the point of impingement with the pool surface. The later may be characterised by the Reynolds Number (Re), the boundary layer development within the jet δ/D or even the type of outlet device, whether nozzle or orifice.

The question which remains is, what effect does air entrainment have on the pressure fluctuation values ? The answer in fact is difficult to ascertain in this work, because air injection was by purely natural means and hence closely allied with the ratio L/LB as well as the impact turbulence level. Previous research has clearly shown that air entrainment increases as the level of jet surface disturbances increase. Research has also shown that more turbulent jets entrain more air, at least at lower velocity ranges. This means that there is difficulty (in this data set) in separating the air bubble effect from that of increased turbulence due to uneven and greatly disrupted impinging jets.

It was decided however to attempt some form of analysis, albeit limited, to derive more understanding of the influence of air bubbles in plunge pools, especially with regard to their influence in supressing or magnifying pressure fluctuations. It was decided that if L/LB was the main parameter influencing pressure fluctuations, then it is a necessity to plot the data for constant L/L_B values but at different rates of air entrainment. This is shown in Figs. 7.57 to 7.61 for L/LB values in the range 0.04 to 0.41. The difficulty arose in obtaining variations in air entrainment rate but with constant L/LB ratios.

Figs. 7.57 to 7.61 are plots of the RMS pressure fluctuation value Cp' plotted against the plunge pool depth (Y/Di). The graphs in general show at consistent trend in the sense that Cp' increases with the L/LB ratio, as discovered previously. This is shown clearly in Fig. 7.62 showing the trend from L/L_B = 0.04 to L/LB = 0.4. Only the upper and lower curves are shown for clarity.

Returning to Figs. 7.57 to 7.61, it should be clarified that these graphs are for nozzles only and exclude orifice data. The reason for this is straightforward. An impinging jet will produce turbulence in the pool with magnitude depending on:

(i) Jet surface disturbances (L/LB).
(ii) Jet internal turbulence at impact (Tui).
(iii) Rate of air entrainment (βi).

If we keep L/LB constant then any variations in Cp' will result from variations in Tui and βi, neither of which were measured in this work. Therefore if we confine our analysis to the nozzle jets only, then it seems that the variation in turbulence is minimised to the range Tu ≈ 0.003 to 0.01, as seen in Fig. 7.41(a). Orifice turbulence readings at higher velocities suddenly increase substantially above these values.

Therefore with a constant L/LB range and a reasonably constant Tu range, we may be able to detect variations in Cp' due to air entrainment rates.

Fig. 7.57 shows the variation in Cp' for a constant L/LB = 0.04→0.07 for two jet diameters. In this particular case both the jet Reynolds Numbers and air

entrainment rates (see Table 6.2 for air entrainment rates) are almost identical. This is reflected in the small data spread. In fact this is the only test series with all three parameters constant L/LB, βi, and Re_o for two jet diameters.

Fig. 7.58 shows the Cp' variation for a constant L/LB in the range of 0.08 to 0.14, for all three jet nozzle diameters. The range of Reynolds Number is approximately constant $2.5x10^5$ to $3x10^5$, but the air entrainment rate varies from 0.29 to 0.8, measured in terms of air/water ratio. This graph gives a reasonable idea as to the likely effect of air entrainment, as the main parameters affecting pool fluctuations are constant (L/LB, Re_o), but βi is varying. Fig. 7.58 shows that for pool depths greater than Y/Di = 6, there appears to be little effect of β, but for shallow pool depths Y/Di < 6, more air entrainment supresses RMS fluctuations, although it should be borne in mind that there is great uncertainty in the estimates of both L_B and βi.

Fig. 7.59 shows the variation in Cp' over the constant range of L/LB of 0.11–0.18, again for all three nozzle diameters. In this case the Reynolds Numbers are similar for the 25mm and 52.5mm nozzles, but much greater for the 78mm nozzle. The values of air/water ratio in this case varied from 0.31 to 0.84. The same general trend is confirmed, with larger air/water ratios producing lower fluctuations, suggesting that air bubbles suppress both mean and fluctuating pressures, EVEN THOUGH jet surface disturbances increase fluctuations and air entrainment rates.

Fig. 7.60 shows the variation in Cp' over the constant L/L_B range of 0.27 to 0.32. In this case the Reynolds Number is reasonably constant for all three nozzle diameters although the ratio of air/water varies considerably in the upper range 0.67 to 1.5. The picture in Fig. 7.60 is more confused, but it does show that the 25mm nozzle with air/water ratio 1.5 produces lower fluctuations than the other two jets in the 0.67 to 0.85 range of βi. There is considerable spread of data in this graph which may reflect inaccurate assessments of the break– up length LB, or even experimental error.

Fig. 7.61 shows the variation in Cp' for the ratio L/LB = 0.41, for two nozzles only, the 25mm and 52.5mm nozzles. Again their Reynolds Numbers are approximately constant, and again the jet with higher air/water ratio, gives the lowest pressure fluctuations.

It might be concluded from the five examples shown in Figs. 7.57 to 7.61 that even though an increase in L/LB increases pressure fluctuations; for a constant L/L_B, an increase in air/water ratio decreases pressure fluctuations. This is a further " conflict of interests", because a large L/LB will make the jet more uneven at impact and produce greater fluctuations; it will also entrain more air which produces lower fluctuations.

An approximate attempt to quantify the effect of air entrainment is shown in Fig. 7.63 for a constant plunge pool depth of Y/Di = 4. The reason for choosing this plunge pool depth for the example was because the air/water ratio appears to have substantial effect at that depth but much smaller effect at depths greater than say, Y/Di> 6.

Fig. 7.63 reveals that pressure fluctuations Cp', do indeed decrease with increasing air entrainment, for constant L/LB ratios, and at a given plunge pool depth.

For convenience the data is plotted in two main bands, the upper band referring to L/LB values between 0.27 and 0.41, whilst the lower band refers to L/L_B values betwen 0.08 to 0.14. The graph shows very clearly how Cp' values increase with L/LB ratio but decrease with larger quantities of air entering the pool. The most marked effect of air seems in the middle range of air/water ratios between βi = 0.5 to 1, with larger increases in βi beyond 1 having less and less effect. A rather more tentative curve is also given for L/L_B = 0.04–0.07 but should be treated with caution until more data points become available.

7.4.7 An impinging jet "Froude" model.

One advantage of covering such a wide range of jet velocity, jet diameter and jet plunge length, is that some of the jets are scale models, (or approximately scale models) of other jets. By definition, a Froude model involves linear scaling of dimensions, to form a scale ratio Lr = $L_{(prototype)}/L_{(model)}$ and hence the velocity scales according to $\sqrt{Lr}$.

If we assume that the larger jet is the 78mm nozzle jet and the smaller jet the 25mm nozzle jet, then Lr ≈ 3.12, and hence the velocity ratio should be √(3.12)= 1.766.

A further condition is that the non–dimensional ratios such as L/Do and Y/Do should remain the same in both nozzles. Therefore it was decided to investigate the 78mm nozzle at the longer droplength of 2230mm–2630mm to give L/Do = 28.6–33.7. This can be compared with the 25mm nozzle at droplength L = 513–913mm giving L/Do = 21–36, which is broadly speaking in the same L/Do range as the 78mm nozzle. Behaviour can be compared over the measured range of Y/Do.

It was decided in the first instance to investigate a nozzle velocity of Uo = 7.1m/s for the 25mm case, and hence Froude scaling would require (1.766)(7.1) = 12.5m/s in the 78mm nozzle. This would produce a nozzle Froude Number of 14.3 in both cases, but would achieve a Reynolds Number of 10^6 in the 78mm nozzle, and only 1.8×10^5 in the 25mm nozzle.

As a further check on the compatibility of these Froudian scale models, the break–up ratio (L/LB) is 0.1–0.18 in the 25mm nozzle, whereas the L/LB for the 78mm nozzle is 0.11–0.12. These are both of the same order of magnitude, with the smaller jet slightly more broken up at impact.

Fig. 7.64 shows the comparison between the two Froudian scale models, for the 78mm jet and the 25mm jet at Froude Number 14.3. The limited amount of data in each case does not provide a great deal of overlap, but it is clearly seen in Fig. 7.64 that there is a reasonable correspondence between data, but not exact. The correspondence between the two lies in the plunge pool depth where maximum fluctuations are achieved Y/Do ≈ 7, although the higher Reynolds Number jet seems to reach slightly higher values of Cp' at that point. The major discrepancy between the two models concerns low pool depths and in particular, the one approximately direct comparison point at Y/Do = 4–4.5. At this point the 25mm jet has a Cp' value over twice that of the 78mm jet, despite the difference in Reynolds Numbers.

The reason for this discrepancy again highlights the sensitivity of the data to the L/LB ratio. For the 25mm jet at Y/Do = 4, the value of L/LB is

approximately 0.18, whereas the 78mm jet at Y/Do = 4, gives L/LB ≈ 0.11. The smaller jet has a more uneven surface at impact.

As well as this, the larger jet has a thinner boundary layer during the plunge ($\delta \propto 1/Re$), although it would have been expected that the larger Reynolds Number would have more than compensated for this effect. The air concentration for the 25mm jet is around 0.43 and is 0.47 in the 78mm jet case. As shown in previous section, the increased air concentration acts to suppress fluctuations at constant L/LB, particularly at low pool depths. This may be another contributory factor for the discrepancy in results at Y/Do= 4– 4.5.

The same procedure was carried out again for the same two nozzle diameters and the same two L/Do ratios, but this time with a 3.4m/s velocity at the 25mm nozzle, and a scaled–up model with 6m/s velocity at the 78mm nozzle. This gave a Froude Number of 6.8 at both nozzles. The result is plotted in Fig. 7.65

Despite the scarcity of data points, both jets appear to peak at Y/D_o = 5–6, with the lower Reynolds Number jet giving slightly lower Cp' values at the peak. The range of Reynolds Numbers in Fig. 7.65 are between 8×10^4 and 5×10^5, somewhat lower than Fig. 7.64.

It is of considerable interest to note that lower pool depths appear to give less discrepancy between the two data sets in this case, and it is also of interest to note that their average values of break–up parameter L/LB, are 0.2 for the 78mm nozzle and 0.24 for the 25mm nozzle, giving much closer correspondence in this case.

Thus it can be concluded that the plunge pool pressure fluctuation data from a Froude model is to be treated with some caution because the values obtained are highly sensitive to the L/LB ratio, which is not a Froude scaled parameter, and in fact is more related to a Weber/Reynolds Number parameter.

It is also of interest to note that the highest values of Cp' do not show great variation with Reynolds Number, and hence a Froude model can be used with some confidence in the highest Cp' values obtained. The reason for this is that the peak Cp' is dominated by large vortex structures which are reproduced in most Froude models, except an extremely small scale.

The main disparity is therefore confined to the initial few jet diameters into the plunge pool where jet surface disturbances may dominate.

7.5 THE DESIGN OF AN IMPINGING JET PLUNGE POOL AND SPILLWAY.

The work of this thesis has concentrated on the physical flow mechanisms and measurement of the behaviour of a circular jet in the atmosphere with subsequent diffusion in a water cushion.

For the jet in the atmosphere, discussion has centred on the development of internal jet turbulence, surface disturbances, break-up length of the vertical impinging jet, as well as estimation of the outer and inner jet diameters at impact along with estimates of the degree of air entrainment at impact point. An understanding of jet conditions at impact has been shown to be important in interpreting the values of mean and fluctuating pressure on the plunge pool floor.

For the jet in the plunge pool, discussion has centred on the variation of mean and fluctuating pressure on the plunge pool floor, both with varying pool depths, but also in the radial direction. Pressure fluctuations have been characterised by the RMS value (Cp') the peak instantaneous value above the mean (Cp^+), the minimum instantaneous peak below the mean (Cp^-), as well as the total pressure envelope. Interpretation and analysis of the mean and fluctuating pressures has only been possible in the light of jet characteristics at the impact point. This has included estimates of the impact jet diameter Di, the jet break-up ratio L/LB, the impact velocity Ui and the impact air/water ratio βi.

The main conclusions from the work are summarised in Chapter 8.

It is incumbent on the author of this work however to provide some comments on the design of impinging jet spillways and plunge pools based on the results of this experimental programme. If this is not done then the research results simply report an interesting Fluid Mechanics situation but make little impact on designers at the sharp-end, making decisions which will affect the performance and life of the structure. Typical designers questions include:

performance and life of the structure. Typical designers questions include:

(i) What is the fluid loading on the plunge pool floor both in magnitude and frequency ?

(ii) What is the optimum plunge pool depth ?

(iii) What factors are involved in the plunge pool floor slab design ?

(iv) What is the optimum jet arrangement for the plunge from dam to pool ?

Each of the above aspects will be covered in the following discussion.

(i) What is the fluid loading on the plunge pool floor in magnitude and frequency ?

The results of this thesis provide the first definitive answer to the above question at least for the range of experimental parameters tested.

- The mean dynamic head for vertical circular jets, along the jet centre-line, is shown in Fig. 6.6

- A comparable graph for rectangular impinging jets is shown in Fig. 6.25. This is a composite of other authors data.

- The variation of RMS pressure fluctuation with plunge pool depth is shown in Fig. 5.50(a). As a rough guideline, the highest Cp' values are around 0.2 at a plunge pool depth Y/Di≈ 6 to 7.

- The variation of the peak fluctuations above the mean is shown in Fig. 5.50(b), revealing maximum Cp^+ values around 0.8 $Ui^2/2g$ above the mean at pool depths of 8 to 10Di.

- The variation of minimum fluctuations below the mean is shown in Fig. 5.50(c), revealing minimum Cp^- values around 0.6 $Ui^2/2g$ below the mean at pool depths around 4 to 6Di.

– The extreme maximum and minimum pressure head field is shown in Fig. 7.66 revealing that in plunge pools, the highest instantaneous pressures reach $1.4Ui^2/2g$ above atmospheric pressure, and reach $0.1Ui^2/2g$ below atmospheric pressure. The latter term means that cavitation is possible for impact velocities above 40m/s, but not likely because of high air content.

The only question remaining is how representative are these values for a prototype situation.

The answer to this question is that the data is reasonably representative of prototype behaviour on all but two counts. The range of velocity is adequate (up to 15 m/s), the range of Reynolds Number is sufficiently high to avoid significant scale effects (Re up to 10^6), the range of pool depths up to Y/Di of 25 is adequate, the range of plunge lengths up to L/Do = 100, is reasonable, but could have been greater, the range of air/water ratio up to $\beta i \approx 1.6$ is good, and the range of outlet devices using both nozzle and orifice provides further insights, although may have been extended to the free overfall situation.

The only doubts about the representative nature of this data concerns the range of jet break–up at impact with most of the data having $L/LB < 0.5$ which represents reasonably intact jets at impact. Castillo's data [13] may be used to complement this data, because of its greater degree of break–up with L/L_B in the 0.65 to 0.85 range. No author has yet managed to provide fluctuation data for jets beyond the break–up point $L/LB > 1$.

The other doubt concerns the internal turbulence levels in the impinging jets with turbulence level less than 1%. Only the orifice jets at high velocity ($Uo > 10$m/s) produced turbuelence values which would be more likely to be found in nature ($Tu \approx 3 \rightarrow 5\%$). Thus the orifice data at high velocity could be taken as the nearest approach to prototype behaviour. Typical graphs for this behaviour are shown in Fig. 7.34 (for values of Cp') and Fig. 7.44, for values of Cp+.

The frequency range to be expected in the plunge pool is generally situated below 50 Hz with the dominant frequency between 0 to 15Hz (Chapter 3). A tentative relationship has been forwarded between this dominant frequency and the parameter Ui/Y, and is given in Equation (7.20). In terms of design, Equation (7.20) is useful to estimate the dominant frequency of fluctuations, due to large

scale vortex structures (Y/Di> 4), once the parameters Ui and Y have been determined for the particular prototype configuration. Consideration of the structures dynamic response can then be undertaken to ensure limitation of vibration problems.

(ii) What is the optimum plunge pool depth ?

In almost all cases of reported damage and vibration in plunge pool structures, the main problem has been due to pressure fluctuations and not due to high mean pressures. A concrete structure can be designed quite easily to withstand high static loadings so in a sense it matters not if the mean dynamic head on the plunge pool floor is $0.1Ui^2/2g$ or $Ui^2/2g$. The fluctuations are more important because their dynamic load may lead to fatigue, cracking, vibration, cavitation or even destruction.

The key point in any design of pool depth should be the avoidance of large pressure fluctuations at the concrete base. Fig. 7.13 is a summary of the pressure fluctuations in this work, revealing the worst negative peaks at a pool depth of 4 – 6 diameters, the RMS fluctations worst at 6–7 diameters into the pool, and the highest positive peaks worst at 10 jet diameters into the pool. This means that all this range should be avoided in any design.

In fact Fig. 7.13 indicates that the optimum pool depth should be of the order of 16–20 jet diameters in depth to avoid serious problems. This may be a very uneconomical excavation if large jets are used in the spillway. At Morrow Point Dam for instance, the equivalent jet diameter is around 3–5m which would mean a pool depth of 50–100m which is almost as high as the dam itself! The obvious answer is to provide small diameter jets which would make a pool depth of 20 diameters economical. The problem then is that a large number of jets would be needed and also that these would need to be spread over a large area, in plan so that they would not overlap too much diffusing in the plunge pool.

The other obvious solution from Fig. 7.13 is the case of a zero pool depth with small fluctuations. This method has already been adopted by Hartung and Hausler [22]. Their method is to design a stilling basin beneath spillway jets which basically dispenses with the tailwater (low depth) and produces a forced hydraulic jump with rotating surface rollers. This assumes that the oncoming jet

is "caught" in a receiving trough and is then diverted smoothly towards the horizontal direction, as shown in Fig. 7.67. High dynamic pressures are prevented from building up under the apron by prestressing the trough horizontally in order to remain crack free under the momentum of the incoming jets.

This type of design may be flawed, however, on at least two major counts:–

(a) If the impinging jet is very much broken–up at impact or L/LB $\longrightarrow$ 1 as in the case of Castillo's data [13], then from Fig. 7.23 we find large pressure fluctuations at zero pool depth. This is seen just as clearly in Fig. 7.24 and points very strongly to the avoidance of zero pool depth. This phenomenon did not show up in the Glasgow data because the jets were relatively intact as impact.

(b) The second possible reason for avoiding a zero pool depth is shown in Fig. 7.6. For zero pool depth with a circular jet, a radial hydraulic jump is formed whose upstream velocity can be as high as Ui, the vertical impact velocity. When the jump forms, RMS fluctuations as high as 0.4 $Ui^2/2g$ will also occur indicating fluctuations (Fig. 7.6) which should be avoided if possible. These values of peak and minimum are 1/2 to 2/3 of the direct impinging jet case. This leaves a recommendation of a pool depth $\approx$ 20 jet diameters.

(iii) <u>What factors are involved in the plunge pool floor slab design ?</u>

For the case of concrete–lined floor slabs the main structural problem concerns the possible ingress of the applied fluid loading on the upper base slab being transmitted to the underside of the base slab, through cracks and joints etc., and, if the circumstances are unfavourable, producing uplift of the concrete floor.

The possibility that one extreme in pressure is followed by the opposite extreme at a time period coincident with the interval required for transmission of the loading to the underside of the base slab is remote but, over the operating life of the structure, it must be considered. In addition to the slab self weight and tailwater head, three load combinations can be envisaged.

(a) Similar to a hydraulic press, the maximum pressure at the top surface of the base slab may be active while at the underside the minimum pressure may be applied. The net result may be a sizeable downward instantaneous pressure, as shown in Fig. 7.68(a).

(b) The opposite situation may occur where the minimum pressure is applied to the top side of the base slab while the maximum pressure, acting in the upward direction, is active at the underside of the base slab, as shown in Fig. 7.68(b). This load combination may produce a sizeable uplift, depending on the relative magnitude of the maximum and minimum heads, the tailwater depth and the dead weight of the concrete slab and reinforcement, which must be considered in the structural design. The form of loading in (a) and (b) means that the fatigue possibilities must also be investigated.

(c) If not ingress of pressure to the underside of the slab is possible by whatever means available, the full maximum pressure head at the slab must be considered. Cavitation at the minimum heads should not be a problem due to the presence of large amounts of air at such plunge pools during spillway jet diffusion.

The other potential problem in floor slab design concerns the frequency of loading which must be considered. To prevent potentially damaging vibration, the natural frequency of the structure must be such that coincidence with the low frequency fluid pressure pulses is prevented. In the present research programme, frequencies in the range of 0 to 15Hz for the dominant fluctuations have been encountered. This has been shown in detail in Fig. 7.12.

The important factor here is to avoid significant overlap between the fluid and the structure frequency spectra as sketched in Fig. 7.69.

The resonant frequency of the structure will be typically less than 1Hz, whereas this work shows typical frequencies around 5Hz. There is however, substantial overlap possibilities which should be investigated if possible.

This raises again one of the main positive points of Hartung and Hausler's solution [22] of zero pool depth, which usually produces much higher frequency fluctuations at the impact point well away from the structures natural frequency.

(iv) What is the optimum jet arrangement for the plunge from dam to pool?

The discussion in (ii) reveals that the optimum pool depth is around 20 jet diameters. This provides low fluctuations on the plunge pool floor. To achieve this depth economically we need the jet as thin as possible at entry. That is, the plunging jets should be as small in diameter as possible at impact, so that 20Di does not involve a deep excavation.

The problem with small diameter jets is that there needs to be a large number of them, preferably spread over the plunge pool plan area, or they need to have very high velocity by exiting much lower in the dam structure. This in turn may cause problems with the placing of the plunge pool location well away from the dam, to accomodate the larger velocity jets with their longer trajectory.

The rectangular nappe overflow such as Crystal Dam (Fig. 1.2) or Castillo's arrangement in Fig. 7.21 is an elegant compromise to this problem. By using a rectangular nappe, the jet is immediately spread over the full width of the plunge pool, rather than say four individual jets as in the case of Morrow Point. This solution is preferred if the discharge per unit width q (m^2/s) is small enough to produce a thin nappe at the impact point. Castillo's work [13] in Fig. 7.23 shows that a pool depth of 20 nappe thickness is sufficient to reduce fluctuations down to manageable levels. This means a small q, large droplength L, and thin nappe at entry can produce an elegant economical solution, with pool depth around 20 Bi

For larger values of unit discharge q (m^2/s), the designer may need a more complex system which attempts to spread the impinging jet (not just over the plunge pool width) but over the plunge pool area. This means one of two things, either, (i) the jet is given a built–in dispersion at the exit point in the dam by the use of crest splitters or dispersion blocks, or (ii) a series of jets are used with different trajectories designed to have impact points over the full plan area of the plunge pool. Both these solutions require extensive model tests.

Although no work has taken place at and beyond the break–up condition for plunging jets, it is thought that, for this situation, the mean and fluctuating

pressures would be smaller than measurements in this work. This is because, at break– up, the jet will fall as discrete droplets into the pool, losing momentum to the surroundings in the process, and hence this impingement mechanism will necessarily produce lower values in pressure head than an intact jet. In this condition (at break– up) maximum entrainment is also achieved which has shown to reduce the magnitude of fluctuations.

The reduction in pressure is indicated, somewhat artifically, in Fig. 7.70. In the case of a reasonably intact jet, similar to this work, the maximum and minimum pressure head will be as shown in Fig. 7.70, corresponding to the appropriate values of Y and Di. Near break– up, however, the intact portion of the jet (core) will only be small percentage of Di, and the maximum and minimum pressures can be extrapolated to much lower values, considering the intact core only. Apart from the artificiality of this linear extrapolation, it should also be remembered that between the conditions of an intact and broken– up jet, maximum fluctuations may be obtained, as in this work (e.g. at L/LB = 0.4).

The objective would be to have a completely dispersed jet at impact by providing a large fall height (L/LB$\rightarrow$1), as noted above, or by interaction of the spillway jets in the atmosphere, causing the flow to fall as a disseminated spray.

REFERENCES FOR CHAPTER 7

1. Toso, J.W., "The Magnitude and Extent of Extreme Pressure Fluctuations in the Hydraulic Jump.", Ph.D. Thesis, University of Minnesota, August, 1986.

2. Rouse, H., Siao, T.T., and Nagaratnam, S., "Turblence Characteristics of the Hydraulic jump.", Trans. A.S.C.E., Vol. 124, 1959.

3. Hinze, J.O., "Turbulence.", Pub: McGraw Hill, New York, 1959.

4. Lopardo, R.A., De Lio, J.C., and Vernet, G.F., "Physical Modelling on Cavitation Tendency for Macroturbulence of Hydraulic Jump.", Int. Conf. on the Hyd. Modelling of Civil Eng. Structures, B.H.R.A. Fluid Eng., Paper C3, Coventry, England, 1982, pp. 109–121.

5. Minami, I., and Aki, S., "A Consideration on the Supervision of a Concrete Arch Dam in the Flood Time.", 10th I.C.O.L.D., Montreal, Q38, R8, 1970, pp. 113–140.

6. Corrsin, S., "Investigation of Flow in an Axially Symmetric Heated Jet of Air.", N.A.C.A. Wartime Report, W–94, 1943.

7. Mansoori, A., "Turbulent Velocity and Pressure Fluctuations Occurring in Water at a Sudden Enlargement.", Ph.D. Thesis, King's College, London, 1988.

8. McKeogh, E.J., "A Study of Air Entrainment Using Plunging Water Jets.", Ph.D. Thesis, Queen's University of Belfast, 1978.

9. Davies, J.T., "Turbulence Phenomena.", Pub: Academic Press Inc., 1972.

10. Thomas, N.H., "Entrapment and Transport of Bubbles by Transient Large Eddies in Multi–Phase Turbulent Shear Flows.", Int. Conf. on the Phy. Mod. of Multi–Phase Flow, Coventry, 1983, pp. 169–184.

11. Kamoi, A., and Tanaka, H., "Measurements of Wall Shear Stress, Wall Pressure and Fluctuations in the Stagnation Region Produced by Oblique Jet

Impingement.", Proc. DISA Conf., Univ. of Leicester, 1972, pp. 217–227.

12. Hydraulic Research Limited, "Impact Pressure in Falling–Jet Energy Dissipators.", Preliminary Report No. SR 124, 1987.

13. Castillo, L., "Metodologia Experimental Y Numerica Para La Caracterization Del Campo De Presiones En Los Disipadores De Energia Hidraulica.", Ph.D. Thesis, Universitat Politechica de Catalunya, Barcelona, 1989.

14. Horeni, P., Disintegration of a Free Jet of Water in Air.", Byzkumny ustav vodohospodarsky prace a Studie, Sesit 93, Praha–Podbaba, 1956.

15. Corps. of Engineers U.S. Army, "Cavitation at Baffle Piers.", Miscellaneous Paper No. 2–154, Vicksburg, Mississippi, 1956.

16. Petrikat, K., Abdul Khader, M.H., Knoll, M., "Vibration due to Pressure Fluctuations of Baffle Piers in Cavitating–Supercavitating Flows.", Proc. 13th I.A.H.R. Congress, Kyoto, 1969.

17. Lowe, J., Chaw, P.C., and Luecker, A.R., "Tarbela Service Spillway Plunge Pool Development.", Water Power and Dam Construction, 1979, pp. 85–90.

18. Lopardo, R.A., Orellano, J.A., and Vernet, G.F., "Baffle Piers Subjected to Flow–Induced Vibrations.", Proc. 17th I.A.H.R. Congress, 1977, pp. 445–452.

19. Akbari, M.E., Mittal, M.K., and Pande, P.K., "Pressure Fluctuations on the Floor of Free and Forced Hydraulic Jumps.", Proc. Int. Conf. on Hydraulic Modelling of Civil Engineering Structures, B.H.R.A., Coventry, Paper C1, 1982, pp. 87–96.

20. Narasimhan, S., and Bhargava, V.P., "Pressure Fluctuations in Submerged Jump.", A.S.C.E., Jour. Hyd. Div., Paper 12004, HY3, 1976, pp. 339–350.

21. Locher, F.A., "Some Characteristics of Pressure Fluctuations on Low–Ogee Crest Spillways Relevant to Flow Induced Structural Vibrations.", U.S. Army Engineers Waterways Experiment Station, Vicksburg, Contract. Report No. H–71–1, 1971.

22. Hartung, F., and Hausler, E., "Scours, Stilling Basins and Downstream Protection Under Free Overfall Jets at Dams.", Commission Internationale Des Grandes Barrages, Madrid, Q42, R3, 1973, pp. 39–56.

CHAPTER 8

CONCLUSIONS AND SUGGESTIONS FOR FUTURE RESEARCH

CONTENTS

CHAPTER 8

8.1 INTRODUCTION

There is not doubt about the need to define the magnitude, frequency and extent of pressure fluctuations in plunge pools below freely impinging jets. Damage to the plunge pool lining at Granget Dam, increasing deepening of the scour hole at Kariba Dam, as well as the possibility of vibration damage at Morrow Point Dam (USA), have all ensured the importance of this work. The question is whether this research has added significantly to the body of understanding of such complex chaotic flows as jets plunging through the atmosphere, beginning to disintegrate, forming a two-phase highly turbulent mixture in the plunge pool with the resulting range of mean and fluctuating pressures on the plunge pool floor.

On the positive side, the following points can be made:-

(i) An experimental rig was designed and constructed and a method developed to obtain instantaneous pressures over the plunge pool floor.

(ii) A sophisticated data aquisition system was designed to link pressure data directly with a micro computer, with software control (ASYST), with the ability to process the data into any desired form including mean pressures, RMS pressure fluctuations, skewness, kurtosis, Fast Fourier power spectra, and many other features.

(iii) A technique was used to measure turbulence intensities within the plunging jet both in the radial and longitaudinal direction. This parameter later proved important in determining pressure fluctuations on the plunge pool floor.

(iv) One of the most positive aspects of this work was the wide range of velocities used from 3 m/s to 20 m/s, effectively covering model and prototype values. This is the largest range ever tested in this area of research.

(v) The use of two outlet forms (nozzles and orifices) was also a novel innovation, reflecting the different types of outlet device used in dams.

(vi) The range of diameters from 25mm up to 78mm was also larger than most previous studies, and hopefully relatively free of scale effects as the resultant Reynolds Number range was usually between 10^5 and 10^6, which is high by modelling standards.

(vii) The range of jet fall lengths from 513mm to 2630mm was slighly limited, but nevertheless produced jets of non–dimensional droplength L/Do up to 100.

(viii) The work also investigated the effect of plunge pool depth in great detail, covering the normal range of non–dimensional pool depths Y/Do up to 20, or Y/Di up to around 32.

The main criticisms of the work might centre on the degree of disintegration which occurred in the plunging jets as well as their shape.

It is clear that the use of more disintegrated jets would have been informative, but this was precluded because of the lack of vertical space in the laboratory. Much smaller jets could have been used, but this would have introduced significant Reynolds and Weber Number scale effects.

The use of rectangular nappes rather than just circular jets would have been useful. At the time of starting this work H.R.Ltd. Wallingford were in the process of studying rectangular jets and Glasgow agreed to complement this by studying circular jets. In any case, the time span was too short to investigate both shapes of jet.

By sheer coincidence, recent work from Barcelona (Spain) has reported on rectangular plunging nappes with a large degree of jet break–up and disintegration.

8.2 MAIN CONCLUSIONS

8.2.1 Mean pressures

(i) The most significant finding of this work concerns the variation of mean

dynamic head at the jet centre line, as it varies with plunge pool depth. When the mean head is normalised by the impact velocity head ($Ui^2/2g$) and the plunge pool depth is normalised by the measured jet diameter at impact (Di), then the results collapse onto one curve. This is surprising in view of the large range of velocity, jet diameter and fall height tested, although tempered to some extent by the narrow range of jet disintegration $0 < L/L_B < 0.4$.

(ii) In order to use this design curve for mean dynamic heads, the author has devised a method of calculating the actual jet diameter at the impact point with the free water surface (Di). The method involves the combined use of jet turbulence at the outlet device, gravitational acceleration as well as a probability density function used to describe the edge of the plunging jet from its solid core to the extreme edges of the jet. These predictions correlated well with measured jet diameter values.

(iii) The method in (ii) was extended to predict the jet length that the solid inner jet core tends towards a zero diameter. This was assumed to be the break–up length of the jet (L_B) and was compared with a range of experimental data for measured break–up lengths. The comparison was again favourable, and furthermore showed that the ratio of (L/L_B) would be a useful parameter in describing the degree of jet disintegration at the impact point.

(iv) The variation of mean dynamic head with plunge pool depth have been summarized by empirical expressions given by Equations (6.59), (6.60) and (6.61).

It is interesting to note that the mean dynamic head remained constant to a plunge pool depth of 4Di, indicating an inner core which is shorter than that predicted for submerged jets.

(v) A comparison of the authors variation of mean dynamic head with pool depth was done with previous authors data. The result was favourable for previous circular jet data (see Fig. 6.22) although is less favourable if compared with rectangular jet data (see Fig. 6.25)

(vi) The influence of jet break–up parameter (L/L_B) on the mean dynamic heads was assessed in some detail. Surprisingly there was no correlation between the two parameters which may have reflected the narrow range of L/L_B in these

tests. Most of the values ranged only up to 0.4, representing relatively intact jets at impact.

In this situation it would be expected that as the ratio of L/L_B is increased, and hence extra turbulence is produced in the pool, the corresponding mean pressure heads would be reduced, due to shorter pool core lengths, faster decay of velocity etc. However, the main device for increasing the ratio L/L_B was to reduce the jet outlet velocity which results in reduction of the Reynolds Number of the flow, the internal turbulence of the jet and the degree of air entrainment in the pool, and hence these effects work to increase the mean dynamic head in the pool. This highlights one of the numerous "conflict of interests" that are inherent when studying this complex phenomena.

(vii) The author used a relationship by Ervine to predict the rate of air entrainment into the plunge pool, and hence the initial air concentration near impact (Ci). The influence of Ci was then investigated in some detail to determine its effect on mean dynamic heads. The result is given by Fig. 6.26 showing a clear correlation of mean dynamic head and initial air concentration especially at pool depths $Y/Di > 10$.

(viii) From this work it is clear that initial air concentration is a very important parameter in defining the mean dynamic head at any plunge pool depth. The work also shows that L/L_B is a less important parameter at least over the range of L/L_B up to 0.4. It must be stressed however that work to be published soon by Armengou with a totally disintegrated jet $L/L_B \approx 2$, shows significant influence of L/L_B on the mean dynamic heads along the jet centre line.

8.2.2 Pressure fluctuations

(i) A study of RMS pressure fluctuations (Cp') and turbulent velocities (Tu) for a hydraulic jump showed an approximate relationship $Cp' \approx 10(Tu)^2$. A similar relationship was shown to be true for plunge pool RMS fluctuations.

(ii) At least three mechanisms have been established, each contributing to presure fluctuations at a plunge pool floor:

(a) large eddies occupying the pool depth Y, forming low frequency eddies whose dominant frequency is of the order of 0.01Ui/Y.(Hz).

(b) coherent vortex structures in the plunge pool shear layer producing eddies and fluctuations of higher frequency of ther order of 0.25Ui/Y(Hz).

(c) random turbulence in the pool made up the third component, producing even higher frequencies but at lower power density.

(iii) The orientation of coherent vortex structures in the plunge pool shear layer, offered an explanation for the skewness of peak and minimum fluctuations about the mean.

(iv) The variation of pressure fluctuations in the radial direction correlates strongly with the variation of turbulence in the radial direction. In the zone of established flow, Cp' decreases in the radial direction. In the zone of flow establishment ($Y/Di < 4$), pressure fluctuations peak at a radial distance of approximately $R/D \approx 0.5$.

(v) The variation of pressure fluctuations with plunge pool depth shows maximum values of Cp' around 0.2, at a pool depth of $Y/Di \approx 6-7$. This is significantly greater than parallel flows such as a hydraulic jump, where Cp' reaches values only of the order of 0.05. Both types of structures however approximate to the relationship $Cp' \approx 10(Tu)^2$.

(vi) A comparison with other authors centred on recent work by Castillo [29] using rectangular jets. In this case the highest values of Cp' were of the order of 0.12 to 0.16. Castillo's jets were more disintegrated at the impact point highlighting a key parameter in determining fluctuation values. A comparison with fluctuation values on the front face of a baffle block, showed very similar of Cp' to this work.

(vii) When analysing the data trend of pressure fluctuations with plunge pool depth it was found that the key to interpreting the results lay in three parameters. These were (a) L/L_B for the degree of jet break-up, (b) the air entrainment rate at impact (βi) and (c) the jet turbulence intensity at the centre line at impact. The latter effect involves the boundary layer thickness at impact

and also the Reynolds Number at impact. A conflict was highlighted between these two parameters in that a high velocity jet would have a larger turbulence level than a low velocity jet but would be more intact because of longer break–up lengths.

(viii) In essence, increases in jet disintegration produced larger pressure fluctuations. This statement has to be tempered with the fact that values of L/L_B only up to 0.4 were tested, meaning that most of the jets were relatively intact at impact.

Castillo's data with the jet near the point of disintegration, $L/L_B \rightarrow 1$, shows lower fluctuation values. Clearly a totally broken–up jet (into droplets) will produce lower Cp' values still. This has been discovered in recent tests by Armengou with $L/L_B > 2$ showing negligible fluctuations.

The value of L/L_B is therefore a key parameter in determining both Cp', Cp^- and Cp^+, as well as the overall envelope.

(ix) The influence of air entrainment βi on the level of fluctuations was also investigated and revealed that for a given degree of break–up (L/L_B), and at a given plunge pool depth (Y/Di), pressure fluctuations Cp' decreased with increasing air entrainment. This represents a "conflict of interests", because a large L/L_B will make the jet more uneven at impact and produce greater fluctuations; it will also entrain more air which produces lower fluctuations. This observation is true over the narow range of L/L_B tested, but when $L/L_B > 1$, the fluctuations reduce substantially.

(x) A significant feature of this work was the measurement of internal jet turbulence in the plunging circular jet. The nozzle jets showed an increasing boundary layer width with increasing plunge length, revealing a gradual transmission of edge turbulence towards the jet centre line. The orifice jet showed much larger turbulence levels at high velocity but nozzle type turbulence at low velocity.

The work clearly shows that higher internal turbulence jets produce a more uneven jet surface at impact. The higher levels of impinging jet turbulence seem to be transmitted into the plunge pool at least for the shallow plunge pool

depths, until a point is reached where shear layer turbulence dominates at Y/Di > 6 approximately. This means that high turbulence impinging jets produce larger presure fluctuations at least up to plunge pool depth of Y/Di ≈ 6.

(xi) The combination of jet disintegration (viii) and high internal turbulence means that the highest possible pressure fluctuations are produced by an almost broken−up jet ($L/L_B \rightarrow 1$) with a high internal turbulence intensity at impact.

The nearest these tests have approached this condition, and most akin to a prototype structure, was that of an orifice jet at high velocity with break−up parameter $L/L_B \approx 0.3-0.4$ and internal turbulence ≈ 4%. A typical result is shown in Fig. 7.39 indicating that prototype jets will have substantial levels of pressure fuctuations, especially at the powest pool depths.

(xii) Variations of Cp^+, highest peaks above the mean, and Cp^- lowest minimums below the mean, have also been investigated with increasing plunge pool depth.

The largest values of Cp^+ are approximately 0.8 when Y/Di= 8−10, and the largest values of Cp^- are around 0.6 when Y/Di= 4−6. Therefore in a plunge pool, presure fluctuations are negatively skewed at small pool depths and positively skewed at greater pool depths.

(xiii) The total pressure envelope revealed the maximum instantaneous head (mean + fluctuating) to be 1.4 to $1.6Ui^2/2g$ with the minimum instantaneous head around $-0.1Ui^2/2g$. The latter effect would produce cavitation at velocities Ui> 45m/s, but this is highly unlikely because of large air bubble concentrations in plunge pools.

(xiv) The main scale effects in this work are viscous and surface tension scale effects in the impinging jets. Because of non−scaling of these factors, a prototype jet will:

(a) produce more self aeration into the jet
(b) produce more air entrainment into the plunge pool
(c) cause more spray and droplets than the model
(d) produce faster jet disintegration than the model

(e) have higher internal turbulence than a model

(a) (b) and (c) will generally produce lower pressure fluctuations whereas (d) and (e) may well produce larger pressure fluctuations. The net effect is likely to be comparable model/prototype fluctuations at lower frequencies, but higher prototype fluctuations at higher frequencies. Mean dynamic heads are almost certain to be less in a prototype structure.

(xv) Finally, application of the results in terms of structural design, illustration of the potential damage mechanism, as well as suggestions for the most suitable arrangement of spillway and plunge pool structure were provided.

8.3 SUGGESTIONS FOR FUTURE RESEARCH.

Due to time limitations, and in some cases space confinement, various areas in this highly complex phenomena could not be adequately covered. The following is a list of topics that the author suggests need research to further refine the present experimental results.

(i) Further data on pressure fluctuations from prototype and large scale models is needed. Scale effects could be better understood from this data and could be used to further extend the present results. The micro-computer has proved to be very suited for this work.

(ii) One major defect of this research was that no impinging jets were completely disintegrated at impact. Research with jet droplengths at and above the break-up length would be invaluable to confirm some of the proposals made in this work. The nearest that this condition has been reached is from the data of Castillo with $L/L_B = 0.65-0.85$ which confirm and partially extend the present experimental results.

(iii) The parameters that have been highlighted in Chapter 3, but were not varied, should be considered to asses any effect on the present results and provide a more complete picture of the flow phenomena. These include inclination of the outlet device (non-vertical), alteration of the plunge pool dimensions (and shape) and testing multiple jets with interactions in the atmosphere. The latter effect may also shed some light on topic (ii) above as

the jet condition at impact may be highly diffused due to jet interaction in the atmosphere.

(iv) Conflict was found in many instances due to the alteration of influencing parameters such as jet break–up lengths, pool air concentrations, internal jet turbulence level etc. by simply varying the flow outlet velocity. More precise evaluation of effects may be obtained by alteration of these parameters by other means, for instance, by injecting known quantities of air into the jet at the outlet.

(v) Video recording of the flow in conjunction with synchronised records of pressure fluctuations would capture more information on jet behaviour in the atmosphere than still photography, as used in this work, and would probe further at the mechanics of the flow which cause the peak pressures.

APPENDICES

Appendix A

Included in this appendix are the main sampling routine and the data processing routine (Samprot) for the pressure transducers located at the plunge pool floor. The program is for simultaneous samples from 3 channels and can store 24,000 data points. Sample rates are inputed at execution of the program, e.g. 100 sample. 1, up to 200 Hz.

The example given is heavily commented to explain each of the individual activities. Similar comments are applicable to the other cited programs in the appendices, and are therefore omitted. This program has been discussed in Sections 3.6.5 and 3.7.2 of the main text, and consists of an Asyst structure with assembly language sub– routines.

Appendix B

Special routines:

(1) Stationarity test for raw data (Station. one). Program .to sample centrally located plunge pool transducer for different input durations. Several test runs taken at stipulated time period. The sample period is then increased, i.e. scalar W altered, until no significant difference is found in the statistical properties of the raw data. Minimum test periods are then determined to ensure that results are independent of time.

(2) Routine to determine time period required to define limiting maximum pressure value (Limitmax.one). Continuous test for 24 minutes. After each minute, maximum and mean values of raw data determined and stored. Time period found from results for which maximum pressure reaches limiting value. Time drift effects are also investigated.

Both programs in this appendix are discussed in Section 3.6.9 of the main text.

Appendix C

Graphics routine: Waveform and spectrum of raw data for samples at 100Hz (Specdist. 100).

Asyst language routine to plot 10 second excerpts of waveform. Program also determines and graphically displays a 2048 point power spectrum from sections of the raw data. This program has been discussed in Section 3.7.4 of the main text.

Appendix D

The programs in this appendix have been developed (in Basic) to calculate the core dimensions of a plunging jet which is spreading in the atmosphere, and have been discussed in Section 6.3.4 of the main text. As per the outlined theory, the jet core diameter is calculated for each droplength increment in an iterative manner. When the core has diminished the jet is considered to have broken– up. Once this condition is satisfied, the respective plunge length from the outlet is taken as being representative of the jet break– up length.

Input of the flow outlet diameter, jet turbulence intensity and the overall droplength investigated is required before program operation. The first listed program provides numerical output while the second generates a graphical representation of the results.

```
\  SAMPLE ROUTINE ( SAMPROT ) USING ASYST
\  SAMPLE PROGRAM 1 -- ANALOG INPUT WITH PCI-20002M
\  THIS PROGRAM READS AN ANALOG INPUT WITH A PCI-20002M-1
\  USING THE FOLLOWING PCI-20046S-1 INSTRUCTIONS:
\
\       SYSINIT     INIT     ERR.SYS     CNF.AI
\       READ.CH
\
\  DESIGNATE SCALARS
INTEGER SCALAR ERROR.CODE
INTEGER SCALAR SEGMT
INTEGER SCALAR CHN
INTEGER SCALAR GAIN
INTEGER SCALAR Z.CHN
INTEGER SCALAR RANGE
INTEGER SCALAR ADATA
INTEGER SCALAR W
REAL SCALAR DEG0
REAL SCALAR DEG1
REAL SCALAR DEG2
REAL SCALAR DEG3
\  DATA BUFFER ARRAYS TO CONTAIN SCAN DATA
INTEGER DIM[ 8000 ] ARRAY POSITION1
INTEGER DIM[ 8000 ] ARRAY POSITION2
INTEGER DIM[ 8000 ] ARRAY POSITION3
\
\  DEFINE A GENERAL PURPOSE ERROR PROCESSING ROUTINE.
\
: ERROR?              \ ( String --- )
   CALL[ PCI46S , ERR.SYS , ERROR.CODE ]
   ERROR.CODE 0 <> IF
      "TYPE ERROR.CODE . CR
   ELSE
      "DROP
   THEN
;
: SAMPLE.1
\
CR ." SETTING ARRAYS TO ZERO"
0 POSITION1 :=
0 POSITION2 :=
0 POSITION3 :=
\
\  INITIALISE THE PCI-20046S-4 SYSTEM.  THIS SEQUENCE MUST BE
\  GIVEN PRIOR TO CALLING ANY OTHER PCI-20046S-4 INSTRUCTION.
\
   CR
   " 61"H SET.VECT
   CALL[ PCI46S , SYSINIT ]
\
\  SEGMT, DEFINED BELOW, CONTAINS THE BASE ADDRESS OF THE CARRIER.
\  USING " C000H, BUT IT CAN BE SET ANYWHERE.
\  [ PCI46S , INIT , SEGMT ] MUST BE CALLED ONCE FOR EACH CARRIER
\  IN THE SYSTEM, EACH WITH ITS OWN ADDRESS.
\
   " C000"H SEGMT :=
   CALL[ PCI46S , INIT , SEGMT ]
\
\  CHECK FOR A SYSTEM ERROR.  DURING DEBUG, CALL ERR.SYS OFTEN,
\  POSSIBLY AFTER EVERY CALL TO THE PCI-20046S-4.
\  ERR.SYS CALLS IN FINISHED PROGRAM TO
\  MONITOR THE STATUS OF THE SYSTEM.
\
   " ERROR FOUND DURING INIT" ERROR?
\
```

```
\
\
   CR ." PROGRAM SAMPLE.1"
   CR
   CR ." SETTING GAIN AND RANGE"
   CR ." GAIN ?"
   " INPUT GAIN :=
   -1 Z.CHN :=
   1 RANGE :=
   " FLUID TEMP. ?"
   "INPUT DEGO :=
\  TEMPERATURE COEFFICIENTS
   1.25 DEGO  0.0125 * - DEG1 :=
   1.286 DEGO 0.0143 * - DEG2 :=
   1.263 DEGO 0.0132 * - DEG3 :=
\  W IS THE NUMBER OF READINGS +1 ON EACH CHANNEL
   8001 W :=
\
   CR
   CR ." CONFIGURING CHANNELS"
   4 1 DO
   CR ." CHANNEL NUMBER" I .
   I CHN :=
   CALL[ PCI46S , CNF.AI , CHN , GAIN , Z.CHN , RANGE ]
   " ERROR FOUND DURING CNF.AI" ERROR?
   LOOP
\
\  READ THE ANALOG INPUT CHANNEL.
\
   CR
   CR ." READING CHANNELS"
\
\  SCAN CHANNELS SIMULTANEOUSLY AT VARIABLE RATE UP TO 200 Hz
   SYNC.ERROR.ON
   INV 1000. *
   SYNC.PERIOD
   W 1 DO
      SYNCHRONIZE
      1 CHN :=

      CALL[ PCI46S , READ.CH , AI.T , CHN , ADATA ]


\  GIVE ADC READING, ADATA, TO ARRAY AND CONVERT.

      ADATA POSITION1 [ I ] :=

      2 CHN :=

      CALL[ PCI46S , READ.CH , AI.T , CHN , ADATA ]
      ADATA POSITION2 [ I ] :=

      3 CHN :=

      CALL[ PCI46S , READ.CH , AI.T , CHN , ADATA ]
      ADATA POSITION3 [ I ] :=

\  THE ASSUMPTION IS THAT THE PCI-20002M-1 MODULE IS SET
\  UP FOR +/- 10 VOLTS.
\
```

```
\
\  THE FOLLOWING TABLE GIVES THE GENERAL EQUATIONS TO BE USED IN PLACE
\  OF THE EQUATION BELOW FOR OTHER THAN +/- 10 VOLTS.
\
\    +/- 5          ADATA 10.0 * 4096.0 / 5.0 - GAIN / FDATA :=
\    0 TO 10        ADATA 10.0 * 4096.0 / GAIN / FDATA :=
\

\
   LOOP
   CR ." END OF ACQUISITION LOOP"
\ PRE-PROCESSING
\ CONVERT ARRAY FROM ANALOGUE VOLTAGE TO DIGITAL VOLTAGE TO PRESSURE

   POSITION1 20.0 * 4096.0 / 10.0 - GAIN / 7.2371 * DEG1 / POSITION1 :=
   POSITION2 20.0 * 4096.0 / 10.0 - GAIN / 7.3337 * DEG2 / POSITION2 :=
   POSITION3 20.0 * 4096.0 / 10.0 - GAIN / 7.2439 * DEG3 / POSITION3 :=
   CR ." NUMBER OF READINGS ON EACH CHANNEL WAS" W 1 - .
   CR
;
\  STORE RAW DATA

\  PRINT OUT DIMENSIONS OF EXPERIMENT FROM PREVIOUSLY
\  INPUTED DATA AND STORE AS COMMENTS ON TEST CONDITIONS
   20 STRING DATE1
   REAL SCALAR FALL
   REAL SCALAR DEPTHS
   REAL SCALAR DIA.
   REAL SCALAR MAN
   REAL SCALAR VELO
   REAL SCALAR VEL1
   REAL SCALAR HEAD
   12 STRING RUN_No
   REAL SCALAR LOC2
   REAL SCALAR LOC3

:  INPUTS1-3
   CR ." TRANSDUCER RESULTS ( CHANNELS 1-3 )"
   CR
   CR DATE1 "TYPE
   CR RUN_No "TYPE
   CR ." FALL HEIGHT =" FALL . ." m"
   CR ." POOL DEPTH =" DEPTHS . ." m"
   CR ." NOZZLE DIAMETER =" DIA. . ." m"
   CR ." MANOMETER READING ( MERCURY ) =" MAN . ." m"
   MAN .4931 ** .548 * PI / DIA. 2. ** / VELO :=
   19.62 FALL * VELO 2. ** + SQRT VEL1 :=
   CR ." MEAN JET OUTLET VELOCITY =" VELO . ." m/s"
   CR ." THEORETICAL IMPACT VELOCITY =" VEL1 . ." m/s"
   VEL1 2. ** 19.62 / HEAD :=
   CR
;

\  DATA PROCESSING ROUTINE
\  DETERMINE STATISTICAL PROPERTIES FOR EACH CHANNEL.
\  PRINT OUT AND STORE WITH PHYISICAL PARAMETERS ON FILE
   REAL DIM[ 10 ] ARRAY TEMP1
   REAL DIM[ 10 ] ARRAY TEMP2
   REAL DIM[ 10 ] ARRAY TEMP3
```

```
: RESULTS1-3
  CR RUN_No "TYPE

  CR ." CHANNEL 1 (CENTRE LINE TRANSDUCER)"
  CR
  POSITION1 MEAN TEMP1 [ 1 ] :=
  CR ." MEAN PRESSURE=" TEMP1 [ 1 ] . ." M"
  POSITION1 VARIANCE SQRT TEMP1 [ 2 ] :=
  CR ." STANDARD DEVIATION OF PRESSURE FLUCTS.=" TEMP1 [ 2 ] . ." M"
  POSITION1 []MAX TEMP1 [ 3 ] :=
  CR ." MAXIMUM PRESSURE=" TEMP1 [ 3 ] . ." M"
  POSITION1 []MIN TEMP1 [ 4 ] :=
  CR ." MINIMUM PRESSURE=" TEMP1 [ 4 ] . ." M"
  TEMP1 [ 3 ] TEMP1 [ 1 ] - TEMP1 [ 1 ] / 100 * TEMP1 [ 5 ] :=
  CR ." PEAK/MEAN RATIO=" TEMP1 [ 5 ] . ." %"
  TEMP1 [ 2 ] HEAD / TEMP1 [ 6 ] :=
  CR ." RMS PRESSURE COEFF. ( Cp' )=" TEMP1 [ 6 ] .
  TEMP1 [ 3 ] TEMP1 [ 1 ] - HEAD / TEMP1 [ 7 ] :=
  CR ." MAX PRESSURE COEFF. ( Cp+ )=" TEMP1 [ 7 ] .
  TEMP1 [ 1 ] TEMP1 [ 4 ] - HEAD / TEMP1 [ 8 ] :=
  CR ." MIN PRESSURE COEFF. ( Cp- )=" TEMP1 [ 8 ] .
  POSITION1 TEMP1 [ 1 ] - 3. ** []SUM 8000 / TEMP1 [ 2 ] 3. ** /
  TEMP1 [ 9 ] :=
  CR ." SKEWNESS=" TEMP1 [ 9 ] .
  POSITION1 TEMP1 [ 1 ] - 4. ** []SUM 8000 / TEMP1 [ 2 ] 4. ** /
  TEMP1 [ 10 ] :=
  CR ." KURTOSIS=" TEMP1 [ 10 ] .
  CR


  CR ." CHANNEL 2 (INTERMEDIATE TRANSDUCER)"
  CR
  CR ." LOCATION OF TRANSDUCER=" LOC2 . ." R/Do"
  POSITION2 MEAN TEMP2 [ 1 ] :=
  CR ." MEAN PRESSURE=" TEMP2 [ 1 ] . ." M"
  POSITION2 VARIANCE SQRT TEMP2 [ 2 ] :=
  CR ." STANDARD DEVIATION OF PRESSURE FLUCTS.=" TEMP2 [ 2 ] . ." M"
  POSITION2 []MAX TEMP2 [ 3 ] :=
  CR ." MAXIMUM PRESSURE=" TEMP2 [ 3 ] . ." M"
  POSITION2 []MIN TEMP2 [ 4 ] :=
  CR ." MINIMUM PRESSURE=" TEMP2 [ 4 ] . ." M"
  TEMP2 [ 3 ] TEMP2 [ 1 ] - TEMP2 [ 1 ] / 100 * TEMP2 [ 5 ] :=
  CR ." PEAK/MEAN RATIO=" TEMP2 [ 5 ] . ." %"
  TEMP2 [ 2 ] HEAD / TEMP2 [ 6 ] :=
  CR ." RMS PRESSURE COEFF. ( Cp' )=" TEMP2 [ 6 ] .
  TEMP2 [ 3 ] TEMP2 [ 1 ] - HEAD / TEMP2 [ 7 ] :=
  CR ." MAX PRESSURE COEFF. ( Cp+ )=" TEMP2 [ 7 ] .
  TEMP2 [ 1 ] TEMP2 [ 4 ] - HEAD / TEMP2 [ 8 ] :=
  CR ." MIN PRESSURE COEFF. ( Cp- )=" TEMP2 [ 8 ] .
  POSITION2 TEMP2 [ 1 ] - 3. ** []SUM 8000 / TEMP2 [ 2 ] 3. ** /
  TEMP2 [ 9 ] :=
  CR ." SKEWNESS=" TEMP2 [ 9 ] .
  POSITION2 TEMP2 [ 1 ] - 4. ** []SUM 8000 / TEMP2 [ 2 ] 4. ** /
  TEMP2 [ 10 ] :=
  CR ." KURTOSIS=" TEMP2 [ 10 ] .
  CR
```

```
   CR ." CHANNEL 3 (OUTER TRANSDUCER)"
   CR
   CR ." LOCATION OF TRANSDUCER=" LOC3 . ." R/Do"
   POSITION3 MEAN TEMP3 [ 1 ] :=
   CR ." MEAN PRESSURE=" TEMP3 [ 1 ] . ." M"
   POSITION3 VARIANCE SQRT TEMP3 [ 2 ] :=
   CR ." STANDARD DEVIATION OF PRESSURE FLUCTS.=" TEMP3 [ 2 ] . ." M"
   POSITION3 []MAX TEMP3 [ 3 ] :=
   CR ." MAXIMUM PRESSURE=" TEMP3 [ 3 ] . ." M"
   POSITION3 []MIN TEMP3 [ 4 ] :=
   CR ." MINIMUM PRESSURE=" TEMP3 [ 4 ] . ." M"
   TEMP3 [ 3 ] TEMP3 [ 1 ] - TEMP3 [ 1 ] / 100 * TEMP3 [ 5 ] :=
   CR ." PEAK/MEAN RATIO=" TEMP3 [ 5 ] . ." %"
   TEMP3 [ 2 ] HEAD /  TEMP3 [ 6 ] :=
   CR ." RMS PRESSURE COEFF. ( Cp' )=" TEMP3 [ 6 ] .
   TEMP3 [ 3 ] TEMP3 [ 1 ] - HEAD / TEMP3 [ 7 ] :=
   CR ." MAX PRESSURE COEFF. ( Cp+ )=" TEMP3 [ 7 ] .
   TEMP3 [ 1 ] TEMP3 [ 4 ] - HEAD / TEMP3 [ 8 ] :=
   CR ." MIN PRESSURE COEFF. ( Cp- )=" TEMP3 [ 8 ] .
   POSITION3 TEMP3 [ 1 ] - 3. ** []SUM 8000 / TEMP3 [ 2 ] 3. ** /
   TEMP3 [ 9 ] :=
   CR ." SKEWNESS=" TEMP3 [ 9 ] .
   POSITION3 TEMP3 [ 1 ] - 4. ** []SUM 8000 / TEMP3 [ 2 ] 4. ** /
   TEMP3 [ 10 ] :=
   CR ." KURTOSIS=" TEMP3 [ 10 ] .
   CR
;
```

```
\  STATION.ONE - PROGRAM TO DETERMINE MEAN AND RMS
\  FOR DIFFERENT INPUTED TIME PERIODS.CHANNEL ONE ONLY
\  STATIONARITY TEST OF RAW DATA.
INTEGER SCALAR ERROR.CODE
INTEGER SCALAR SEGMT
INTEGER SCALAR CHN
INTEGER SCALAR GAIN
INTEGER SCALAR Z.CHN
INTEGER SCALAR RANGE
INTEGER SCALAR ADATA
REAL SCALAR W
REAL SCALAR DEG0
REAL SCALAR DEG1
\ INTEGER ARRAY TO CONTAIN SCAN DATA
INTEGER DIM[ 6000 ] ARRAY POSITION1
\  DEFINE A GENERAL PURPOSE ERROR PROCESSING ROUTINE.
\
: ERROR?                \ ( String --- )
   CALL[ PCI46S , ERR.SYS , ERROR.CODE ]
   ERROR.CODE 0 <> IF
      "TYPE ERROR.CODE . CR
   ELSE
      "DROP
   THEN
;
: SAMPLE.1
\
CR ." SETTING ARRAYS TO ZERO"
0 POSITION1 :=

   " 61"H SET.VECT
   CALL[ PCI46S , SYSINIT ]
\
   " C000"H SEGMT :=
   CALL[ PCI46S , INIT , SEGMT ]
\
   " ERROR FOUND DURING INIT" ERROR?
\
\
   CR ." PROGRAM SAMPLE.1"
   CR
   CR ." SETTING GAIN AND RANGE"
   CR ." GAIN ?"
   "INPUT GAIN :=
   -1 Z.CHN :=
   1 RANGE :=
   CR ." FLUID TEMP ="
   "INPUT DEG0 :=
   1.25 DEG0 0.0125 * - DEG1 :=
\  W IS THE NUMBER OF READINGS +1 ON EACH CHANNEL
\  VALUE OF W INPUTED TO DETERMINE TEST TIME PERIOD
   CR
   CR ." CONFIGURING CHANNELS"
   4 1 DO
   CR ." CHANNEL NUMBER" I .
   I CHN :=
   CALL[ PCI46S , CNF.AI , CHN , GAIN , Z.CHN , RANGE ]
   " ERROR FOUND DURING CNF.AI" ERROR?
   LOOP
```

App. B1 : Stationarity Test.Page 1 of 2

```
\  READ THE ANALOG INPUT CHANNEL.
\
   CR
   CR ." READING CHANNELS"
\
\  SCAN CHANNEL 1 AT 100 Hz .PROCESS REPEATED TO DETERMINE
\  PRESSURE VARIATION FOR EACH TIME PERIOD.
   SYNC.ERROR.ON


   1 CHN :=
   INV 1000. *
   SYNC.PERIOD

   W 1 DO
      SYNCHRONIZE


      CALL[ PCI46S , READ.CH , AI.T , CHN , ADATA ]

\
   ADATA POSITION1 [ I ] :=
\
   LOOP

\ CONVERT ARRAY FROM ANALOGUE VOLTAGE TO DIGITAL VOLTAGE TO PRESSURE
CR ." DATA CONVERSION"
   POSITION1 20.0 * 4096.0 / 10.0 - GAIN / 7.2371 * DEG1 / POSITION1 :=
\  PRINT OUT NUMBER OF READINGS
   CR ." NUMBER OF READINGS ON CHANNEL 1 WAS" W 1 - .
;

\ PRINT OUT DIMENSIONS OF EXPERIMENT
\ FROM PREVIOUSLY INPUTED DATA
20 STRING DATE1
REAL SCALAR FALL
REAL SCALAR DEPTHS
REAL SCALAR DIA.
REAL SCALAR MAN
REAL SCALAR VELO
REAL SCALAR VEL1
REAL SCALAR HEAD
12 STRING RUN_No
: INPUTS1
CR ." CENTRE LINE TRANSDUCER RESULTS"
CR ." STATIONARITY TEST"
CR
CR DATE1 "TYPE
CR RUN_No "TYPE
CR ." NOZZLE DIAMETER=" DIA. . ." m"
CR ." FALL HEIGHT=" FALL . ." m"
CR ." POOL DEPTH=" DEPTHS . ." m"
CR ." MANOMETER READING (MERCURY)=" MAN . ." m"
MAN .4931 ** .548 * PI / DIA. 2. ** / VELO :=
19.62 FALL * VELO 2. ** + SQRT VEL1 :=
VEL1 2. ** 19.62 / HEAD :=
CR ." MEAN JET OUTLET VELOCITY=" VELO . ." m/s"
CR ." THEORETICAL IMPACT VELOCITY=" VEL1 . ." m/s"
CR ." DYNAMIC HEAD=" HEAD . ." m"
CR ." TIME PERIOD=" W 1 - 100 / . ." s"
CR
CR ." MEAN PRESSURE (m)"
POSITION1 SUB[ 1 , W 1 - ] MEAN .
CR ." RMS PRESSURE (m)"
POSITION1 SUB[ 1 , W 1 - ] VARIANCE SQRT .
CR
;
```

```
\  LIMITMAX.ONE - PROGRAM TO DETERMINE MAXIMUM PRESSURE
\  AFTER EACH MINUTE OF CONTINUOUS TEST.
\
INTEGER SCALAR ERROR.CODE
INTEGER SCALAR SEGMT
INTEGER SCALAR CHN
INTEGER SCALAR GAIN
INTEGER SCALAR Z.CHN
INTEGER SCALAR RANGE
INTEGER SCALAR ADATA
INTEGER SCALAR W
REAL SCALAR DEG0
REAL SCALAR DEG1
\ SCALAR FOR TOTAL TIME PERIOD
INTEGER SCALAR T
\ INTEGER ARRAY TO CONTAIN SCAN DATA.CHANNEL 1 ONLY
INTEGER DIM[ 6000 ] ARRAY POSITION1
\ TEMPORARY ARRAYS TO HOLD MEAN AND MAXIMUM VALUES
  REAL DIM[ 24 ] ARRAY TEMPMAX
  REAL DIM[ 24 ] ARRAY TEMPMEAN
\  DEFINE A GENERAL PURPOSE ERROR PROCESSING ROUTINE.
\
: ERROR?              \ ( String --- )
   CALL[ PCI46S , ERR.SYS , ERROR.CODE ]
   ERROR.CODE 0 <> IF
      "TYPE ERROR.CODE . CR
   ELSE
      "DROP
   THEN
;
\ INITIALISE CHANNELS.REQUIRED ONLY ONCE
: SAMPLE.1
\
CR ." SETTING ARRAYS TO ZERO"
0 POSITION1 :=
0 TEMPMAX :=
0 TEMPMEAN :=
\
\
   CR
   " 61"H SET.VECT
   CALL[ PCI46S , SYSINIT ]
\
\
   " C000"H SEGMT :=
   CALL[ PCI46S , INIT , SEGMT ]
\
\
   " ERROR FOUND DURING INIT" ERROR?
```

App. B2 : Limiting Maximum Value Routine.Page 1 of 3

```
   CR ." PROGRAM SAMPLE.1"
   CR
   CR ." SETTING GAIN AND RANGE"
   CR ." GAIN ?"
   "INPUT GAIN :=
   CR ." FLUID TEMP. ="
   "INPUT DEGO :=
   -1 Z.CHN :=
   1 RANGE :=
   1.25 DEGO 0.0125 * - DEG1 :=
\  W IS THE NUMBER OF READINGS +1 ON EACH CHANNEL
   6001 W :=
   25 T :=
   CR
   CR ." CONFIGURING CHANNELS"
   4 1 DO
   CR ." CHANNEL NUMBER" I .
   I CHN :=
   CALL[ PCI46S , CNF.AI , CHN , GAIN , Z.CHN , RANGE ]
   " ERROR FOUND DURING CNF.AI" ERROR?
   LOOP
;
: TIMED
\  READ THE ANALOG INPUT CHANNEL.
\
   CR
   CR ." READING CHANNELS"
\
\  SCAN CHANNEL 1 AT 100 Hz .PROCESS REPEATED TO DETERMINE
\  PRESSURE VARIATION WITH TIME. SEE CP V TIME LOOP
   SYNC.ERROR.ON

   1 CHN :=
   INV 1000. *
   SYNC.PERIOD
\  ONE MINUTE LOOP
   W 1 DO
     SYNCHRONIZE

      CALL[ PCI46S , READ.CH , AI.T , CHN , ADATA ]

   ADATA POSITION1 [ I ] :=

   LOOP

\
\ CONVERT ARRAY FROM ANALOGUE VOLTAGE TO DIGITAL VOLTAGE TO PRESSURE

   POSITION1 20.0 * 4096.0 / 10.0 - GAIN / 7.2371 * DEG1 / POSITION1 :=
\  SAVE ONLY MAXIMUM AND MEAN PRESSURE

CR   I .
   POSITION1 []MAX TEMPMAX [ I ] :=
   POSITION1 MEAN TEMPMEAN [ I ] :=
```

```
;
\ READ CHANNEL FOR 24 MINUTES WITH MEAN AND MAX. SAVED AFTER EACH MINUTE

: CPVTIME
  T 1 DO 100 TIMED
  LOOP
;

\ PRINT OUT DIMENSIONS OF EXPERIMENT
\ FROM PREVIOUSLY INPUTED DATA
REAL DIM[ 24 ] ARRAY TEMPHEAD
20 STRING DATE1
REAL SCALAR FALL
REAL SCALAR DEPTHS
REAL SCALAR DIA.
REAL SCALAR MAN
REAL SCALAR VELO
REAL SCALAR VEL1
REAL SCALAR HEAD
12 STRING RUN_No
: INPUTS1
CR ." CENTRE LINE TRANSDUCER RESULTS"
CR ." VARIATION OF PRESSURE WITH TIME"
CR
CR DATE1 "TYPE
CR RUN_No "TYPE
CR ." NOZZLE DIAMETER=" DIA. . ." m"
CR ." FALL HEIGHT=" FALL . ." m"
CR ." POOL DEPTH=" DEPTHS . ." m"
CR ." MANOMETER READING (MERCURY)=" MAN . ." m"
MAN .4931 ** .548 * PI / DIA. 2. ** / VELO :=
19.62 FALL * VELO 2. ** + SQRT VEL1 :=
VEL1 2. ** 19.62 / HEAD :=
CR ." MEAN JET OUTLET VELOCITY=" VELO . ." m/s"
CR ." THEORETICAL IMPACT VELOCITY=" VEL1 . ." m/s"
CR ." DYNAMIC HEAD=" HEAD . ." m"
CR
CR ." MAXIMUM PRESSURE (m)"
TEMPMAX .
CR
CR ." MEAN PRESSURE (m)"
TEMPMEAN .
TEMPMAX TEMPMEAN - HEAD / TEMPHEAD :=
CR
CR ." MAX PRESSURE COEFF. (Cp+)"
TEMPHEAD .
;
```

```
\ SPECDIST.100
\ PROGRAM TO PLOT POWER SPECTRUM AND
\ SCAN OF DATA. SAMPLING AT 100Hz


REAL DIM[ 2048 ] ARRAY POSITION?
20 STRING TEST
REAL DIM[ 2048 ] ARRAY FREQS
2048 REAL RAMP
1 - 100 * 2048 / FREQS :=
REAL DIM[ 2048 ] ARRAY PSPECTRUM
: SPECTRUM?
  POSITION? FFT
  ZMAG DUP * PSPECTRUM :=

  VERTICAL LOGARITHMIC
  -1.2 0 10 LABEL.FORMAT
  FREQS SUB[ 1 , 1024 , 1 ]
  PSPECTRUM SUB[ 1 , 1024 , 1 ]
  XY.AUTO.PLOT
  NORMAL.COORDS
  0 LABEL.DIR 0 CHAR.DIR
  .7 .05 POSITION " FREQUENCY (Hz)" LABEL
  .4 .975 POSITION TEST LABEL
  .17 .9 POSITION " MAGNITUDE=(FFT)^2" LABEL
  .5 .9 POSITION " POWER SPECTRUM" LABEL
  OUTLINE
  CURSOR.OFF
  WORLD.COORDS
;
REAL DIM[ 1000 ] ARRAY TIMES
TIMES []RAMP
TIMES 1 - 100 / TIMES :=
15 STRING UNITS
: SCAN?
  TIMES
  POSITION? SUB[ 1 , 1000 , 1 ]
  VERTICAL LINEAR
  AXIS.DEFAULTS
  XY.AUTO.PLOT
  NORMAL.COORDS
  CURSOR.ON
  0 LABEL.DIR 0 CHAR.DIR
  .7 .08 POSITION " TIME (Sec.)" LABEL
  .3 .03 POSITION " SCAN OF FLUCTUATIONS" LABEL
  .4 .975 POSITION TEST LABEL
  90 LABEL.DIR 90 CHAR.DIR
  .025 .6 POSITION UNITS LABEL
  OUTLINE
  CURSOR.OFF
  WORLD.COORDS
;
```

1. Numerical output of jet dimensions.

```
 10 INPUT "FLOW(M^3/S)";Q
 20 INPUT "ORIFICE DIA.(M)";D
 30 U=4*Q/(D^2*PI)
 40 R0=D/2
 50 INPUT "TURBULENCE INTENSITY(LATERAL)%";A
 60 V1=U*(A/100)
 70 INPUT "FALL LENGTH(M)";L
 80 G=9.81
 85 @%=&2040C
 90 PRINT TAB(6);"DROP";SPC(4);"OUTER";SPC(4);"CORE";SPC(3);"LAMINAR"
100 FOR S=0 TO L STEP L/100
110 E=SQR(U^2+2*G*S)
120 T=(-U+E)/G
130 V=E
140 X=V1*T
150 R=X+R0
160 B=(R0^2*U)/V
170 C=SQR(B)
180 Y=S/R0:X1=R/R0
190 F=(R*V*0.4)^2-(R0^2*-U*1.51*V)-(R^2*V^2*0.336)
210 IF F>=0 F=SQR(F)
215 IF F<0 R1=-(R*0.53)
220 R1=(-V*R*0.4+F)/(V*0.76)
230 X2=R1/R0
240 IF F<=(R*V*0.4) X2=0*X2
245 PRINT Y;"  ";X1;"  ";X2;"  ";C
248 IF X2=0 I=4.5*(R0^2*U)/(R^2*V):PRINT I
250 NEXT S
260 END
```

2. Graphical output of jet dimensions.

```
 10 INPUT "FLOW(M^3/S)";Q
 20 INPUT "ORIFICE DIA.(M)";D
 30 U=4*Q/(D^2*PI)
 40 R0=D/2
 50 INPUT "TURBULENCE INTENSITY(LATERAL)%";A
 60 V1=U*(A/100)
 70 INPUT "FALL LENGTH(M)";L
 80 G=9.81
 85 @%=&2040C
 90 MODE 0
100 FOR S=0 TO L STEP L/100
110 E=SQR(U^2+2*G*S)
120 T=(-U+E)/G
130 V=E
140 X=V1*T
150 R=X+R0
160 B=(R0^2*U)/V
170 C=SQR(B)
180 Y=(S/R0)*10:X1=(R/R0)*250
190 F=(R*V*0.4)^2-(R0^2*-U*1.51*V)-(R^2*V^2*0.336)
210 IF F>=0 F=SQR(F)
215 IF F<0 R1=-(R*0.53)
220 R1=(-V*R*0.4+F)/(0.76*V)
230 X2=(R1/R0)*250
235 IF F<=(R*V*0.4) X2=0*X2
240 IF S=0 THEN 290
250 MOVE OLDX1,OLDY
260 DRAW X1,Y
270 MOVE OLDX2,OLDY
280 DRAW X2,Y
290 OLDX1=X1
300 OLDX2=X2
310 OLDY=Y
330 NEXT S
340 PRINT "PICTURE OF PROFILE"
350 PRINT "FLOW = ";Q
360 PRINT "DIA. = ";D
370 PRINT "TU = ";A/100
380 END
```